Title
THE INITIATION OF NATURAL CONVECTION CAUSED BY TIME-DEPENDENT PROFILES

Author
Davenport, Ian Frank

Publication Date
1972-06-01

LBL-660

THE INITIATION OF NATURAL CONVECTION CAUSED BY TIME-DEPENDENT PROFILES

Ian Frank Davenport* and C. Judson King

June 1972

AEC Contract No. W-7405-eng-48

*Filed as a Ph. D. Thesis

LBL-660

DISCLAIMER

THE INITIATION OF NATURAL CONVECTION CAUSED BY TIME-DEPENDENT PROFILES

Contents

THE INITIATION OF NATURAL CONVECTION CAUSED BY TIME-DEPENDENT PROFILES

Ian Frank Davenport and C. Judson King

Department of Chemical Engineering and
Lawrence Berkeley Laboratory
University of California
Berkeley, California 94720

June 1972

ABSTRACT

This experimental study is concerned with the initiation of convection in deep pools (penetration depth is small compared with the fluid depth) and shallow pools (penetration depth is comparable to the fluid depth). Fluids covering a wide range of Prandtl number, Pr, were either cooled from above through a gas-liquid surface where both surface tension and density forces were expected to contribute to the convection, or heated from below where only the density forces were present. The study of these two systems simultaneously allowed identification and separation of density and surface tension effects. The results were then used to evaluate current models of convection initiation driven by either density forces, surface tension forces or a combination of both over a wide range of experimental conditions.

The onset of convection in deep pools driven by density forces was observed to be described by high Prandtl number and low Prandtl number phenomenon. The high Prandtl number phenomenon was observed to behave similar to the onset of convection from a linear density gradient across the fluid (shallow pool). However, the striking dissimilarity between the deep pool and shallow pool phenomena was that the critical Rayleigh

number in the deep pool case was independent of the rigidity of the heating or cooling boundary, which is opposite to that found in the shallow pool case. The understanding of the low Prandtl number, deep pool phenomenon has yet to be developed.

Convection initiation driven by surface tension forces was observed not to occur in fluids with planar surfaces, and one dimension temperature gradients. However, some important conditions for surface-tension motion at a gas-liquid interface were identified, including surface deformation, i.e. waves, meniscus, and point source surface-tension sinks.

Prediction of steady state convection heat transfer coefficients, using Howard's (1966) model of density boundary layer growth and destruction and convection initiation data, appears limited when the predicted values are compared with experimental values.

I. INTRODUCTION

Natural convection has been a popular topic of research over the past decade. This stems from researchers in disciplines such as oceanography and atmospheric sciences working with large-scale systems, and chemical and mechanical engineers working with small-scale systems, desiring to understand the fundamentals of convection so as to allow them to be more precise in their predictions. There is no doubt that the availability of large computers to solve the governing equations numerically has also opened up avenues of research on this topic. Consequently, many aspects of natural convection have been explored and some of these understood, but reliable predictions for many applications are still unavailable.

Natural convection is observed when the temperature or composition gradient in a fluid-phase heat or mass transfer process produces an unstable hydrodynamic situation. This situation can arise when a more dense layer is formed on top of a less dense layer, or when surface tension inequalities exist along a phase boundary. At a liquid-liquid or gas-liquid boundary, both density and surface tension instabilities have been observed, whereas at a gas-solid or liquid-solid boundary the density effects have been observed to be dominant.

Convective motion driven by these instabilities can be sustained if the driving forces are large enough to overcome the viscous and conduction stabilizing forces. This condition for motion is met when the Rayleigh number (Ra) (see Table 1), which expresses the ratio of the bouyancy forces to the viscous and conduction stabilizing forces in density driven flow, and the Marangoni number (M) (see Table 1), which

Table 1. Definitions of Rayleigh and Marangoni Numbers

$$Ra_H = \frac{\rho g \beta \, \Delta T \, H^3}{\mu \alpha}$$ - Rayleigh number based on fluid depth (H) (I-1)

$$Ra_t = \frac{\rho g \beta \, \Delta T \, \alpha^{1/2} t^{3/2}}{\mu}$$ - Rayleigh number based on thermal boundary layer thickness $(\alpha t)^{1/2}$ (I-2)

$$M_H = \frac{\Delta \sigma \, H}{\mu \alpha}$$ - Marangoni number based on fluid depth (H) (I-3)

$$M_t = \frac{\Delta \sigma \, t^{1/2}}{\mu \alpha^{1/2}}$$ - Marangoni number based on thermal boundary layer thickness $(\alpha t)^{1/2}$ (I-4)

$$\frac{Ra_t}{M_t} = \frac{\rho g \frac{\partial \rho}{\partial T} \alpha \, t_c}{\frac{\partial \sigma}{\partial T}}$$ - thermal driven (I-5)

$$\frac{Ra_t}{M_t} = \frac{\rho g \frac{\partial \rho}{\partial c} \mathscr{D} t_c}{\frac{\partial \sigma}{\partial c}}$$ - composition driven (I-6)

$$\frac{(Ra_t)_{THERMAL}}{(Ra_t)_{MASS}} = \frac{\frac{\partial \rho}{\partial T} \alpha^{1/2} \Delta T}{\frac{\partial \rho}{\partial \psi} \mathscr{D}^{1/2} \Delta \psi}$$ (I-7)

$$\frac{(M_t)_{MASS}}{(M_t)_{THERMAL}} = \frac{\frac{\partial \sigma}{\partial \psi} \alpha^{1/2} \Delta \psi}{\frac{\partial \sigma}{\partial T} \mathscr{D}^{1/2} \Delta T}$$ (I-8)

expresses the ratio of surface tension forces to conduction and viscous forces in surface tension flow, are greater than some critical value.

The research and application of natural convection motion revolves around two concepts: the conditions for initiation of convective motion from the static conduction state (the conditions at which the driving forces are just great enough to overcome the viscous and conduction stabilizing forces), and the transfer coefficient resulting from sustained convective motion.

The objective of this thesis is to expand the experimental data reported in the literature on density-driven ("natural") convection initiation for cases where the ratio of the fluid depth to transfer boundary layer thickness varies from large values (deep pool) to small values (shallow pool). These data are useful for evaluation of current models of convection initiation and in providing physical insight into time-dependent convection initiation phenomena.

In addition, the current theories of steady-state turbulent natural convection (discussed in Chapter VIII) suggest a similarity between the initiation and steady-state phenomena (Burger, 1970 and Foster, 1971). The information developed from a turbulent convection initiation investigation is useful for evaluation of this similarity hypothesis.

II. CONVECTION INITIATION

This chapter will review the literature on convection initiation by either density or surface tension driving forces, or a combination of both, and will introduce the goals of the experimental work.

1. Density-Driven Convection Initiation

When a fluid is heated from below or cooled from above, bouyancy forces can be generated which lead to sustained motion. The form of motion depends upon the ratio of the rate of generation of the buoyancy forces to the growth rate of the stable forms of motion, the ratio of the buoyancy forces to the viscous and conduction stabilizing forces (Rayleigh number), and the ratio of the conduction to the viscous stabilizing forces (Prandtl number).

Provided the rate of increase of the buoyancy force is slow in comparison with the growth rate of the stable convective patterns of motion (time-independent case), the first intense motion will be in a cellular form (Rayleigh, 1916; Stuart, 1964). If the rate of increase of the buoyancy force is much faster (time-dependent case), the first convective motion will be in the form of thermals (Howard, 1966), which are turbulent periodic bursts of fluid from the heated or cooled surface.

At high enough values of the Rayleigh number (Ra_H), cellular flow will become unstable regardless of the heating rate, and the flow will be turbulent. This is known as the onset of turbulence in the time-independent case.

1.1. Time-Independent or Cellular Convection Initiation

For a linear density gradient through the fluid, the onset of cellular convection from the "motionless fluid" state occurs at a value of the Rayleigh number ("first transitional Rayleigh number") well established theoretically and experimentally. It has a value on the order of 1000, and increases with increasing rigidity at the boundaries and is higher as the conductivity of the boundary increases. The topic has been extensively reviewed by Chandrasekhar (1961) and Berg, et al. (1966). The critical Rayleigh number for fluid contained between two perfectly conducting, rigid boundaries is approximately 1704. For fluid contained between two perfectly conducting boundaries, with one rigid and the other free, the Rayleigh number is approximately 1100. Finite-amplitude disturbance studies (using a perturbation expansion (v) with terms (ε) raised to integer powers i.e. $v = \varepsilon + \varepsilon^2 + \varepsilon^3 \ldots$) by Malkus and Veronis (1958) and Busse (1967) have shown theoretically that the observed cellular convection at onset is the one maximizing heat transport. When the Boussinesq approximation (all fluid properties other than density are independent of temperature) is valid, the cellular pattern is two-dimensional roll cells; whereas if the Boussinesq approximation is not valid, hexagonal cells can be stable for a short range of super-critical Rayleigh number, whereupon they are replaced by roll cells at higher values of Rayleigh number. The predictions agree well with the observations of Bénard (1900), Silveston (1958), and Somerscales and Dougherty (1970).

The form of cellular motion for supercritical Rayleigh numbers has been studied theoretically and experimentally. Busse (1967) predicted,

for fluids with infinite values of the Prandtl number, that the roll cell would be stable to infinitesimal disturbances up to a Rayleigh number of about 22,000, provided the roll cell wavelength was within a narrow bandwidth. Experimental observations by Rossby (1966), Chen and Whitehead (1969), Krishnamurti (1968, 1970), Koshmeider (1966), and Busse and Whitehead (1971) have supported these predictions and have identified features associated with the development and breakdown of the two-dimensional roll cell structure. The width of the roll cell increases with increasing Rayleigh number. Photos reported by Busse and Whitehead (1971) show that at conditions of instability the roll cell boundaries transform to either a zig-zag pattern or a rectangular pattern, which has the appearance of cross-roll cells with their axis at 90° to each other (bimodal convection). This is the second transition, which occurs at a Rayleigh number that is dependent on Prandtl number (Krishnamurti, 1970).

1.2. Turbulent Convection Onset in the Time-Independent Case

The bimodal, or three-dimensional, regular hexagonal form of convection succeeds the roll cell pattern and persists as the Rayleigh number is increased, until at sufficiently high values of the Rayleigh number (Ra_H) periodic temperature fluctuations appear with magnitude and frequency increasing as the Rayleigh number is increased. Eventually, at very high Rayleigh numbers a time-dependent flow, appearing as turbulence, replaces the cellular flow. The first appearance of time-dependent characteristics is the third transition and is Prandtl-number dependent. This represents the start of the breakdown of cellular convection.

Experimentally observed values of the Rayleigh number at the second and third transitions are tabulated in Table 2.

The cellular transitions and breakdown have only been recently investigated closely, notably by Busse (1967), Krishnamurti (1970), and Busse and Whitehead (1971), and the mechanisms involved in these phenomena are not well established. However, the observations of these investigators, with some interpretation by the present author based on physical reasoning, provide generalized information on cellular mechanics.

The convective flow pattern involves circulation of fluid. The driving force for circulation is the buoyancy force, and the resistance to motion is due to fluid viscosity and to shear effects at the fluid boundaries. Primary conduction across the fluid layer establishes the critical buoyancy force necessary for convection, but motion is sustained by density differences in the horizontal planes of the fluid. Consequently, the temperature profile in a cell must be two-dimensional. The horizontal gradients are maintained by convective heat transfer associated with the fluid motion. However, secondary conduction effects tend to conduct heat in the opposite direction of the convective heat flow, and so resist the establishment of these horizontal gradients. It is a balance between secondary conduction and convective heat transfer processes which determine the temperature distribution and hence the velocity and heat transfer characteristics of the cellular motion. Figure II-1 displays the relationship between the temperature and the velocity in cellular flow.

The convective velocity is limited by the viscous drag and the shear at the boundaries, and the thermal diffusivity of the fluid determines the influence of the secondary conduction transfer. For a situation where

Table 2. Rayleigh Number at Convection Pattern Transformation

a) Transition from Two-Dimensional Roll Cells to Three-Dimensional Cells:

Investigator	Prandtl Number	Rayleigh Number $(Ra_H)_{II}$
Krishnamurti (1970)	6.7	17,000
	57	22,000
	100	22,000
	860	22,000
	8500	17,000

b) Rayleigh Number at Third Transition:

Investigator	Prandtl No.	Rayleigh No. $(Ra_H)_{III}$	Comments
Schmidt and Saunders (1938)	5	48,000	
Silveston (1958)	5 to 35	50,000	
Rossby (1966)	0.023	1700 approx.	Krishnamurti (1970) suggests that this transition was probably that observed for fully developed turbulence rather than the first signs of turbulence.
	6.8	44,000	
	39	82,000	
	61	175,000	
	104	210,000	
	403	426,000	
		940,000	
	880	1,600,000	
Willis and Deardorff (1967)	0.7	5,500	
	6.8	35,000	
	18	120,000	
	57	140,000	
Krishnamurti (1970)	0.7	4,800	(1) External conditions steady to allow precision in long period, low Ra_H readings.
	6.7	30,500	
	57	47,600	
	100	56,000	

(continued)

Table 2. (continued)

b) Rayleigh Number at Third Transition:

Investigator	Prandtl No.	Rayleigh No. $(Ra_H)_{III}$	Comments
Krishnamurti (1970)	200	56,000	(2) Many temperature probes.
	860	58,000	
	8500	56,000	(3) Observed transition with onset temperature fluctuations and change in slope of heat flux vs. ΔT

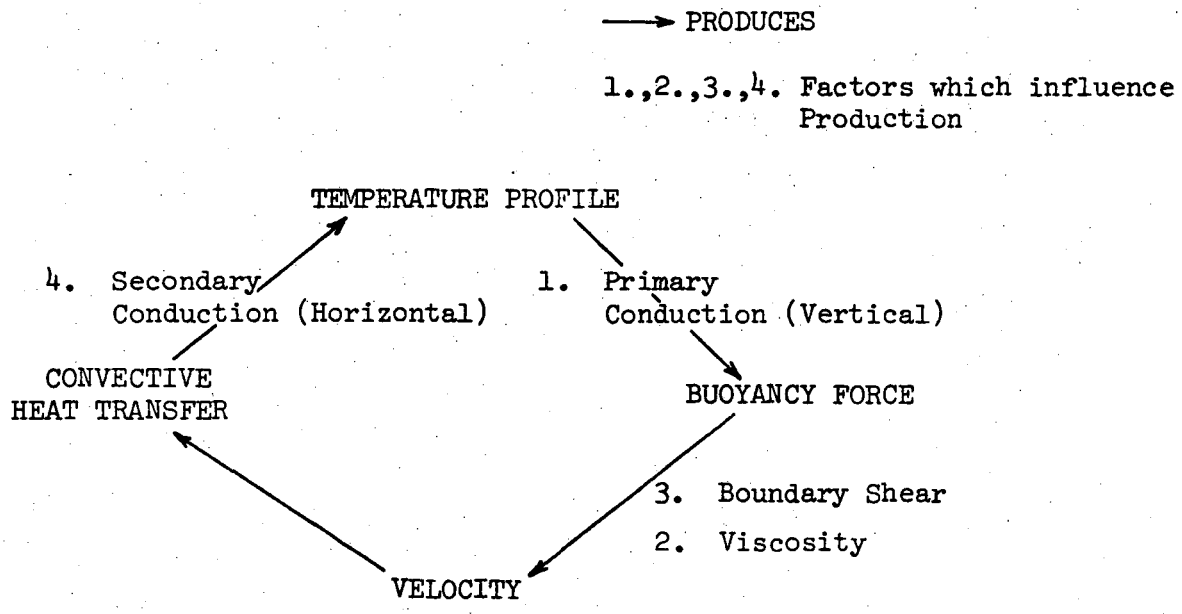

Fig. II-1. The Interdependence of the Temperature and Momentum Fields in Laminar Cellular Flow.

the rigidity at the boundaries is constant, the ratio of the convective transport to the conduction transport can be given by the ratio of the viscous properties to the conduction properties of the fluid, which is the Prandtl number.

The breakdown of a cellular structure occurs when the convective transfer process cannot maintain the necessary balance with the conduction transport in shaping the temperature profile and so provide a high enough velocity to give the necessary convective transfer. As the Rayleigh number (Ra_H) increases, the temperature gradient across the fluid increases, and from dimensional analysis considerations, it can be expected that the absolute temperature gradient in the horizontal direction will increase. This represents an increase in the magnitude of the secondary conduction transport which eventually leads to the breakdown of the cellular pattern discussed above. The Rayleigh number (Ra_H) corresponding to cellular breakdown should be higher as the Prandtl number is increased, since this higher Prandtl number represents a relative increase in the ratio of the viscosity to the thermal diffusivity involved in secondary conduction. (See Table 2.)

Krishnamurti (1970) observed that at cellular breakdown packets of hot fluid appeared in the cellular flow and corresponded with the first signs of temperature fluctuations. She postulated that these packets of fluid were carried by the cellular motion at approximately the orbit velocity. However, her interpretation is suspect since, if the conductive heat transfer is influential enough to resist convective alteration of the temperature field (discussed above), it is doubtful that the hot packets of fluid could resist conductive dissipation so as to retain

their identity for even a fraction of the orbit period. On the other hand, in the cell pattern, it can be expected, from observed temperature isotherm patterns in the cell by Willis and Deardorff (1969), and by Silveston (1958), that there are regions in the cell where a perturbation produces a significant alteration of temperature and velocity in that region. Because of the delicate balance between conduction and convection processes, this region is probably the site for initial cell breakdown. If the cell structure is unstable, the heat conducted to this site should be greater than the heat removed by convection, which will decrease the density gradients and lessen the convection velocity in this region. Decreased convection heat transfer will result in an increase in the temperature of the region over the steady-state value in the cellular flow. This will create a localized hot packet of fluid. The growth of the hot packet in temperature and elevation, and in size is ensured by the fact that the increase in temperature deflects the currents further from the site and lessens the heat convected away. The hot packet of fluid will become mobile when the buoyancy forces overcome the viscous and conduction stabilizing forces. The packet should then dissipate its heat as it rises through the fluid.

In order to describe the appearance of the hot packets, the following dimensional analysis appears valid. The velocity and temperature distribution in the cell pattern can be described by Ra_H and Pr. After onset of the periodic appearance of hot packets, the period (or time between appearance of thermals) is an additional dependent variable in describing the cell flow. Dimensional Analysis requires another dimensionless group to account for the period. Rossby (1966) suggested the

time-dependent Rayleigh number (Ra_t - see Table 1) as this other group. He and Krishnamurti (1970) found experimentally that a constant value of Ra_t when a thermal is released could adequately describe the periodicity over decades of change in Ra_H. They measured the period between temperature fluctuations by suspending thermocouples in the cell flow, and used the total temperature drop across the fluid in evaluating Ra_t. In this manner, they determined that the critical Ra_t for thermal generation decreases slightly as Pr increased in the range of Pr from 6 to 8500, where cellular flow was still observable. Willis and Deardorff (1971) measured frequency data for fluctuations in air (Pr = 0.7) in the range of Ra_H from 4,500 to 30,000, where the flow changed from cellular flow to turbulent flow. They observed that the value of Ra_t increased by almost 50% as the Rayleigh number Ra_H increased. This trend was also noted in Krishnamurti's results, but the increase in value of Ra_t did not appear to be as significant.

In summary, the transition from cellular or laminar flow to turbulent flow highlights the importance of the balance between the convective and conduction transfer processes in determining the pattern of the convection flow.

1.3. Onset of Turbulent Convection from a Time-Dependent Profile

1.3.1. Theoretical. In an infinitely deep pool of fluid, all patterns of convection motion can grow, in theory, as a result of an adverse density profile in the fluid (Howard, 1966). However, the growth rates of these patterns vary, and the observed initiation

phenomenon corresponds to that pattern having the fastest growth from the conduction state to the observed convection state. Foster (1965, 1968) has calculated the growth rates of a class of cellular convection patterns for this situation and has shown that the fastest growing cell is that with a length scale on the order of the thickness of the density boundary layer at first observable convection.

When the fluid is deep enough so that the density profile never "feels" the non-heating or non-cooling boundary, the phenomenon is confined to the region of the boundary producing the adverse density gradient. In this case, the density profile extends into a semi-infinite medium and is therefore transient. Consequently, the magnitude of the buoyancy force at a given point in the fluid changes with time. This introduces into the convection initiation problem an extra dimension which was not considered in the time-independent problem discussed in Section I-1. The growth rates of the convective patterns, which are dependent on the buoyancy force magnitude and distribution, must change with time as the temperature profile changes. Thus, prediction of convection initiation for the boundary layer case necessitates an understanding of the relationship between the growth rates of the convection patterns, on the one hand, and the rate of change of the density profile, on the other. Different models have been advanced postulating this relationship.

The earliest attempts to predict the onset of convection from a transient profile assumed that the growth of the observed convective mode was infinitely fast compared with the rate of change of the density profile. This became known as the Quasi-Steady-State Assumption (Q.S.A.), and included the work of Morton (1958), Lick (1964), and Currie (1967). This

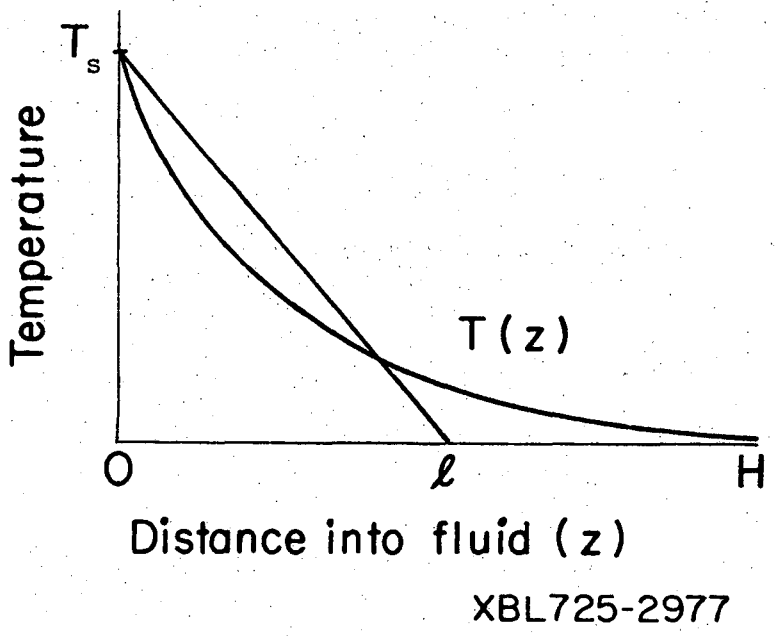

Fig. II-2. The Segment Approximation of a Curved Profile. The areas under the curved profile and linear approximation are equal. Thus according to Lick (1965),

$$1/2\ T_s \times \ell = \int_0^H T\ dz$$

or

$$\ell = 2\int_0^H T/T_s\ dz$$

analysis was a modification of the analysis used to study convective initiation from the time-independent linear conduction profile. The time-dependent curved profile was divided into two linear segments (Fig. II-2), one segment containing all of the density change and the other segment having zero density change. The critical Rayleigh number (Ra_H) based on the total fluid depth (H) was found as a function of the ratio (ℓ/H), by finding the wave number of the disturbance which gave the minimum value of Ra_H that corresponded to fluid motion. The Rayleigh number Ra_H found from the analysis increased as the ratio (ℓ/H) decreased, so that in the limit of small (ℓ/H), which corresponds to a boundary layer gradient, the group $Ra_H(\frac{\ell}{H})^3$ was constant. This introduced the importance of the Rayleigh number Ra_ℓ, based on the boundary layer depth (ℓ), for describing boundary-layer convection initiation. However, the weakness of this analysis has been discussed by Robinson (1966) who showed that the growth rate of the cellular patterns of convection over most of the growth period was comparable to the rate of change of the density profile for thermal diffusion in a semi-infinite-medium. This contradicts the Q.S.A., discussed earlier.

Attempts to investigate convection initiation where growth rates of cellular convective patterns are considered to be comparable to the rate of change of the density profile have been made by Foster (1965, 1968), Mahler and Schechter (1970), and Gresho and Sani (1970). The basis of this approach was to consider the growth of a velocity perturbation in a time-dependent adverse density field ("Amplification" Theory). The fluid is assumed to be in motion at all times, and the assumption is made that this motion contains a wide range of fundamental wavelengths. The

adverse density profile encourages preferential growth of the vertical velocity components of a narrow bandwidth of wavelengths, until the convection reaches some finite observable size.

This situation is treated mathematically by integrating the time-dependent equations of motion with a given time-dependent temperature profile, and a specified initial velocity profile. The time taken for the amplitude of the initial velocity component to be magnified by a given factor (commonly 1000) is found from this integration. The model cannot predict the amount of amplification necessary for observable convection, but in principle a small number of experiments could be performed to determine the amplification factor corresponding to observable convection. Once determined, this amplification factor should be constant for that given initial velocity profile, and all other variables constant.

The disadvantages of this approach are

(1) The amplification factor required for observable convection is dependent upon the initial amplitude of the fundamental wavelengths. Thus, as the velocity source varies (e.g., with location of the experiment), the initial amplitudes of the various wavelengths can be expected to vary, and thus invalidate the use of a generalized correlation for convection initiation.

Comment (1) could also be important in scale-up considerations.

(2) The mathematics are simplified by linearizing the equations of motion about the pure conduction solution before integration. This action is justified by assuming that all perturbations in velocity and temperature profiles are small up to the time

shortly before convection begins to be observed. The linearized equations are not expected to be valid once large-scale motion begins. Further, inertial effects are neglected in linear theory because they involve the product of two small quantities ($V.\nabla V$), which could be important in the acceleration or growth period. The disadvantage of linearized mathematics is their range of validity. However, this linearized approach gives an indication of the relationship between different dimensionless groups, which forms the basis for experimental correlation.

The theoretical results from Amplification Theory for the critical time (t_c) and the critical wave number (a_c) functions of Prandtl number for the fastest growing wave in a continuous wave spectrum, for a specified amplification factor, have been published (Foster, 1965, 1968; Mahler and Schechter, 1970; Gresho and Sani, 1971). The two density profiles examined have been responses to a step change and to a linear change in surface conditions with time, where the thermal boundary layer thickness is much smaller than the liquid depth.

The dimensionless group for convection initiation have been utilized in Amplification Theory with specific connotations applied to them. However, these groups arise from the dimensional analysis of the basic equations of motion and the relevant boundary conditions, and need not necessarily have the Amplification Theory connotations applied to them. The following are the dimensionless groups for this phenomenon.

$\pi_1 = Ra_t$ = dimensionless conduction time before first observable convection

$\pi_2 = Pr$

$\pi_3 = \frac{\alpha t}{H^2}$ = effect of fluid depth

$\pi_4 = \frac{\alpha t}{W^2}$ = effect of fluid width

$\pi_5 = M_t$ = Marangoni number to describe the importance of surface tension effects

π_6 = group to describe initial velocity condition

π_7 = group to describe degree of rigidity at boundaries

π_8 = group to define type of condition temperature profile (e.g., step change at surface)

1.3.2. Experimental. Several experimental studies on time-dependent convection initiation have been reported in the literature.

Foster (1965) evaporated water from a quiescent pool and measured the surface temperature optically as a function of time. Prior to a run, the water was allowed to reach thermal equilibrium with its container and enclosed gas space. The run was started by removing the equilibrium conditions from the gas phase. Convection onset was defined as being where the surface temperature vs. time changed from a negative to a positive slope, since convection enhanced heat transfer, and in this case lowered the temperature difference between the bulk and the surface which had been established during the conduction period. The surface temperature during the conduction period, was approximated by a linear decay with time. The time-dependent Rayleigh number for the linear surface temperature change was defined as

$$Ra_t = \frac{\rho g \beta (\frac{\partial T_s}{\partial t}) \alpha^{1/2} t_c^{5/2}}{\mu} \quad .$$

The time derivative of the surface temperature ($\frac{\partial T_s}{\partial t}$) was varied and the results verified the relationship ($\frac{\partial T_s}{\partial t} \cdot t_c^{5/2}$) = constant. In another series of experiments, Foster (1969) heated water from below so that the bottom surface temperature increased linearly with time. The heating rate was varied, and the results again verified the relationship ($\frac{\partial T_s}{\partial t} \cdot t_c^{5/2}$ = constant).

The first signs of convection were observed by noticing movement in a thin layer of dark, fine particles lying on the bottom of the fluid. At the time when convection was indicated by a change in surface temperature slope, the ink was observed to move at random points in the ink layer. After a short time, the area exhibiting convection increased. In an area where convection was observable, the distance between centers of motion was found to be dependent on the thickness of the thermal layer, as had been predicted by Amplification Theory.

In the heating experiments, the surface was described as "fixed", because the heat transfer was across a solid-liquid phase boundary; whereas in the evaporation experiments the heat transfer experiments were described as "free", because the cooling was across an air-liquid surface. It should be noted that free surfaces are treated mathematically by the boundary condition $\frac{\partial^2 V}{\partial z^2} = 0$, and fixed surfaces by the boundary condition $\frac{\partial V}{\partial z} = 0$. Generally the predicted fixed-surface Rayleigh number from Amplification Theory is from two to three times that in the free surface case, depending on the Prandtl number (see Chapter VI, Sec. 1.1). The amplification factor found by Foster (1965, 1969) comparing experimental and theoretical Rayleigh numbers for the free surface was in the range 10^1 to 10^2; whereas the fixed surface amplification factor was determined

as 10^3 to 10^5. The presence of surface waves in the evaporation experiments was suggested as a possible cause for the difference in amplification factor between the free and fixed surface experiments.

Blair and Quinn (1968) performed mass transfer experiments by absorbing gases into water. A high-pressure reservoir was connected to a pair of experimental cells, one containing no liquid and one containing liquid and gas in equilibrium. The pressure in both cells was increased simultaneously, and the moles of gas absorbed (measured as the pressure differential between the two cells) was recorded as a function of time. The conditions at onset of convection were identified by the first departure from a linear relationship between the moles of gas absorbed and the square root of the time of the run. Critical conditions were verified by Schlieren techniques. In these experiments the change in surface conditions was approximated by a step function. The Rayleigh number for a step function was defined as

$$Ra_t = \frac{g \frac{\partial \rho}{\partial \Delta P} \Delta P \, t_c^{3/2} \rho^{1/2}}{\mu} \quad .$$

By varying the driving force for absorption (ΔP), the relationship ($\Delta P \cdot t_c^{3/2}$ = constant) was verified. In a separate series of experiments, the inverse relationship with viscosity in the Rayleigh number was verified by increasing the viscosity of the water with a thickening agent. The water-air surface was contaminated and shown to have a fixed surface character. The apparent amplification factor was in the range of 10^5 to 10^6.

The first convection motion at high density-gradient driving forces appeared as a combination of rings, plunging columns or droplets, and sheet-like streamers. For smaller density-gradient driving forces, the initial motion appeared in the form of plunging sheets, without the columnar mode.

Mahler and Schechter (1970) performed experiments similar to those of Blair and Quinn with clean and contaminated aqueous surfaces. The results were interpreted by defining different degrees of surface contamination; the more contaminated the surface, the greater the surface rigidity and hence the greater the critical Rayleigh number. With this interpretation the results agreed well with the theoretical predictions for an amplification factor of 10^3. However, important surface tension and surface wave effects were not considered in their interpretation. These are discussed in Chapter VI, Sec. 1-2.

Onat and Grigull (1970) heated a wide range of fluids from below with a linear time increase of temperature, to determine the relationship of Ra_t with Prandtl number. Their results agreed well with Foster's (1968) calculated functionality for an amplification factor of approximately 10^1. Interferometric studies showed the development of the convection initiation. Prior to the breakdown of pure conduction, the boundary region had planar isotherms. However, at the point where the surface temperature deviated from the linear slope in time, bumps in the isotherms were observed to appear at the outer region of the boundary layer. These grew rapidly into packets of hot fluid resting on an almost planar boundary layer, and broke off upon reaching a certain size.

The above discussion highlights the practical weakness of Amplification Theory, since the observed amplification factors corresponding to experimental convection initiation varied from 10^1 to 10^5. As can be seen from Fig. II-3 for an example published by Foster (1969) simulating an actual experiment, this range of amplification factor produces a wide variation in convection onset time. Obviously further refinement of Amplification Theory is needed before reliable predictions can be made.

2. Surface-Tension-Driven Convection Initiation

Observation since the time of Thompson (1870) has shown that surface-tension gradients, produced by either composition or temperature gradients, can cause liquid motion. Surface-tension-driven motion has been observed in gas-liquid (Ellis and Biddulph, 1966; Berg et al., 1966), liquid-liquid (Orell and Westwater, 1962; Bakker, et al., 1966), and gas-liquid-solid (Hrma, 1970) systems. Often, the same composition or temperature profiles that cause surface-tension-driven motion also cause density-driven stabilizing or destabilizing effects. Some experimental conditions, however, are thought to be dominated by the surface tension effects, and in the mathematical analysis of these cases the body forces are neglected (Levich, 1962). These include cases where the surface tension gradient is parallel to the liquid-air surface, or in shallow pools where the gradient is normal to the liquid-air surface.

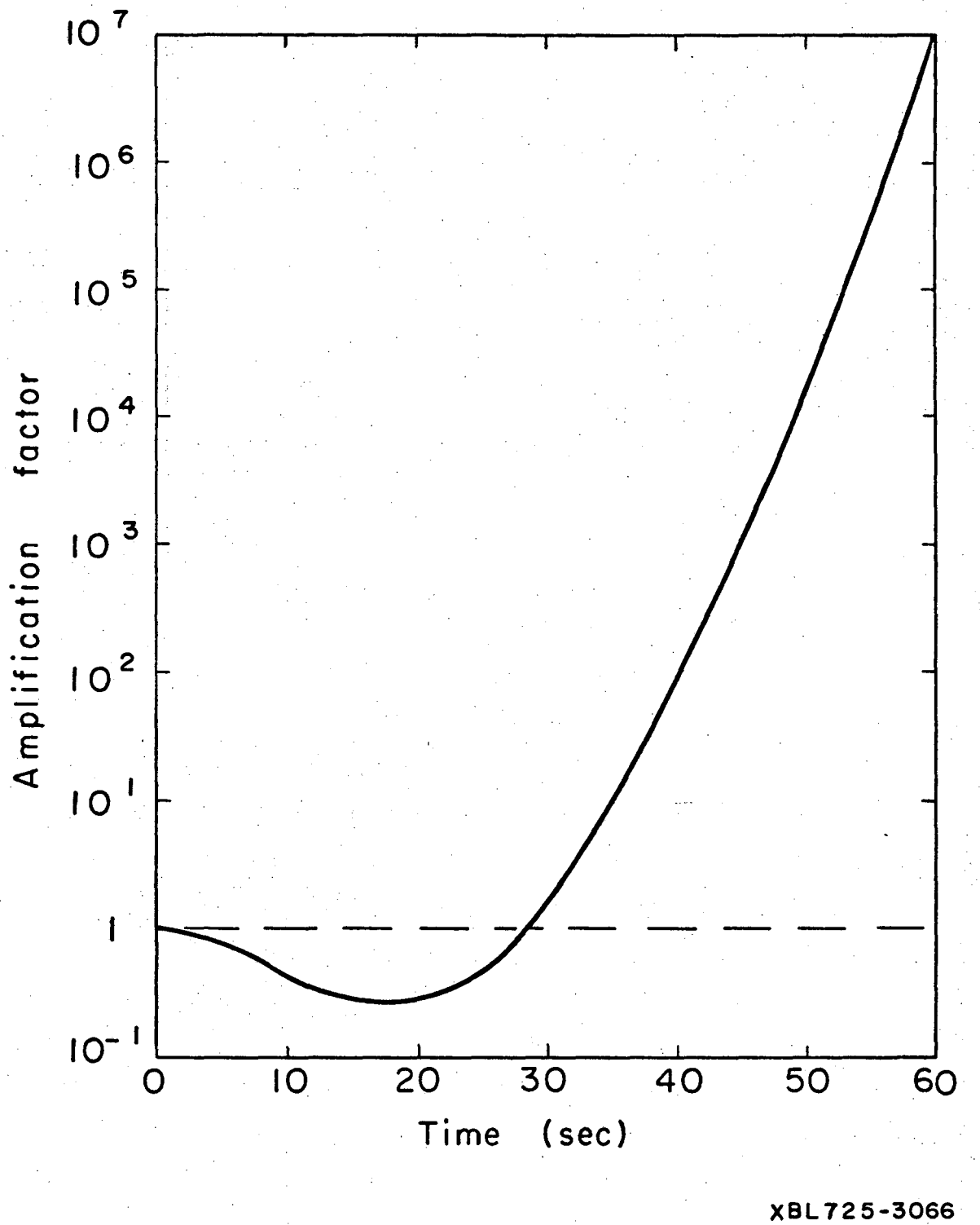

Fig. II-3. Amplification of the Fastest Growing Wave as a Function of Time in Foster's (1969) example.

2.1. Surface-Tension-Driven Motion Produced by a Gradient Normal to the Liquid Surface

2.1.1. Theory. If liquid at a surface has a higher value of surface tension than would be produced if bulk liquid were at the surface, convection can persist. The driving force for motion is the reduction in surface energy which results when the bulk liquid is brought to the surface. This is usually described as the "Marangoni Effect".

Pearson (1958) used an approach for theoretical analysis of surface-tension-driven motion similar to that employed for the density-driven convection problem with a linear temperature gradient through the fluid. Motion was found to persist if the critical conditions, as indicated by the Marangoni number (see Table 1) were surpassed ($M_H > 80$). Extensions of his approach have been made so as to include surface deformation, surface rigidity, various thermal boundary conditions (Berg, 1966), and the effect of Gibbs adsorption (Brian, 1971).

Vidal and Acrivos (1967) have extended the method adopted by Pearson to non-linear temperature or composition profiles in the liquid, using the same approximations as Morton, Lick, and Currie, mentioned earlier. This approach may well be subject to the same criticisms as the Q.S.A. approach to density-driven convection, but no time-dependent convection studies using the Amplification Theory have yet been published for surface-tension-driven convection so as to allow an evaluation of the Q.S.A. validity. The theoretical predictions of Vidal and Acrivos agreed only qualitatively with their experimental results, as was the case for the aforementioned density-driven convection studies which compared experimental results with Q.S.A.-based predictions.

2.1.2. Experimental. Dimensional analysis of this phenomenon suggests that the same groups are important as were mentioned for density-driven convection initiation in Sec. 1.3.1. However, in this case the density effects are negligible ($Ra \simeq 0$), and the Marangoni number is the important group.

Clark and King (1970) used a rectangular channel device to evaporate four solutes (see Appendix A) from n-tridecane into nitrogen, both streams moving in horizontal laminar flow. The onset of cellular motion was recognized by an increase in the liquid phase mass transfer coefficient, and could be described by a unique value of the time-dependent Marangoni number (= 4500) for each solute.

Blair and Quinn (1969) correlated instabilities in a mass transfer system with the relation ($\Delta P \cdot t_c^{1/2}$ = constant), with a similar technique to that described in Sec. 1.3.2. They found that surface-active agents added to the solvent changed the relationship to $\Delta P t_c^{3/2}$ = constant.* Since the change in surface tension and in density in these experiments was linear with ΔP, they verified the Marangoni relationship $\Delta\sigma t_c^{1/2}$ = constant and the Rayleigh relationship $\Delta\rho t_c^{3/2}$ = constant in these different experiments. Rough calculations indicated that the critical Marangoni number was about 3100 (see Appendix A).

Mayr et al. (1971) carried out desorption in a short, vertical wetted-wall column with solutes acetone, ethyl ether, and triethylamine desorbing from an aqueous solution into a cocurrent nitrogen stream. Each

*The Marangoni number (M_t) for this experiment is:

$$M_t = \frac{\Delta\sigma\, t^{1/2}}{\mu\mathscr{D}^{1/2}}$$

The Rayleigh number was described earlier in Sec. 1.3.2.

system showed convection effects, and the critical Marangoni number was reported to decrease as the Biot number decreased.

2.2. Surface-Tension-Driven Flow Produced by Gradients Parallel to the Liquid Surface

Kenny (1968) has reviewed the literature on this topic (101 articles), including the effects of surface tension gradients on the flow of bubbles through a fluid, on cellular motion in evaporating thin pools of liquid, and on the prevention of surface tension-driven flow by surfactants.

Berg and Morig (1969) and Kayser and Berg (1971) have investigated the effect of surface tension gradients at meniscuses in liquid-liquid systems. They observed that, when the surface tension along the interface increased in the direction away from the wall, cellular eddies were larger than if the surface tension decreased away from the wall.

3. Combined Surface Tension and Density Driven Convection Initiation

3.1. Theory

When surface tension and density effects occur together, they can either reinforce or offset each other. Nield (1964) published the first theoretical study of the coupling effect for the case of a linear gradient normal to the liquid surface. The analysis was similar to that of Pearson, but the body forces, which are important for the density-driven convection portion of the analysis, were included. Numerical computation showed that, to an approximation, the normalized Rayleigh number and the normalized Marangoni number were additive.

$$\frac{Ra_H}{Ra_{Ho}} + \frac{M_H}{M_{Ho}} = 1$$

(Ra_{Ho} and M_{Ho} are the values in the absence of the other phenomenon. Ra_H and M_H are the values in the presence of the other phenomenon.)

Extensions of this approach have been published for a parabolic gradient, and the results are similar (Debler and Wolf, 1970).

3.2. Experimental

Berg and Palmer (1971) and Koshmeider (1967) performed similar experiments in partially verifying Nield's theoretical predictions. A liquid with a free surface was heated very slowly from below to ensure a linear temperature gradient. Convection onset was detected when the linearity ceased between the heat flux and the temperature difference across the liquid. The ratio of Rayleigh number to Marangoni number was increased by increasing the liquid depth. The results show some scatter, but approximately follow the predicted relationship.

The treatment of transient profiles for mixed driving forces has not appeared in the literature, from either the experimental or theoretical aspect. However, Davenport and King (1972) observed an apparent effect of stabilizing surface tension effects on an adverse density gradient in analyzing the data of Mahler and Schechter (1970) for the absorption of sulfur dioxide into water. In this case, the critical Rayleigh number was almost doubled by the presence of the stabilizing influence.

4. Goals of the Present Convective Initiation Investigation

4.1. Experimental Goals

There appears to be a need for experimental data to evaluate the predictions of Amplification Theory and possibly expand the concepts presently associated with convection initiation.

The experimental data which it appears necessary to gather include:

(1) Determining the critical Rayleigh number (Ra_t) vs. Prandtl number relationship.

(2) Investigating the effects of vibration. Amplification Theory suggests that the observed results should be dependent on the form of the initial velocity distribution in the fluid.

(3) Examining the difference between convection initiation at a "free" (gas-liquid) and "fixed" (solid-liquid) surface. Present models of both time-dependent and time-independent convection indicate that the higher shear at a fixed surface will increase the critical value of Ra_t as opposed to that for a free surface.

(4) Examining the dependence of Ra_t on the depth of the fluid. As the thickness of the boundary layer approaches the fluid depth, the mechanism of initiation should change. When the fluid depth is much larger than the thickness of the boundary layer, the fluid motion will correspond to a deep-pool mechanism. When the fluid depth and boundary layer thickness are comparable, the fluid motion will correspond to a shallow-pool mechanism.

(5) Examining the dependence of Ra_t on the width of the fluid container. Wave analysis does not take into account the wall discontinuity effects, and experimental determination of the phenomenon in a narrow fluid container appears more straight forward than the numerical approach.

(6) Examining the dependence of convection initiation on the shape of the density profile in the fluid. A step change in surface conditions will produce a different shape of density profile vs. time than will a linear change.

(7) Examining coupling effects of surface tension and density forces as the fluid depth changes from a deep pool to a shallow pool. Evaporation from deep pools of liquid (5 cm or more) has produced convection which is density-driven, as was shown by Foster (1965). However, at small fluid depth (5 mm or less) with gas-liquid interfaces, convective flow produced by evaporation has been attributed to surface tension effects rather than density effects (Berg et al., 1966; Vidal and Acrivos, 1969). As the fluid depth is decreased to fulfill Objective 4, the transition from density-driven flow to surface-tension-driven flow can be investigated.

The experiments investigating density effects alone were carried out by heating a liquid from below in a completely confined container. This arrangement should be free of surface tension effects because of the lack of a free surface. Foster (1969) has shown that this arrangement produces density-driven convection.

Careful experiments with free surfaces can yield results where both surface tension and density forces are present. With the knowledge of how the density-driven convection should behave, derived from the fixed-surface heating experiments, the surface tension effects can be separated and correlated. In this project the free surface experiments were performed by carefully cooling the liquid from above.

The experiments were performed in stationary pools of liquid with heat transfer providing both an adverse density gradient and an adverse surface tension gradient. The temperature fields were established so as to be very nearly one-dimensional in the vertical direction. This was necessary since the theories being assessed picture a one-dimension vertical temperature gradient. Further, gradients along the liquid-gas surface were found to produce undesirable types of surface-tension-driven effects.

Although the results were derived from heat transfer experiments, their applicability to mass transfer will be assumed through the Prandtl number to Schmidt number analogy. Thus heat transfer experiments with fluids of Pr = 1000 will be analogous to mass transfer with Sc = 1000.

One limitation of this experimetnal approach lies in the extension of the results to moving liquids. The experimental correlations are derived from stagnant pool experiments, which is not necessarily the same basis as streams in laminar or turbulent flow. This was illustrated by Burger (1970) who showed in a series of experiments when sulfur dioxide was absorbed into water that liquid phase stirring decreased the onset time. However, the stagnant-pool experiments appear to be the simplest arrangement for study of density and surface tension effects, with the current understanding of the phenomenon.

4.2. Theoretical Goals

Wave analysis has been assumed valid in the treatment of time-dependent boundary layer convection, because it has been successfully

used to describe time-independent convection initiation. Such an assumption necessitates that the velocity distribution in the horizontal plane have its nodal points predetermined in the fluid. It appears inconsistent to see the same fluid providing the initial velocity distribution in the form of waves which are compatible with the mass transfer scale (0.01 cm) and the heat transfer scale (0.1 to 1.0 cm). In the time-independent problem, the density gradient was linear, the only scale was the fluid depth, and the motion had an infinite amount of time (theoretically) to settle into the least energetic convection pattern, which was on the scale of the fluid depth. In the time-dependent problem, the initial "stagnant" pool necessarily has some slow motion within it with dimensions on the scale of the fluid container (Muller and Ibl, 1958; Muller, 1956). It does not appear obvious why this motion should be treated in a wave form. Instead, the initiation mechanism appears to be connected to the process by which this slow, large-scale motion interacts with the buoyancy field to produce localized small-scale motion.

Investigation along these lines appears worthwhile since it should provide deeper insight into the convection initiation mechanism.

III. FIXED SURFACE EXPERIMENTS: APPARATUS AND PROCEDURE

1. Introduction

Heating an enclosed liquid from below provides a situation where density-driven convection should be free from surface tension effects. Using this experimental approach Objectives 1, 2, 3, 4, and 5 outlined in Chapter II, Sec. 4.1 were fulfilled or partially fulfilled. The remaining objectives were fulfilled using the free surface apparatus.

2. Apparatus and Procedure

2.1. Introduction

The method used to detect the onset of convection involved monitoring the temperature of the liquid-solid interface and observing the first deviation from a conduction profile. Figure III-1 shows a typical surface temperature response in these experiments. Foster (1965, 1969) showed that this deviation from the conduction profile corresponded to the first observable motion in the fluid. The conditions at the onset of convection were recorded as surface temperature change (ΔT_c) and time of heating by conduction (t_c). All of the results in this dissertation were derived from responses similar to that shown in Fig. III-1.

The surface temperature increased linearly with time before the onset of convection, and consequently the results are an extension of the work reported by Foster (1969), and Onat and Grigull (1970).

2.2. Fixed Surface Apparatus

The apparatus was designed to produce a one-dimensional temperature profile in the vertical direction in the fluid. This was accomplished by

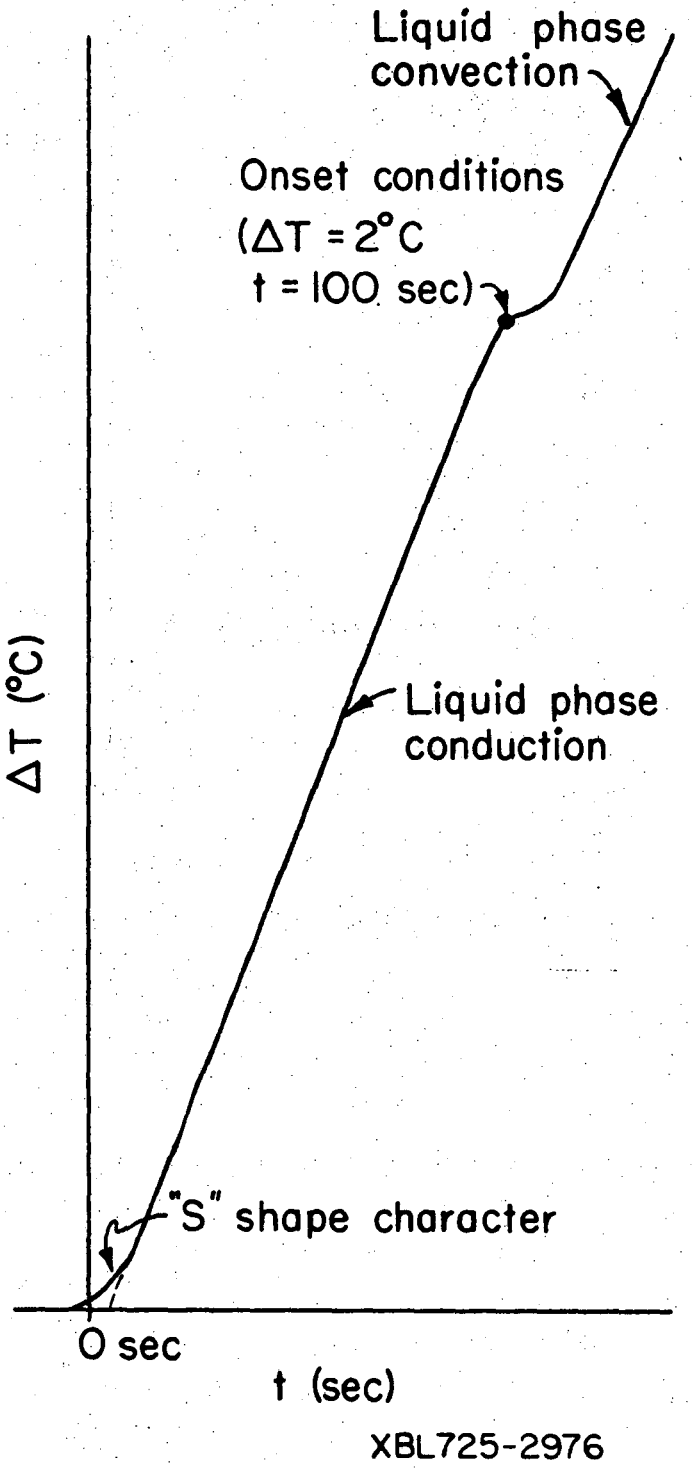

Fig. III-1. Response of the Metal-Liquid Surface Temperature During a Fixed Surface Run.

using a heating surface with a uniform temperature, and selecting the liquid and its container so that both had similar thermal properties.

2.2.1. Design of Apparatus. The apparatus consisted of a Plexiglass cylinder attached to a 750 watt heater with an isothermal heat surface (Fig. III-2). The heating element was a metallic, electrical-resistance-type, annulus plate heater manufactured by Kamlrok, U.S.A., and available from the LBL stockroom. The annulus heater was the only type easily available which did not have severe temperature gradients across the heating surface. This particular model was chosen because it had the largest outside diameter of those available with a small inside diameter. The isothermal heating surface was produced by alternating layers of aluminum and paper (one layer of aluminum 1.5 mm thick, and two layers each of aluminum and paper, each 0.5 mm thick). These were attached to the annulus heating surface, so as to increase the effective thermal conductivity in the horizontal direction compared to that in the vertical direction. This design suppressed the effects of any two-dimensionality in the temperature on the surface of the heater (Fig. III-3).

The heating surface was made horizontal by using a level and adjusting three screws in the leveling table. The screws were placed in a tripod design, and the leveling principle was the same as in a set of weighing scales. The lid was fitted tightly, but was removable in order to clean the interior of the vessel. The rubber stoppers and holes enable the liquid to be made flush with the lid and thus "fix" the upper surface.

The dimensions of the apparatus are given in Fig. III-2.

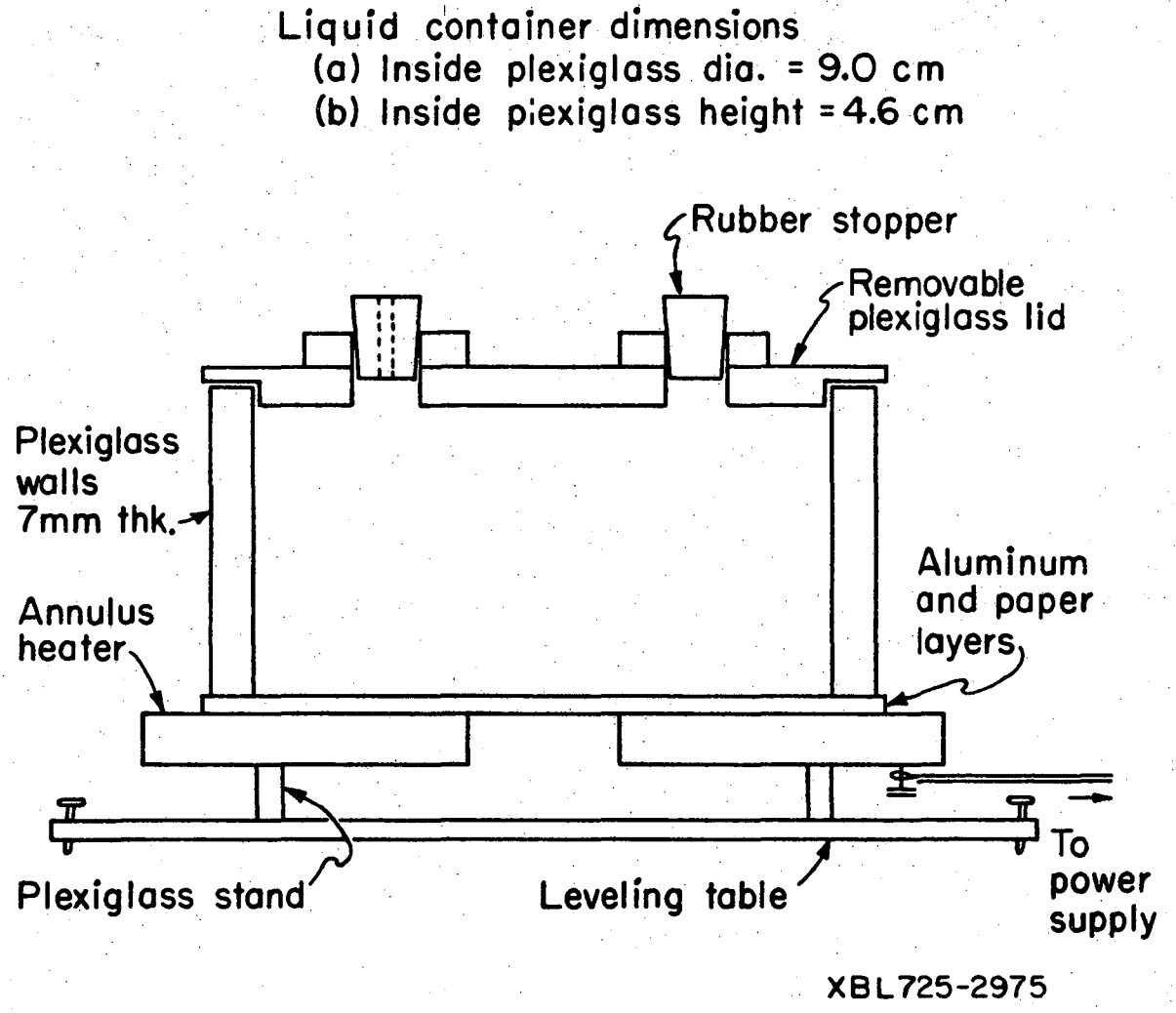

Fig. III-2. Schematic diagram showing design of the Fixed Surface Apparatus.

2.2.2. Isothermal Plate Testing. The temperature profile of the bare plate of the annulus heater (and subsequent surface of the aluminum and paper layers) in both the radial and circumferential directions was found by putting a thermocouple attached to a metal block (1 cm diameter, 1 cm high) at different points across the surface. The radial units were 5 mm apart and the angle directions were at 0°, 90°, 180°. The thermocouple and plate were allowed to come to equilibrium, and then the heater current was switched on. The plate was allowed to cool after a run. The bare heater surface profile and the profiles of the final design are given in Fig. III-3.

2.2.3. Selection of Solid and Liquid: Thermal and Corrosion Matching

2.2.3.1. Thermal Matching of Liquid with Container. A one-dimensional temperature profile necessitates a similar temperature profile in both the liquid and the container. From examination of the thermal conduction equations and boundary conditions, this condition can be obtained only when the thermal diffusivity (α) and the thermal conductivity (k) of both liquid and container are equal. Most organic liquids have values of k in the range 2.7 to 4.2×10^{-4} cal/sec cm°C and $\alpha = 10^{-3}$ cm^2/sec (Reid and Sherwood, 1966). Solids normally have higher values of both properties, but some plastics fall in the liquid range (Appendix D).

2.2.3.2. Corrosion Matching of Solid and Liquid. Care must be taken to choose test liquids which will not dissolve the solid plastic. Many plastics are soluble in ketones, esters, aromatics and chlorinated hydrocarbons.

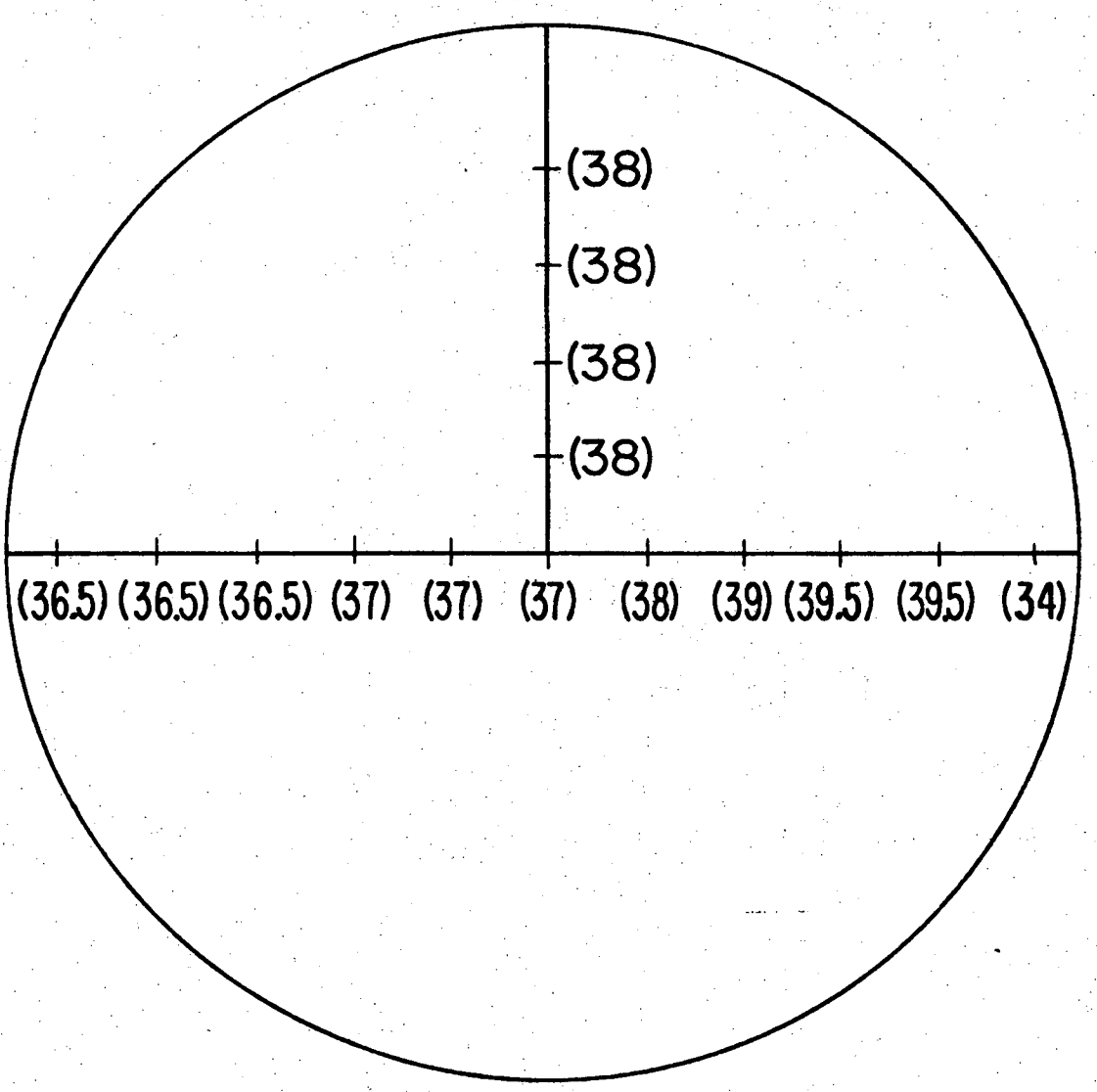

Fig. III-3. Temperature Distribution of the Heated surface in the Fixed Surface Apparatus. The measured temperatures (arbitrary units) after 12 seconds of heating are shown in brackets.

2.2.3.3. Choice of Solid. Plexiglass was chosen because it has thermal properties in the liquid range and it is not chemically attacked by some organics. It was readily available, and its transparency was useful for observing large-scale convection effects.

2.2.3.4. Evaluation of Plexiglass Thermal Properties. Many organics with varying thermal properties were cooled in the final design container (Fig. III-2), and their surface temperature responses were compared with that of Plexiglass. The tests showed that the plastic thermal conductivity was about 3.7×10^{-4} cal/cm sec °C and the thermal diffusivity about 10^{-3} cm^2/sec. These values are in the range quoted in the Plastics Encyclopedia (1970).

2.2.3.5. Choice of Liquids. Using the above corrosion and thermal matching criteria, the following test liquids were chosen (see Appendix D for values of physical properties).

Liquid	Prandtl Number
Methanol	7.4
n-Decane	13.7
n-Butanol	43
n-Octanol	108
Silicone Oil, 50 cs.	465
Silicone Oil, 100 cs.	890
Silicone Oil, 1000 cs.	8500

2.2.4. Surface Temperature Measurement. The surface temperature of the heated surface was measured by placing a Copper-Constantan thermocouple

on the surface of the isothermal plate, approximately in the center. It was insulated from the metal plate by a thin sheet of mica. The mica had been glued to the metal surface with Kodak 910 adhesive and sand-papered down until only a thin layer of mica remained. The 0.001 inch diameter thermocouple junction was then attached to the mica with the above adhesive.

2.3. Variation of Depth of Liquid

The apparatus as shown in Fig. III-2 was used to conduct the deep pool experiments. The shallow pool experiments were carried out using a smaller diameter Plexiglass annulus, temporarily placed on the apparatus, but not glued to any part of the equipment. A large aluminum cylinder, 50 mm high and with a diameter slightly less than the permanent Plexiglass annulus, was placed on top of the temporarily placed annulus (Fig. III-4).

In the shallow depth experiments, it was realized that the temperature profile would be affected by the boundary conditions at the upper surface. If this surface was adiabatic, the temperature at the upper boundary surface would change with time, and more variables would have to be measured and correlated than if the upper surface temperature was kept at a constant value. Although the adiabatic condition is more similar to most ultimate practical situations, the constant temperature condition was chosen because of the potential of an easier correlation where no guidelines existed theoretically for small depth convection. Figure III-5 shows the extent to which this temperature was kept constant.

The liquid was poured into the apparatus so that the liquid just covered the smaller annulus. The metal block was lowered so that the

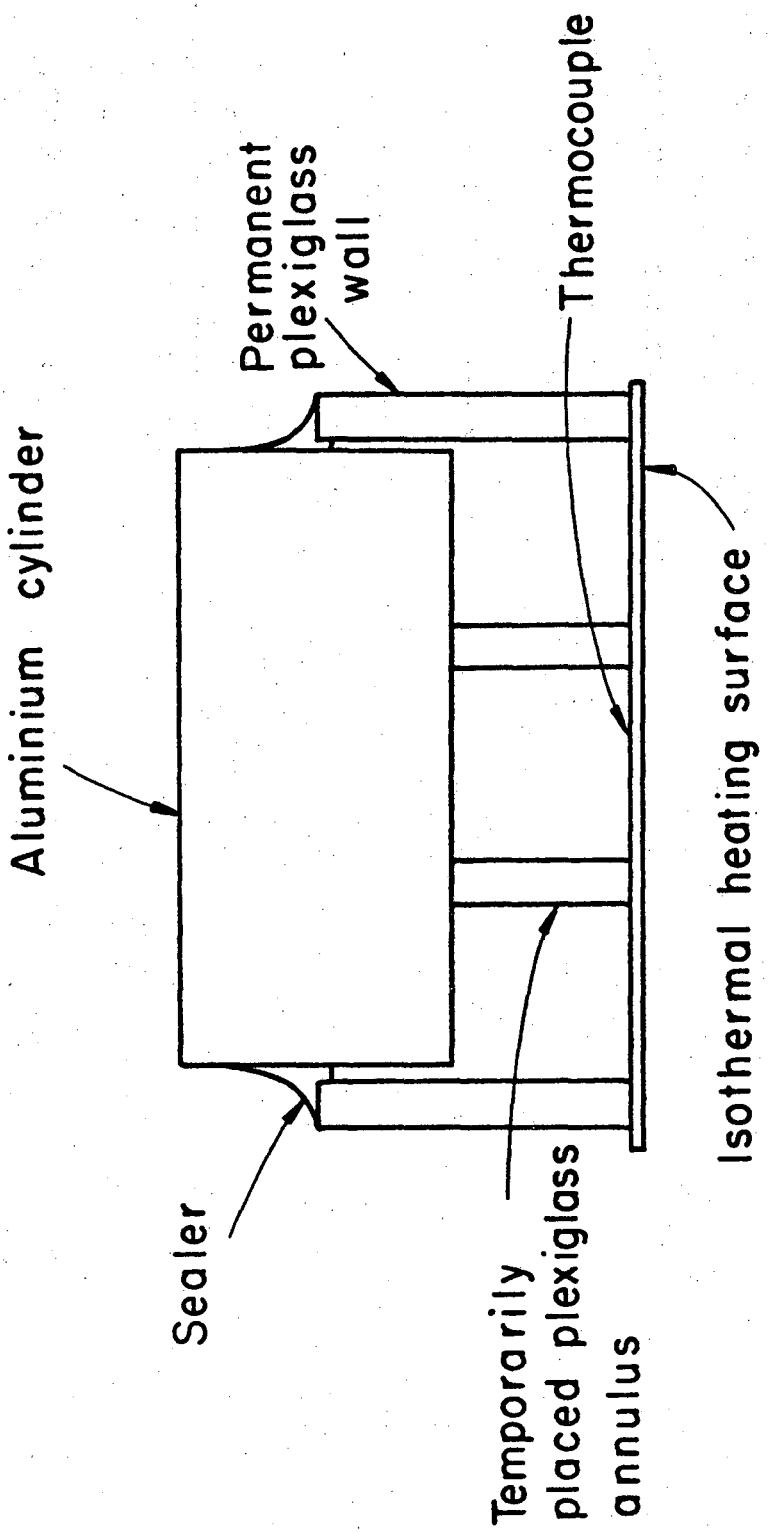

Fig. III-4. Adaption of Fixed Surface Apparatus to vary Fluid Depth and Width.

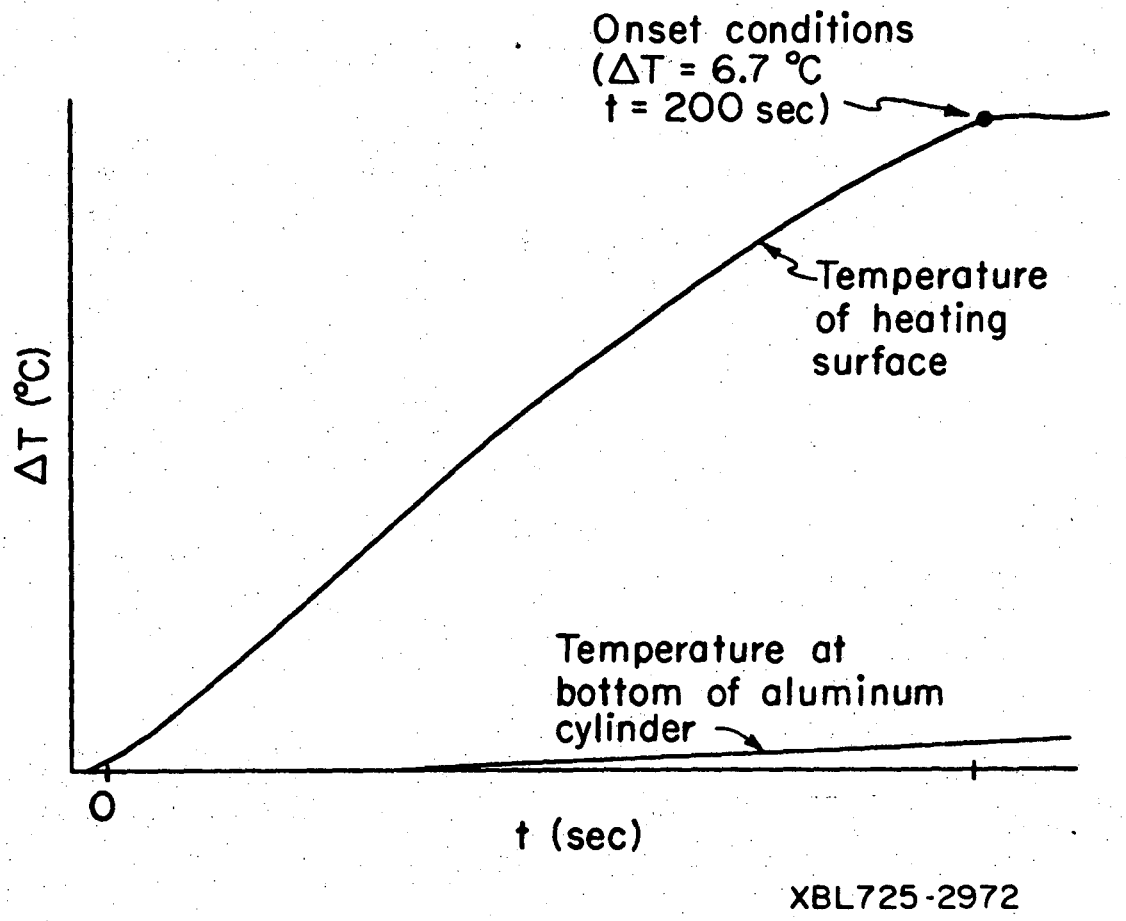

Fig. III-5. Temperature Response During a Shallow Pool Run (Fluid depth of 2.06 mm) showing the Approximate Constant Temperature of the Upper Liquid Surface (or bottom surface of Aluminum).

metal-liquid surface was observed to contain no air bubbles. The liquid was allowed to rise between the metal walls and the permanent Plexiglass walls. A putty was then used to seal the top of the metal with the permanent wall. A thermocouple was attached to the bottom of the metal cylinder to evaluate how constant the temperature of the upper liquid surface remained.

The heights of the temporary annuli were 36.5 mm, 11.9 mm, 6.2 mm, 3.48 mm, and 2.06 mm, each with an inside diameter of 36.5 mm and wall thickness of 7 mm.

2.4. Variation of Wall Diameter

The diameter of the temporarily placed annulus could be varied so as to estimate the influence of the wall spacing on convection initiation. Because of the flexibility of the fixed-surface design over the free-surface apparatus, the effects of the walls could be more easily tested in the fixed-surface apparatus. The three diameters used were 90 mm (height 44 mm), 69 mm (height 11.9 mm), 36.5 mm (heights listed in Sec. 2.3.).

Holes with diameters of 5.7 mm and 8.7 mm were drilled through a Plexiglass cube (side 25 mm) and were used to find extreme wall effects.

2.5. Limitations of Apparatus

One obvious limitation in this apparatus is the narrow range of liquid type which can be used and not be corrosive to the Plexiglass. The lowest Prandtl number that can be obtained with non-corrosive and thermally matching liquids is 6.6 (methanol). Acetone, which is corrosive, has a Prandtl number of about 3 at room temperature, and air and liquid metals, which are not thermally suitable, have Prandtl numbers in the range 0.01 to 0.7.

Another limitation arises from the difference in thermal expansion coefficients between the Plexiglass and the metal surface to which it is glued. As the temperature is increased the thermal stresses at the Plexiglass-metal bond increase, so that leaks can rapidly occur. The higher temperatures were necessary only for the very viscous liquids.

The time duration for the experimental runs was limited from about 40 seconds to 250 seconds. The attachment provided the isothermal heating with a substantial heat transfer resistance which added to the time delay of the heated surface response. This was manifested by a curved gradient during the initial stages of heating (Fig. III-1). The effective starting time has to be estimated, so as to allow for heating which does not occur under the steady temperature gradient.

The time is limited to less than 250 seconds because the heater response becomes curved at longer times. Even when adjustments were made to the heating rate during a run, the linearity of the response became difficult to control beyond this point. The difficulty associated with observing convection onset at long conduction times is discussed in Chapter IV, Sec. 4.

3. Auxiliary Equipment

3.1. Temperature Recording

The temperatures for both the free-surface and the fixed-surface experiments were monitored by Copper-Constantan thermocouples (0.001 inch diameter), purchased commercially from Omega Engineering Inc., Stamford, Connecticut. The response was recorded on a Leeds-Northrup recorder

especially adapted to measure in the ranges 50 μv, 100 μv, 200 μv, 500 μv, 1 mv, 2 mv. Two recorders were available, with speeds of 9 inches per hour, 60 inches per hour, and 90 inches per hour.

The thermocouple calibration is shown in Fig. III-6. It was taken by fastening a thermocouple to a bulb thermometer with the junction attached to the bulb, and stirring water at various temperatures with the thermometer. The difference in temperature between this thermometer reading and the thermocouple reference was plotted against the thermocouple e.m.f. registered on a temperature recorder mentioned above.

Some experiments were run with critical temperatures as low as 0.1 °C. Since the thermocouple e.m.f. is proportional to the difference between the junction and the reference temperature, greatest sensitivity is obtained when the temperature change of the junction is proportional to the magnitude of the e.m.f. produced. This procedure is arranged by keeping the reference temperature at the bulk (and surface) fluid temperature, which is the room temperature in these experiments. In this manner, small temperature changes can be read with accuracy. The procedure permitted use of the 50 μv scale, rather than the 1 mv scale which would have been necessary had the ice-water reference been used. The reference temperature might have varied by one Centigrade degree over a day, but this slow rate did not show during runs. Further, the experiment required only the difference between the surface and bulk temperatures of the test liquid, not the absolute values, so that precise knowledge of the reference temperature was not critical.

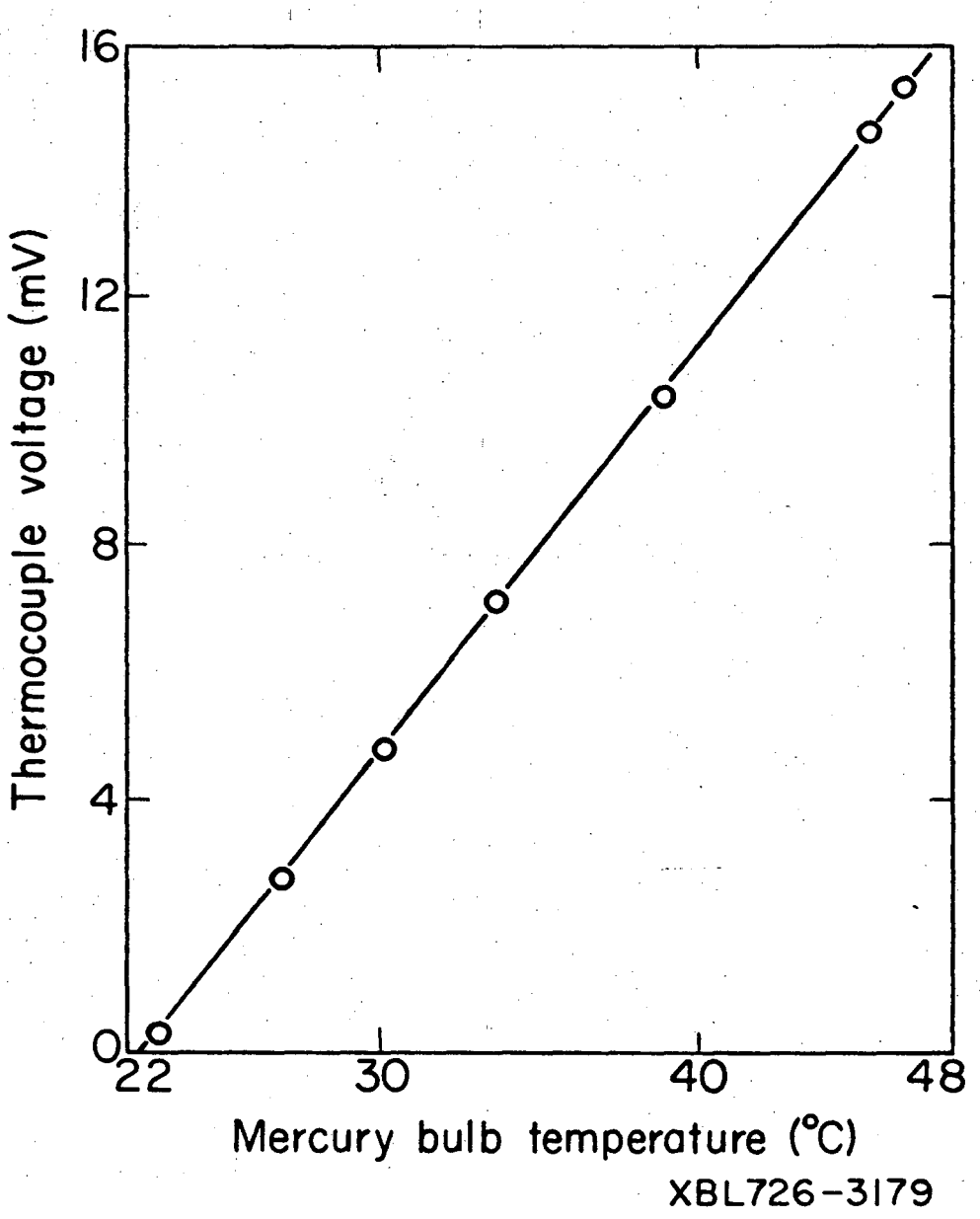

Fig. III-6. The Copper-Constantan Thermocouple Calibration. Reference junction was kept at 22°C. Slope is 1.6°C/mV.

3.2. Vibration Equipment

The vibration generating equipment was designed to provide a forced vibration to the heating apparatus and a contained liquid which had either a fixed or free upper surface. A schematic diagram of the apparatus of the final design is shown in Fig. III-7.

The major component of this system is a vibration exciter (MB model EA1250) with an electronic power amplifier (MB model EA 1500 PM), both available commercially from MB Electronics, New Haven, Connecticut. The vibration exciter was designed on the same principle as a loud speaker. An alternating electric field interacts with a permanent magnetic field to produce an oscillating force on a metallic cone.

An accelerometer was attached to the metal cone. It produced a voltage directly proportional to the movement of the cylinder cone. The voltage was measured on an oscilloscope. For the machine used in these experiments the accelerometer was calibrated by

$$11.2 \text{ mV} = 0.0512 \, f^2 \, (\text{D.A.})$$

where

mV = voltage output in millivolts

f = frequency of vibration in c.p.s.

D.A. = displacement of cone, peak to peak - inches.

The accelerometer was supplied with the other two components from MB Electronics.

The function generator was a Hewlett Packard Company 202 Clow Frequency Oscillator with a range of 1 - 10^5 c.p.s. and a variable

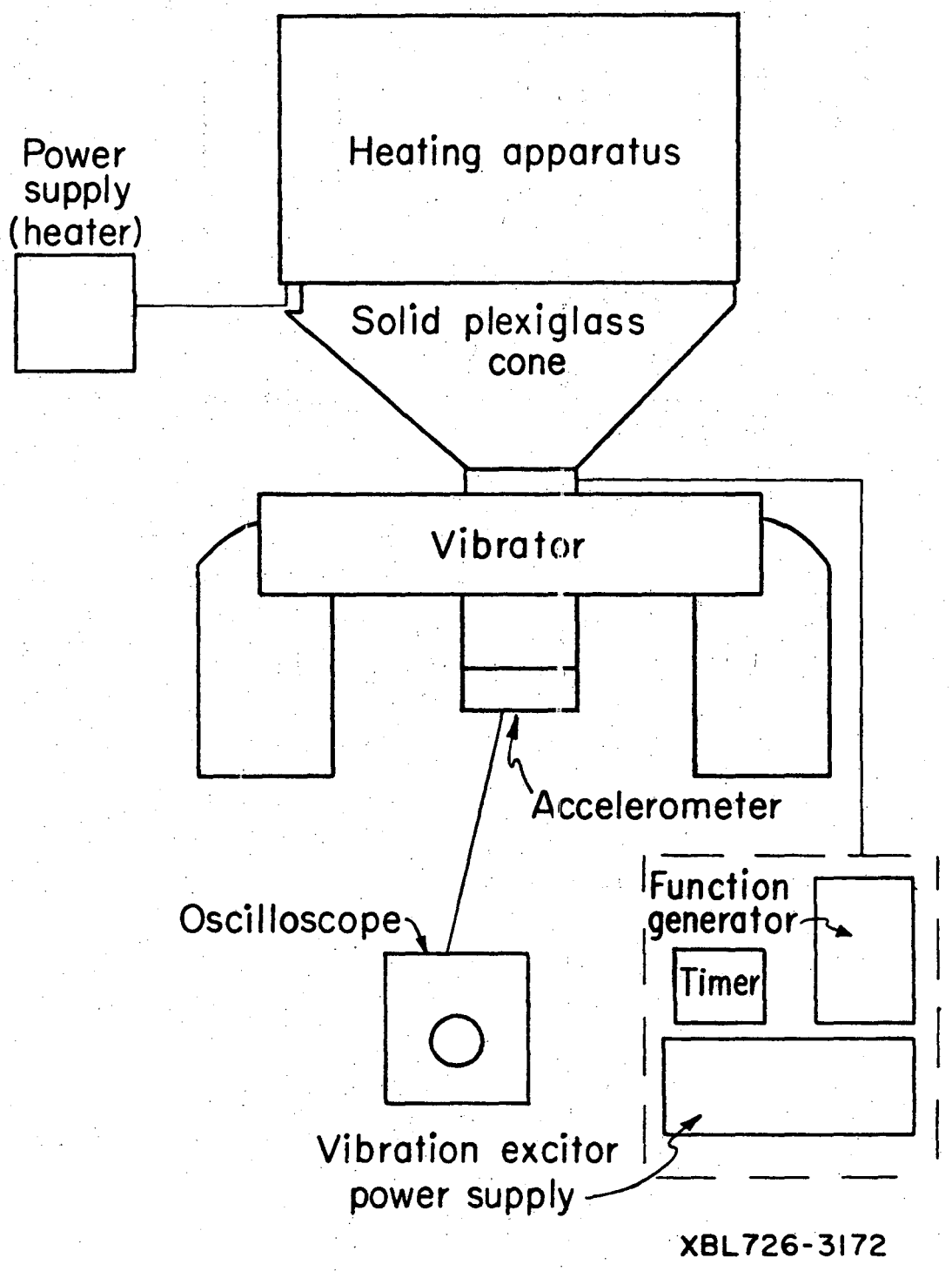

Fig. III-7. Schematic diagram showing Fixed Surface Apparatus attached to the vibration equipment.

amplitude of 1 - 100%. The instrument could be considered as a 20 volt generator with a 600 ohm internal impedance.

A timer was used to limit the duration of a run. This instrument would break the circuit after a specified time.

The apparatus was allowed to run for about one minute before the heating began in each run. This was to ensure steady state in the initial motion, which was verified by looking at the oscilloscope.

3.3. Experimental Technique for the Vibration Experiments

Two different wave forms in the liquid were produced by having either a fixed or free upper surface. Amplification Theory suggests that growth time will vary with different vibration forms.

Only two liquids were used--methanol, a non-viscous liquid, and n-octanol, a viscous liquid. It was anticipated that the vibration wave form produced in the liquid by environmental vibration would be dependent to some extent upon the viscosity of the liquid. For a given environmental vibration wave form, a viscous liquid might not have as large a vibration amplitude as a non-viscous liquid. Thus the amplification factor required might be expected to increase with increasing viscosity.

A parameter which might be important in describing the results is the power input to the liquid. If the liquid is assumed to be in phase with, and have the same amplitude as the vibrator, and the vibration motion is assumed to be sinusoidal, then the following analysis is valid.

Power input is the change in energy per unit time. The change in energy is associated with the difference in kinetic energy at zero

displacement (kinetic energy is $\frac{1}{2m} A^2w^2$) and at maximum displacement (zero kinetic energy). Changes in potential energy are too small to be considered. The time for this change in kinetic energy is $\frac{\pi}{2w}$. Hence, the power input is $\frac{mA^2w^3}{\pi}$ where

m = mass of system

A = amplitude of vibration

w = frequency of vibration

For convenience, the power input in these experiments was taken as A^2w^3, which is proportional to the power input per unit mass.

The limitations of the apparatus are as follows:

1) When the power input to the liquid was high enough, the liquid motion appeared to generate heating within the liquid. This invalidated the temperature field which we intended to work with, and thus did not permit comparison with results where internal heating was negligible. It is unlikely that common environmental vibration would be strong enough to produce internal heating. However, this factor limited the amplitude that could be reached at a particular frequency.

2) In the experiments with a free upper surface, the liquid could become wavy or turbulent at high amplitudes. This motion would destroy the heat flow by conduction and thus invalidate the experiment. Thus vibration amplitudes were further limited with the free upper surface experiments.

3) The vibration frequency was limited to the range $10^1 - 10^4$ c.p.s. by design. Below 10 c.p.s., the amplitude could not be registered by the accelerometer. However, conditions which would probably be met in practice

were covered in this range of frequency and amplitude. The range of operation is shown in Fig. III-8.

4) The accelerometer was not sensitive enough to measure the vibrations of the "vibration-free" table described in Sec. 4. Further, the accelerometer was not sensitive enough to measure below a certain amplitude for each frequency. This limited the lower amplitudes that could be obtained at frequencies below about 2000 c.p.s. and hence prevented the experiment from being carried out with constant amplitude over a wide range of frequencies.

4. Vibration-Free Table

A site was recognized as having a constant vibration frequency and amplitude was located at Lawrence Berkeley Laboratory, Building 70, Room 136. The experiments were carried out on a table which was 20 feet by 2 feet, with two layers of concrete 6 inches thick separated by rubber cushions 2 inches thick. The table rested on three concrete supports which went through the building foundation to rest on rock. This table had been in use for some very precise laser experiments. The table was located in a special soundproof room and was isolated during the experiments. The recorders and other electronic equipment were positioned outside the room to reduce the vibration level in the room.

5. Performance of Apparatus

In this equipment, only conduction and initiation of convection are strictly in a one-dimensional temperature field. Once convection has

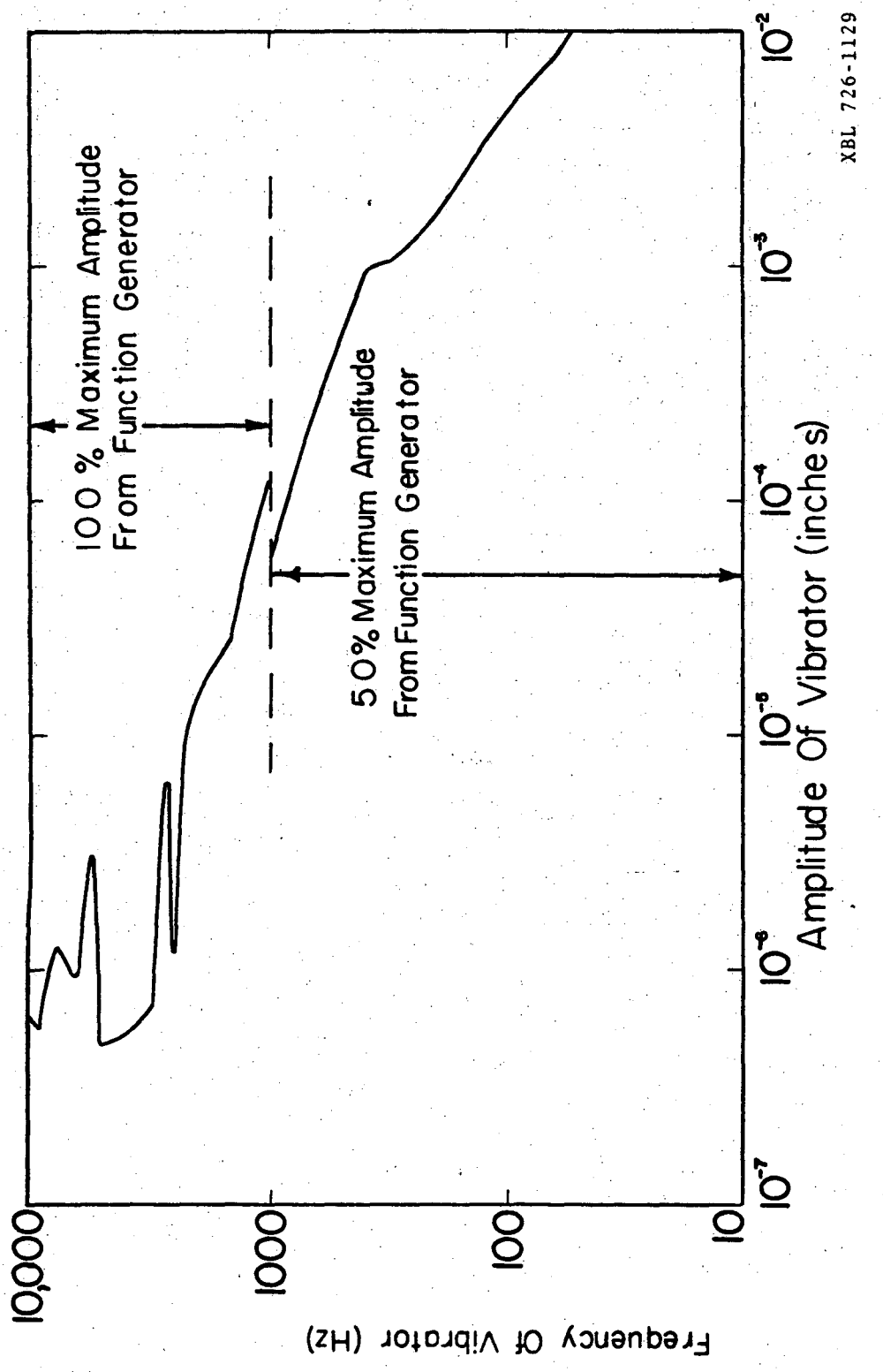

Fig. III-8. Operating Characteristics of the Vibrator - MB Electronics model E-A-1250.

increased the liquid temperature, and the solid temperature continues to increase by conduction, a two-dimensional temperature field will result. The heat transfer coefficient in the liquid will be greater than that in the solid, and so the two-dimensional character will persist. This means that any transition or steady state responses seen in this equipment will be a result of a two-dimensional field. However, the response shortly after convection begins should yield meaningful data on the transition region. Steady-state natural convection in a one-dimensional potential gradient field should best be studied in mass transfer systems where the wall does not introduce two-dimensional effects.

IV. FREE SURFACE EXPERIMENTS: PROCEDURE AND APPARATUS

1. Objectives

The aim of the experiments described in this chapter is to investigate convection adjacent to a free surface and to try to establish further characteristics of density-driven and surface-tension-driven flow, including

a) identification of both types of motion,

b) separation of the effects, so as to study them individually,

c) understanding coupling effects between density and surface tension forces,

d) identification of conditions of instability.

2. Selection of Procedure

Previous experimentation has been concerned with evaporation from quiescent pools (Spangenberg and Rowland, 1961; Foster, 1965; Vidal and Acrivos, 1968). That experimental system is inherently difficult to control, as well as having a limited range of surface heat flux. These limitations were later overcome using mass transfer systems, but the experiments were limited to high values of Sc (Blair and Quinn, 1969; Mahler and Schechter, 1970).

In order to extend the work of these latter workers, it is the aim of the present work to investigate

a) ranges of Sc and Pr lower than 600 (heat transfer in organic liquids),

b) a wide range of surface temperature functions,

c) the effect of depth on the motion.

Heat transfer experiments are relatively simple and offer a wide range of Pr, especially in the region where the theoretically predicted asymptotes for Ra_t versus small Pr and large Pr meet (Foster, 1968). Further, the thermal properties of common liquids are well known and easily available. Heat transfer experiments can be performed by:

a) evaporation from quiescent pools

b) evaporation from pools controlled by a draft of air blown over the liquid surface

c) a heat sink placed above the liquid, with no intentional evaporation.

Because method (a) involves quiescent pools, the initial velocity field in the liquid (produced by building vibrations, etc.) should be maintained uniform during a series of experimental runs; this requires that the environmental vibrations be steady. The vibrations should also be minimized to reduce surface deformation, which might enhance surface-tension-driven motion (Berg, 1964 and Scriven and Sternling, 1964) in an uncontrolled manner. This method, however, has the disadvantage of providing a narrow range of heat flux at the liquid surface. Since the cooling is generated by evaporation, which in turn is proportional to the difference in humidity between the bulk gas and the liquid interface, a system to control the bulk humidity is needed. There is also difficulty in producing a sharp change in conditions at time $t = 0$. If the lid is lifted from a container with the liquid and gas phases in equilibrium, and if the gas phase will then be at room conditions, the experiment is limited to the one driving force. Another disadvantage, discussed in Appendix B, is that evaporation causes two-dimensional effects near the

container walls. This is the result of a cooling liquid surface lying adjacent to a non-cooling container surface, thus producing a temperature gradient along the liquid surface. This effect, combined with the meniscus producing a two-dimensional geometry, can lead to complicating types of surface-tension-driven motion (Kayser and Berg, 1971).

Method (b) has the advantage of producing a wide range of heat fluxes at the surface from varying the draft velocity, and causing a sharp change in conditions at time t = 0 by switching the draft on or off. This method has the disadvantage of not being able to reproduce the same liquid velocity field for varying draft velocity, and this violates the conditions for a constant amplification factor. Consequently, testing of the Amplification Theory would be very difficult using this method.

Method (c) has the advantages of (a) and (b) and none of the disadvantages, provided the equipment can be designed to produce a one-dimensional temperature field. The stagnant pool has a constant-vibration field when placed in a steady environment. Both the solid container surface and liquid surface will have the same temperature profile, provided the cooler has a one-dimensional character and the solid and liquid have similar thermal properties. This method was therefore chosen as the basis of free surface experimentation.

3. Apparatus and Procedure

3.1. Introduction

The method used to detect the point of instability involved monitoring the temperature of the gas-liquid and surface observing when it first deviates from a conduction profile.

The apparatus was designed so that the whole liquid surface was isothermal, by moving the effects far from the liquid surface. The one-dimensional character in the apparatus was based on the existence of three separate thermal regions--(1) cooler, (2) air space and cooler support, and (3) the liquid and its container--each section having planar parallel boundaries and uniform thermal properties (refer to Fig. IV-1). The development of the apparatus design is traced in Appendix B.

3.2. The Liquid and Its Container

3.2.1. Planar Geometry of the Liquid Surface. The liquid and container surfaces must be on the same plane for two reasons:

(1) a difference in level will mean a difference in gap space above the liquid and solid. If the liquid surface is below the solid surface, the resistance to heat transfer will be greater through the gap space above the liquid, and this will result in the solid surface heating up faster.

(2) a meniscus provides a two-dimensional geometry. The result of either of these effects is an undesirable two-dimensional temperature profile along the liquid surface.

The remedy was found by designing the container surface flat and with a sharp, right-angled corner at the edge adjacent to the liquid. The liquid surface could then be brought to the level of the container walls without bursting the edges, provided the container surface was horizontally leveled. The risk of liquid bursting the edges was further minimized by securing the container firmly.

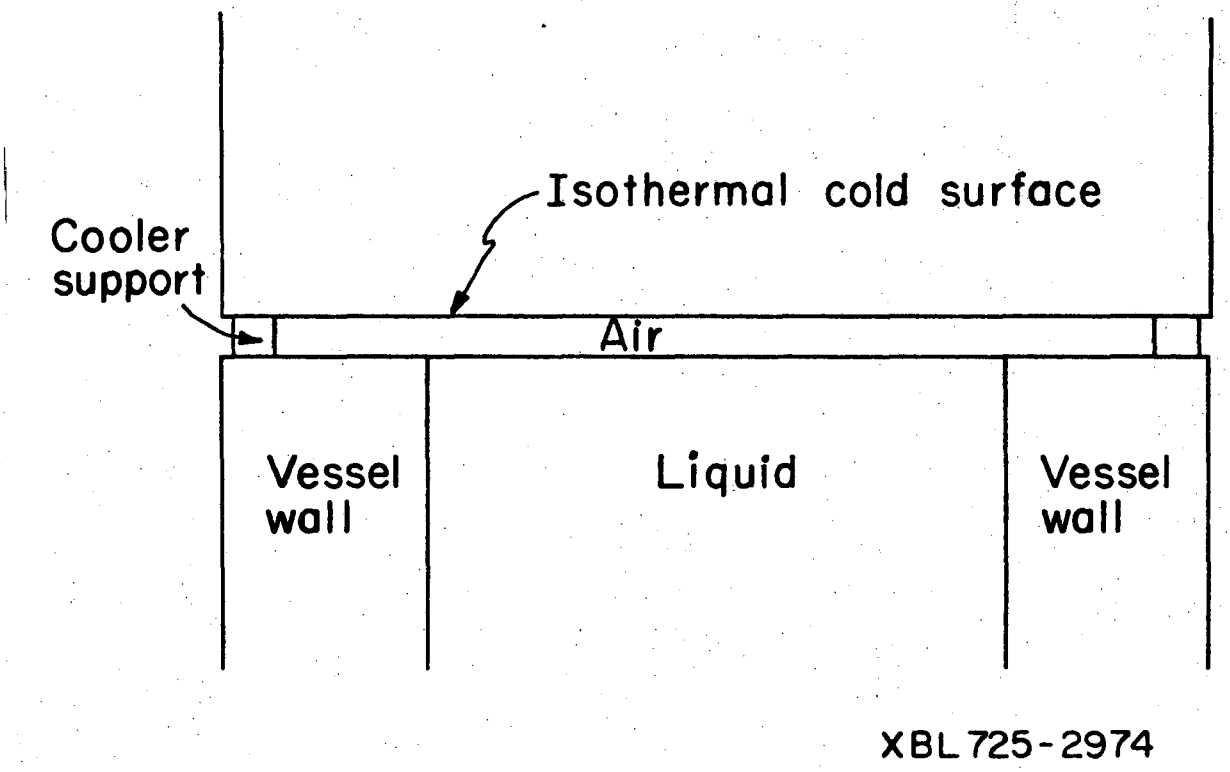

Fig. IV-1. Free Surface Apparatus Strategy.

3.2.2. Selection of Solid and Liquid. The liquids and the Plexiglass as chosen for the fixed surface experiments on the basis of corrosion and thermal compatibility (Chapter III, Sec. 2.2.3.5.) were used in the free surface experiments, except for methanol. This exclusion arose because liquids in the free surface experiments had to be non-volatile for several reasons. First, liquid height control is important, especially in maintaining the planar liquid and solid surface. Secondly, an evaporating liquid will condense on the cooling surface which is directly above the liquid and alter the planar surface of the cooler, as well as condensing on the foam cooler supports (see below) and establishing a short circuit for heat transfer through the air gap region.

n-Undecane (Pr - 17) was included in the list of test liquids to substantiate findings at low Prandtl number.

3.2.3. Liquid Container Design. Containers were built to suit both the deep pool and the shallow pool experiments. The width (36.5 mm) in each design was constant and limited by the size of the thermo-electric cooler.

3.2.3.1. Deep Pool Design (Fig. IV-2). The vessel had an inside width and depth of 36.5 mm, and a wall thickness of 7 mm. The ends were perpendicular to the walls, and a copper plate was glued to the lower end. A thick slab of cardboard was glued to the outside wall, about halfway up the wall. Foam insulation was fashioned to fit around the vessel and sandwich the cardboard. The insulated vessel was held to a leveling table by elastic bands which gave rigidity to the vessel.

The top surface of the vessel was made horizontal by placing a level on it and adjusting the leveling table described in Chapter III, Sec. 2.2.

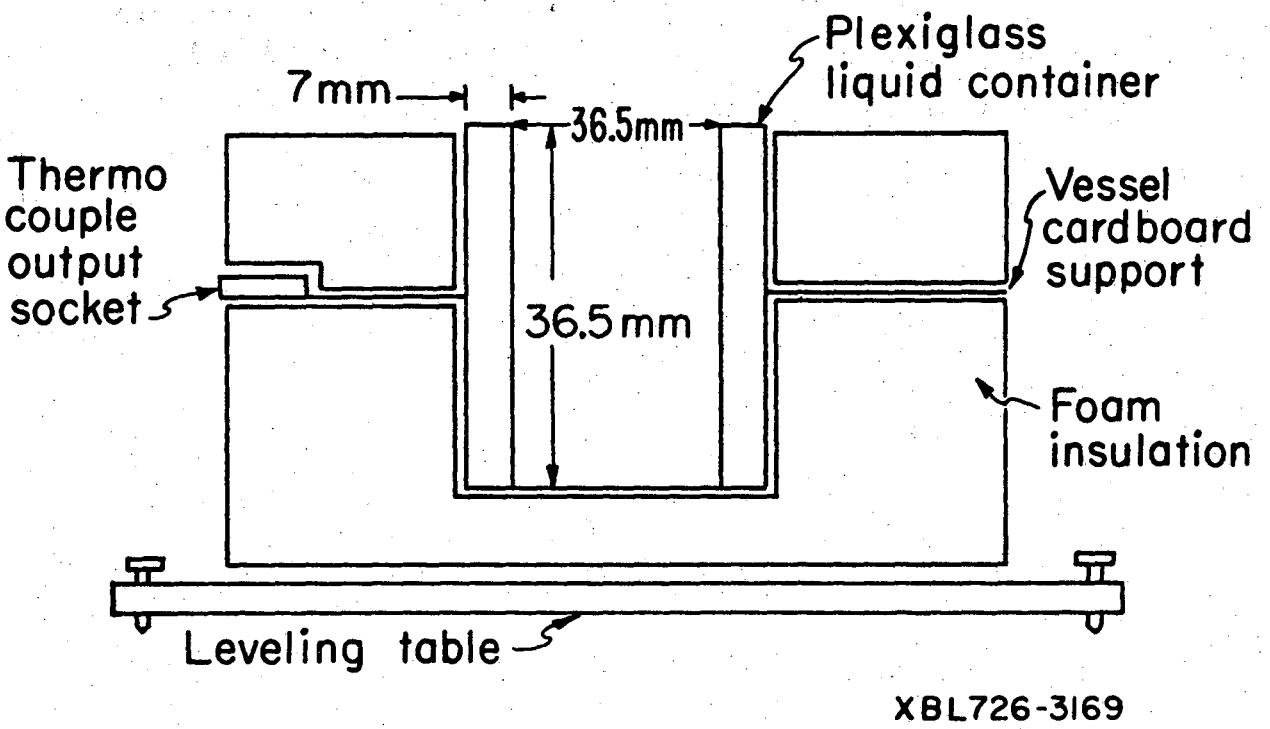

Fig. IV-2. Design and Dimensions of Free Surface Deep Pool Apparatus.

3.2.3.2. Shallow Pool Design (Fig. IV-3). The lower boundary of the liquid was held at a constant temperature by a block of copper which was glued to the bottom surface of the container. This followed the procedure adopted in Chapter III, Sec. 2.3. The copper block was glued to a Plexiglass stand, and foam insulation surrounded the vessel and copper. Several models were constructed, each having a different Plexiglass height.

The apparatus was leveled in the same way as in the deep pool apparatus.

3.2.3.3. Thermocouples. The thermocouple junctions should be placed on the surface, and the thermocouple leads should lie as close to the surface as possible, so as to eliminate a temperature gradient in the wires near the thermocouple junction.

One way of positioning the thermocouple wires and junction to achieve this condition would be to lay taut wires across the Plexiglass, so that the wires are at the surface. The disadvantage of this method was found to be that the liquid creeps along the wire and wets the top of the Plexiglass.

An alternate approach, which was the one utilized in the present work, is that illustrated in Fig. IV-4. The glass leads support the thermocouple, and, because they are not glued to the Plexiglass, these leads can be adjusted so that the tips are in line with the plane of the Plexiglass, these leads can be adjusted so that the tips are in line with the plane of the Plexiglass surface. This design overcomes the problem of the liquid wetting the Plexiglass surface, but it does introduce a hydrodynamic hindrance and an inhomogeneity of the thermal properties in

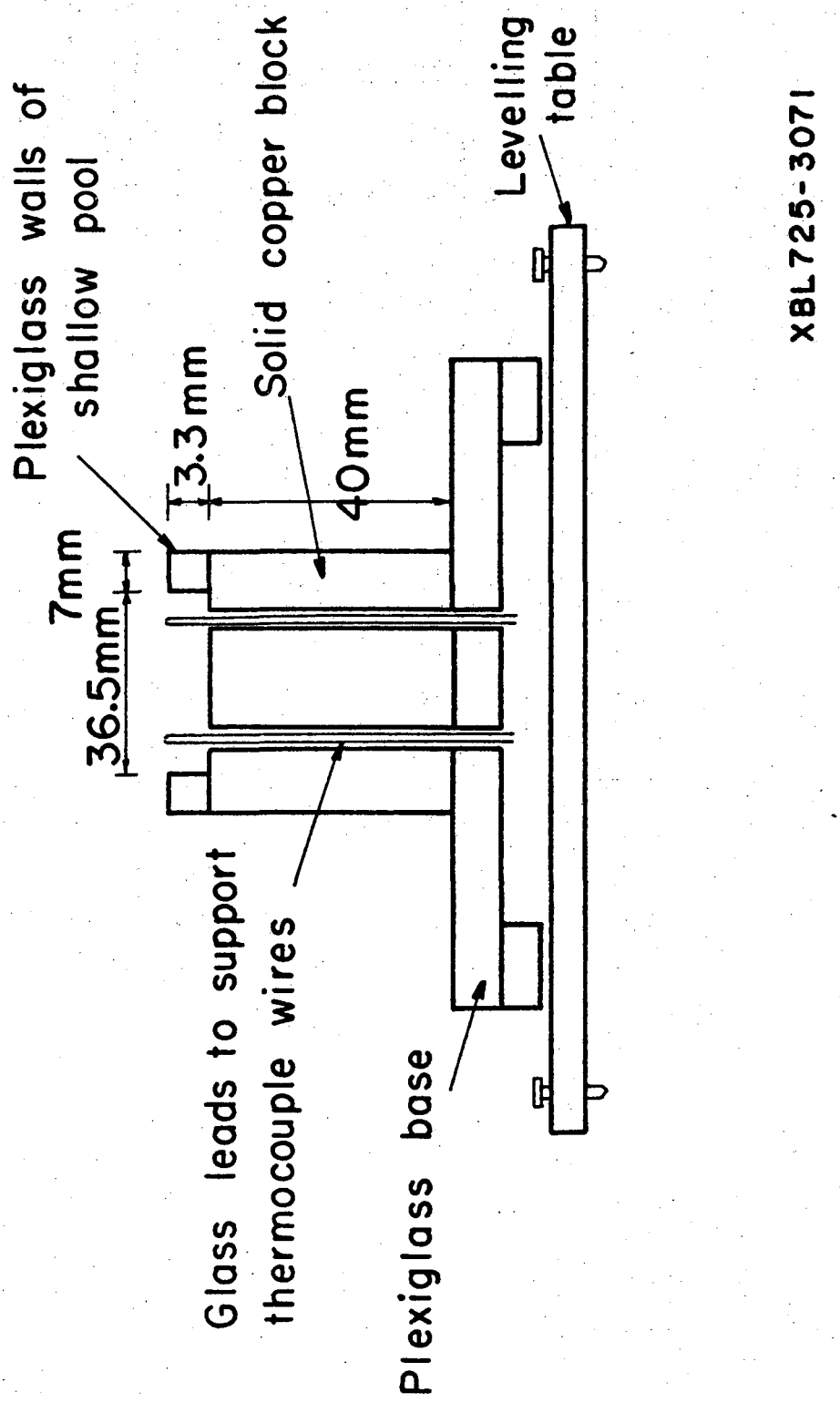

Fig. IV-3. Design and Dimensions of Free Surface, Shallow Pool Apparatus.

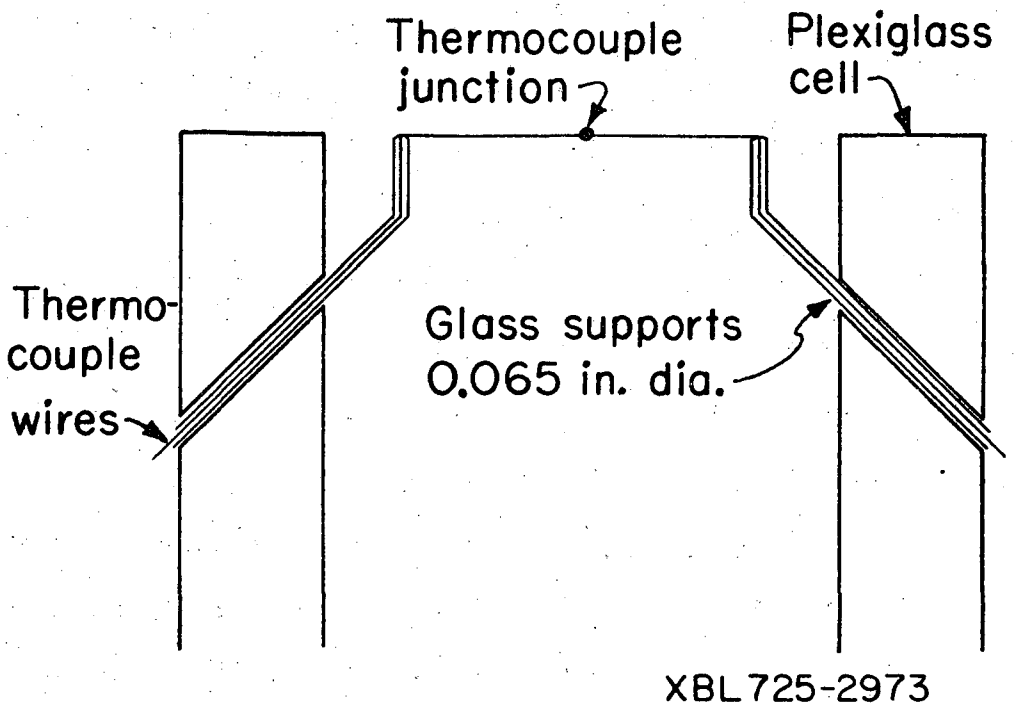

Fig. IV-4. Thermocouple Suspension in the Free Surface, Deep Pool Apparatus.

the liquid, because glass and organic liquids have dissimilar thermal properties.

Because the walls of the shallow pool do not have sufficient height of Plexiglass through which to introduce the thermocouple leads, an alternate design had to be found for the shallow pool equipment. The most convenient method was to put the glass leads through the metal block, and adjust the height of the thermocouple by adjusting the glass leads, as shown in Fig. IV-3.

Copper-Constantan thermocouples, as described in Chapter III, Sec. 3.1., were used in the apparatus.

3.2.3.4. Liquid Level Measurement. Because the thermocouples were designed to be along the surface of the liquid, the thermocouples were positioned carefully by manipulating the glass leads and the tension in the wire so that the wire along the surface was in the same plane as the surface of the container walls. The liquid height was then raised until the thermocouple was in the plane of the liquid surface. This method worked well.

3.3. Design of Cooler Support

In the overall design strategy (refer Fig. IV-1), this section was a composite of support and air, sandwiched between two planar boundaries. Provided the support could be made so that it had an even thickness, the only matching to be investigated concerned the thermal properties of the air and the support.

3.3.1. Material Selection. Because air at room temperature is so much less dense, it has thermal properties different from most solids. The

only materials which have approximately the same values of thermal properties as air are the very porous (and therefore nearly all air) foamed solids. Polystyrene foam, being among the most porous and yet having the mechanical strength to act as a support, was selected.

3.3.2. Dimension Selection. In the design of a cooler which was parallel and opposite to a surface of solid and liquid, edge effects were to be expected, similar to edge effects in a parallel-plate capacitor. The design strategy demanded that these edge effects were to be far enough away from the liquid portion of the surface so that the liquid could remain in the one-dimensional heat transfer region.

Some experiments were performed with a cooler resting on top of a Plexiglass cylinder. The temperature response on the cylinder surface was measured. Results indicated that two-dimensional effects were only significant in the region between the wall and 1.5 times the height away from the wall. Best results were obtained when the cooler diameter was about the same size or slightly larger than the cylinder diameter. The thickness of the wall of the Plexiglass vessel which was finally used was 7 mm, and the height of the foam support was 1.5 - 2 mm, which would isolate the two-dimensional effects from the liquid surface.

3.3.3. Manufacture of Foam Support. The foam has very little mechanical strength and is difficult to machine, especially to the accuracy required in this apparatus, i.e., to a uniform thickness of 1.5 mm.

The technique used to manufacture these supports involved making a mold out of cardboard, with a hole having the same diameter as the outer annulus diameter of the foam, and having a depth of 1.5 mm. Foam was cut into a cylindrical form with the same diameter as the hole, and

one end was smoothed on a sandpaper machine. The foam cylinder was cut so that its thickness was about 5 mm. It was next placed in the mold and machined on a sandpaper machine until the foam was level with the top of the mold. The foam annulus was then cut from this.

3.3.4. Final Comments on Foam Support. One of the most important functions of the foam support is to stop any air convection which might be produced by the cooler and which might sweep across the surface of the liquid from outside the equipment. This is one of the reasons why the support was made in an annular shape.

Another important comment is that the foam has to be produced and maintained so that it does not lose its porosity. If the porosity is decreased, the support will become a much better heat conductor than the air and short circuit the air gap. This would result in two-dimensional effects.

3.4. Cooler Design and Performance

The cooling apparatus is required to provide an isothermal cold plate, the temperature of which can be controlled and varied. The two systems used were a thermo-electric cooler and a cold-liquid sprayer. The sprayer had the advantage of being able to provide a variety of temperature profiles on the liquid surface, whereas the thermo-electric cooler was not as flexible and was limited to a linear decay in surface temperature. However, the sprayer had the disadvantage of introducing variable vibrations into the system because of the spraying mechanism. The thermo-electric cooler had no moving parts and was essentially vibration-free; therefore it was used to represent the "stillest" possible condition for free-surface convection.

3.4.1. Thermo-electric Cooler. The thermo-electric cooler works on a thermodynamic cycle of transferring heat from a heat source to a heat sink by putting work into the system.

The components of the thermo-electric cooler are arranged so that heat is transferred by using N and P type semiconductors connected electrically in series and thermally in parallel. The direction of heat transfer is governed by the current direction. Thus the thermo-electric cooler can heat or cool by reversing the direction of the current.

The operating characteristics of the thermo-electric cooler are very sensitive to the temperatures of the source and sink, and for reliable operation the heat sink must be efficient in removing heat in order to keep the hot surface from overheating (i.e., there must be a good thermal junction between the pump and the sink). The heat transfer capacity of the pump decreases as the temperature difference between the source and the sink increases (Fig. IV-5).

3.4.1.1. Cooler Design. The thermo-electric cooler chosen was a Cambion model 3953-2; available commercially from Cambion Thermionic Corp., Cambridge, Massachusetts. The operating characteristics are shown in Fig. IV-5. This model was chosen because of its circular cooling plate and because it had a high heat pump capacity for its size.

The heat sink was a copper cylinder, filled with water and attached to the heat pump with glue. The heat transfer junction between the sink and the heat pump was improved using a thermal interface compound (Cambion Silicon Grease #630-7208).

3.4.1.2. Isothermal Character of Thermo-Electric Cold Plate. The temperature profile on the cold plate was measured and was found to be

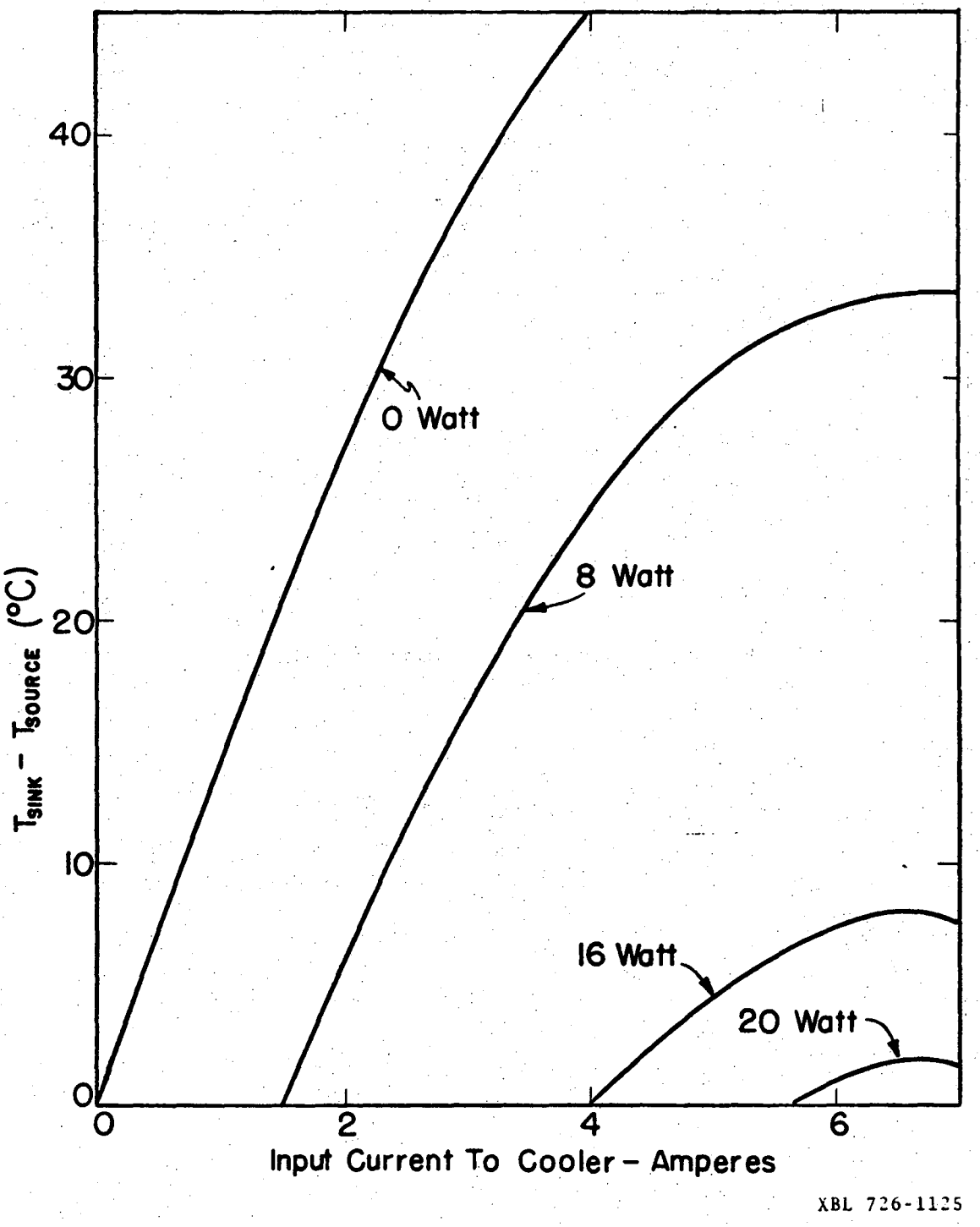

Fig. IV-5. Operating Characteristics of Thermo-electric Cooler (Cambion model 3953). The data is from a Cambion Brochure for a sink temperature of 50°C.

colder near the edges and warmest at the center (Fig. IV-6). The temperature profile measurements were performed by placing the cooler on top of a metallic cylinder with a thermocouple junction attached to its furface. The position of the thermocouple was marked on the surface so that the temperature response at any point on the cooler could be recorded by moving the cooler to different positions. Since the response was transient, the temperature after a standard period of time was taken as the measured quantity.

Various methods were devised to make the cold surface isothermal. Each was aimed at decreasing the heat transfer at the edges, by increasing the heat transfer resistance there, and increasing the heat transfer to the center. The final design involved layers of copper, sandwiching a composite layer with radially varying heat transfer resistance, attached to the cold side of the heat pump. The final form of the composite layer and resultant temperature profile are shown in Figs. IV-6 and IV-7. The heat transfer resistance decreased in the order: paper, cellulose, copper.

3.4.1.3. Thermo-electric Cooler Operation. Some tests were made to increase the rate of cooling, by using cold solvent as the sink fluid. The observations made were as follows:

(1) More heat transfer resulted from conduction than from the thermo-electric process. This was seen when the rate of heat transfer measured increased only slightly when the current was on. When the heat pump acted as a heater, it blocked the conduction process so that the temperature of the bottom cold side could be controlled. This observation introduced the possibility of using the cold solvent, and the heat pump acting as a heater, as a means of varying the surface temperature profile from a linear decay to a step change.

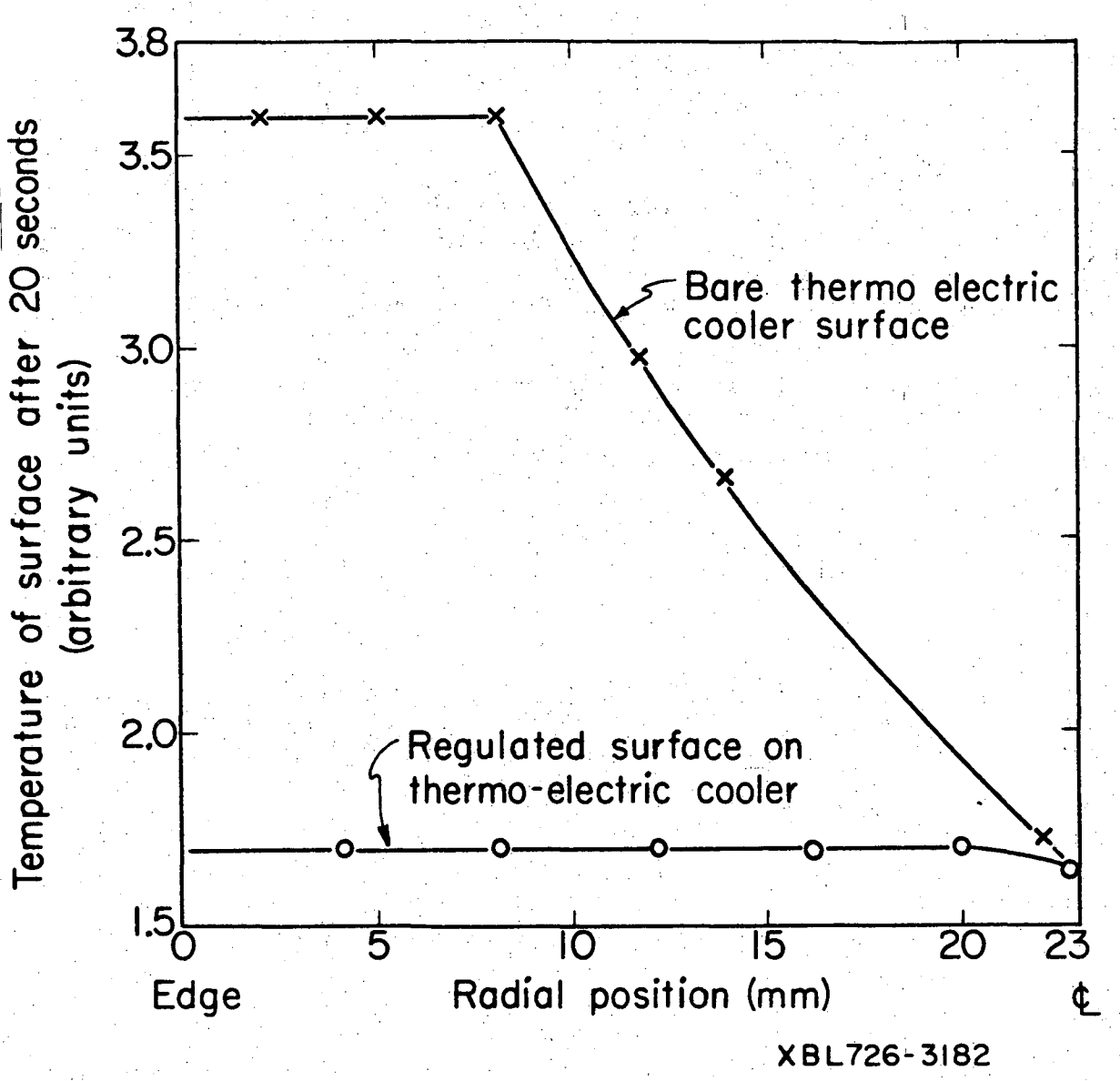

Fig. IV-6. Temperature Response on the Thermo-electric Cooler's Cold Surface Before and After the Addition of the Surface Regulator which is shown in Fig. IV-7.

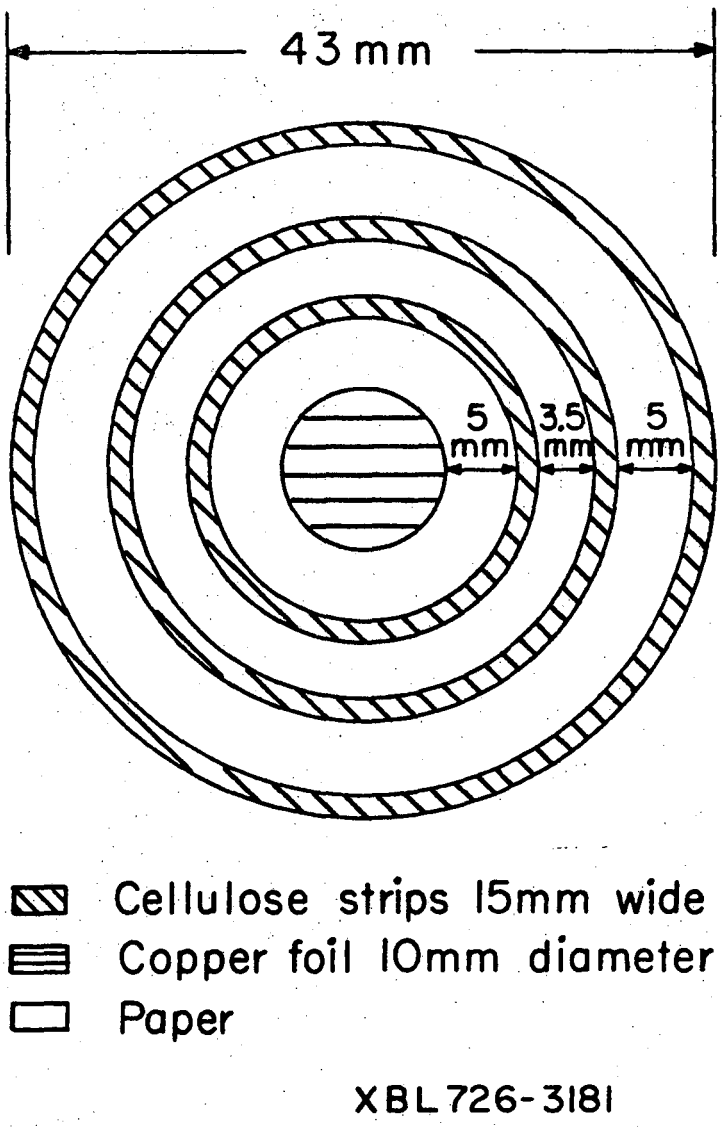

Fig. IV-7. Pattern of the heat transfer Resistance layer Applied to the Bare Thermo-electric Cold Surface to make it more Isothermal. In order of heat transfer conductance: Copper > Cellulose tape > Paper.

(2) The cold solvent does not permit a steady state of the liquid surface temperature to evolve in the way that it would if the solvent was at room temperature. This has the disadvantage of requiring that the cold solvent be poured into the sink container just as the thermo-electric cooler is switched on, thus defeating the purpose of the vibration-free experiment.

As a result of these investigations, the sink liquid temperature was kept at room temperature. This had the additional advantage of allowing the equipment to be set up with liquid in place. Also the apparatus did not have to be dismantled after each run to bring the system back to thermal equilibrium. With this arrangement heat could be added via the heat pump, and cold liquid could be easily added to the sink if required.

3.4.2. Spray Cooler. The spray cooler was developed to overcome the limitations of the thermo-electric cooler, by producing a variety of liquid surface temperature functions, from linear decay to step functions.

A step function on the liquid surface can be produced only approximately when the cooling surface is separated from the liquid by an air space. However, a linear surface temperature profile can be obtained by slowly decreasing the temperature of the cooling plate, the exact temperature history required for the cooling plate being determined experimentally. The temperature profiles for the linear decay resemble those shown in Fig. IV-8.

A step function profile on the liquid surface can be approximated by two linear segments (Fig. IV-9), the earlier segment having a very steep

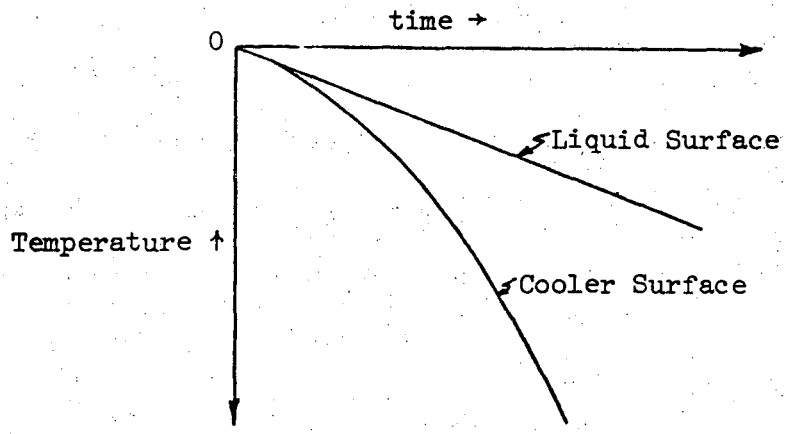

Fig. IV-8. Shape of linear decay temperature profiles.

gradient and the latter a very shallow gradient. This can be achieved by using a very high driving force during the lifetime of the first segment and then decreasing the driving force during the lifetime of the second segment. The shape of the temperature history of the cold plate during the second segment can be estimated according to the following analysis:

A heat balance at the liquid surface for a constant temperature at the liquid surface gives:

$$k_{air} \left.\frac{\partial T_{air}}{\partial z}\right|_{z=0} = k_{liq} \left.\frac{\partial T_{liq}}{\partial z}\right|_{z=0}$$

The relaxation time in the air space to a change in temperature can be approximated as very small so that the temperature gradient across the air gap can be assumed almost linear. Preliminary experimental and theoretical investigation supported this assumption for this equipment. Thus

$$k_{air} \frac{\Delta T}{\ell} = k_{liq} \left.\frac{\partial T_{liq}}{\partial z}\right|_{z=0}$$

or

$$\Delta T = \frac{k_{liq}}{k_{air}} \cdot \ell \cdot \left.\frac{\partial T_{liq}}{\partial z}\right|_{z = 0}$$

where ΔT = temperature difference between cooler and liquid surfaces and ℓ = air gap spacing.

During the second segment period, it can be shown that $\left.\frac{\partial T_{liq}}{\partial z}\right|_{z = 0}$ will fall sharply at first and then flatten out later. Since ΔT is proportional to $\left.\frac{\partial T_{liq}}{\partial z}\right|_{z = 0}$, the temperature of the cold surface and the liquid surface will be in the shape shown in Fig. IV-9.

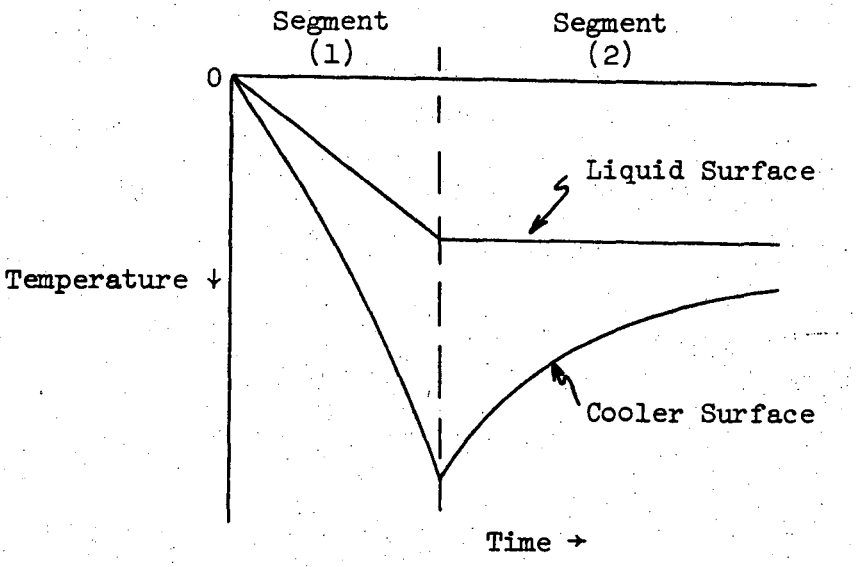

Fig. IV-9. Shape of "Step Function" surface temperature change.

3.4.2.1. Spray Cooler Design. From the foregoing discussion, the spray cooler had to be designed so as to (1) provide as large a driving force as possible during Segment 1, (2) keep the time of Segment 1 short, and (3) control the temperature of the cooling plate during Segment 2 in order to obtain the desired liquid surface temperature.

These above demands were achieved by spraying cold solvent (-60° C to -10° C) onto the cooling surface and then evaporating the

solvent with a forced draft (Figs. IV-10 and IV-11). The cold solvent lowers the temperature of the cooling plate quickly and provides the initial driving force. However, the system cannot sustain this low temperature for long because of heat flow to it, and this provides the rapid rise in temperature during Segment 2. The temperature drop of the cold plate is controlled by the temperature of the cold solvent, and the duration of Segment 1 is controlled by the quantity of cold solvent. The flow of the draft air controls the evaporation cooling of Segment 2.

3.4.2.2. Spray Cooler Apparatus. Apparatus to control these actions is shown in Figs. IV-10 and IV-11. Cold liquid is held under pressure in the syringe and the sprayer. When the clip is opened, the liquid enters the sprayer and is distributed onto the bottom side of the cooler before running out the eight exit tubes. The air pressure is adjusted to control the flow of air through the apparatus. This is set before the cold liquid and the stopper are placed in the syringe. The syringe is calibrated to facilitate measuring the amount of cold liquid to be pumped through the cooler.

3.4.2.3. Distributor Section (Fig. IV-10). The principle of this section is to provide the cooling surface with equal amounts of cold liquid over its area simultaneously. This even distribution is especially important when liquid is first introduced and the greatest changes in the plate temperature take place. Experience has shown that when the plate is not uniform in temperature, motion driven by lateral gradients in surface tension sets in.

The greatest challenge with the spray section is in obtaining the right sort of spray. To a large extent, this is governed by the gap

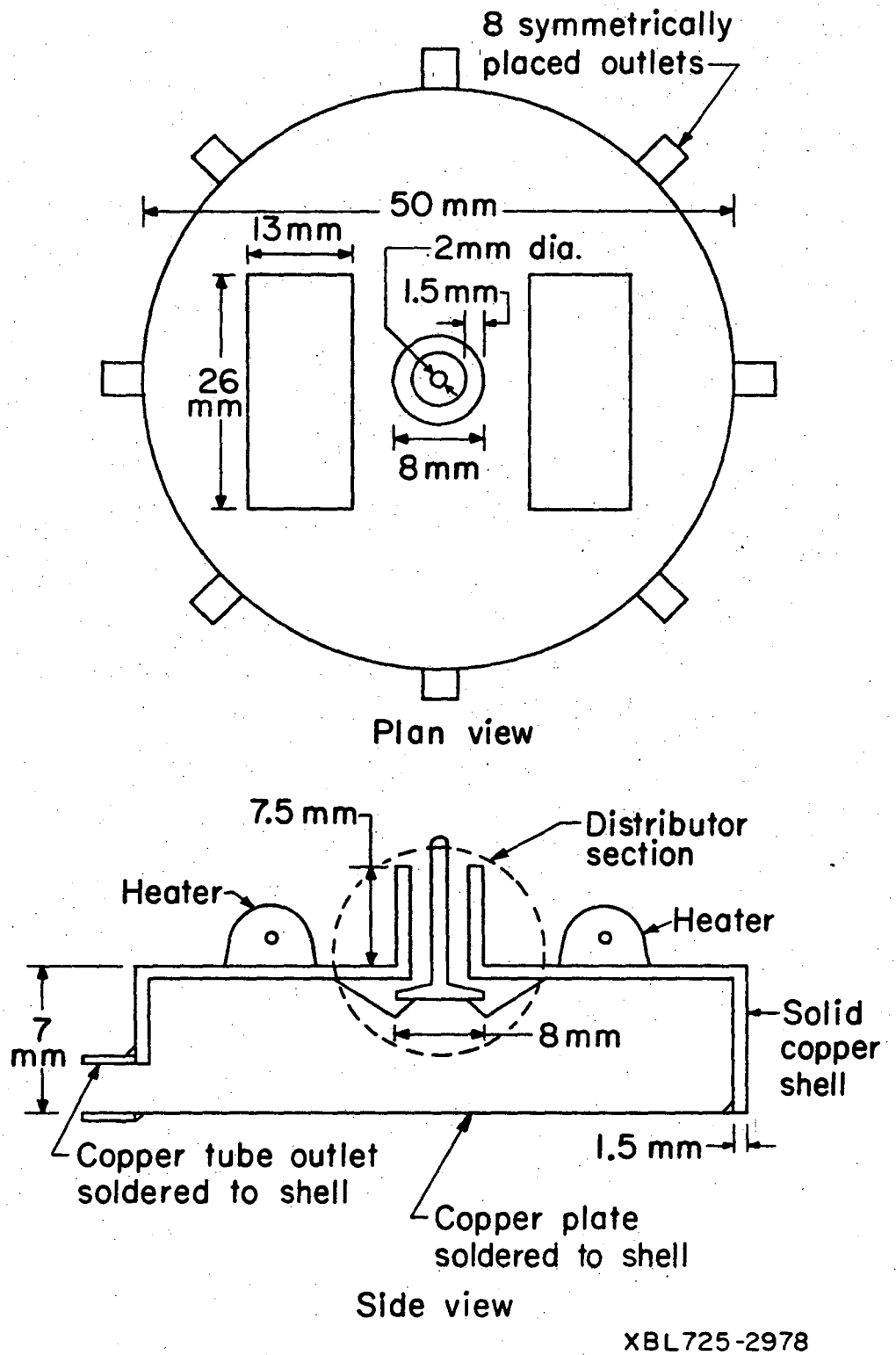

Fig. IV-10. Free Surface Spray Cooler Design and Dimensions.

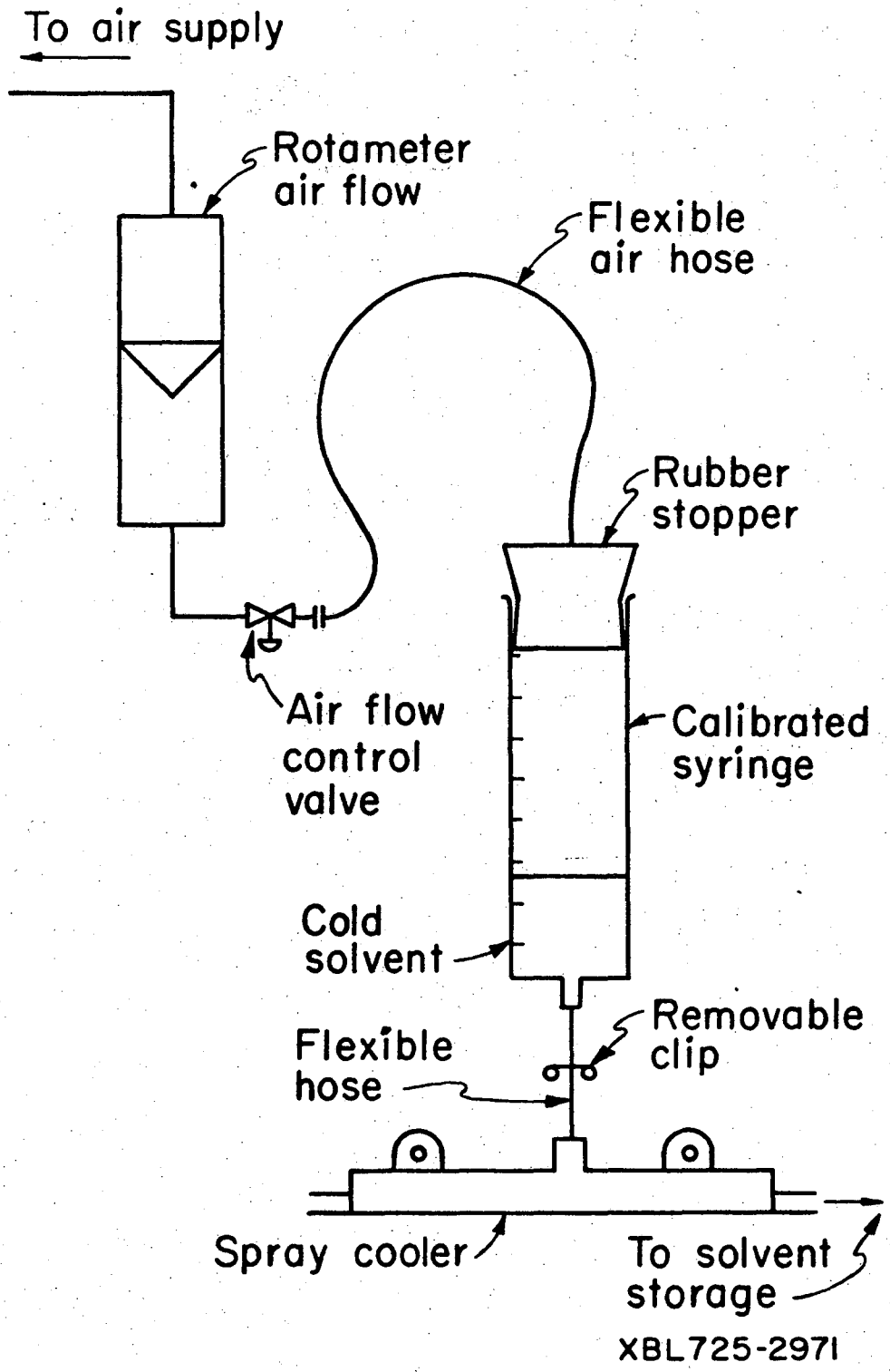

Fig. IV-11. Schematic Diagram for Spray Cooler Operation.

distance between the distributor plate and the copper shell. Because the leads holding the distributor plate were made of 20 gauge copper wire, the position of the distributor plate could be adjusted to give an observed good spray. This was tested before the cooling surface was soldered to the shell.

3.4.2.4. Outlet Systems. In order to ensure quick and even drainage, eight outlets were positioned in the walls of the cooler. Each outlet had an opening size of 1.5 mm and was placed so that the base of the cooler was level with the opening of the outlet or with the bottom wall of the pipe, which was about 3/4 mm thickness. The variation in the vertical positioning of those outlets whose opening was flush with the cooler plate was random and was caused by imperfect machining. However, drainage results showed that each section was well drained and that minor adjustments were necessary on only two of the outlets to ensure even flow.

The outlets were drained by rubber hoses and combined into pairs, the hoses for which were laid on the foam insulation. The exit liquid was collected from these outlets.

3.4.2.5. Heaters (Fig. IV-10). Heating to bring the system back to the operating temperature was accomplished with two 25-watt resistance heaters attached to the upper surface of the copper shell connected to a power supply. The response of this system was fast. The environmental temperature could be controlled with either the heating or cooling system to bring about approximate steady state within three minutes.

3.4.2.6. Two-Dimensional Temperature Suppressor for Spray Cooler. The isothermal character of the cooling plate was further improved by

gluing a layer of paper to the plate. This increased the resistance to heat transfer in the vertical direction and promoted evening out any two-dimensional character in the plate temperature.

3.5. Convection in the Air Gap

While there is an adverse temperature gradient in the air gap, there is no verified time-dependent correlation available to predict convection in that phase. However, some runs were taken with a thermocouple monitoring the air side of the cooler plate. Convection responses were noted when the air space was about 6 inches deep, but were not observed for 3 mm depths. This confirms that the source of convective motion is in the liquid phase rather than in the air phase in these experiments.

3.6. Performance and Operation of Equipment

The electric cooler was found to maintain a linear profile over a greater range than the spray cooler. The spray cooler produced the two extreme surface functions--linear decay and step function--as well as intermediate types (see Fig. IV-12).

4. Comparison of Free and Fixed Surface Onset Conditions

The major difference in performance between the free and fixed surface experiments was in the detection of instability. The point of instability for a fixed surface was taken as the first departure from pure-conduction behavior in the bottom liquid surface temperature. However, after the convection had begun, the temperature difference between surface and bulk for the fixed surface continued to increase rather than to decrease.

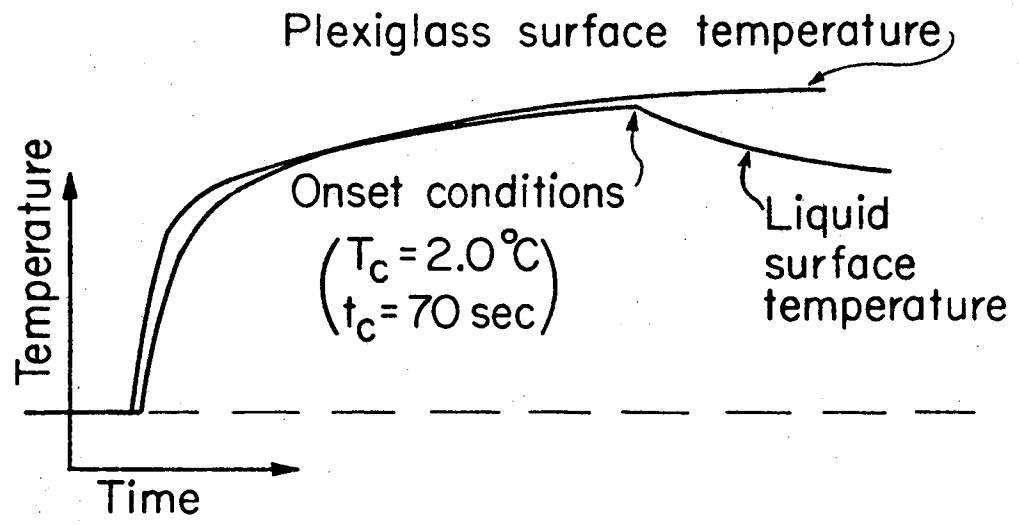

(a) Step change in surface temperature

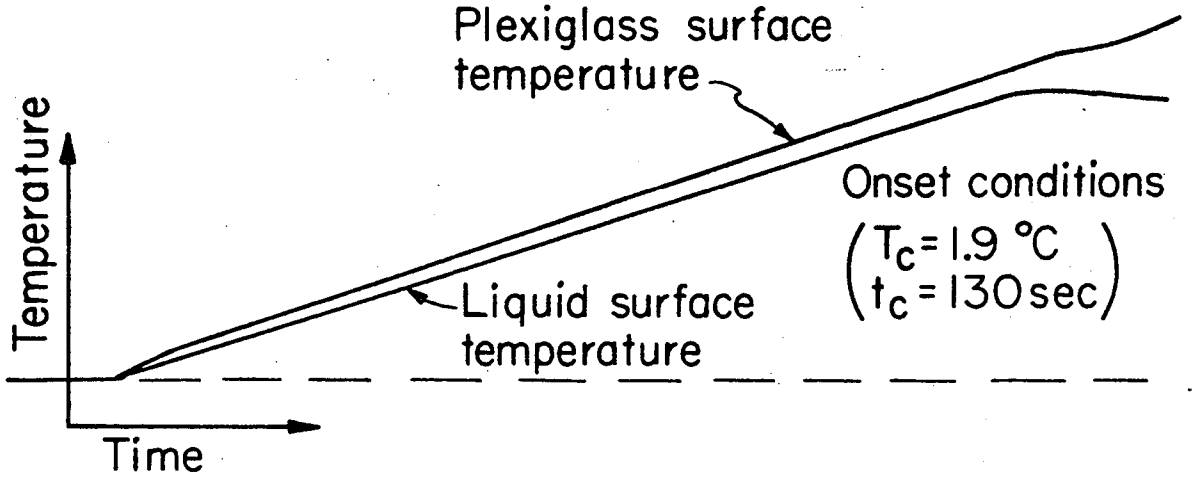

(b) Linear time decay of surface temperature

XBL726-3175

Fig. IV-12. Experimental Temperature Responses on the Gas-Liquid and Plexiglass surfaces using the Spray Cooler. The Surface Temperature of the Plexiglass is shown to Display the Conduction Response which was used as a Reference in Identifying the Onset of Convection.

This difference is due to the ratio of heat flux in the air to heat flux in the liquid being less in the free surface case than the ratio of heat flux in the annulus heater to heat flux in the liquid in the fixed surface case. The lack of temperature decrease in the fixed surface experiments added difficulty to detecting convection onset with curves having an onset time greater than 250 seconds.

V. FIXED SURFACE RESULTS

1. Deep Pool Results

1.1. Convection Free of Wall, Depth, and Vibration Effects

In these experiments, the heating rate and the fluid viscosity were varied so as to verify the internal consistency of the time-dependent Rayleigh number and determine its dependence on the Prandtl number. The depth of the fluid was either 4.5 cm or 5.6 cm, $\frac{\alpha t}{H^2}$ was always less than 0.01, and $\frac{\alpha t}{D^2}$ was always less than 0.01. The experiments were performed on the vibration-free table, except for those described in Sec. 1-3. All runs were made with a bottom surface temperature which increased linearly with time.

1.1.1. Internal Consistency of the Rayleigh Number. The time-dependent critical Rayleigh number may be partitioned into two groups, one dependent upon the physical properties of the liquid and the other dependent upon the nature of the imposed surface temperature.

$$Ra_t = \frac{\rho g \beta \, \Delta T (\alpha t)^{3/2}}{\mu \alpha} = \left(\frac{\rho g \beta \alpha^{1/2}}{\mu} \right) \quad (\Delta T \, t_c^{3/2})$$

(ΔT is the temperature drop across the fluid.)

For any given liquid in which the physical properties do not vary significantly, the first group in the Rayleigh number ($\frac{\rho g \beta \alpha^{1/2}}{\mu}$) and the Prandtl number are constant. Thus the theory would predict that Ra_t for a particular fluid is proportional to $\Delta T \, t_c^{3/2}$, provided the initial disturbance spectrum is constant.

The experimental conditions for first observable convection (refer to Fig. III-1) are plotted on Fig. V-1 for the following liquids; methanol

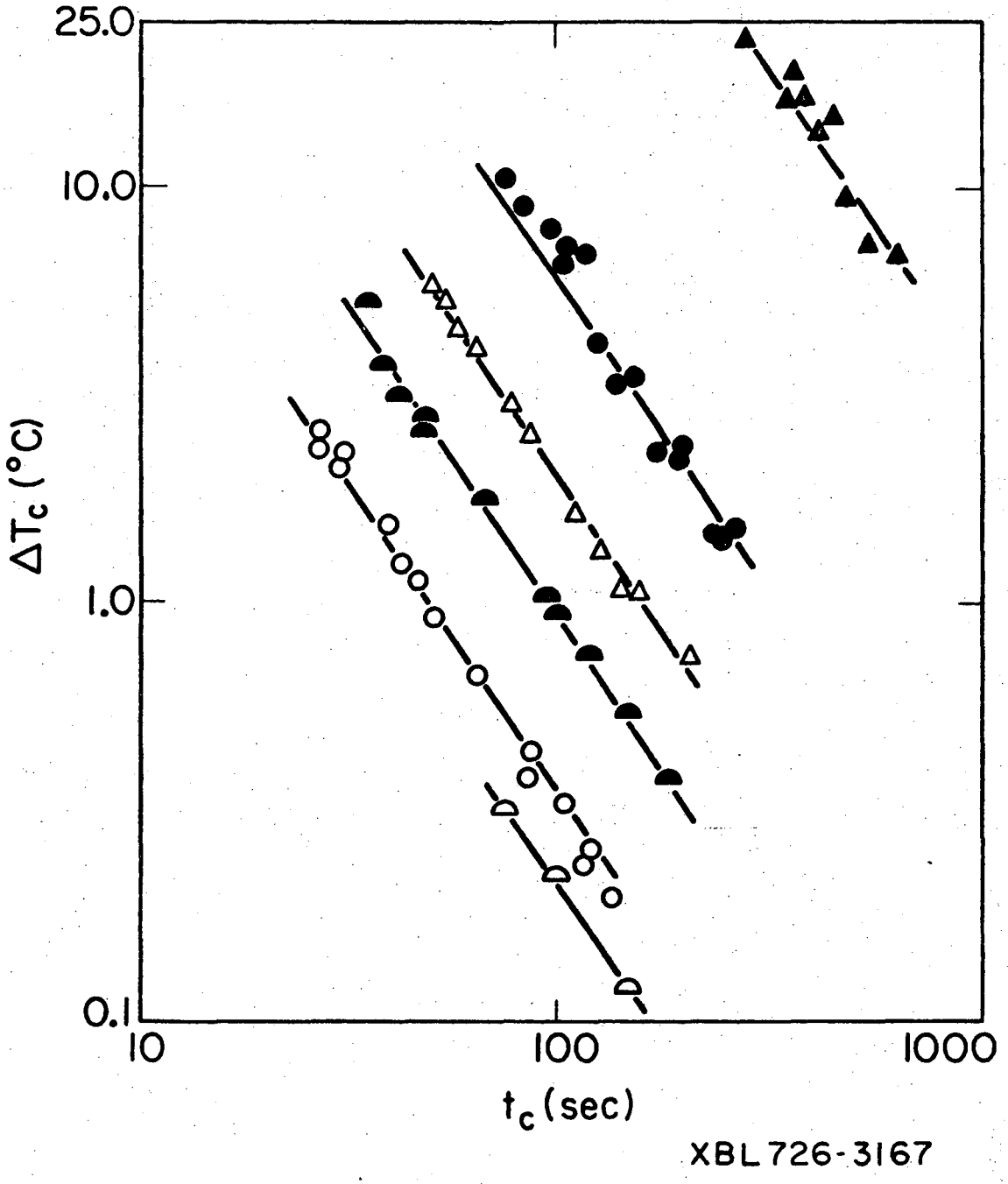

Fig. V-1. Experimentally Determined Conditions for the Onset of Convection for a linear temperature decay at a Fixed Surface in a Deep Pool. △ Methanol, ○ n-Decane, ◮ n-Butanol, Δ n-Octanol, ● Silicon Oil 50 cs., ▲ Silicone Oil 1000 cs. Bulk liquid temperature at 25.0 ± 0.2°C.

(Pr = 6.6), n-decane (Pr = 13), n-butanol (Pr = 43), n-octanol (Pr = 108), and Silicone Oils 50 cs (Pr = 450) and 1000 cs (Pr = 8500).

The results verify the relation ($\Delta T\ t_c^{3/2}$ = constant) for each fluid tested in this apparatus, and support the findings of Foster (1969) for water. Although his results were reported as ($\frac{\partial T_s}{\partial t} \cdot t_c^{5/2}$ = constant), the results here were reported in the form $\Delta T\ t_c^{3/2}$ for the following reasons:

(1) $\Delta T\ t_c^{3/2}$ is the simplest and the most uniform combination of surface temperature and onset time for any surface temperature history. The approach of using $\frac{\partial T_s}{\partial t} \cdot t_c^{5/2}$ utilizes a characteristic of the surface temperature history ($\frac{\partial T_s}{\partial t}$), which will vary from one surface temperature history to another.

(2) ΔT can be more easily identified as a physical quantity than ($\frac{\partial T_s}{\partial t}$) or any other surface temperature characteristic. Thus this form of correlation should have a greater general utility than other forms.

The disadvantage of this approach in practice is that the critical conditions (ΔT, t_c) are found by simultaneously solving the heat conduction equation with the appropriate boundary conditions, along with the $\Delta T \cdot t_c^{3/2}$ plot. This is in contrast to reading the critical conditions directly from a plot for a given type of heating (i.e. constant flux).

1.1.2. Functionality Between Ra_t and Pr. The values of Ra_t for each fluid were found from the results of Fig. V-1, and from values of physical properties obtained from the literature. These properties are listed in Appendix D. The results have been plotted in Fig. V-2 so as to show the average value and the range of values obtained from Fig. V-1.

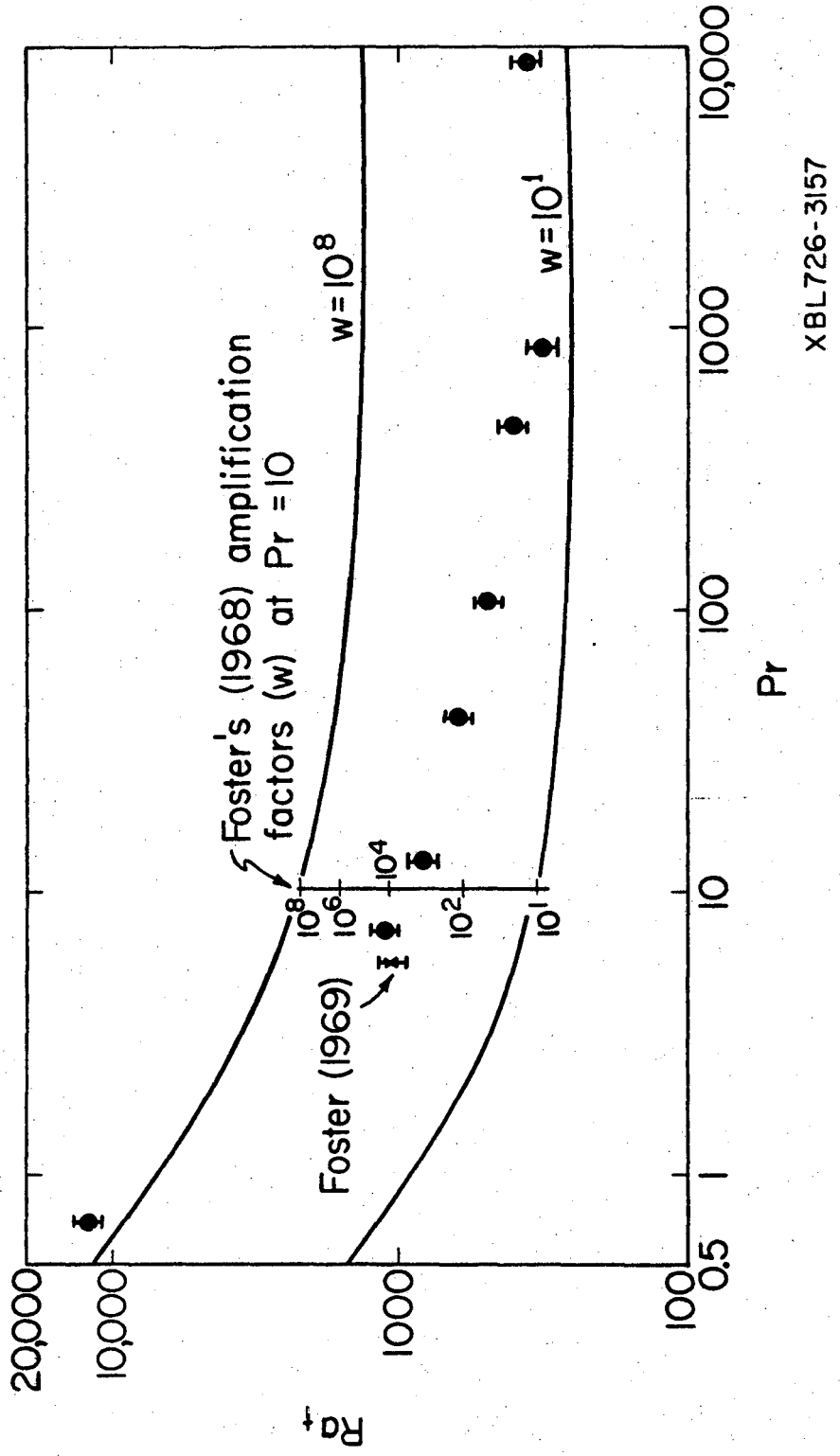

Fig. V-2. Experimental Values of Ra_t versus Pr for a linear temperature decay at a Fixed Surface in a Deep Pool.

± Experimental Data

—Foster's (1968) theoretical curve for constant Amplification Factors of 10^1 and 10^8.

The heating apparatus was also used to estimate Ra_t for air (Pr = 0.7) (refer to Appendix F). Even though the temperature profile was two-dimensional near the walls because of the difference in thermal properties between air and Plexiglass the region in the center of the plate was thought to be nearly one-dimensional. The apparatus had to be modified so as to detect instability. A thin thermocouple was suspended 1 mm (approx.) above the surface and this detected the onset of convection much better than the thermocouple on the air-solid surface. The results and calculations are presented in Appendix F.

Predicted relationships between Ra_t and Pr calculated by Foster (1968) using Amplification Theory with constant amplification factors of 10^8 and 10^1 has also been plotted on Fig. V-2. The data show that the apparent amplification factor corresponding to onset decreases as the Pr increases. However, the data do fall in the ranges reported in the literature and reported in Chapter II, Sec. 1.3.2. The predicted curve is qualitatively correct insofar that it predicts Ra_t approaching a constant value at high values of Pr, and Ra_t increasing as Pr decreases.

A more thorough test of the shape of this curve would be to extend this work into the liquid metal domain (low Pr). The apparatus used in this work was thermally incompatible with liquid metals and therefore not suitable for the necessary extension, but the design principles used in this work could be extended to liquid metal experiments.

Foster (1969) published results for heating water in an apparatus similar to that used in this report. With Pr = 6.6, he correlated his results with an amplification factor of 10^3 to 10^5, which agrees well with the results in this study.

1.2. Effect of Wall Spacing

The solution to the Amplification and Q.S.A. theories assumes an infinite horizontal layer so that wall effects do not enter the problem. Although this is an unrealistic assumption, it simplifies the analysis. Krishnamurti (1970) commented that the fringing of the isotherms in the vicinity of the walls introduces a horizontal temperature gradient into the fluid which leads to sub-critical (i.e. two-dimensional) motion. Sub-critical motion at walls was observed by Koshmeider (1966).

The effect of wall spacing on the linear-density-profile convection onset problem has been discussed theoretically (Davis, 1967; Davies-Jones 1970) as well as experimentally (Heitz and Westwater, 1971; Deardorff and Willis, 1965; Quinn and Mitchell, 1966); these results may serve as a guideline for transient convection. The critical Rayleigh number was found to increase as the ratio of the wall spacing (D) to the fluid depth (H) decreased. This increase was due to both the effect of shear stress at the walls and the rearrangement of the convective motion to circulate in a confined space. With an infinite horizontal layer, the convective cell takes on dimensions corresponding to the minimum energy for convection. When the wall spacing has dimensions similar to or less than the lowest energy convective cell, the liquid has to circulate with a cell dimension dependent upon the size of the wall spacing. Convective circulation with this restriction requires a higher energy level. Heitz and Westwater (1971) found that for convection in a vessel with square horizontal cross section, the Rayleigh number (Ra_H) increased for $\frac{D}{H} < 2$, but that for $\frac{D}{H} > 2$ the Rayleigh number did not increase significantly. Similar results using gases have been reported by Deardorff and Willis (1965), and Quinn and Mitchell (1965).

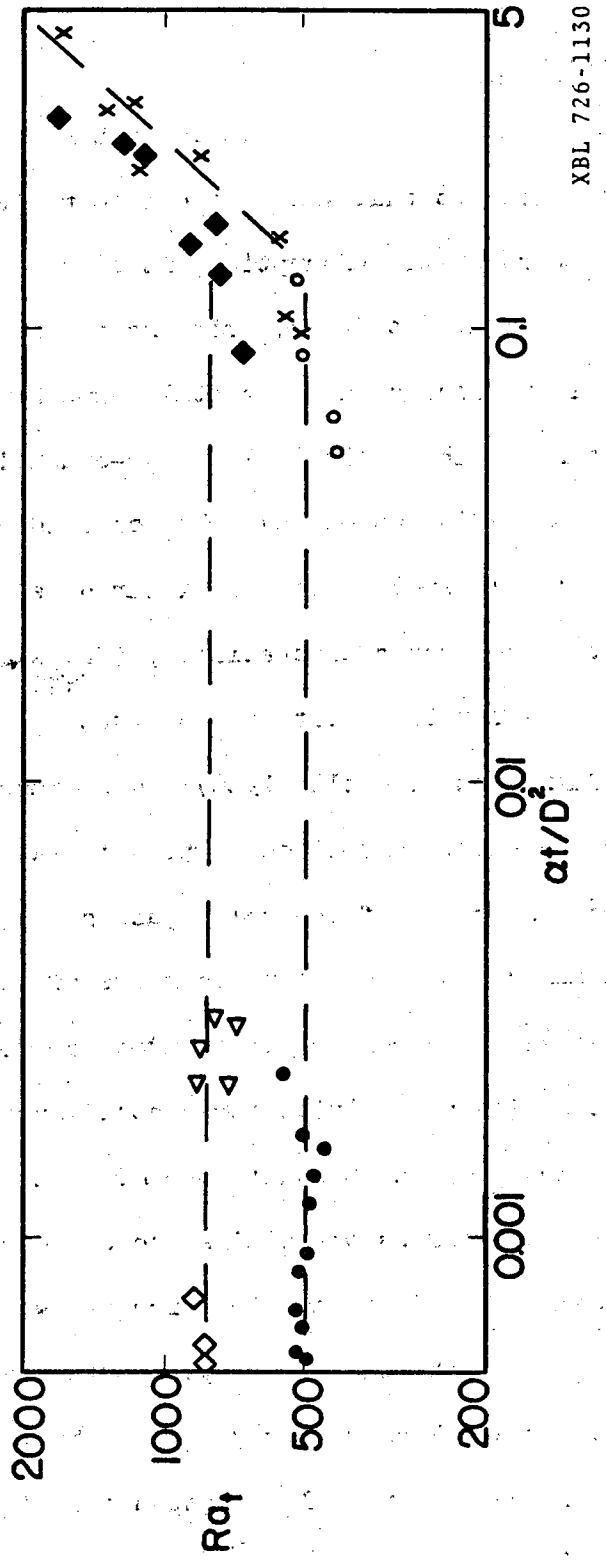

Fig. V-3. Experimental values of Ra_t versus width factor ($\alpha t/D^2$) for the Fixed Surface Deep Pool Case.

n-Octanol: ● D = 8.9 cm ○ D = 0.87 cm X D = 0.57 cm

n-Decane: ◊ D = 8.9 cm Δ D = 5.9 cm ♦ D = 0.57 cm

Foster (1969) reported photos of the incipient observable convective cell patterns. From such photos, it was observed that only the cells next to the wall of the container were affected by the presence of the walls, and Foster made the generalization that the walls have only a minor effect on the conditions necessary for observable convection. In these experiments, the width of the tank was 30 cm, and the penetration depth was never more than 1 cm.

Although the mechanisms in the time-dependent and time-independent convection cases may be different, the equivalent of $\frac{H}{D}$ in the linear profile case should probably be proportional to $\sqrt{\frac{\alpha t}{D^2}}$ in the transient case. Experiments were run with the apparatus and technique described in Chapter III, Sec. 2.4. The results have been tabulated in Appendix C, and plotted in Fig. V-3. It can be seen that wall effects are negligible for n-octanol (Pr = 108) and n-decane (Pr - 13), provided $\frac{\alpha t}{D^2} < 0.1$. For greater values of $\frac{\alpha t}{D^2}$, Ra_t rises sharply. The dependence of Ra_t on Pr for $\frac{\alpha t}{D^2} > 0.1$ was not clearly distinguishable.

1.3. Effect of Variable Vibration in the Vertical Direction

The influence of different forms of vibration on the onset time as reflected by Ra_t was studied using the equipment and technique discussed in Chapter III, Secs. 3.2 and 3.3.

Results reported in Figs. V-4 and V-5 and in Tables 3 to 6 show that as the forcing vibration decreases in frequency and increases in amplitude, the onset of convection occurs earlier. Since the vibration conditions employed in these experiments represent the extremes expected in practice, the upper extreme representing conditions just prior to

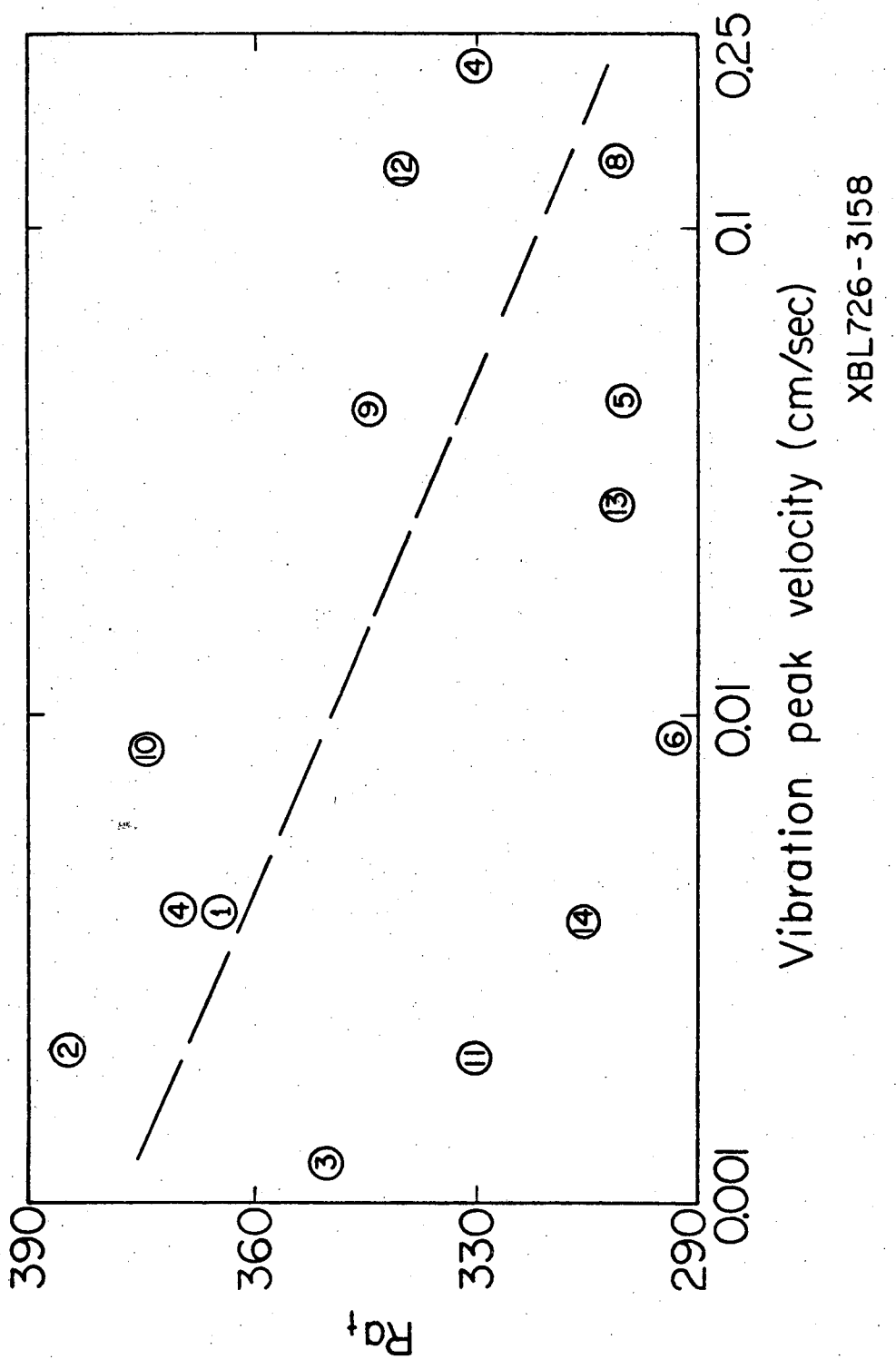

Fig. V-4. Experimental Values of Ra_t for various vibration conditions for n-Octanol at a Fixed Surface. The Numbers in the Circles Correspond to Series of Runs listed in Tables 3 and 4.

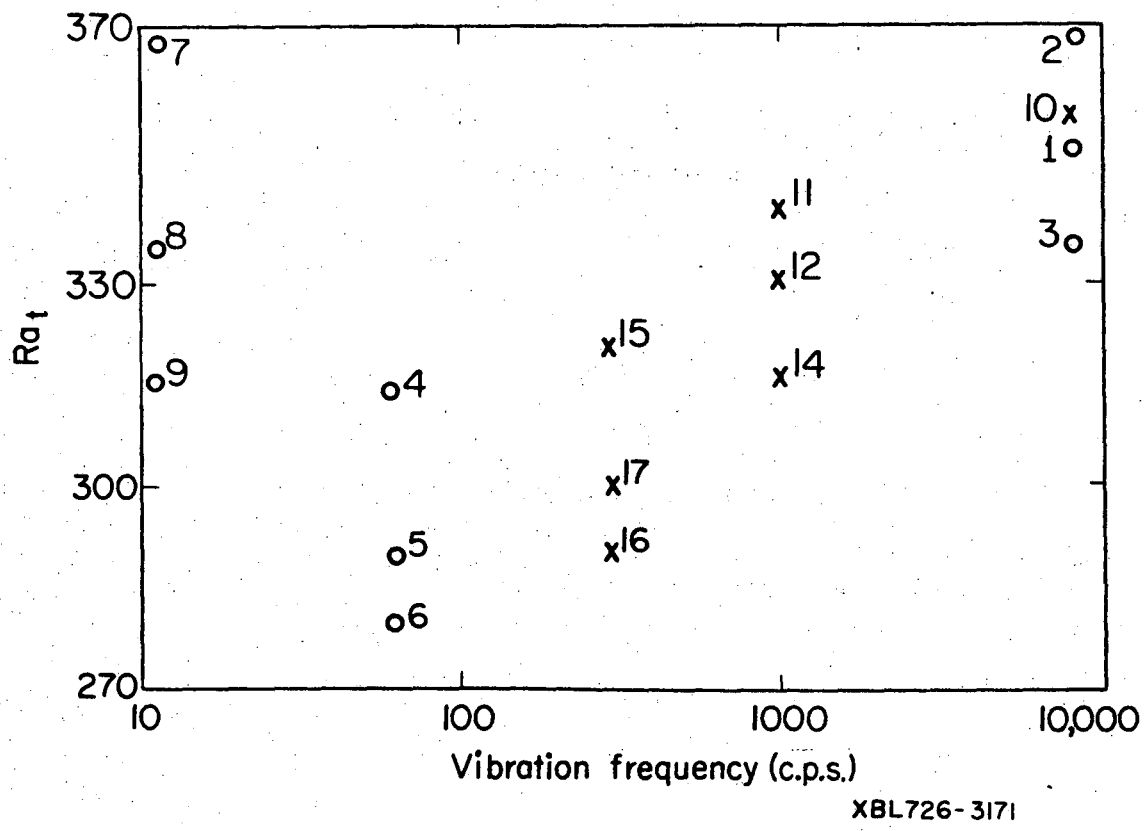

Fig. V-5. Experimental Values of Ra_t as a Function of Vibration Frequency for n-Octanol at a Fixed Surface. The Numbers on the Plot Correspond to Series of Runs Listed in Tables 3 and 4. For a specified frequency and for either a fixed (x) or a free (0) upper surface, the amplitude decreases with increasing numbers. Ra_t on the vibration free table was 450 - 520.

Table 3. Fluid: Octanol; Upper Fluid Surface: Fixed

Identification Number for Fig. 5	Vibrator Frequency (w)(c.p.s.)	Vibrator Amplitude(A) (inches)	Vibrator Power (A^2w^3) (inches^{2}c.p.s.^{3})	Average Rayleigh No.	Maximum Vibration Velocity (cm/sec)	Number of Runs
1	8100	4×10^{-7}	8.5×10^{-2}	350	3.2×10^{-3}	2
2		2.1×10^{-7}	2.3×10^{-2}	370	1.6×10^{-3}	2
3		1.2×10^{-7}	7.7×10^{-3}	335	1×10^{-3}	2
4	60	3×10^{-3}	2.1	315	1.8×10^{-1}	4
5		6×10^{-4}	7×10^{-2}	290	3.6×10^{-2}	2
6		1.2×10^{-4}	3×10^{-3}	280	7×10^{-3}	1
7	10	$.10_e$	10	385	1	2
8		6×10^{-2}	3.6	335	6×10^{-1}	2
9		4.5×10^{-3}	2×10^{-2}	315	4.5×10^{-2}	2

Table 4. Fluid: Octanol; Upper Fluid Surface: Free

Identification Number for Fig. 5	Vibrator Frequency (w)(c.p.s.)	Vibrator Amplitude(A) (inches)	Vibrator Power (A^2w^3) (inches^{2}c.p.s.^{3})	Average Rayleigh No.	Maximum Vibration Velocity (cm/sec)	Number of Runs
10	8100	4×10^{-7}	8.5×10^{-2}	355	3.2×10^{-3}	2
11	1000	1.07×10^{-4}	12	340	1×10^{-1}	4
12		3.4×10^{-5}	1.2	330	3.4×10^{-2}	4
13		6.9×10^{-6}	4.8×10^{-2}	360	7×10^{-3}	4
14		1.56×10^{-6}	2.4×10^{-3}	315	1.6×10^{-3}	4
15	300	3.5×10^{-4}	3.2	320	1×10^{-1}	4
16		7.0×10^{-5}	1.3×10^{-1}	290	2.1×10^{-2}	3
17		1×10^{-5}	3×10^{-3}	300	3×10^{-3}	3
18	10	6×10^{-2}	3.6	270	6×10^{-1}	2

*Vibration Free: Ra_t = 500 to 550.

Table 5. Fluid: Methanol; Upper Fluid Surface: Fixed

Vibrator Frequency (c.p.s.)	Vibrator Amplitude (inches)	Vibrator Power (A^2w^3)	Maximum Vibration Velocity (cm/sec)	Average Rayleigh No.	Average $\frac{\partial T_s}{\partial t} \times 10^2$ °C/sec	Number of Runs
8100	1.37×10^{-7}	9×10^{-3}	1.5×10^{-3}	1050	2.8	1
	3.9×10^{-7}	8×10^{-2}	3.2×10^{-3}	865	2.7	2
6000	3.9×10^{-7}	3.2×10^{-2}	2.5×10^{-3}	800	2.6	1
4000	3.9×10^{-7}	9.5×10^{-3}	1.6×10^{-3}	1000	2.7	1
3000	3.9×10^{-7}	4×10^{-3}	1.2×10^{-3}	800	3.1	1
2000	3.9×10^{-7}	2.4×10^{-3}	7.8×10^{-4}	800	3.2	2
1000	8.7×10^{-5}	7.6	8.7×10^{-2}	900	2.7	1
300	3.9×10^{-4}	4.1	1.2×10^{-1}	920	2.9	1
	8.7×10^{-5}	2×10^{-1}	2.6×10^{-2}	850	2.8	1
60	2.9×10^{-3}	1.8	1.8×10^{-1}	1000	2.3	1
10	$10^{-1}_{(e)}$	10	1	860	2.8	1
	$10^{-2}_{(e)}$	-1	10^{-1}	750	3.0	1

*Vibration Free: Ra_t = 1100 to 1200.

Table 6. Fluid: Octanol; First Observation of Viscous Heating

Vibrator Frequency (c.p.s.)	8100	1000	300
Vibrator Amplitude (inches)	5.3×10^{-7}	7×10^{-5}	7.8×10^{-4}

viscous heating (see Chapter III, Sec. 3.3), it would appear that vibrations of approximately 60 c.p.s. and amplitude of 0.001 inches have the greatest destabilizing effect, lowering Ra_t by 40% from the value obtained with a very low-vibration environment.

The two different wave forms produced in the liquid with free and fixed upper liquid surfaces did not produce results which were significantly different from each other, except at low frequencies and high amplitude with the free upper surface where the liquid was almost turbulent, which lowered Ra_t significantly.

The conclusion from the results is that vigorous vibration lowers the onset time, but not as severely as Gresho and Sani (1970) and Foster (1968) anticipated using Amplification Theory. Levels of vibration can be expected to vary with the location of the fluid container, but the experimental results show that under average conditions, Ra_t may change up to 15% as a result of variation in environmental vibration. This is to be compared with the 10% variation in Ra_t for the heating experiments reported in Sec. 1.1. In that case, the vibration environment was constant.

Figure V-5 shows 10 c.p.s. to be more stable than 60 c.p.s., which was against the trend of the higher frequencies. The accelerometer showed that vibration motion below 60 c.p.s. was erratic, and at 10 c.p.s. it was very irregular. Consequently, the vibration motion in the two cases was very different, but the results show the motion at 60 c.p.s. to be more destabilizing.

The possibility of something else other than environmental vibration triggering the convection initiation appears real from the

spread in the results so far obtained. Observation from experiment suggests that this is tied to temperature nonhomogeneities in the fluid, although this is difficult to prove. This point is discussed further in Chapter VII, Sec. 2.

1.4. Effect of Varying Physical Properties in the Thermal Layer

Because some physical properties (e.g., viscosity) are temperature-dependent, values of physical properties in the thermal layer will differ from the bulk conditions. Properties in our experiments were evaluated at bulk conditions. Both Ra_t and Pr will be affected, but as can be seen from Fig. V-6, only the viscosity is significantly affected by temperature. Although the calculations for Fig. V-6 are for octanol, this trend is general for all the liquids tested.

In heating experiments viscosity decreases in the thermal layer. This would increase Ra_t and decrease Pr as compared to the values computed at bulk conditions. At low values of Pr, Ra_t increases with decreasing Pr, and so the viscosity effect would not be as noticeable. At higher Pr, Ra_t is independent of Pr and the indicated Ra_t would be higher than that estimated using physical properties at bulk conditions.

In Fig. V-1, variable viscosity effects would be observed through the results for high temperature differences ΔT falling below the line with -1.5 slope drawn through the lower ΔT results, especially with the Dow Corning Silicone fluids. The opposite was observed; this could be due to the slight difference in shape of the surface temperature curves for rapid and slow heating (refer to Chapter V, Figs. VI-6 to 10; Chapter VII, Sec. 1.2.). At rapid heating rates, the surface temperature curve was found to increase above the linear form (i.e. arch upward, $S < 0.5$),

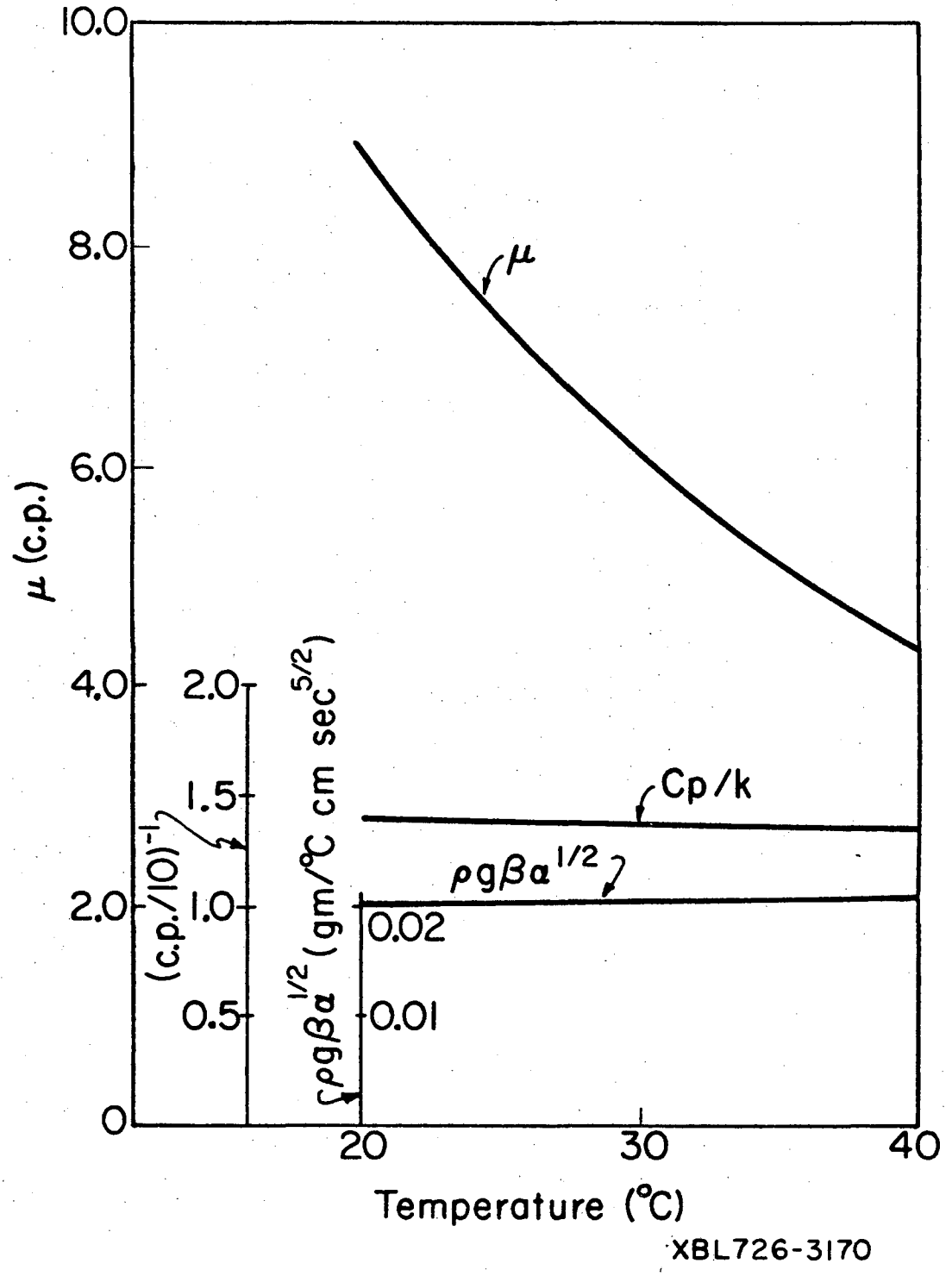

Fig. V-6. The Temperature effect on groups in the Rayleigh number and Prandtl number for n-Octanol.

which would produce a higher value of Ra_t than expected from a linear temperature response. At slow heating rates, the surface temperature dropped below the linear response at long times ($S > 0.5$), and this would produce Ra_t lower than expected from a linear temperature response. Thus, at high ΔT the increase in Ra_t from the slight change in surface temperature linearity probably more than compensated for the slight decrease with changing viscosity.

In the experimental analysis of convection along vertical cylinders (Fuji et al. 1970), the viscosity effect is accounted for by the term $(\frac{\mu}{\mu w})^{1/5}$, where μw is the viscosity at the wall and μ is the viscosity in the bulk. For 1000 cs Silicone Oil, a temperature increase of 24.5° C would produce a 30% decrease in viscosity.

$$(\frac{\mu}{\mu w})^{1/5} = (1.30)^{1/5} = 1.05$$

In this case, the viscosity effect would produce a 5% reduction in Ra_t, which is less than the scatter in the results.

In the linear theoretical analysis by Palm (1960) and Segal and Stuart (1962) for a fluid with both surfaces "free" and at a constant temperature, the effect of variable viscosity through the fluid was shown to be

$$\frac{Ra_H}{(Ra_H)_b} = 1 - 0.048\ (\frac{\mu w - \mu}{\mu})^2$$

For the change in properties in the 1000 cs Silicone Oil as before, this relation would again indicate a 5% reduction in Ra_t.

The above discussion leads to the conclusion that variable viscosity effects are probably not important enough in these results to affect the conclusions.

2. Shallow Pool Results

The shallow pool experiments were carried out using the technique and apparatus described in Chapter III, Sec. 2-3. As outlined in Sec. 1, the correlating parameter to show the increase in Rayleigh number, based on either fluid depth (Ra_H) or penetration depth (Ra_t) at shallow depths and constant Prandtl number is $\frac{\alpha t}{H^2}$. The observed results have been plotted in Figs. V-7 and V-8 for three fluids and for liquid depths down to 2.05 mm, and the results are tabulated in Appendix C.

The transition from deep pool mechanism to a shallow pool mechanism is clearly seen in Fig. V-7. The shallow pool data converge on an asymptote which is independent of Pr and t_c, and dependent on fluid depth (H). The lack of Pr dependence in shallow pools is discussed in Chapter VII, Sec. 1.4. The shift in dependence from t_c to H is discussed in Chapter VII, Sec. 1.3. The deep pool asymptotes are independent of $\frac{\alpha t}{H^2}$ but are dependent on Pr, as reported in Fig. V-2.

The effect of non-linearity of a density profile in a shallow pool is seen in Fig. V-8 where the shallow pool data of Fig. V-7 have been replotted as $Ra_H [= Ra_t \left(\frac{H^2}{\alpha t}\right)^{3/2}]$ versus $\frac{\alpha t}{H^2}$.

The data at large $\left(\frac{\alpha t}{H^2}\right)$ converge on the asymptote $Ra_H = 1700$, which is the solution to the linear density profile and time-independent convection initiation problem (refer to Chapter II, Sec. 1.1).

The comparison of the data with theory is made in Chapter VII, Sec. 1.3.

There are no published shallow pool experimental results for constant temperature at the upper surface. However, some shallow pool experimental results for an adiabatic upper surface have been published. Soberman's

(1958) results for a step increase at the lower boundary have been reported in Appendix A on coordinates that allow comparison with our work. The values of Ra_H are below our results and lower than theoretically predicted by Currie using the Q.S.A. approach. This could indicate that there is some error in Soberman's results (refer to Chapter VII, Sec. 1.3 for evaluation of Q.S.A.).

Foster (1969) reported values for convection onset in shallow pools with a linear increase in the lower surface temperature with time. The liquid at the upper surface was open to the air and so was closer to an insulated surface than to an isothermal surface. The critical Rayleigh numbers (see Appendix A) were estimated to be Ra_t = 10,800 to 12,700 at $\frac{\alpha t}{H^2} = 1.8$, as shown in Fig. V-7. Considering that it was possible that the upper surface did not act as a perfect insulator, in which case Ra_t would be overestimated, and that the temperature profile in the liquid differs from that in this experiment, it appears possible that the shallow pool mechanism is not very dependent on the shape of the temperature profile in the liquid. This point is discussed further in Chapter VII, Sec. 1.3.

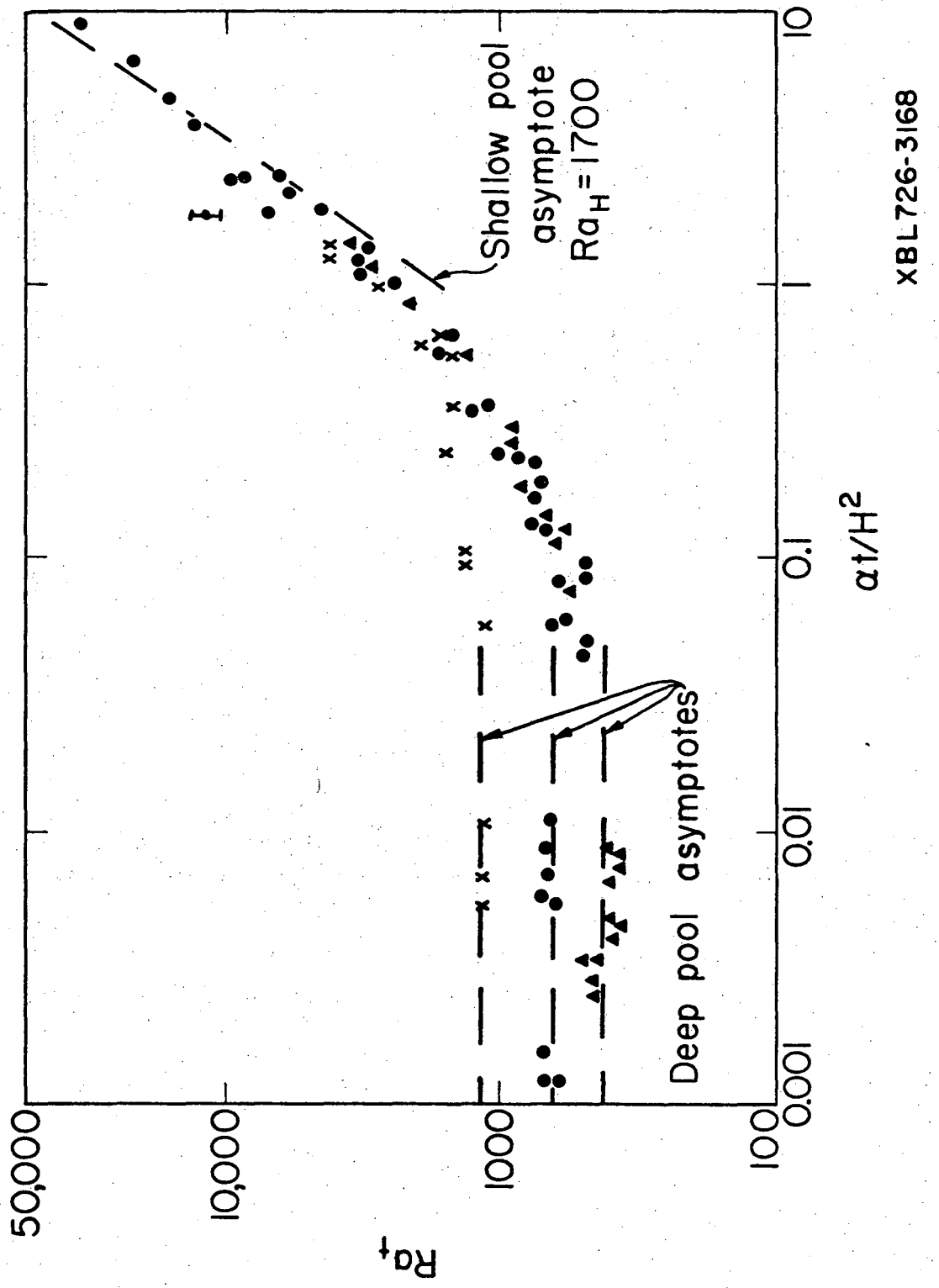

Fig. V-7. Experimental values of Ra_t versus Depth Factor ($\alpha t/H^2$) Showing the Transition from Deep to Shallow Pool Conditions for the Fixed Surface Case. X Methanol, Pr = 7.6, O Butanol, Pr = 43, Δ Silicone Oil 50 cs, Pr = 450. ⧫ Foster's (1969) datum point for water.

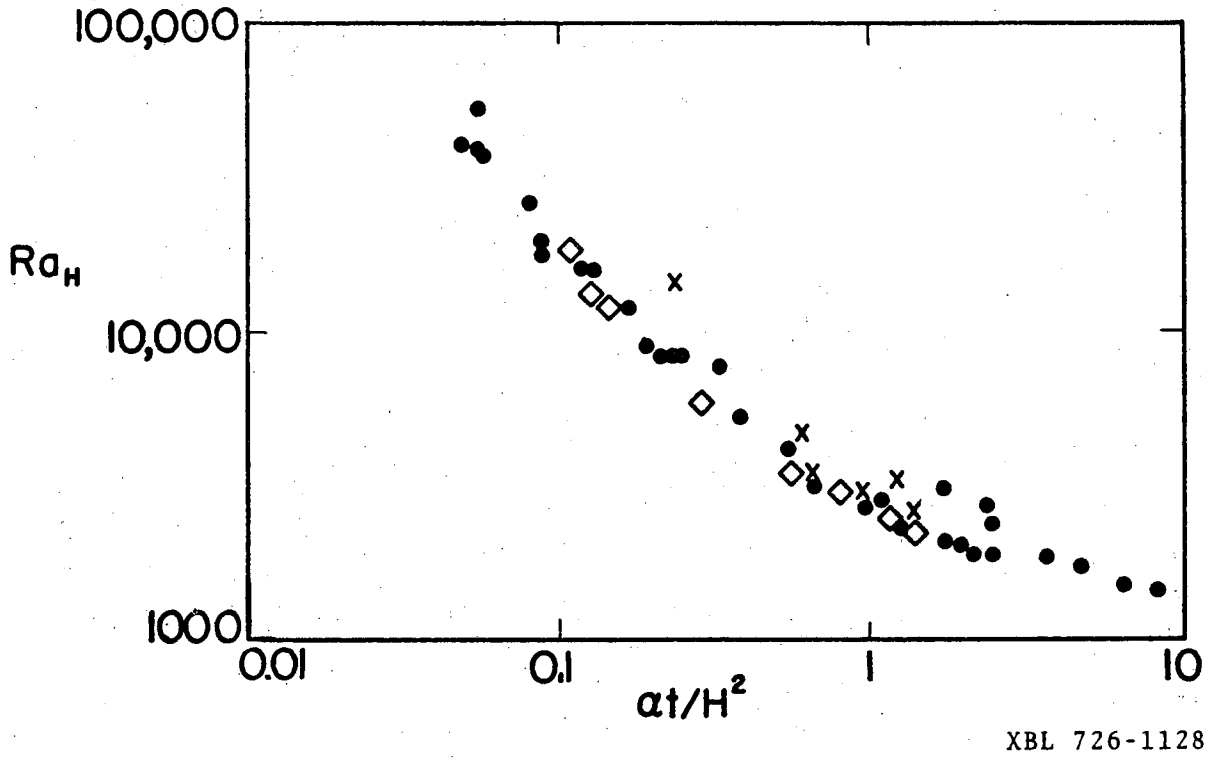

Fig. V-8. Experimental values of Ra_H versus Depth Factor ($\alpha t/H^2$) for the Shallow Pool Data.

X Methanol Pr = 7.6
○ Butanol Pr = 43
Δ Silicone Oil 50 cs Pr = 465

VI. FREE SURFACE RESULTS

With free surface convection, both density and surface tension effects can be expected. These effects can be separated using the relation ($\Delta T \cdot t_c^{3/2}$ = constant) verified in Chapter V to identify density influences, and ($\Delta T \cdot t_c^{1/2}$ = constant) to identify surface tension influence (refer to Chapter II, Sec. 2.1.2.).

1. Deep Pool Results

In the deep pool experiments, the thermo-electric cooler was used with the technique and apparatus described in Chapter IV, Sec. 3.4., to identify the type of convection at a free surface for a linear decrease in surface temperature with time. The spray cooler, with technique and apparatus described in Chapter IV, Sec. 3.4., was used to investigate the effect of varying the shape of the surface temperature-versus-time curve. The liquid container used was designed from results obtained in Chapter V, Secs. 1.2. and 2., to be free of wall and lower boundary effects. It was assumed that free surface and fixed surface convection behave similarly with respect to fluid width.

1.1. Characterizing Free Surface Convection and Comparing it with Fixed Surface Data

The results of the deep pool, thermo-electric cooler experiments have been tabulated in Appendix E and are plotted on Figs. VI-1, 2, 3, and 4. The fixed surface results, as shown in Chapter V, Fig. V-1 have been plotted with the free surface results to permit clearer identification of density-driven effects.

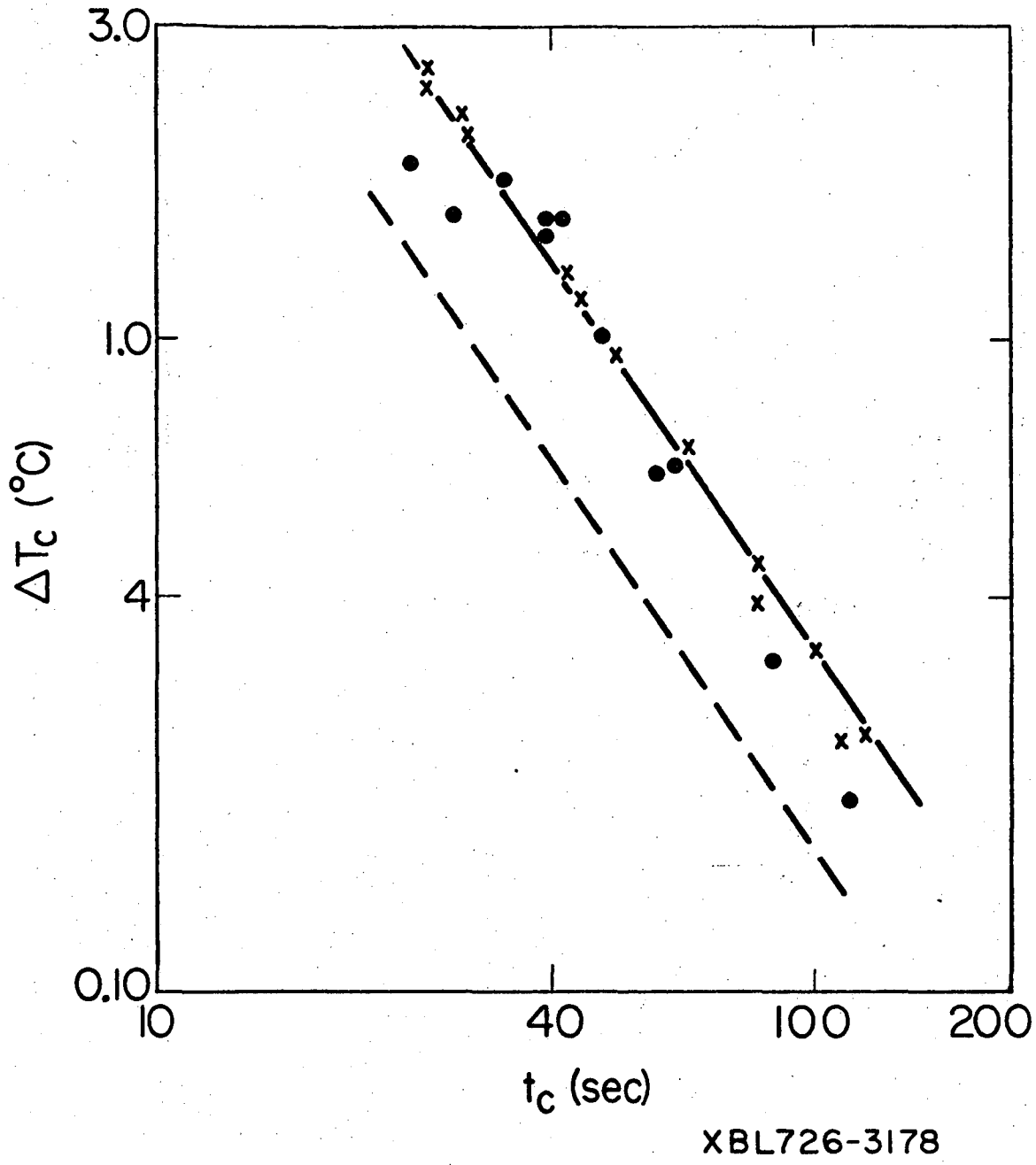

Fig. VI-1. Experimental Conditions of Onset of Convection in n-Decane (Pr = 13) for a linear surface temperature decay in a deep pool using the Thermoelectric Cooler. X Fixed Surface data, ● Free Surface data, - - Free Surface Predictions of Mahler (1970).

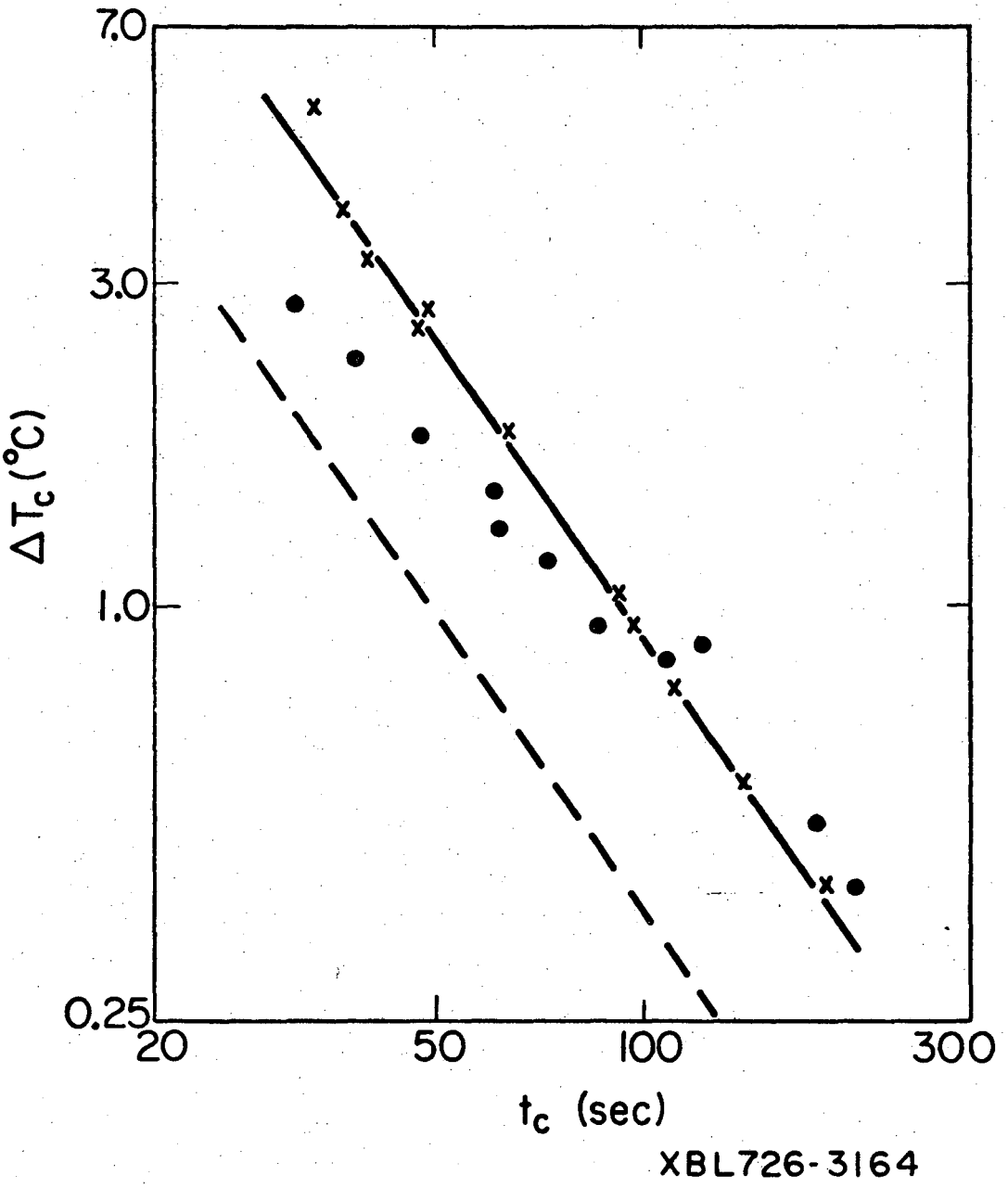

Fig. VI-2. Experimental Conditions of Onset of Convection in n-Butanol (Pr = 43) for a linear surface temperature decay in a deep pool using the Thermoelectric Cooler. X Fixed Surface data, ● Free Surface data, - - Free Surface Predictions of Mahler (1970).

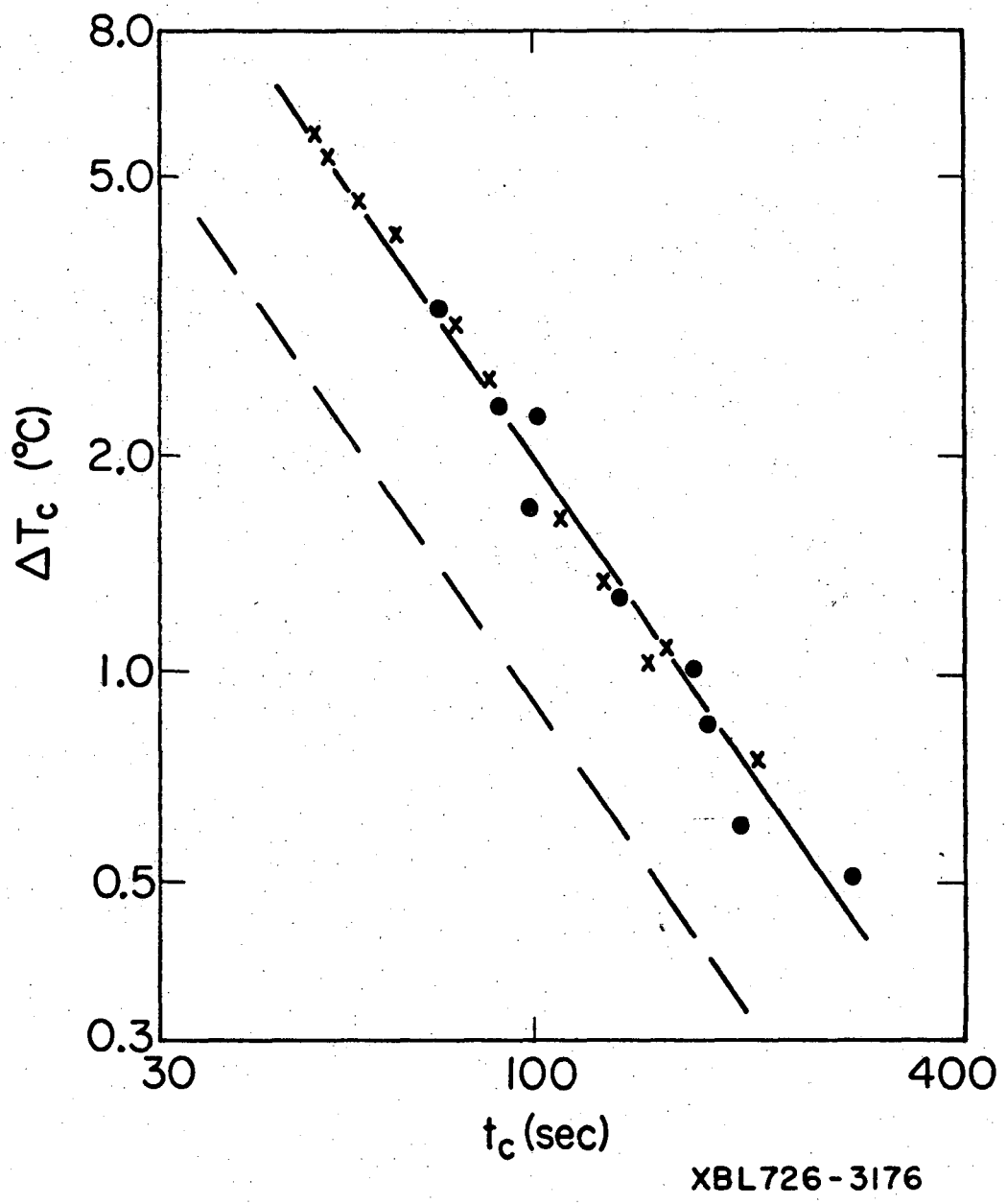

Fig. VI-3. Experimental Conditions of Onset of Convection in n-Octanol (Pr = 108) for a linear surface temperature decay in a deep pool using the Thermoelectric Cooler. X Fixed Surface data, ● Free Surface data, - - Free Surface Predictions of Mahler (1970).

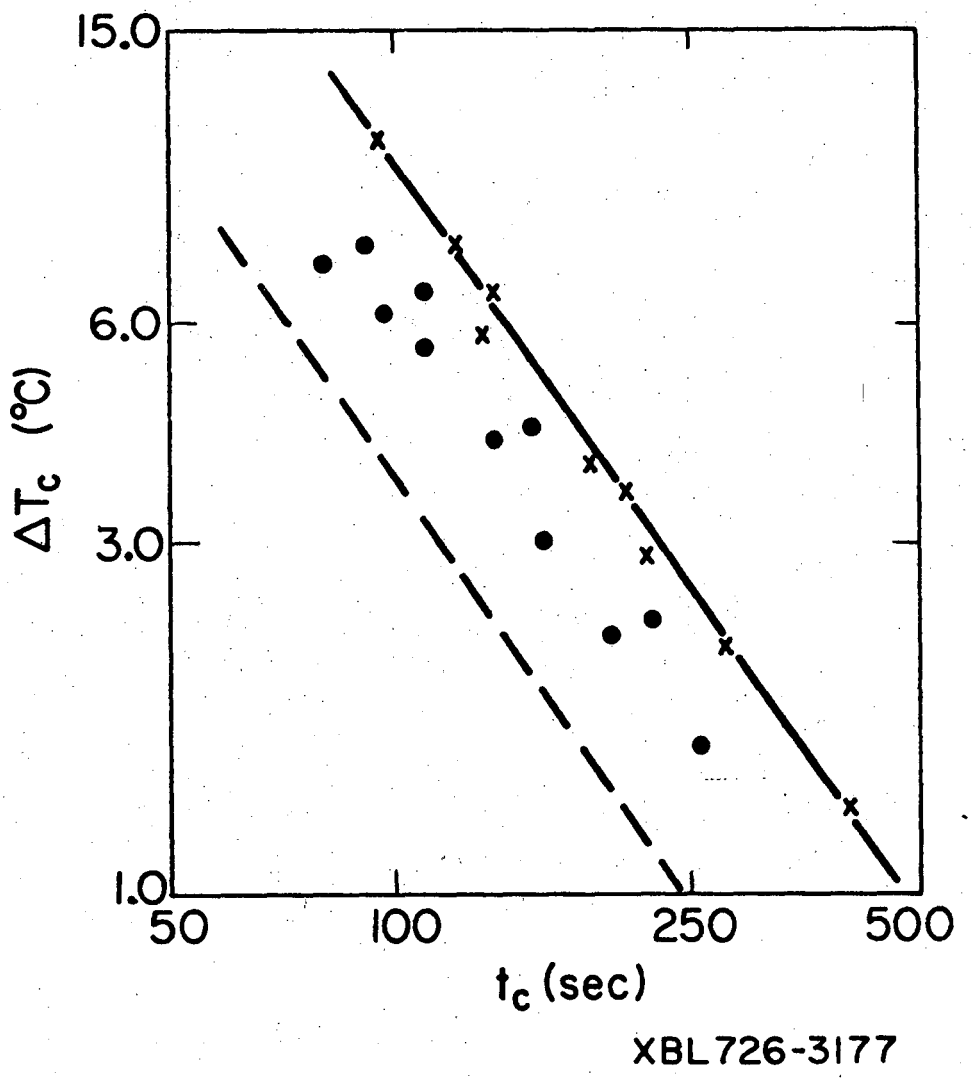

Fig. VI-4. Experimental Conditions of Onset of Convection in Silicone Oil 100 cs (Pr = 890) for a linear surface temperature decay in a deep pool using the Thermoelectric Cooler. X Fixed Surface data, ● Free Surface data, - - Free Surface Predictions of Mahler (1970).

The results for n-decane, n-butanol, n-octanol, and 100 cs Silicone Oil at the slower heating rates (large t_c, small ΔT_c) obey the relation $\Delta T\, t_c^{3/2}$ = constant. This indicates that convection at these conditions is density-driven.

Mahler, et al. (1970) using Amplification Theory calculated the ratio of the Rayleigh numbers at fixed and free surfaces for a step change in surface conditions and an amplification factor of 1000. The ratio was found to be 1.93 at Pr = 7 and 2.62 at Pr = 600. Foster (1968) calculated this ratio as 1.95 for infinite value of Pr and a step change of surface conditions.

Q.S.A. has been used to calculate Ra_t = 32 for two fixed surfaces (Currie, 1967) and Ra_t = 5.4 for two free surfaces (Lick, 1965). By comparing the results of different shear conditions for the linear density profile, which have been tabulated by Berg et al. (1966) and which are: fixed-fixed (Ra_H = 1700), fixed-free (Ra_H = 1100), free-free (Ra_H = 650), and assuming that the ratios between these results holds for the Q.S.A. analysis, the ratio of fixed to free surface deep pool Rayleigh number according to Q.S.A. would be 3.5 ($= \frac{32}{1700} \times \frac{650}{5.4} \times \frac{1700}{1100}$).

Generally, the free surface results in Figs. VI-1, 2, and 3 have the same value as the fixed surface results, and when they fall below the fixed surface results it is not as low as the current theories predict. The free surface results are lower than the fixed surface results only in experimental regions of high driving force (low t_c-- Fig. VI-2) or long conduction times (Fig. VI-4). It is in these experimental regions that

(1) surface tension-density force coupling, and/or

(2) side effects inherent in the experimental equipment

become important as destabilizing effects. These are discussed in the following paragraphs.

The ratio of surface tension forces to density forces ($= M_t/Ra_t$) in the deep pool case for a particular fluid is proportional to $1/t_c$. Thus, as t_c increases, coupling between surface tension and density driving forces would become increasingly important and could lead to the decrease in stability of the fluid.

The side effects are possibly due to two-dimensional character in the liquid surface temperature. At high cooling rates (small t_c, large ΔT_c) there was a greater possibility for the cooler surface to develop a two-dimensional character inherent within the design of the thermo-electric cooler. This effect was demonstrated with the 100 cs Silicone Oil results. These results initially showed free-surface Rayleigh numbers about a factor of three lower than the fixed surface results. On the supposition that the layer between the heat pump and the cold plate could have been damaged, which would permit two-dimensional character on the cold plate, the layer was relaid and the free surface Rayleigh numbers were found to be only slightly less than the fixed surface results, as shown in Fig. VI-4.

For longer cooling periods, as in the 100 cs Silicone Oil experiments, the difference in thermal properties between the Plexiglass and the liquid could become important.

The meniscus effect, which had been minimized in this apparatus, could also have been important if a two-dimensional character of the

surface temperature developed. It was found in preliminary experiments that the presence of a surface-temperature gradient could lower the critical Rayleigh number, even without surface-tension-driven motion. This is also in agreement with the observations of Burger (1971), and Berg and Morig (1969).

The observations that improved, i.e., more isothermal, thermoelectric cooling surfaces increased the value of the critical conditions (t_c, T_c) significantly, and that most of the free surface results lay on a -3/2 slope, indicate that lateral temperature gradients rather than surface tension-driven coupling from the vertical gradient was the cause of destabilization in these experiments.

The experimental regions where the free surface data have values similar to the fixed surface data are least influenced by the above destabilizing effects. Thus, the results show that convection initiation is independent of the shear conditions at the heating or cooling boundary, in the absence of destabilizing effects in a vertical one-dimensional, deep pool density field.

This result differs from the predictions of both Q.S.A. and Amplification Theories, a point which is considered further in Chapter VII, Sec. 1.4. This conclusion also differs from the conclusion and experimental results of Mahler and Schechter (1970). They observed that the onset time at a contaminated aqueous surface (defined as a fixed surface) was almost double that at a non-contaminated surface, defined as free surface. The experimental conditions in these experiments (see Chapter II, Sec. 1.3.2.) and in the present study were different. In

order to appreciate this difference, the experimental conditions of Mahler and Schechter and their forerunners, Blair and Quinn (1969), will be considered briefly.

Sulfur dioxide was absorbed into water to produce the unstable density gradient in both studies. Blair and Quinn observed that when a wire mesh was held across the contaminated aqueous surface, the onset times were the same as those without the wire mesh, after the absorption rate had been corrected for the reduction in transfer area by the wire mesh. They concluded that this showed that a contaminated aqueous surface acted like a fixed surface.

When the water surface was partially covered with natural contaminant (insoluble surfactant) and partially covered with oleic acid (soluble surfactant) so that the surface pressure across the surface was at equilibrium, the onset time under the contaminant was 24 seconds while the onset time under the oleic acid was 20 seconds. The form of motion under each surface was also observed to be different. The difference between the two surfaces was attributed to differences in surface compressibility, which effected the lateral rigidity of the surface. Thus, Blair and Quinn concluded that the less rigid the surface, the earlier the onset time. Mahler and Schechter extended this work by observing the effect of different types of surfactants.

There appear to be two possible explanations of these results of these two previous studies:

1) Less rigid surfaces have smaller onset times in one-dimensional, density-driven convection.
2) There is a side effect in the experiments which lowers the onset time as the surface rigidity is decreased.

Mahler and Schechter assumed Explanation 1 without considering Explanation 2. If (2) is possible, what effects can lower the stability at a gas-liquid interface? Experiments have shown that the presence of surface waves at a gas-liquid interface can lower onset times. See for example, Chapter VI, Sec. 1.2., where the spray cooler generated surface waves and produced onset times in n-decane which were approximately 50% lower than those produced by the vibration-free thermo-electric cooler. As the liquid viscosity increased, the effect of surface waves decreased, and the density boundary layer at the onset was generally thicker (see Fig. V-1).

When the instability is produced in water by mass transfer, both the viscosity and the density boundary layer thicknesses are in the range where surface waves should be important. The surface waves are generated by building vibrations, but are reduced in special cases, such as in the vibration-free table described in Chapter III, Sec. 4. The second source of vibration is in the mechanical action which increased the sulfur dioxide partial pressure suddnely so as to approximate a step change in these experiments. Since the instability occurred between 10 and 20 seconds, this mechanical action would be significant. The magnitude of the surface waves would be expected to decrease as the surface rigidity increased. The presence of surfactants would increase stability (i.e., lengthen onset times) because they increase the surface rigidity and dampen the surface wave action.

These comments apply equally to the results of Mahler and Schechter and those of Blair and Quinn. The conclusion from comparison of the sulfur dioxide-water absorption experiments with the heat transfer results is that surface waves on a gas-liquid interface, rather than the surface

rigidity, are the cause for the difference found between onset times at "free" and "fixed" surfaces in the sulfur dioxide-water absorption experiments.

1.2. Effect of Variation of Surface Temperature Profile

The results of the deep-pool spray-cooler experiments have been tabulated in Appendix F and are plotted in Figs. VI-6 through VI-11.

The correlating parameter used to describe the shape of the surface temperature vs. time profile was

$$S = \frac{\text{area under surface temperature curve up to } (t_c, \Delta T_c)}{\text{area given by } t_c \times \Delta T_c}$$

$S = 1$ for a step change, and

$S = 0.5$ for a linear decay

This was the simplest parameter that could describe the surface temperature curve. It has the drawback that several curve shapes can be described by a given value of S (see Fig. VI-5). An additional parameter, a non-dimensional first moment of the curve about the temperature axis, was used to differentiate qualitatively between curves with similar values of S, but different curve shapes.

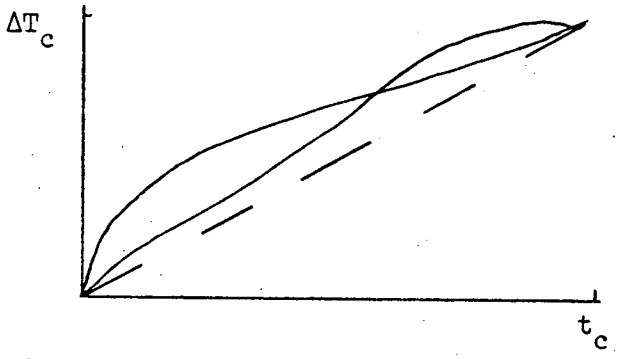

Fig. VI-5. Curves with different shapes but same value of Shape Factor S.

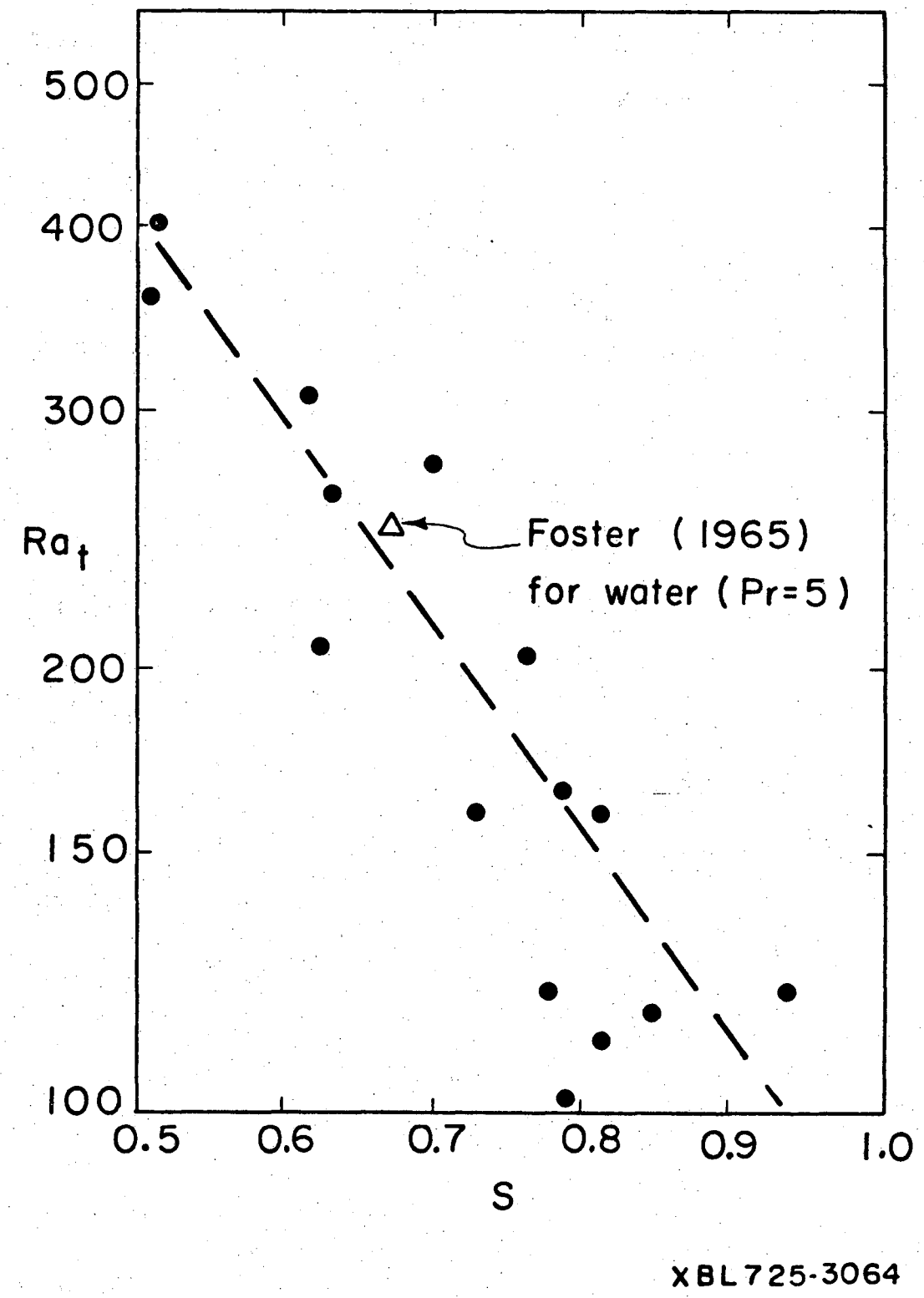

Fig. VI-6. Experimental values of Ra_t as a function of the Surface Temperature Shape Factor(S) for n-Decane in the Deep Pool Case using the Spray Cooler.

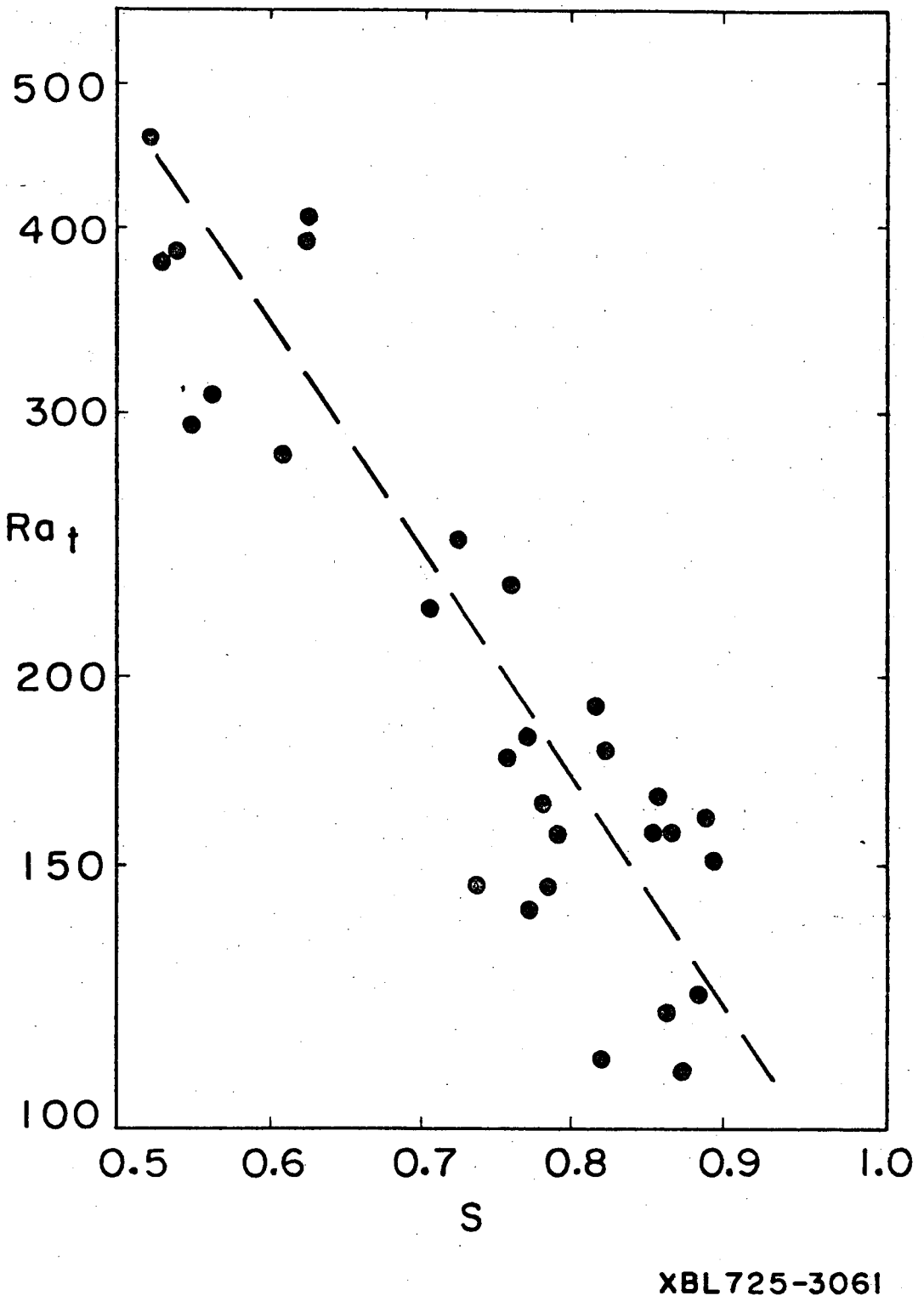

Fig. VI-7. Experimental values of Ra_t as a function of the Surface Temperature Shape Factor(S) for n-Undecane in the Deep Pool Case using the Spray Cooler.

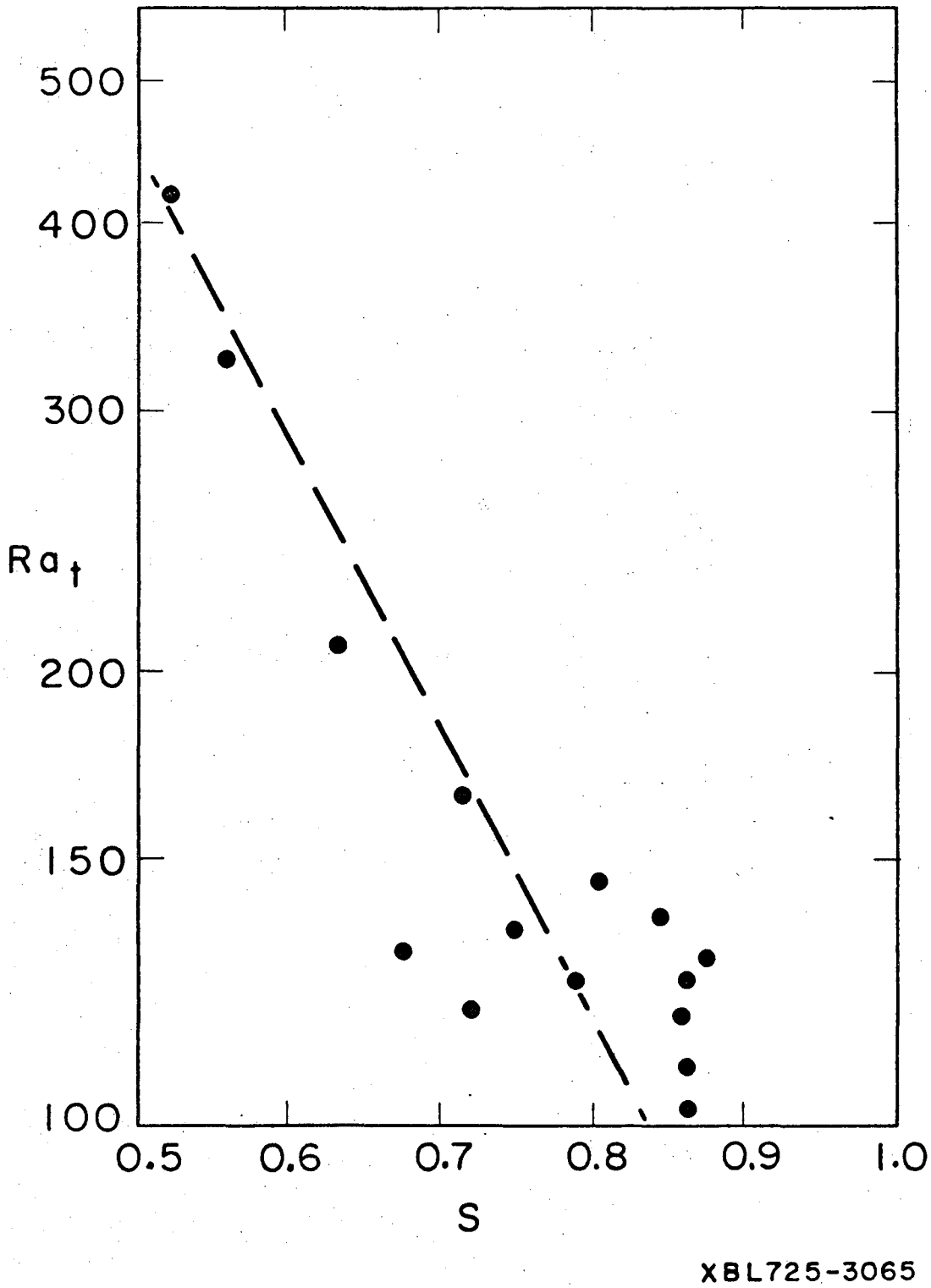

Fig. VI-8. Experimental values of Ra_t as a function of the Surface Temperature Shape Factor(S) for n-Butanol in the Deep Pool Case using the Spray Cooler.

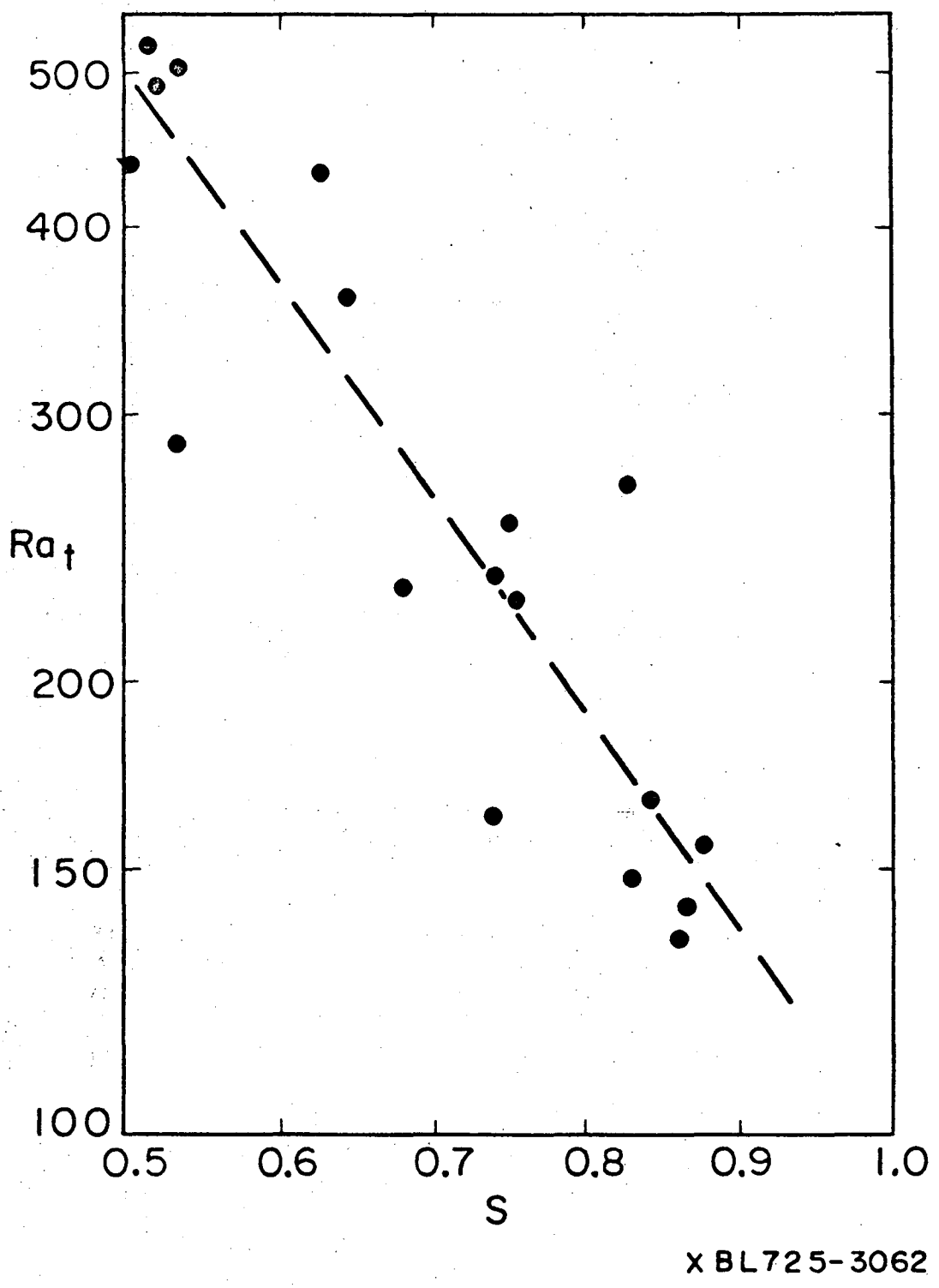

Fig. VI-9. Experimental values of Ra_t as a function of the Surface Temperature Shape Factor(S) for n-Hexanol in the Deep Pool Case using the Spray Cooler.

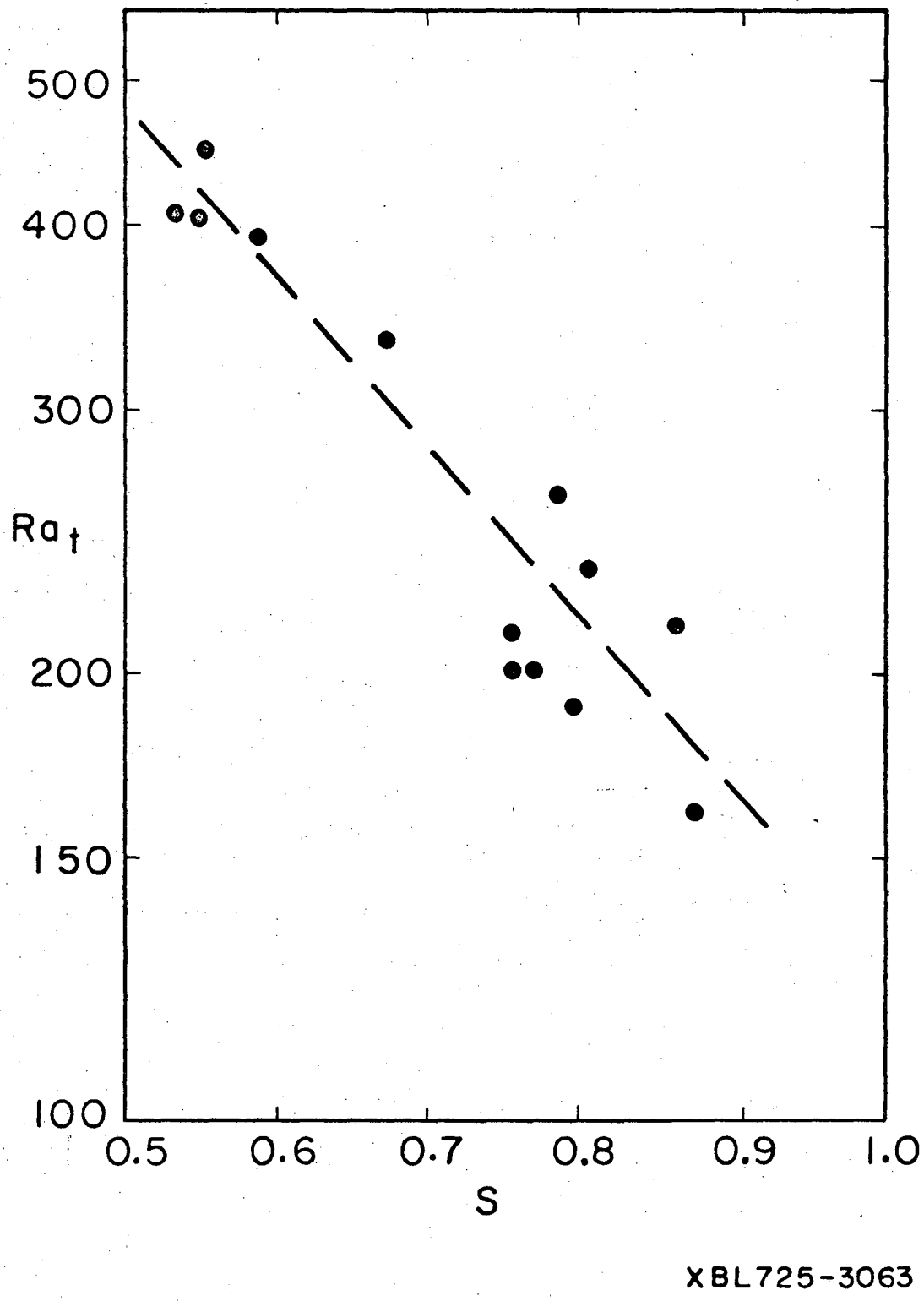

Fig. VI-10. Experimental values of Ra_t as a function of the Surface Temperature Shape Factor(S) for n-Octanol in the Deep Pool Case using the Spray Cooler.

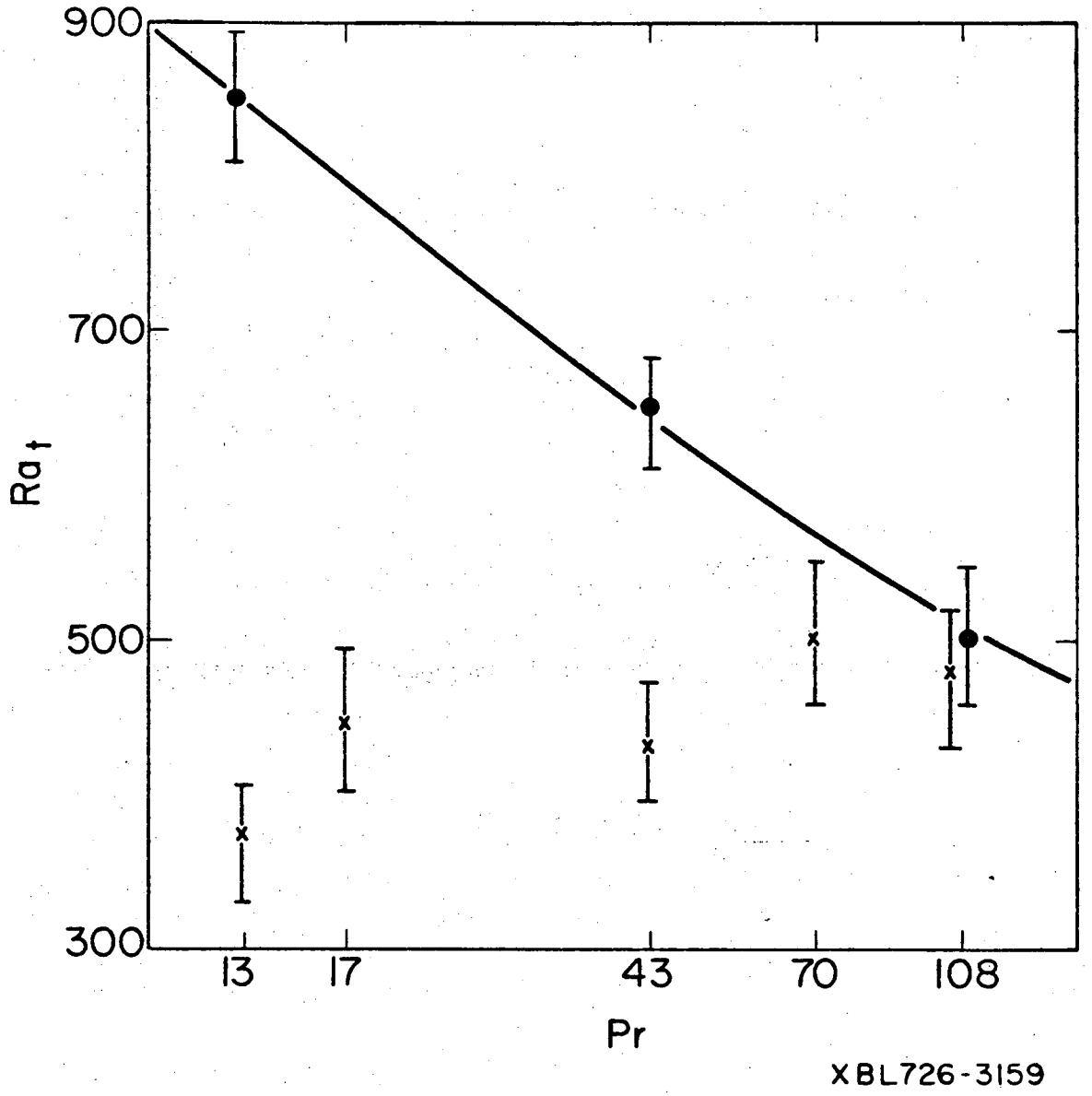

Fig. VI-11. Comparison of Values of Ra_t at a Free-surface determined with the Spray Cooler (⊼) and the Thermoelectric cooler (⊥), for a linear surface temperature decay (S = 0.5).

The results show that Ra_t decreases as S increases in the range $0.5 < S < 0.85$. Curves with $S > 0.85$ were difficult to produce, because of the shallowness of the initial slope and its rounding off into the plateau temperature segment. These same limitations would hold for almost any type of step-function production where the time to reach the plateau is comparable to the convection time.

The scatter is probably due to a number of causes. First, the definition of S did not uniquely describe a curve, as pointed out above. The curves were reviewed to see if there was a trend with respect to the first moment of the curve, but no significant trend was found. This could be due to the fact that the decrease in Rayleigh number in the Rayleigh number-vs-S relationship occurs most sharply for curves with only small deviations from linear profiles in which S almost uniquely describes the curves (refer to Fig. VI-5).

The second possible reason for scatter in the effect of gravity upon the instability. Due to the spray action in the spray cooler, vibrations could have been introduced into the system and could have produced waves on the surface of the liquid. The presence of surface waves would account for the difference in Ra_t between the spray cooler results and the fixed surface results at low Pr (Fig. VI-11). The variation in Pr was produced by varying the liquid viscosity, and it is possible that the size of the surface waves and their consequent effect on the stability of the thermal layer increased with decreasing viscosity. A theoretical study by Berg (1966) on surface tension effects showed that surface deformation can result in a decrease of stability.

The third possible reason for scatter is the coupling effect between surface-tension and density-driven convection. However, the results of Sec. 1.1. imply that the coupling effect is probably negligible in these experiments.

From the foregoing, the more viscous liquids, n-octanol and n-hexanol, appear to have less surface deformation than the less viscous liquids, and hence should be closer to the theoretically analyzed cases. Indeed, the linear surface temperature (S = 0.5) decay for n-octanol can be extrapolated to Ra_t = 500, which is the same result as obtained with the thermo-electric cooler which was free of surface waves (refer to Figs. VI-10 and VI-11). Comparison of the results with theoretical predictions is discussed in Chapter VII, Sec. 1.2.

1.3. Comparison of Deep Pool, Free Surface Results with Literature Results

Foster (1965) and Spangenberg and Rowland (1959) published results for convection where water was evaporated from stagnant pools. These results have been tabulated in Appendix A. Although Foster identified the surface temperature-vs-time curves as a linear decay of surface temperature with time (S = 0.5), Vidal and Acrivos (1969) found that evaporation from stagnant pools could be better described by a constant flux at the evaporation surface. A curve with constant flux would have S = 0.67. The typical surface temperature curve that Foster worked with, which was published with his results, can also be described by S = 0.67. Foster's results for evaporation of water of Ra_t = 255 with S = 0.67 and Pr = 6.6 agree well with the results of n-decanol (Pr = 13) using the spray cooler (Fig. VI-6). The fact that these data compare better with

the spray cooler results than with the thermo-electric cooler results (refer to Fig. VI-11) indicates the possibility of surface-wave influence in Foster's experiments.

Clark and King (1970) published results for evaporation of carbon disulfide from tridecane solvent (see Appendix A). Although the liquid system was moving in laminar flow, density-driven convection could be identified by Ra_t = 285, S = 0.62, for thermal-driven convection at Pr = 27. Comparison with the spray cooler results for n-butanol (Pr = 48) and n-undecane (Pr = 18) is good, considering the hydrodynamic difference between a stagnant pool and a laminar flowing stream.

Ball and Himmelblau (1967) identified density-driven convection for the absorption of carbon dioxide into a laminar flowing aqueous stream (see Appendix A). The mass-transfer-driven Rayleigh number (Ra_t) was reported at 785 with Sc = 300, but the thermal-driven Rayleigh number was not reported. Since the absorption was exothermic, the thermal gradient would tend to stabilize the system, which may account for the high value of Ra_t when compared with the present results where no stabilizing influence was present.

2. Shallow Pool Results

The results of the shallow pool experiments using both the spray cooler and thermo-electric cooler have been recorded in Appendix F, and are plotted on Figs. VI-12, 13, 14, and 15. The apparatus and experimental technique used were described in Chapter IV, Sec. 3.2. The surface temperature changed linearly with time so as to be compared with the fixed-surface, shallow-pool data of Chapter V, Sec. 2.

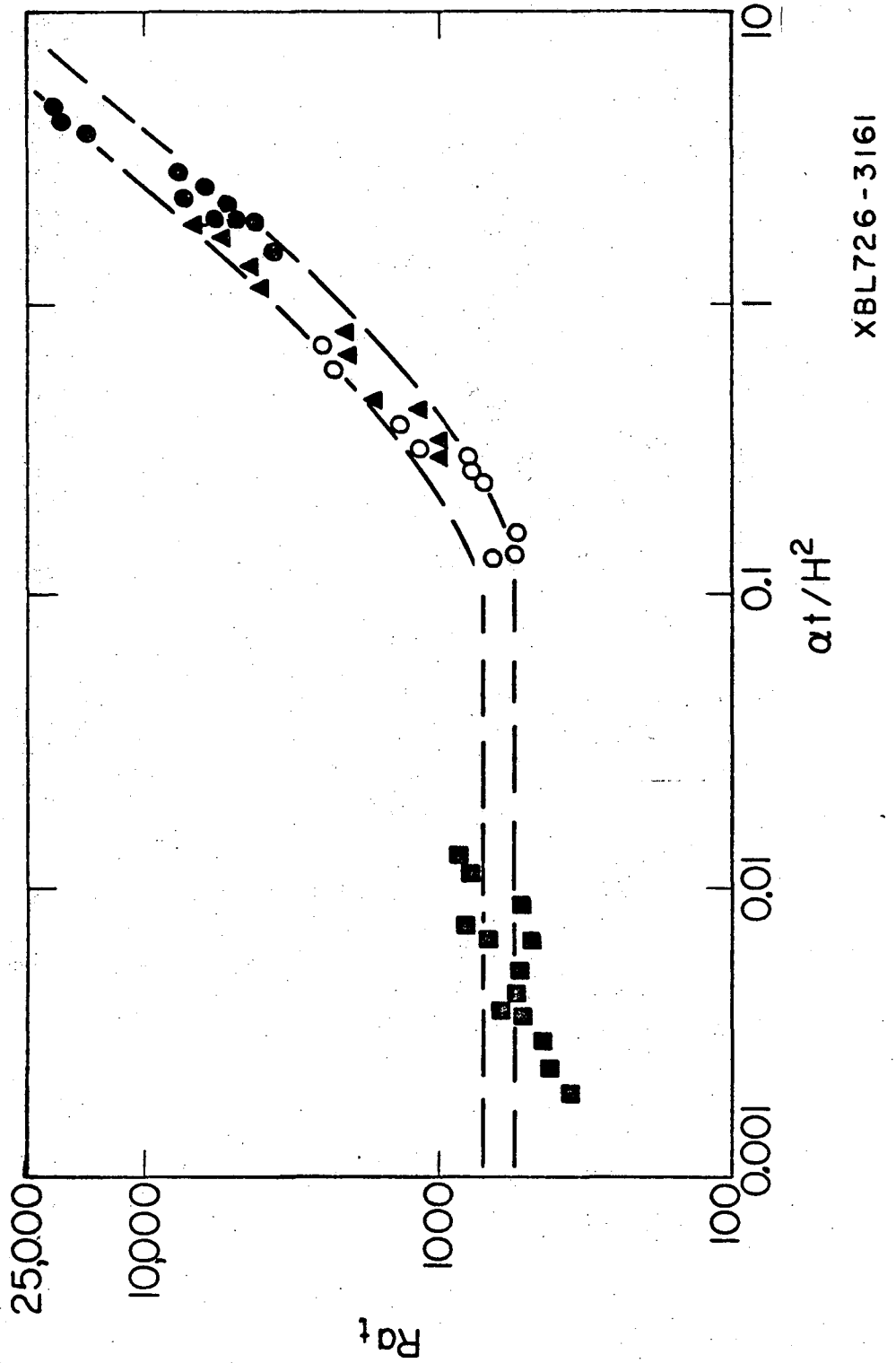

Fig. VI-12. Experimental values of Ra_t at a Free Surface as a Function of Depth Factor ($\alpha t/H^2$) for n-Butanol. The linear decay of surface temperature with time was produced with a thermoelectric cooler.

Fluid Depth: ■ 36.5 mm ▲ 3.3 mm
○ 5.0 mm ● 2.16 mm

- - Limits of Fixed Surface Results from Fig. V-7.

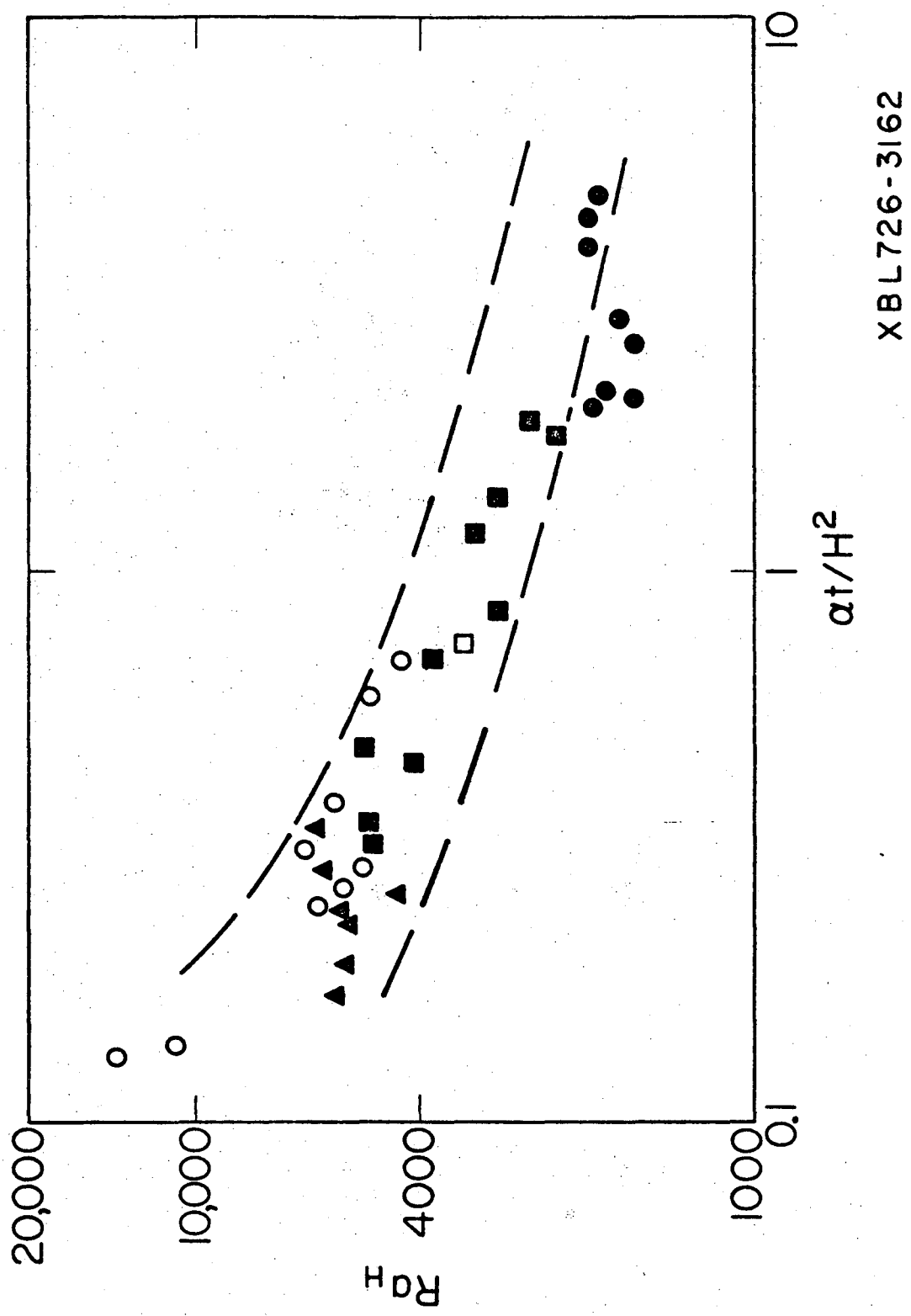

Fig. VI-13. Experimental values of Ra_H at a Free Surface as a Function of Depth Factor ($\alpha t/H^2$) for n-Butanol using the Thermoelectric Cooler. Fluid Depth: ○ 5.0 mm, ■ 3.3 mm, ● 2.16 mm. Spray Cooler data for $0.5 < S < 0.6$, see Fig. VI-15. ▲ n-Butanol, □ n-Octanol, - - - Boundaries of Spray Cooler data for $0.5 < S < 0.8$.

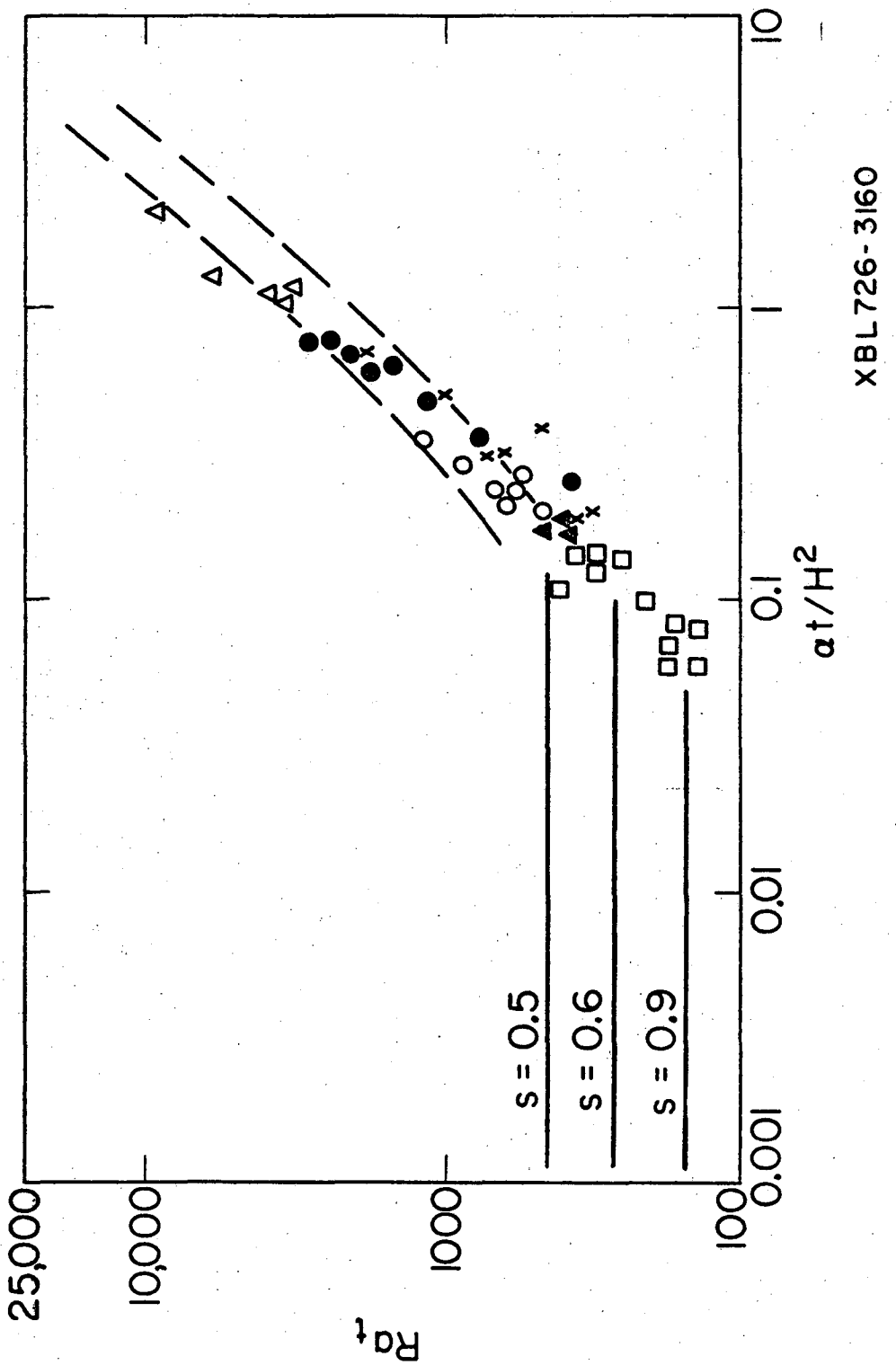

Fig. VI-14. Shallow pool results for Surface Curves produced by the spray cooler and with $0.5 < S < 0.8$. Ra_t vs. $(\alpha t/H^2)$. Fluid depth: n-Butanol ○ 5.0 mm $0.5 < S < 0.6$, ▲ 5.0 mm $0.6 < S < 0.7$, □ 5.0 mm $0.7 < S < 0.8$, Δ 3.3 mm $0.6 < S < 0.7$, 3.3 mm $0.7 < S < 0.8$, n-Octanol X 5.00 mm
– – Boundaries of fixed surface data for S = 0.5.
—— Deep pool asymptote for various values of S.

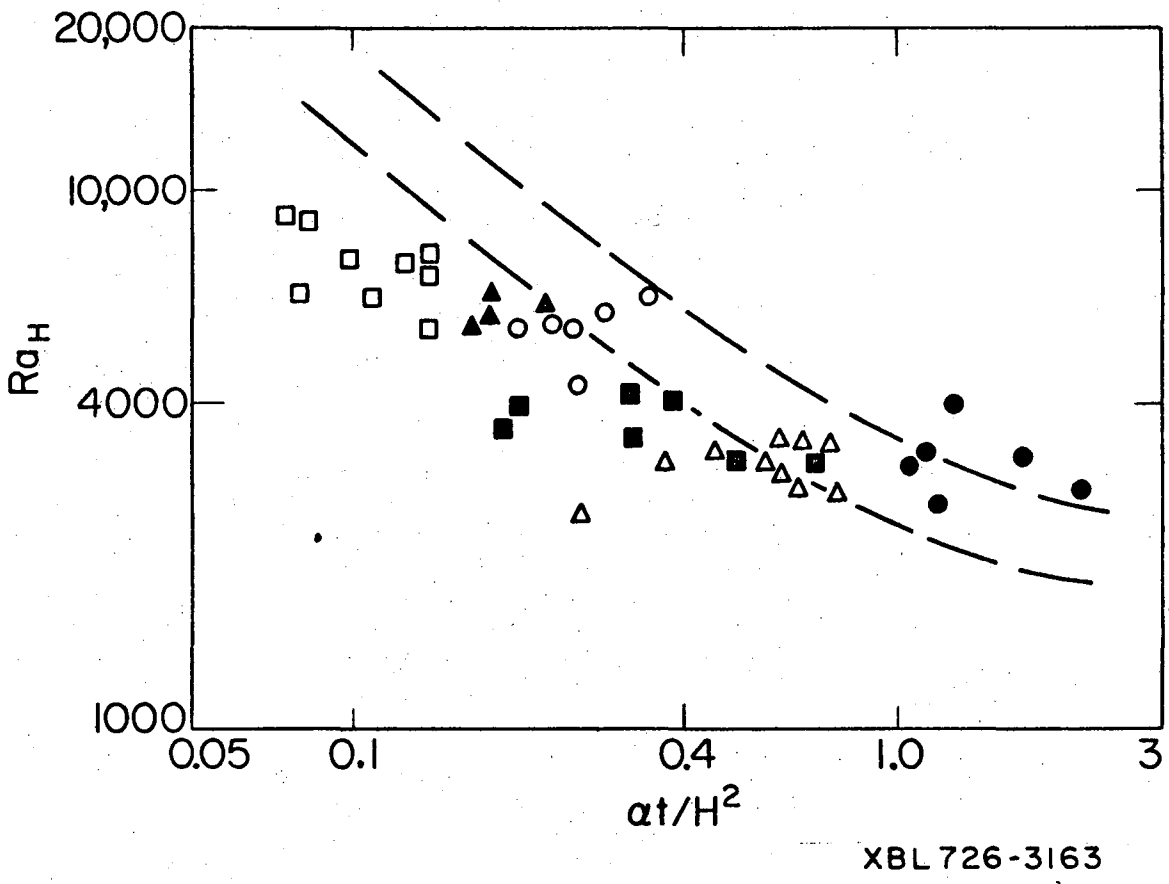

Fig. VI-15. Shallow pool results for Surface Curves produced by the spray cooler and with $0.5 < S < 0.8$. Ra_H VS. $(\alpha t/H^2)$. Fluid depth:

n-Butanol
- ○ 5.0 mm $0.5 < S < 0.6$
- ▲ 5.0 mm $0.6 < S < 0.7$
- □ 5.0 mm $0.7 < S < 0.8$
- ● 3.3 mm $0.6 < S < 0.7$
- △ 3.3 mm $0.7 < S < 0.8$

n-Octanol
- ■ 5.00 mm

- - Boundaries of fixed surface data for S = 0.5

From the results of the fixed-surface, shallow-pool data it was apparent that both time (t_c) and fluid depth (H) were important in the description of shallow-pool convection initiation. Consequently the data have been plotted in terms of Ra_t (time-dependent Rayleigh number, Figs. VI-12, 14) and Ra_H (fluid-depth dependent Rayleigh number, Figs. VI-13, 15) to illustrate the time and fluid depth effects.

The free-surface, shallow-pool data (Figs. VI-12, 13, 14, and 15) appear to have the same values as the fixed-surface, shallow-pool data. This shows that the mechanism for convection initiation at these two surfaces in the shallow pool case is the same, or that convection onset in these experimental conditions for free-surface, shallow pools is density-driven. This is true even for thin liquid films (2 mm) and high values of Marangoni number (M_t = 10,500; M_H = 5,200).

This conclusion is in contradistinction to previously published work on convection initiation in thin films of evaporating, pure, organic liquids. Berg, et al. (1965), and Vidal and Acrivos (1967) found convection initiation at Ra_H much below 1700 and so ascribed surface-tension force as the driving force. These results were duplicated in our laboratory when a temperature gradient existed along the liquid surface, which can be expected in evaporation experiments (see Appendix B). When this surface gradient was eliminated, the results could be described by Figs. VI-12 to 15. Thus, this study shows that previously published results for thin-film, free-surface, thermal convection produced by evaporation did not conform to the theoretical models used to describe surface-tension-driven and density-driven convection, because of the temperature gradient along the liquid surface in those experiments.

The comparison between the spray cooler and thermo-electric cooler results given on Fig. VI-13, shows that the influence of the vibrations is not important in shallow-pool convection. This is probably due to the size of the gravity waves in this experimental apparatus being reduced by the shallow depth of liquid.

The scatter in results can possibly be identified with uncertainty in the height of the liquid used. Although care was taken to fill the vessels to the planar level of the top of the walls, the liquid heights could have been slightly less than those recorded. This would account for some free-surface values lying above the fixed-surface results on Fig. VI-14. There could also have been some surface tension-density coupling, but this was difficult to determine since one plot could not separate the following two effects:

1) Marangoni force-Density force coupling

2) Marangoni number vs $\frac{\alpha t}{H^2}$ relationship.

Some scatter could also arise from side effects discussed in Sec. 1.1.

VII. DISCUSSION OF RESULTS

1. Evaluation of Models Describing Time-Dependent Convection in Deep Pools

The models describing density-driven convection initiation have been discussed in Chapter II, Sec. 1.3. and are briefly summarized as follows. They fall into two classes depending upon the relative magnitude of the time to establish an unstable density gradient, and the growth time of the disturbance. When the growth time is assumed negligible the marginal stability assumption is invoked. The type of model used then depends upon the nature of the density gradient through the fluid layer. A linear gradient through the fluid has been successfully examined using the time-independent model. The curved density gradient, arising in transient transfer processes, has been examined using the Q.S.A. approach, which freezes the density profile in time. When the growth time is comparable to the time to establish the unstable density profile, the marginal stability assumption has been shown to be invalid (Robinson, 1965). Under these conditions, the phenomenon has been studied using Amplification Theory.

The purpose of this section is to evaluate the strengths and weaknesses of the Q.S.A. and Amplification theories describing convection initiation in a wide, deep pool. The shallow-pool, time-independent model has been well established theoretically and experimentally and can be used as a reference for judging the validity of the marginal stability assumption when applied to non-linear density profiles. Mathematical comparison between the Q.S.A. and Amplification theories by Robinson (1965), Foster (1968), and Gresho and Sani (1970) has highlighted features of both theories and rejected the Q.S.A. approach as invalid for deep pool analysis.

Such a comparison is suspect since the form of the developing disturbance has not yet been established and therefore has to be assumed. This assumption is the basis for the "mathematical" comparison. The analysis in this section compares the predictions of the two theories with experimental evidence. Such a comparison has no assumed basis as for the former comparison, and would therefore appear to be more practical in its evaluation.

The equations of motion, linearized around zero fluid velocity and the conduction profile $\frac{\partial T}{\partial z}$, are shown below (refer to Chandreskhar, 1962) to illustrate the effect of invoking the marginal stability assumption, a factor which distinguishes between Q.S.A. and Amplification theories. Prior to making the assumption, the equations are as follows (as used in Amplification theory):

$$\frac{\partial T}{\partial z^2} = \frac{\partial T}{\partial t} \tag{VII-1}$$

$$(\frac{\partial}{\partial t} - \nabla^2)\theta = - \sqrt{Ra}\, w \frac{\partial T}{\partial z} \tag{VII-2}$$

$$[\frac{1}{Pr} \frac{\partial}{\partial t} - \nabla^2]\, \nabla^2 w = - \sqrt{Ra}\, \nabla_2{}^2 \theta \tag{VII-3}$$

Assumption of marginal stability causes the time derivatives to be eliminated from these above equations. Thus the equations used with this assumption are:

$$\frac{\partial^2 T}{\partial z^2} = 0 \tag{VII-4}$$

$$- \nabla^2 \theta = - \sqrt{Ra}\, w \frac{\partial T}{\partial z} \tag{VII-5}$$

$$- \nabla^4 w = - \sqrt{Ra}\, \nabla_2^2 \theta \qquad \text{(VII-6)}$$

1.1. Ra_t Independent of Heating Rate

Both Q.S.A. and Amplification theories predict that Ra_t is independent of heating rate for a specified type of heating, and all other conditions constant.

Experimental results reported in Chapter V, Sec. 1., and the results of Foster (1969) verified this prediction for a linear change in surface temperature with time. Other types of density change which have also shown this conclusion include Blair and Quinn (1969) using a step change in surface conditions, and Onat and Grigull (1970) and Foster (1965) using a constant flux at the surface.

1.2. Variation of Ra_ℓ with the Shape of the Density Profile in the Liquid

Currie (1967), using Q.S.A. theory, predicted that Ra_ℓ, where ℓ is the effective thermal depth (refer to Chapter II, Fig. II-2), was independent of the shape of the density profile in the fluid. Ra_ℓ $(= Ra_H \cdot (\frac{\ell}{H})^3)$ was calculated as a function of $(\frac{\ell}{H})$, and the time required to attain Ra_ℓ for a specified value of $(\frac{\ell}{H})$ was governed by the shape of the density profile in the fluid.

Foster (1968), using Amplification Theory, studied the cases of a step change in the surface temperature (Case A), and a linear change of surface temperature with time (Case B). From Figs. 3 and 5 of his paper, the ratio of the time-dependent Rayleigh number Ra_t at the large Pr asymptote and an amplification factor of 10^8 for the two cases was read

and evaluated as 3.0. The same ratio at the small Pr asymptote ($Ra_t \cdot Pr$ = constant) was read and evaluated at 2.3. The ratio of effective thermal layer depth (ℓ) to penetration depth ($\sqrt{\alpha t}$) was different for each case (refer to Fig. VII-1), but after Ra_t was transformed to Ra_ℓ, the values of Ra_ℓ for each case at high Pr were approximately equal. At the low Pr asymptote, the value of Ra_ℓ for the step function was approximately 45% greater than that for a linear decay. Considering the accuracy involved in reading data from Foster's paper, it would appear that Amplification theory agrees with Q.S.A. theory at high values of Pr in predicting Ra_ℓ to be independent of the shape of the density profile in the fluid, and hence the nature of the forcing function.

The experimental data were measured in the form Ra_t (Chapter V, Sec. 1.) for n-octanol (Pr = 108), a high Pr fluid. The values of Ra_ℓ were derived through the transformation $Ra_\ell = Ra_t \cdot \left(\frac{\ell}{\sqrt{\alpha t}} \cdot A\right)^3$ where A is a constant relating ℓ to the penetration depth scale ($\sqrt{\alpha t}$) and has a value dependent upon the form of the forcing function, as can be seen from Fig. VII-1. The transformation requires a knowledge of A^3 as a function of density profile shape in the fluid, which in turn is dependent upon the surface temperature-versus-time relationship. This can be seen from the following equations:

$$\frac{1}{2}(\ell/H) = \int_0^1 T(z)/T(0) \cdot d(z/H) \quad \text{(from Fig. II-2)} \tag{VII-7}$$

$$T(z,t) = f(T(0,\tau),\ T(1,\tau),\ \frac{\alpha t}{H^2}) \tag{VII-8}$$

$$S = \frac{\int_0^t T(0,\tau)d\tau}{T(0,t) \cdot t} \quad \text{- assuming } T(1,\tau) = 0 \tag{VII-9}$$

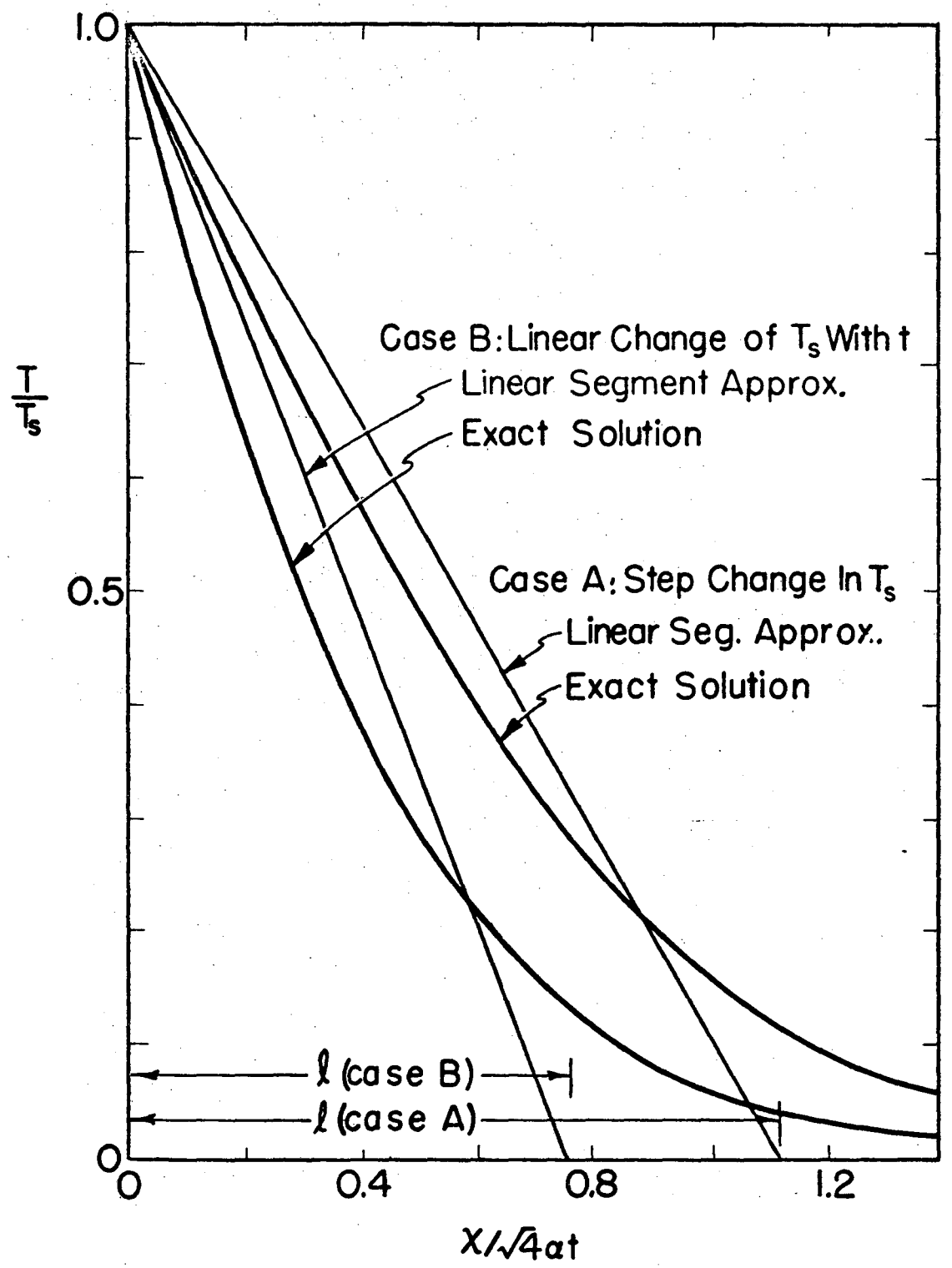

XBL 726-1127

Fig. VII-1. Effective Thermal Depths (ℓ) for a step change in surface temperature (Case A) and a linear Change in Surface Temperature with Time (Case B).

The surface temperature-versus-time curve can be described to a first approximation by the shape factor "S" (refer to Chapter VI, Sec. 1.2.). In order to calculate A as a function of S, the temperature profile in the fluid has to be expressed as a function of S. An observation of the mathematical equations involved shows that this is virtually impossible for the general case. However, the family of curves described by $T_s = kt^{n/2}$ can be used to find values of S and values of A for a particular value of n, which can lead to a relation between S and A for this family of curves. This relation can be used generally to give A for any T_s-versus-time function, if it is assumed that the values of A for all possible T_s-versus-time curves with the same value of S fall within a narrow range about that calculated above using the $T_s = kt^{n/2}$ family of curves. The following analysis is based on this assumption, since there did not appear to be any other reasonable alternative to find a general relationship between A and S. Calculations for A vs. S for the family of curves given by $T_s = kt^{n/2}$ for conduction into a semi-infinite medium have been discussed and plotted in Appendix H.

The values of Ra_t versus S obtained experimentally and reported in Chapter VI, Sec. 1.2. and Appendix I for fixed and free surfaces were cross-plotted with the relation between A versus S described above to give values of Ra_ℓ versus S (Fig. VII-2). The results show that Ra_ℓ is essentially independent of shape factor S at high values of Pr, as predicted from both theories. The scatter was probably due to the assumed generalized relation between A and S. The scatter for the linear time decay of T_s (S = 0.5) is shown to compare the scatter obtained for a particular type of T_s-versus-time curve.

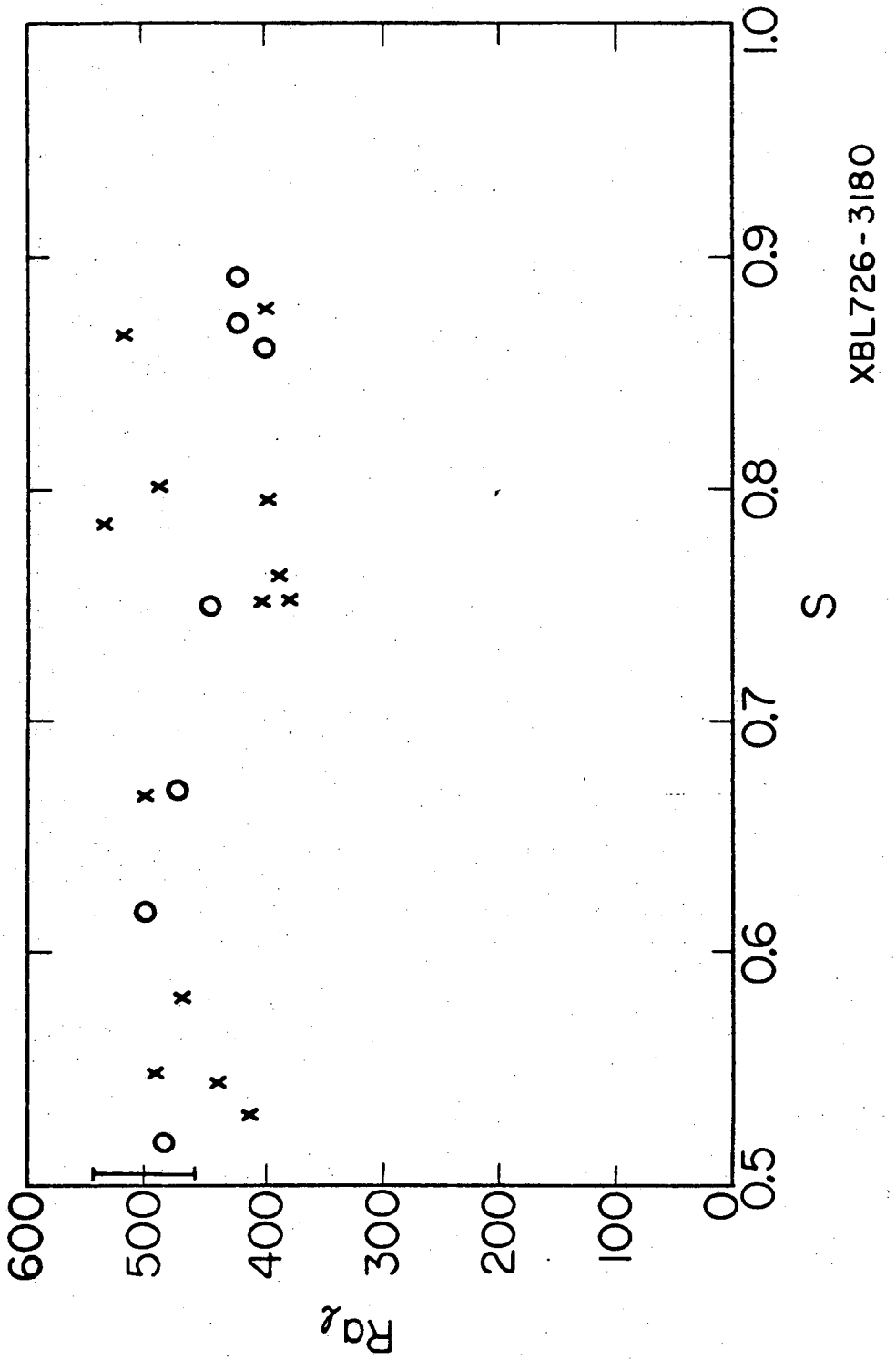

Fig. VII-2. Experimental values of Ra_ℓ for n-Octanol as a Function of the Surface Temperature Shape Factor S in the Deep Pool Case. O Fixed Surface, X Free Surface. I Scatter for linear decay of Surface Temperature using the thermoelectric cooler.

The possibility of Ra_ℓ being density-profile-shape dependent for a low Pr fluid, as predicted from Amplification theory, was not investigated. Air, a low Pr fluid could be used to study this effect.

1.3. Variation of Ra_ℓ with the Ratio of Thermal Depth to Fluid Depth

Currie (1967) used Q.S.A. theory to calculate Ra_H as a function of ℓ/H for a fluid bounded by two, perfectly conducting surfaces. His results were transformed into the form Ra_ℓ versus τ and plotted on Fig. VII-3.

There are no calculations published showing Ra_t as a function of $\frac{\alpha t}{H^2}$ using Amplification Theory. However, Mahler (1969) has shown that with shallow depths Amplification Theory predicts a maximum in the amplification factor versus time. This was interpreted by Mahler as showing that convection would not be observed if the maximum amplification factor was not great enough, even though the value of Ra_H was above the critical condition calculated using time-independent theory. For example, for a free-plus-fixed-surface shear case the time-independent critical condition was given by $Ra_H = 1100$, which has been observed experimentally by Berg and Palmer (1971). Mahler calculated that the maximum amplification factor for $Ra_H = 2000$ was 40, and previously he had correlated deep-pool convection onset with an amplification factor of 1000. The indecisive nature of Amplification Theory in this example places suspicion on the utility of that theory at shallow depths, or low values of Ra_H.

The fixed-surface experimental results were recorded in Chapter V, Sec. 2 as Ra_t versus $\frac{\alpha t}{H^2}$. The values of Ra_t were transformed into Ra_ℓ

using the relationship between A and $\frac{\alpha t}{H^2}$ (refer to Sec. 1.2.) for a linear surface temperature change with time, which has been calculated and plotted in Appendix H. Ra_ℓ versus $\frac{\alpha t}{H^2}$ has been plotted on Fig. VII-3. The asymptotic value (Pr independent) at high values of $\frac{\alpha t}{H^2}$ is in the range of $Ra_\ell = 1700$, which is the time-independent solution for a linear gradient with fixed, perfectly conducting surfaces, and also the solution for Ra_ℓ where the marginal stability assumption has been shown to be valid (Chandrasekhar, 1962). Figure VII-3 shows that, for a fluid with an infinite Prandtl number, Ra_ℓ is essentially independent of $\frac{\alpha t}{H^2}$. This shows that the marginal stability assumption appears valid for deep pools, and infinite Pr fluids if the length scale in the equations of motion is taken as ℓ defined in Chapter II, Fig. II-2. This assumption is not true for all Pr since Ra_ℓ is Pr dependent, contrary to predictions using the marginal stability assumption. This result is discussed further in Sec. 1.4.

The Q.S.A. predictions can be compared with the infinite Pr results, since the marginal stability assumption appears valid for these results. From Fig. VII-3, it can be seen that Q.S.A. underestimates the deep pool experimental results by almost a factor of 40. The Q.S.A. theory predicts that the presence of the bulk fluid causes the thermal layer to be less stable, which from the experimental results appears to be incorrect. The experimental results for the infinite Prandtl number fluid show that convection initiation could have been predicted using the marginal stability assumption and a linear gradient through the thermal layer, and neglecting the presence of the bulk fluid. The error in the frozen-profile approach appears to be tied to separating the thermal

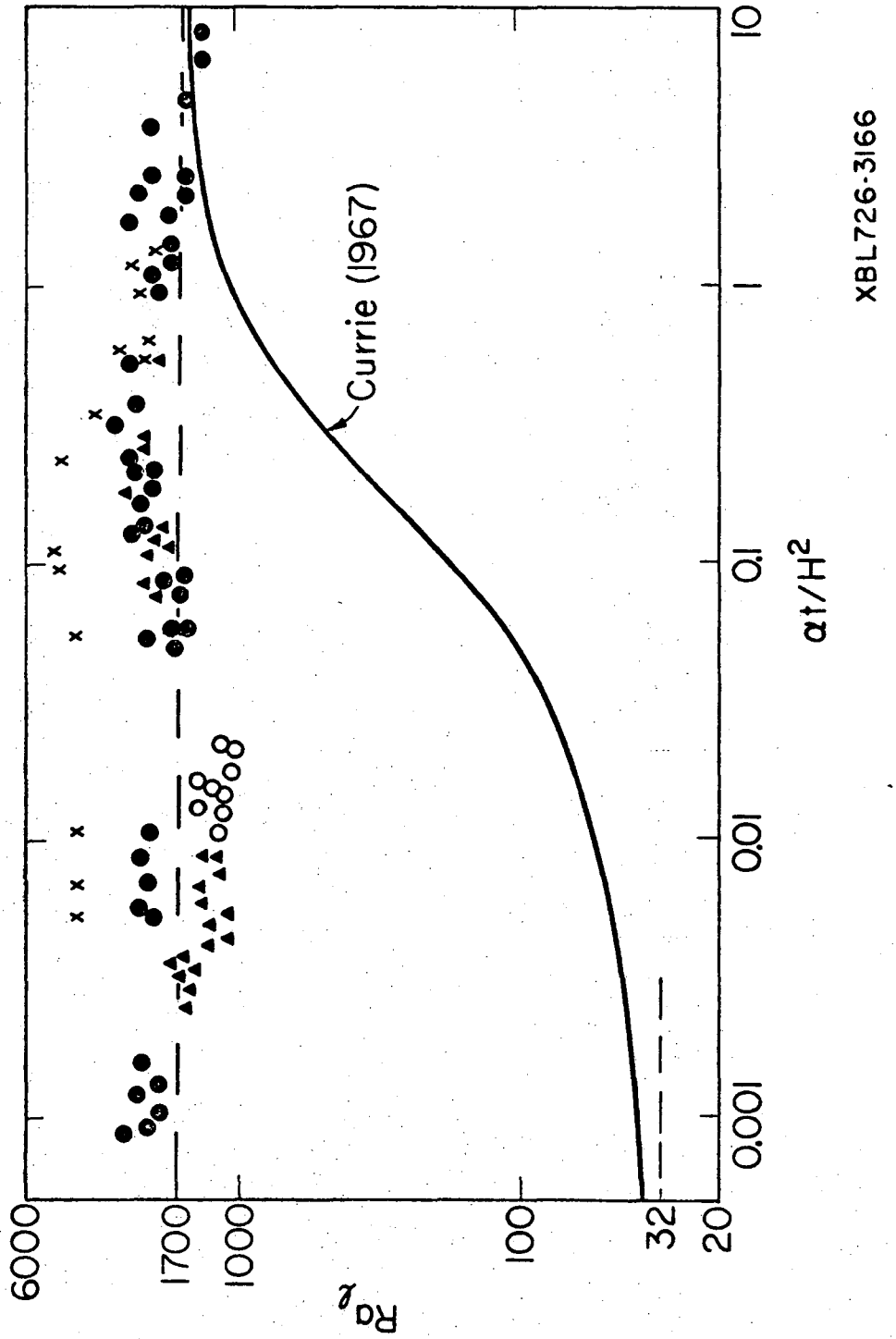

Fig. VII-3. Experimental values of Ra_ℓ as a Function of the Depth Factor $(\alpha t/H^2)$ for the Fixed Surface Case. X Methanol Pr = 7.6
n-Butanol Pr = 43
▲ Silicone Oil 50 cs Pr = 465
○ Silicone Oil 1000 cs Pr = 8500

layer from the bulk fluid and then considering the interactions of one upon the other. The experimental results suggest that it is better to neglect the presence of the bulk fluid and then consider the bulk fluid side of the thermal layer as having shear conditions between a free and a fixed nature. The deep pool asymptote as low values of $\frac{\alpha t}{H^2}$ shows Ra_ℓ = 1200 to 1350 for high Pr.

The relationship between A and $\frac{\alpha t}{H^2}$ plotted in Appendix H, Fig. H-3 shows that Ra_t and Ra_ℓ become independent of Shape Factor at high values of $\frac{\alpha t}{H^2}$. This was found experimentally for the results with the spray cooler for shallow pool convection plotted in Chapter VI, Fig. VI-15. The values of Ra_t at high values of $\frac{\alpha t}{H^2}$ appear to be independent of shape factor (S) for the range $0.5 < S < 0.8$. Further evidence for this concept is seen in the closeness of Foster's (1969) shallow pool datum point for water with an adiabatic non-heating surface and the present work where the non-heating surface temperature was held constant (refer to Chapter V, Sec. 2.). The temperature profiles in each case would be different, but the pools are shallow enough so that this difference is not important.

1.4. Influence of Prandtl Number on Ra_t

The marginal-stability assumption eliminates the Prandtl number from the equations of motion. In the case of the linear density gradient in the fluid theory using the marginal-stability assumption and experiment both show that the onset of convection is independent of the Prandtl number. Experimental results cover a range of Prandtl number from 0.023 to 8,500 (Silveston, 1958; Rossby, 1966). Thus an established test of

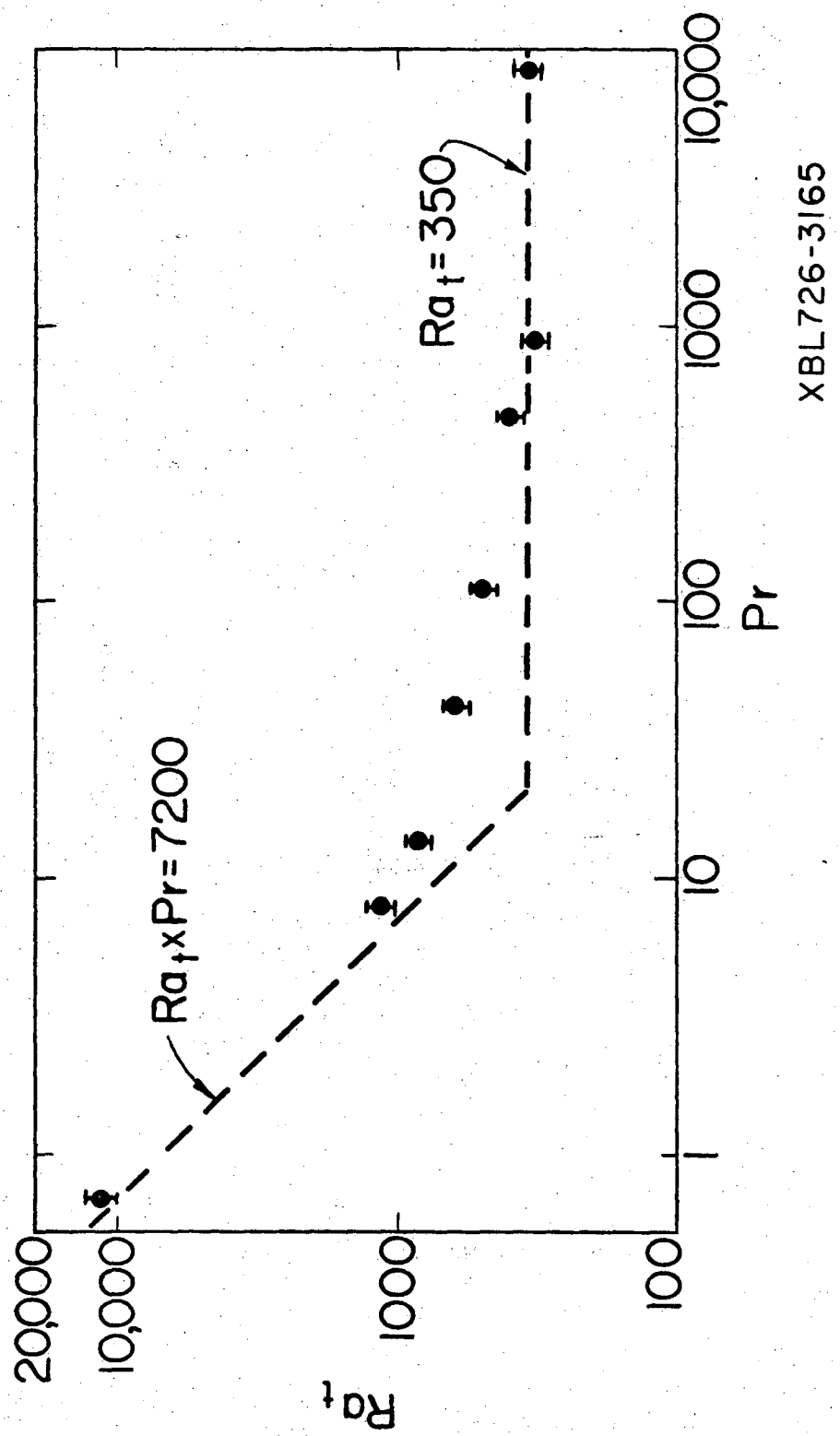

Fig. VII-4. Experimental Values of Ra_t for a linear surface temperature decay at a fixed surface as a Function of Pr showing the Two Experimentally Fitted Asymptotes.

the validity of the marginal-stability assumption is that the onset of convection be Prandtl-number independent.

The Q.S.A. approach uses the marginal-stability assumption to describe the onset of convection in the transient or boundary-layer density profile. As a consequence, the critical Rayleigh number (Ra_ℓ) is predicted to be independent of the Prandtl number.

Amplification theory assumes the time-dependent terms in the equations of motion to have equal weight with other terms. Consequently, the amplification time is a function of the Prandtl number, with two asymptotic solutions. At very low Prandtl number, $Ra_t \cdot Pr$ = constant, and at very high Prandtl number Ra_t = constant. The significant difference between these two asymptotes is that $Ra_t \cdot Pr$ has no viscosity term in it while Ra_t does. Thus, $Ra_t \cdot Pr$ shows the region where only conduction is the important stabilizing force, and Ra_t shows the region where both conduction and viscosity are important stabilizing forces.

The experimental results of Chapter V, Fig. V-2, show that Ra_t increases as Pr decreases, which is in qualitative agreement with Amplification Theory, but not Q.S.A. Theory. These data are poorly fitted with a constant amplification factor, but are fitted well with just the two asymptotes discussed above (Fig. VII-4). In light of the discussion of Sec. 1.3., the concept of amplification to describe the very high Pr asymptote does not appear valid. Rather, in light of the marginal stability assumption appearing valid at these asymptotic conditions, this asymptote should be a consequence of a disturbance displaying convective influence almost immediately after the conditions for first instability have been reached on the scale of the thermal

boundary layer thickness. The asymptote for small Pr appears to be tied to the growth rate of the disturbance from an infinitesimal to an observable size. This arises from the observation that Pr precedes the perturbation of the time derivative of the velocity in the equations of motion. As Pr decreases and approaches zero, the term $\frac{1}{Pr}\frac{\partial w}{\partial t}$ in the equations of motion will become increasingly important. Thus Ra_t and Pr will be important in the initiation phenomena for low Pr. In the limit of very low Pr, the equations of motion (Eqs. VII-1, 2, and 3) are made dimensionless through the group $Ra_t \cdot Pr$. Consequently, the convection onset conditions would be expected to be correlated by Ra_t = constant and $Ra_t \cdot Pr$ = constant at extreme values of Pr. Amplification theory predicts these two asymptotes from dimensional analysis and their values are reported by Foster (1968) and Gresho and Sani (1970) for constant amplification factors (w). The data could be fitted by the asymptotes $Ra_t = 350$ ($w \simeq 10^2$) and $Ra_t \cdot Pr = 7200$ ($w \simeq 10^{20}$) as shown in Fig. VII-3. Note that these asymptotes correspond to widely different amplification factors.

The observation that the Q.S.A. theory predicted Ra_t to be independent of Pr for deep pools, which was contrary to experiment, shows that the marginal stability concept is not applicable to deep-pool convection initiation except at very high values of Pr as discussed in Sec. 1.3. In light of the results presented in Sec. 1.3. and in this section, new features of the mathematical description appear to be important. The variation in fluid-depth experiments showed that if Ra_ℓ is used to non-dimensionalize the equations of motion, the following inequalities explain the apparent validity of the marginal stability assumption in both deep and shallow pools for a very high Pr fluid:

$$\frac{\partial \sigma}{\partial t} << \frac{\partial^2 \sigma}{\partial \psi^2}$$

$$\frac{1}{Pr} \frac{\partial w}{\partial t} << \frac{\partial^2 w}{\partial \psi^2}$$

Variation of Pr showed that as Pr decreases, the group $Ra_\ell \cdot Pr$ becomes increasingly important. This suggests that as Pr decreases, the term $\frac{1}{Pr} \frac{\partial w}{\partial t}$ becomes comparable to and eventually much greater than $\frac{\partial^2 w}{\partial \psi^2}$ in the asymptotic limit.

The Pr dependence in deep pools shows that the ratio of the thickness of the conduction boundary layer to the thickness of the momentum boundary layer changes as Pr decreases. This is reflected by the change in asymptote from Ra_t = constant to $Ra_t \cdot Pr$ = constant. The lack of Pr dependence and consequent lack of change in boundary layer thickness ratio does not occur in shallow pools because the thicknesses of these effects are constrained by the fluid depth; i.e., the temperature profile is almost linear across the fluid layer, and the motion is restricted to the fluid depth. It is only in deep pools where the fluid layer is unconstrained by the geometry that the Pr-dependence is observed.

In summary, a simple model for computing Ra_ℓ in the deep pool case

(a) considers the density boundary layer profile to be approximated by a linear segment as described in Chapter II, Fig. II-2. The equations of motion are made dimensionless using the length scale in Fig. II-2.

(b) neglects the presence of the bulk fluid.

(c) postulates a shear condition at the bulk-fluid edge of the density boundary layer that is between those of fixed and free surfaces.

(d) assumes the relation $\frac{\partial \sigma}{\partial} << \frac{\partial^2 \sigma}{\partial \psi^2}$.

(e) assumes the term $\frac{1}{Pr} \frac{\partial w}{\partial t}$ to be less than, greater than or comparable to $\frac{\partial^2 w}{\partial \psi^2}$, depending on the value of Pr. It appears from experiment that $\frac{1}{Pr} \frac{\partial w}{\partial t} >> \frac{\partial^2 w}{\partial \psi^2}$ for $Pr < 1$

$$\frac{1}{Pr} \frac{\partial w}{\partial t} << \frac{\partial^2 w}{\partial \psi^2} \text{ for } Pr > 1000$$

1.5. Effect of Vibration on Ra_t

The Q.S.A. theory has been used to investigate the behavior of only infinitesimal disturbances in an adverse density field. The effect of finite disturbances in a linear, time-independent profile through the fluid has been mentioned in Chapter II, Sec. 1.1. It was discussed how finite-amplitude disturbances can cause convection onset at a lower value of the Rayleigh number (Ra_H) than infinitesimal disturbances. This concept can be applied to Q.S.A. predictions and would be applicable in the case of vibrating fluids where the amplitude of the disturbances would be expected to be of greater magnitude than in a "stagnant" pool. The theory would predict that Ra_t will decrease as the vibration effect increases.

Amplification Theory predicts the time for amplification of a disturbance. Consequently, this theory predicts that the amplification time would decrease as the initial amplitude of the disturbance is increased, which is the same conclusion as the Q.S.A. theory.

The experimental results of Chapter V, Sec. 1.3. showed that vibration effects can decrease the value of Ra_t or Ra_ℓ. Although the

external vibration conditions were known, the velocity distribution in the fluid was unknown, which eliminated the possibility of quantitative comparison with the predictions of Amplification Theory. However, the experimental results allow some qualitative discussion of Amplification Theory. Vibration in the fluid could produce sound waves and bulk fluid motion to initiate convection. The sound wavelengths are much longer (approximately 1000 cm at 100 c.p.s.) than the observed initial convection wavelength (in the range of 0.2 to 5 cm). Further, the wavelengths of the bulk fluid motion, and hence initial convection conditions, will be dependent upon the size of the container relative to the size of the incipient thermal. The opposite was observed. Instead the value of Ra_t was observed in Chapter V, Secs. 1.2. and 2., to be independent of the fluid width and depth provided the fluid boundaries were greater than the size of the thermal. These observations suggest that the wavelength of the motion produced by the environmental vibrations is probably not the basic wavelength of the incipient thermal, which is in contrast to the initial conditions assumed in Amplification Theory. Rather, this basic wavelength could be derived from a breakdown of some bulk-fluid motion effect. Possible sources of this bulk-fluid effect are discussed in Sec. 2. of this chapter.

1.6. Effect of Rigidity of the Heat Transfer Surface on Ra_t

Both Q.S.A. and Amplification theories use the velocity perturbation (v) expansion form $v = g(x,y,t)f(z)$, where $f(z)$ is the vertical component and is a continuous function of "z" through the fluid satisfying the shear boundary conditions at the upper and lower fluid surfaces. The function for

f(z) at a free surface will differ from that at a fixed surface because of the differences in rigidity between the two boundaries. It is from this reasoning that both theories predict that Ra_t at a fixed surface will be higher than that at a free surface.

The experimental evidence shows that in the case of a linear, time-independent density gradient through the fluid, the difference between the critical Rayleigh number at a free surface (Berg and Palmer, 1971) and at a fixed surface (Silveston, 1958; Rossby, 1966) is as predicted theoretically. However, the experimental evidence presented in Chapter VI, Sec. 1.1., shows that with deep-pool, penetration-type density profiles, the degree of rigidity at the heat-transfer boundary has no influence on the value of Ra_t for convection initiation.

These deep-pool results, together with the interferometric photos of Onat and Grigull (1970), indicate that the first motion occurs in the bulk of the fluid, and more specifically at the bulk edge of the density boundary layer. This initial motion is apparently not strong enough to penetrate the density boundary layer and "feel" the rigidity of the heat transfer surface. Both the Q.S.A. and Amplification Theories incorrectly assume a form of initial motion which is distributed through the density layer and influenced by the rigidity of the heat transfer surface.

A possible reason why large-scale convection first appears at the outer edge of the boundary layer is that this is the region where the conduction thermal gradients are weak enough to be comparable to stray convection thermal gradients, which appears necessary for horizontal

temperature variation, which in turn is a prerequisite for thermal production. At the same time the conduction thermal gradients at the edge of the thermal boundary layer are significant enough to support the initiation process.

The shallow-pool data for free and fixed surfaces are difficult to compare because of the uncertainty in the liquid depth in the free-surface experiments. The shallow pool convection initiation data showed Ra_H at approximately 1800. From the linear, time-independent density profile studies by Berg and Palmer (1971), the high $\alpha t/H^2$ data should fall along Ra_H = 1100. The reason for the discrepancy probably lies in

(1) the difference between the assumed and the actual fluid depths. If there was a meniscus on the liquid surface, the liquid depths would be lower than that assumed and consequently, the actual values of Ra_H would be less than the calculated values. In the fixed surface results, the wall height was equal to the fluid depth because of the geometry of the apparatus.

(2) the difference in surface rigidity is only felt at high values of $\frac{\alpha t}{H^2}$ and the experimental values were not high enough. The time-independent, linear profile results of Berg and Palmer (1971) appear to be at $\frac{\alpha t}{H^2}$ of at least an order of magnitude larger than the present results.

1.7. Comparison of Mass Transfer Results with Heat Transfer Results

Both Q.S.A. and Amplification theory predictions do not distinguish between adverse density gradients produced by heat or mass transfer. The relevant thermal or mass diffusivity and coefficient of expansion due to either a change in temperature or composition in the definitions of Ra_t and Pr account for the nature of the density gradient.

The experimental results using gas absorption or desorption in aqueous systems have involved a step change in density at the gas-liquid surface, and a contaminated aqueous surface. A summary of these results is given in Table 7. Generally, the Ra_ℓ are higher than the heat-transfer, high-Pr value of Ra_ℓ, which is 1400. The increase could be due to several effects, including:

(1) Solute was absorbed out of an air mixture, so that there could be gas-phase resistance due to the presence of the air, which was neglected.

(2) There could have been resistance to mass transfer from the presence of the insoluble surfactant on the contaminated water surface, which was neglected in the calculations. Mahler and Schechter (1970) duplicated Blair and Quinn's (1969) results by placing n-octadecanol, an insoluble surfactant, on the liquid surface. Pigford and Springer (1971) found that insoluble surfactants impeded mass transfer while soluble surfactants had negligible effect. Thompson (1970) found experimentally that the ratio of sulfur dioxide absorption flux in the presence of n-octadecanol to that for clean water was 0.37. A reduction in flux would reduce the concentration

Table 7. Ra_t, Ra_ℓ Determined from Aqueous-Gas Absorption/Desorption Experiments Involving a Step Change in Surface Conditions and a Contaminated Aqueous Surface.

Investigator	Ra_t	Ra_ℓ	Gas
Blair and Quinn (1969)	350	4000	Ethyl Ether - desorption
" " "	320	3650	Ammonia - desorption
" " "	300	3400	Sulfur Dioxide - absorption
" " "	210	2400	Carbon Dioxide - absorption
Mahler and Schechter (1970)	290	3300	Sulfur Dioxide - absorption
Plevan and Quinn (1966)	140	1600	Carbon Dioxide - absorption
Burger (1970)	320	3650	Sulfur Dioxide - absorption
" "	270	3100	Ethyl Ether - desorption

of sulfur dioxide at the top of the fluid and the effective value of Ra_t. Mahler and Schechter found $Ra_t = 190$ for absorption with a soluble surfactant, which would correspond to $Ra_\ell = 2150$. This value would be lowered even further if the surface curve were less than a step function (refer to Appendix H).

(3) The initiation mechanism could be affected by the scale of the density profile depth. In the mass transfer experiments, this scale ($= \sqrt{Dt}$) was approximately 0.01 cm, whereas in the heat transfer experiments, the same scale was approximately 0.35 cm. There is a possibility that the observation of convection initiation is different over this range of density layer thickness.

Reasons (1) and (2) appear to be invalid because the reported mass flux in the SO_2 experiments (see Burger, 1970) was never lower than that predicted from penetration theory using literature values of the diffusivity coefficient of sulfur dioxide in water. The above reasons (1) and (2) would predict a lower flux than that predicted from penetration theory.

Although the number of available experiments to draw a conclusion from is limited, it appears that mass transfer experiments produced values of Ra_t slightly higher than heat transfer experiments. This can be better evaluated when more experimental data with heat and mass transfer are available, and the initiation mechanism is better identified.

2. Nature of the Initial Disturbance

The present experimental study has revealed many aspects of deep-pool convection initiation, and, with the Q.S.A. and Amplification Theories, it has provided a deeper insight into the initiation mechanism than existed before. However, the fundamental questions of what form the instability takes prior to convection, and how it emerges out of the conduction profile have not yet been resolved. The practical aspect of this question concerns the relationship between the critical value of Ra_t and the type of instability. There are many qualitative reports with some conclusions in the literature, and these are reviewed in the following section. These reports are then analyzed to obtain an improved overall picture of the nature of the initial disturbance.

2.1. Qualitative Observations of Convection Initiation

2.1.1. Initiation at a Gas-Liquid Surface. The following studies have been reported.

(1) Spangenberg and Rowland (1962) observed convection onset caused by evaporation in deep pools of water. Schlieren optics showed the thermal layer initially growing with a uniform thickness. After an initial period of cooling, protuberances developed on the leading edge of the thermal layer and then grew and produced plunging sheets of cold liquid. Appearing simultaneously and abruptly with the roughened thermal layer edge, in the view perpendicular to the surface (top view), were stripes which grew in intensity as the plunging sheets developed. Photos reported by those authors showed the length of a stripe in one example to be 8 to 10 cm, whilst the thermal layer thickness was 8 to 10 mm. From these observations,

the mechanism for convection was proposed as an accumulation of cooled liquid along stripes, which caused local thickening of the thermal layer and then instability.

The protuberances retained their identity on the developing stripe and later on the leading edge of the plunging sheets. As the cooling rate increased, more sheets per unit area were observed. Columnar plunging was observed, but its appearance was transient. Columns developed into plunging sheets within a few seconds after formation, so that generally the developed form of convection was plunging sheets.

Interestingly, the thermopile used to record the surface temperature discouraged convective growth. When the thermopile was moved near a stripe, that stripe faded and reformed some distance away from the instrument.

(2) Foster (1965) performed experiments similar to Spangenberg and Rowland, but instead of using Schleiren optics he used a layer of "washable" ink particles on the bottom of the fluid to observe the first signs of motion. This required that the fluid be shallow enough so that plunging convection would disturb the layer of ink. The disturbance observed in the ink layer reflects the nature of the first convection to reach the bottom of the fluid layer, which is not necessarily the same as the form of convection which first forms at the density layer.

The first motion was observed as white spots appearing in the ink layer. Photographs show that these spots were grouped, with as many as five spots in one group. The experimental conditions were similar to Spangenberg and Rowland, and so it is possible that the first developed convection motion could have been isolated plunging sheets with

protuberances on the leading edge causing the spot appearance. Foster did not show side views of the convective motion as Spangenberg and Rowland did, and so it is difficult to assess whether the motion in Foster's experiments was discrete blobs or whether it was sheets.

It is interesting to observe from photos published in Foster's paper that the appearance of white spots was isolated and random, although photos taken shortly after onset showed convection more developed near the walls than in the center of the container.

Foster attempted to correlate the distance between the white spots in a group with the rate of cooling to test Amplification Theory predictions. He observed that the distance between spots in a group decreased as the cooling rate increased. In terms of Amplification Theory, this meant that the distance between the spots should correspond to the wavelength (λ_c) of the fastest growing wave of the disturbance. For a given Prandtl number, this predicted distance is proportional to the thermal-layer thickness, and the correlation of the distance between spots with the thermal layer thickness was observed experimentally ($\lambda_c \sim 7\sqrt{\alpha t}$) by Foster. Furthermore, Spangenberg and Rowland observed that the number of plunging sheets per unit area increased with increasing cooling rate (decreasing thermal layer thickness), which is qualitatively in agreement with the wavelength argument of Foster.

(3) Blair and Quinn (1969) absorbed sulfur dioxide into water, where the aqueous surface was contaminated. They observed the initial forms of convection using Schlieren optics.

The first motion was observed in the meniscus region in the form of plunging sheets. Some time later, convection in the center of the

fluid surface was observed, and its form was dependent upon the driving force, or the time for convection initiation. At high driving forces, both ringlets and columns were observed to plunge into the fluid. The number of ringlets and their time of first appearance was not reproducible, and in some runs only columns were observed. The appearance of ringlets was transient, and they were observed for only a short period before columns and sheets became established. The horizontal distance (λ_c) between neighboring columns was similar to the ring diameter. The results showed approximately $\lambda_c \sim 8\sqrt{\alpha t}$ for this form of initiation.

At low driving forces, rings were not seen, and plunging sheets were the main form of motion observed. However, Rayleigh numbers were the same as for higher driving forces.

The authors concluded that the critical value of the Rayleigh number varied by only a few percent with different degrees of disturbance level and hence different forms of initial convection motion--i.e., ringlets and sheets. To substantiate this, Blair and Quinn made some runs at high driving force with and without a pressure deflecting screen between the gas entry and liquid surface. When the surface was visibly detected without the screen in place, the Rayleigh number was lowered by approximately 15% from the results with the screen in place and no visible deflection. It is important to note that convection onset was observed approximately 20 seconds after the gas entry, and that the surface deflection may have been dampened significantly by the time convection began.

2.1.2. Initiation at a Liquid-Solid Interface. The following two studies have been reported:

(1) Foster (1969) studied the form of convection initiation in water by heating the fluid from below in both shallow-pool and deep-pool cases. A thin layer of washable ink particles was laid on the heating surface, and initial motion was observed by patterns formed in the ink.

Photos were published showing the ink patterns formed just after the onset of convection. Convection was observed to be established near the walls, but there was little ink movement in the center of the vessel.

The deep-pool photos showed a tesselated ink pattern in the areas of convection. There were indications that mushrooming thermals were present in the photos and that the centers of these thermals were over the junctions of lines of ink which had apparently been formed by the sweeping action of the convection process. Foster calculated the wavelength (λ_c) of the initial motion by the square root of the area of an average cell. The results could be correlated approximately by $\lambda_c = 7.5 \sqrt{\alpha t_c}$.

The shallow-pool photos showed that the cell boundaries influenced the form of convection in shallow pools. The patterns formed concentric rings in the ink layer. The photos showed well developed convection patterns at the edge of the fluid, and these do not necessarily correspond to the initial form of motion in these areas. The initial motion may have been more random, but was quickly organized by the wall influence.

The disadvantage of ink studies is that the fluid motion has to be strong enough to sweep the surface. It has not been shown at what stage of convection development the surface motion reaches this strength. The results presented in Sec. 1.6. show that initial motion is at the bulk edge of the density boundary layer. Consequently, the patterns observed in the ink layer probably do not correspond to the very first motion.

(2) Onat and Grigull (1970) observed the onset of convection in various fluids heated from below. Convection was observed using bi-prism interferometry parallel to the development of the thermal layer. Photos at successive stages of initial heating showed the development of bumps in the fluid side isotherms, while the isotherms closer to the heating surface remained planar. The growth of the amplitude of the bumps was fast once they had appeared visible.

2.2. Conclusions from the Above Observations

(1) Convection occurs randomly on a surface, as opposed to the organized motion which is assumed in wave analysis theories.

(2) Initial convection patterns are not consistent in shape.

(3) The initial convection pattern appears to depend upon the density driving force--i.e., a high driving force gives ringlets and a low driving force gives sheets.

(4) The patterns at a gas-liquid surface appear to be influenced by prior surface deformation.

(5) Ra_t can be confined to a narrow range for a number of different forms of convection initiation as shown by Blair and Quinn (1969).

(6) The initial disturbance is one which causes a local thickening of the density boundary layer.

(7) The ratio of distances between protuberances associated with a plunging sheet, column or ringlet to the boundary layer thickness at convection initiation is similar to that most preferred from wave analysis.

(8) Wave analysis has a different meaning in convection initiation than in steady-state convection (regular cellular convection). Initiation is random and appears to be a transformation from a disturbance into a thermal; thus the initial wavelength of the disturbance and its development in the density field, both in possible change of wavelength and amplitude, are important. Steady-state convection appears in well defined symmetrical motion, where the wavelength does not change in time or space and the motion can be described by a wave form. The essential difference between the two cases is in the wave-form description of the motion.

(9) The emergence of the protuberances and their growth appear very fast compared with the accumulation process leading to the thickening of the density boundary layer prior to the appearance of the protuberances.

2.3. Possible Factors Leading to the Local Thickening of the Density Boundary Layer

Protuberances have been observed to occur in groups rather than individually. This suggests that a regime of surface showing the first signs of convection is the real initiator and that the protuberances grow from the disturbance in that regime. For example, Spangenberg and Rowland observed lines of local thickening (the unstable regime) with protuberances growing on them. Further, the growth procedure of the protuberances appears well described by amplification of a favored wavelength (Onat and Grigull), with the prediction for the fastest growing wavelength $\lambda_c \sim 6.5 \sqrt{\alpha t}$ being experimentally observed. However, these observations show that, although linear theory predicts the favored growth pattern of the disturbance, it does not describe the accumulating mechanism which leads to an area being

destabilized. Consequently, large-scale effects (compared to the density boundary layer thickness) causing the destabilization have yet to be identified, and herein lies a possible explanation for the variation of Ra_t from one experiment to another. Such an explanation could be contrasted to the Amplification-Theory concept of the spread in Ra_t being due to variation in the amplification factor required for the appearance of convection from one location to another.

The following are some effects which may classify as large scale disturbances:

(1) Uneven heat transfer over a planar surface. This situation would lead to a sloping density boundary layer,

and the peaks in the density boundary layer might lead to protuberance developments. Irregularities in the transfer process might occur with a non-isothermal heat transfer surface or non-uniform thermal consistency in the heating phase, such as in the wall next to a fluid.

(2) Transfer across a non-planar surface. This would include convection at the meniscus region, where Blair and Quinn observed premature convection. Non-planar free surfaces could also introduce surface tension effects, as Berg and Morig (1969) observed.

(3) Heat transfer across a wavy gas-liquid surface. In this case the surface eddy movement might be influential in redistributing the density boundary layer. This is a possible cause of the ringlet formation observed by Blair and Quinn.

(4) Local temperature variations in the fluid produced by various heat sources, including fluid vibrations. In the vibration experiments

reported in Chapter III, Sec. 3.3., the fluid was observed to heat up quickly at high power inputs. It is possible that at smaller vibration amplitudes (lower power input), the fluid also heated up, although this was not observed by the thermocouple on the metal surface. Since each vibration experiment was started by allowing the vibrator to reach a steady motion and the period to accomplish this was not constant, it seems possible that the amount of internal heating and consequent temperature variation in the fluid would vary from one experiment to the next. This influence may explain the spread in results of the the vibration experiments, and it is therefore difficult to conclude whether the local velocity variations or the temperature variations were the cause of decrease in stability.

(5) Bulk motion in the fluid prior to the start of heat transfer. A fluid with no intentional temperature drop across it normally has some form of fluid circulation generated by non-isothermal boundaries. Photographic studies reported by Muller and Ibl (1958) and Muller (1956) have led to identification of some of the factors promoting this motion. These include

(a) evaporation from the free surface,

(b) heat developed from light absorption,

(c) wind drafts around a container,

(d) fluctuations in room temperature.

Large temperature fluctuations produced motion with velocities on the order of 0.5 mm/sec. This motion was reduced to 0.005 to 0.05 mm/sec by insulating the fluid container and reducing the above four effects. Normally the non-insulated fluid is referred to as "static" because of the slow velocity of these motions.

The advection currents of this motion moving through the thermal boundary layer can provide the initial perturbation. However, this one-dimensional stream must break up into local point sources which grow into thermals. To do this the current must interact with the density field to produce a wavy motion which will then break up into the desired units.

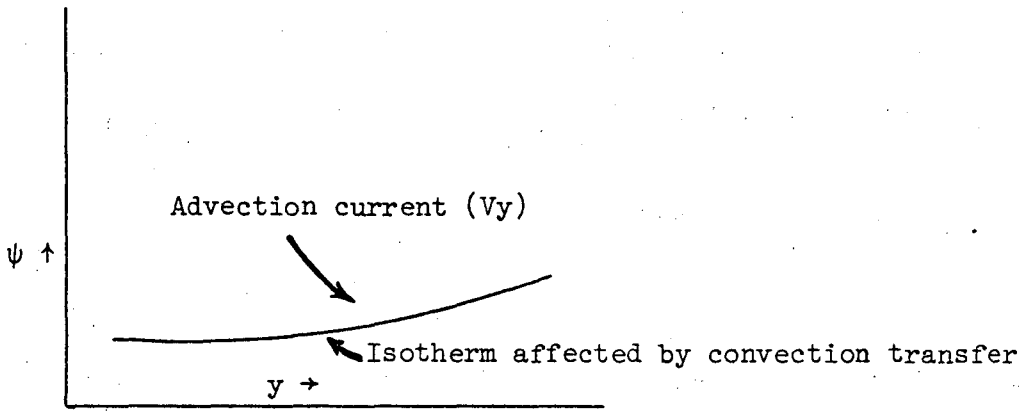

The important dimensionless group relating the advection current to the initiation mechanism appears to be $\frac{V_y}{\sqrt{\alpha/t}}$, where V_y is a standard measure of the advection velocity, and $\sqrt{\frac{\alpha}{t}}$ is a measure of the velocity of the thermal boundary layer edge.

Wavy two-dimensional isotherms were observed by Onat and Grigull (1970). The above form of initial disturbance could be applicable to their results.

Stray large-scale motion could also be a residual effect from a previous heating experiment. Experimental observation in the development of the fixed-surface technique used in this investigation showed that the difference between allowing the fluid to come to rest for a twenty-minute

period and a ninety-minute period after a one-minute run was a lowering of the Rayleigh number by approximately 25% for the shorter rest period. Both residual temperature and velocity variations could be important in this case.

Burger (1970) found that stirring the fluid in a vessel with a gas-liquid surface had a slight destabilizing effect. When the surface became visibly broken, the convection transfer coefficient was much higher and onset was not clearly distinguishable. The form of natural-convection motion in this case is not easily identified.

2.4. Conclusion

Because Ra_t is experimentally the same for fixed and free surfaces, the bulk fluid effects may be expected to be more important than the surface effects as promoters of convection initiation. Since the fluids which had been allowed a long time for thermal equilibrium (12 hours or more) showed convection with onset times only slightly greater than the fluids which had been allowed a 20 minute equilibrium time between runs, the temperature variations in the bulk fluid may only be secondary promoters. Consequently, the residual or bulk fluid motion appears to be the important promoter in forming the disturbance in the density boundary layer. However, more visual observation of the convection initiation phenomenon is needed to identify the primary and secondary promoters better.

3. Deep-Pool, Surface-Tension-Driven Mechanism in Light of the Results of Chapter VI

The free-surface convection initiation results presented in Chapter VI, Sec. 2., showed no surface-tension influence, even to high values of the Marangoni number (M_t = 10,500, M_H = 5,200). This was in the absence of meniscus effects, surface-temperature gradients, and surface waves. This result is in contradistinction to the predictions of Q.S.A. theory developed by Vidal and Acrivos (1969), who proposed a Marangoni number 4 = (M_t) as a critical value in the deep-pool case.

The discrepancy between experiment and theory appears to be connected with the observation of the equivalence of convection initiation at free and fixed surfaces in deep pools. As discussed in Sec. 1.6. of this chapter, the incipient convection is confined to the bulk edge of the density layer and consequently does not feel the rigidity of the transfer surface. Thus, there is no shear variation at the surface due to the incipient convection and consequently no surface deformation. Provided that there are no surface temperature gradients, local surface disturbance or a meniscus, there will be no surface-tension gradients along the surface, and hence surface-tension effects will be absent from the initiation mechanism.

Surface waves and meniscusses have shown that deformed surfaces and surface-tension effects can lower the critical value of Ra_t. Furthermore, in cases where surface-tension effects have appeared to dominate the onset of convection (refer to Appendix A: Clark and King, 1970; Brown and King, 1969; Blair and Quinn, 1969; Mayr, et al., 1971), surface waves have been present and from the above discussion appear to be the important disturbance.

Clark and King (1970), and Brown and King (1969) found that the critical value of M_t decreased from 8500 to 4500 in a horizontal flowing liquid-gas contactor as the liquid flow rate increased from Re_L = 150 to 900. Surface-wave influence should increase as the flow rate was increased.

Blair and Quinn (1969) used a stagnant arrangement which has been shown to have surface waves present, as was discussed in Chapter VI, Sec. 1.1. They found M_t = 3100 approximately.

Mayr, et al., (1971) studied convection onset in a short wetted-wall column in which the falling film always had ripples along its surface. Although they concluded that the Marangoni number was a function of the Biot number, there is evidence to believe that their datum point for acetone desorption was affected by surface-tension gradients along the gas-liquid interface, which enhanced rippling and could have lowered the system stability. This is discussed in Appendix A. Without that datum point, their Marangoni numbers were in the range 3700 to 5700.

One possible reason for the apparent stabilizing surface-tension effect in Mahler and Schechter's (1970) experiments with the absorption of sulfur dioxide into water, discussed by Davenport and King (1972), appears to have been the presence of surface waves in the experiment apparatus (refer to Chapter VI, Sec. 1.1.). Another possible reason is that the density disturbance in its early stage of development caused some surface disturbance and hence caused surface tension stabilization. This stabilizing effect then retarded the observable onset of convection.

Biddulph and Ellis (1966) studied the effect of surface tension forces on the amplitude of waves on a laminar flowing-water stream which was absorbing either acetone or methanol. They observed the amplitude

of the waves to increase by an order of magnitude when the driving force for mass transfer passed a critical value. The authors explained this phenomenon by postulating that the solute absorption across the wavy interface caused sites of low surface tension, and high surface tension gradients along the surface which caused a rapid spreading of surface liquid. This resulted in exposure of bulk liquid to the surface in the center of the site, which increased the surface tension in the exposed region. This caused an annulus of low surface tension fluid and a tendancy to reverse direction of flow. The momentum associated with the spreading and reversal of the low surface tension fluid resulted in a surface ripple.

The above experimental observations suggest that surface waves are important in deep-pool, surface-tension-driven convection initiation. Convection onset involving density forces and surface-tension forces for the case of the time-independent, linear profile in the fluid appears to be in contrast to this absolute need of surface motion. In the analysis of this case, Pearson (1958) and Nield (1964) assumed that the important disturbance for initiation occurs throughout the fluid layer. Their predictions have been experimentally verified by Palmer and Berg (1971) and Koshmeider (1967) . The possible difference between the linear profile, time-independent case and the deep-pool, time-dependent case is that the residual or bulk fluid motion, which could be the initiator of the density convection, is the initiator for the surface-tension-density coupling action, and the time scale for the development of the large-scale observable convection from this initiator could be much longer than that for development from surface waves in the deep-pool case.

Smith (1966) extended the earlier work of Pearson (1958) and Sternling and Scriven (1964) by adding the effect of gravity waves to the linear stability analysis. He found that the critical Marangoni number increased as the wavelength of the surface wave relative to the thermal depth increased. The effect was dominant for thin layers of very viscous fluids. However, the results of the analysis have not yet been correlated with experimental observation.

Experiments were performed to examine the importance of the surface-tension gradient along the surface, and of surface deformation through a meniscus or surface waves; the results are recorded in Appendix J. Pools of liquid were heated with point sources and with uniform temperature gradients along the surface, and in some cases meniscuses were allowed. Surface temperature and the air temperature just above the liquid were monitored to examine surface-tension effects. These results, together with the observations above, show that some necessary conditions for surface-tension-initiated motion are:

(1) a surface tension gradient along the surface,

and (2) surface waves or a meniscus or a point source.

To illustrate the importance of (2), experiments reported in Appendix J showed that a uniform temperature gradient along a planar gas-liquid surface did not produce convection for temperature gradients as high as 3° C/cm in thin pools of decane, 0.75 mm thick.

VIII. PREDICTION OF STEADY-STATE CONVECTION TRANSFER COEFFICIENTS FROM INITIATION DATA

1. Introduction

Measurements of heat transfer coefficients have shown that the transfer mechanism in steady-state, deep-pool (large values of Ra_H) natural convection is a boundary-layer phenomenon. Currently, the boundary-layer thickness is thought to be maintained at an average value by a balance between conduction and convection (release of thermals) processes.

The interaction between the convection and conduction processes has been well described by Howard's (1966) mechanistic theory of steady-state convection. Briefly, it suggests that the boundary layer grows by conduction until it becomes unstable, whereupon a thermal (a plume of hot fluid rising from a heated surface) is generated which destroys the density boundary layer. The boundary layer grows by conduction again and repeats the process in a cyclic fashion. Convection is assumed swift compared with the time of conduction. Consequently, this mechanism can be approximated by a succession of conduction periods where the boundary layer is built up from zero to some unstable thickness. The worth of this model is that it allows prediction of the temperature profile and heat transfer coefficient once the length of the cyclic period is known. This theory is discussed further in Sec. 2. of this chapter.

Foster (1970) and Burger (1970) have postulated models where this cyclic period was equal to the time for convection initiation from a fluid initially at rest. This assumes that the form of the instability for the convection-initiation and steady-state mechanisms are similar.

Obviously if initiation data were available, this method would be a powerful tool for estimating both transient and steady-state transfer coefficients. However, the limitations of both Howard's model, and the above equivalent-forms-of-instability assumption have to be evaluated before this method can be relied upon. There are some data available in the literature and in this dissertation which can help to establish whether such limitations exist.

2. Howard's (1966) Steady-State, Deep-Pool Natural-Convection Mechanism

An excellent review of the steady-state, deep-pool, natural-convection theories which have been proposed has been given by Howard (1966), and the experimental evidence in the literature to test the reliability of these theories has been reviewed by Somerscales and Gazda (1969). The experimental evidence shows Howard's (1966) theory superior in providing a basis for understanding and correlating the steady-state convection mechanism. The important theoretical and experimental conclusions of Howard's theory are discussed in this section.

Townsend (1959), in a study of thermal convection in air over a heated horizontal plate, observed that fluctuations in temperature, temperature gradient, and the rate of change of temperature in the air showed periods of vigorous activity (large fluctuations) alternating with quiescent periods (small fluctuations). The observation was made that the periods of vigorous activity were associated with rising plumes of hot air or thermals passing over the temperature sensor, while the quiescent periods were associated with conditions typical of the bulk

air lying far from the surface. Townsend postulated from his measurements of time-averaged temperature profiles and temperature fluctuations that the thermals probably originated from the edge of a conduction boundary layer, and were dissipated by heat transfer as the thermals ascended through the bulk fluid. This was in qualitative agreement with the Malkus (1954) theory of turbulent natural convection, which emphasized the importance of the conduction layer. However, this and later theories did not predict the periodic nature of turbulent convection, until Howard.

Howard proposed that the periodicity in turbulent convection was a result of the procedure which produced thermals. He proposed that the boundary layer would grow by conduction until it became unstable, whereupon it would produce a thermal which effectively destroyed the boundary layer. Cold bulk fluid would be swept to the heating surface to replace the rising thermal, and the boundary layer would grow by conduction to renew the cycle. By using the Taylor-Rayleigh stability analysis, he calculated that for high Prandtl number fluids, the turbulent process would be fast compared with the time to build up an unstable boundary layer by conduction. Thus if the greater part of the observed period (t^*) was spent in conduction, the instantaneous temperature profile $T(z,t)$ could be described by the error function curve ($T = \Delta T$ erfc ξ) for the case of a constant temperature (ΔT) heating surface. By averaging the error function over the period $(0,t^*)$, the average temperature profile ($\overline{T}$) and transfer coefficient ($\overline{h}$) can be found. Howard gave the result as;

$$\overline{T} = \Delta T \left[(1 + 2\xi^2) \operatorname{erfc} \xi - 2\pi^{-1/2} \xi \operatorname{erfc} \xi\right] \qquad \text{(VIII-1)}$$

$$\overline{h} = \frac{2k}{\delta} \qquad \text{(VIII-2)}$$

where

$$\xi = \frac{z}{\delta}\sqrt{\frac{\pi}{4}} \qquad \text{(VIII-3)}$$

$$\delta = \sqrt{\pi \alpha t^*} \qquad \text{(VIII-4)}$$

The Rayleigh number, based on the boundary layer thickness (δ), at the breakdown of the boundary layer was predicted to be on the order of 1000, from the study of onset of convection from a linear density profile discussed in Chapter II, Sec. 1.1. The soundness of the model can be evaluated by comparing the experimentally observed period (Ra_p), heat transfer coefficient (Ra_{TC}) and average temperature profile (Ra_δ), all defined in Table 8. Howard's model predicts that all three Rayleigh numbers should have approximately similar values.

Average Temperature Profile, Ra_δ

Howard reported that the experimental profiles of Elder (1965) and Townsend (1959) could be fitted with Eq. (VIII-1), above, for values of Ra_δ of 2500 (Pr = 2) and 2800 (Pr = 0.7), respectively.

Somerscales and Gazda (1969) reported experimental temperature profiles. Their data could be fitted with Ra_δ of 1500 (approximately) for Pr in the range of 6 to 20 (see Appendix A). These authors also

Table 8. Characteristic Rayleigh Numbers for Howard's (1966) Theory

$$Ra_P = \frac{\rho g \beta \Delta T}{\mu \alpha} (\pi \alpha \, t_P)^{3/2} ,$$

where t_P is the observed period.

$$Ra_{TC} = \frac{\rho g \beta \Delta T}{\mu \alpha} \ell^3 ,$$

where $\frac{k}{\ell}$ is the transfer coefficient.

$$Ra_\delta = \frac{\rho g \beta \Delta T}{\mu \alpha} \delta^3$$

where δ is a parameter used to fit the experimentally observed temperature profile $T/\Delta T = f(z/\delta)$, and ΔT is the temperature difference across the density boundary layer.

reported temperature profiles from Rossby (1966) for Pr of 840, 104, and 0.023. The data for high Pr were similar to those of Somerscales and Gazda, but the mercury data (Pr = 0.023) showed less steep temperature gradients.

Period, Ra_p

Sparrow et al. (1970) reported Ra_p = 410 for water (Pr = 5), while Somerscales and Gazda (1969) reported Ra_p = 700 for Silicone Oils (Pr = 6 to 20).

The periodic temperature fluctuations observed in the breakdown of cellular flow and reported in the form of Ra_p have shown that Ra_p increases in value as Ra_H increases (see Chapter II, Sec. 1.2.). This effect is probably due to the presence of bulk cellular flow and does not strictly fall in the deep-pool category, which should be free of organized bulk flow. The results of Rossby (1966), Krishnamurti (1970), and Deardorff and Willis (1971) fall into this category, although the latter authors reported Ra_p = 6000 (approximately) in the complete breakdown of cellular motion for air (Pr = 0.7).

Transfer Coefficient, Ra_{TC}

Most experimental heat transfer data reported in the literature have been for the case of constant heat flux through a liquid layer. Consequently, there are boundary layers at both the lower and upper surfaces, with approximately equal transfer coefficients and temperature driving forces (ΔT) (Somerscales and Gazda, 1969). The overall heat transfer coefficient (H_o) has been measured as a function of the driving force across the fluid ($2\Delta T$) and reported in the form;

$$Nu_H = C\ Ra_H^{1/3} \qquad \text{(VIII-5)}$$

From Eq. (VII-2), Howard's model predicts

$$\bar{h} = 2H_o = \frac{2k}{\delta} \qquad \text{(VIII-6)}$$

i.e.

$$\frac{H_o L}{k} = \frac{L}{\delta} = \left[\frac{(2\Delta T)}{2(\Delta T)}\right]^{1/3} \frac{L}{\delta} \qquad \text{(VIII-7)}^*$$

or

$$Nu_H = (1/2\ Ra_{TC})^{1/3}\ Ra_H^{1/3} \qquad \text{(VIII-8)}$$

Values of Ra_{TC} can be found from the experimental data by equating Eq. (VIII-5) with Eq. (VIII-8). There is much scatter of the data reported in the literature for deep-pool natural convection, and this observation has been discussed by Rossby (1966). The results can often be better correlated with an exponent on Ra_H less than 0.33 (Somerscales and Gazda used 0.283 for their best fit). This results indicates that the experiments are not completely fluid-depth independent and thus not strictly deep-pool data. However, the results give an approximate correlation for deep-pool convection (see Fig. VIII-1). Rossby (1966), Somerscales and Gazda (1969) and Globe and Dropkin (1959) report results for high values of Pr which show $Ra_{TC} = 600$ (approximately). As Pr decreases Ra_{TC} increases, so that at Pr = 6, $Ra_{TC} = 1000$ and at Pr = 0.02, $Ra_{TC} = 3000$ to 10,000.

---

*It should be noted that Howard (1966) used Ra_{TC} based on the temperature difference $(2\Delta T)$ across the fluid layer, and Ra_δ based on the temperature difference across one boundary layer (ΔT).

Significance of the Results

The fact that Ra_{TC} was substantially less than Ra_δ shows that conduction accounts for only part of the heat transferred across the boundary layer if Howard's model is used to interpret the results. Since the observed transfer coefficient is proportional to the inverse of the cube root of Ra_{TC} (i.e. $\bar{h} \sim 1/Ra_{TC}^{1/3}$), the heat transfer coefficient by conduction, expressed by $\bar{h} = k/Ra_\delta^{1/3}$, will be less than the observed value of $\bar{h}$ by approximately a factor of $3\sqrt{\frac{2500}{1000}}$ (= 1.32) for water at Pr = 5. Convective transfer must be responsible for making up this factor, which is a substantial portion of the total heat transferred.

Ra_p being less than Ra_δ shows that there is not enough time in a period for the boundary layer to grow by conduction to the observed average thickness, according to Howard's model. This leads to the conclusion that the boundary layer is probably only partially destroyed in each cycle, which is quite possible if the convection currents are centered at the outer edge of the boundary layer. This partial or total destruction has yet to be observed in the established convection, but seems possible since the first convection motion in the initiation phenomena appears to be centered within the fluid, as shown by the interferometric photos of Onat and Grigull (1970) and the lack of dependence of Ra_t on surface rigidity.

If the surface can deform, as in a gas-liquid surface, the possibility of the boundary layer being wiped out intuitively appears to be enhanced, because of the lack of surface rigidity. A rigid surface would be expected to maintain the fluid in a more motionless state near the boundary than a free surface during the plunging of a thermal. Spangenberg

and Rowland (1962) observed depressions in a gas-liquid surface caused by the plunging thermals. However, Schlieren photography used to observe this phenomena could not precisely observe whether the boundary layer was destroyed or not as the thermal plunged. The study did show that the thermal width was narrow compared to the distance between thermals, so that the boundary layer for the whole surface was not destroyed by the thermal plunging action.

However, as the intensity of the plunging is increased at the gas-liquid surface by increased driving forces, there could be a possible change in the extent of the destruction of the boundary layer, and consequent heat transfer resistance.

The results show that the simple model proposed by Howard does not predict some important experimental differences in the several Ra numbers discussed above. The concept of destruction of the boundary layer accounting for the periodic nature of the convection mechanism appears to be more accurately described by an alternate concept, namely a heat sink in the fluid with a periodic varying strength connected with the action of the thermals. This model assumes that the thermal action is confined to the outer edge of the boundary layer rather than distributed through it. Consequently the temperature profile in the boundary layer remains essentially constant with a periodically varying component and with the magnitude of this component increasing toward the center of the thermal action. This contrasts with Howard's model insofar that the transfer coefficient, the periodicity and the temperature profile scale do not necessarily have the same values of Rayleigh number as they should have in Howard's model. Further, Somerscales and Gazda (1969)

using fluids with Pr in the range 6 to 20 have found experimentally that the temperature fluctuations were a maximum (about 0.18 of the temperature drop across the boundary layer) at a vertical distance from the heated surface of approximately three times the conduction boundary layer thickness. The magnitude of the temperature fluctuation between the surface and this maximum site decreased approximately linearly, with an extrapolated value of zero at the surface. Howard (1963) reported Townsend's (1959) results for air (Pr = 0.7) in a form which showed the maximum temperature fluctuation of 0.18 times the temperature drop across the boundary layer occurring approximately at the edge of the conduction boundary layer. These observations appear consistent with the alternate model proposed above.

To investigate the steady-state convection mechanism further, more observation on the behavior of thermals is necessary to establish:

(1) the relation between the period between thermals and the average boundary layer thickness,

(2) the influence that thermals have in governing the rate of transfer across the boundary layer.

3. Comparison of Ra_t (Onset of Convection) with Ra_{TC} (Steady-State Convection)

The discussion in Sec. 2. showed that Howard's (1966) simple model of cyclic boundary layer growth and destruction was not completely adequate in describing experimental observations. Consequently, the concept of using the conditions at the onset of convection (Ra_t) to describe steady-state convection discussed in Sec. 1. may not be

completely valid. However, if the influence of convection and conduction in a cycle remain in a fixed ratio for a given set of conditions, then Ra_t, expressing the conduction influence, may be proportional to Ra_{TC}, i.e. $Ra_{TC} = K \cdot Ra_t$ where K is a constant. If this equality holds, then Ra_t data can be used to predict transfer coefficients through Ra_{TC} and Eq. (VIII-8). Further, there is the possibility of predicting the heat transfer coefficient through Ra_t from linear stability analysis for situations where it is not possible to predict the transfer coefficient mathematically because of the difficulty of mathematically describing the complex thermals. Some of the limitations of using Ra_t in this manner can be established by considering its application to the following cases.

(1) Effect of Pr. Values of Ra_{TC} were found as a function of Pr by using Eq. (VIII-8) and the deep-pool heat-transfer data of Somerscales and Gazda (1969), Silveston (1958), Globe and Dropkin (1959), Malkus (1954), Mull and Reihner (1930), and Rossby (1966). The results have been plotted on Fig. VIII-1, and are recorded in Appendix K. The expected form of Ra_t is that for a step change in boundary conditions. This is because the surface temperature is held constant over many cycles, so that at the start of a cycle the surface temperature is at a steady value. This is best approximated by a step change in surface conditions. The asymptotic values of Ra_t for a step function have been calculated in Appendix K, and plotted in Fig. VIII-1. The intermediate values of Ra_t have not been plotted because it is not known whether the small Pr and hence the intermediate values, are dependent on shape factor. This uncertainty was discussed in Chapter VII, Sec. 1.4. Ra_t has been multiplied by $\pi^{3/2}$ to be on an equivalent length scale with Ra_{TC}.

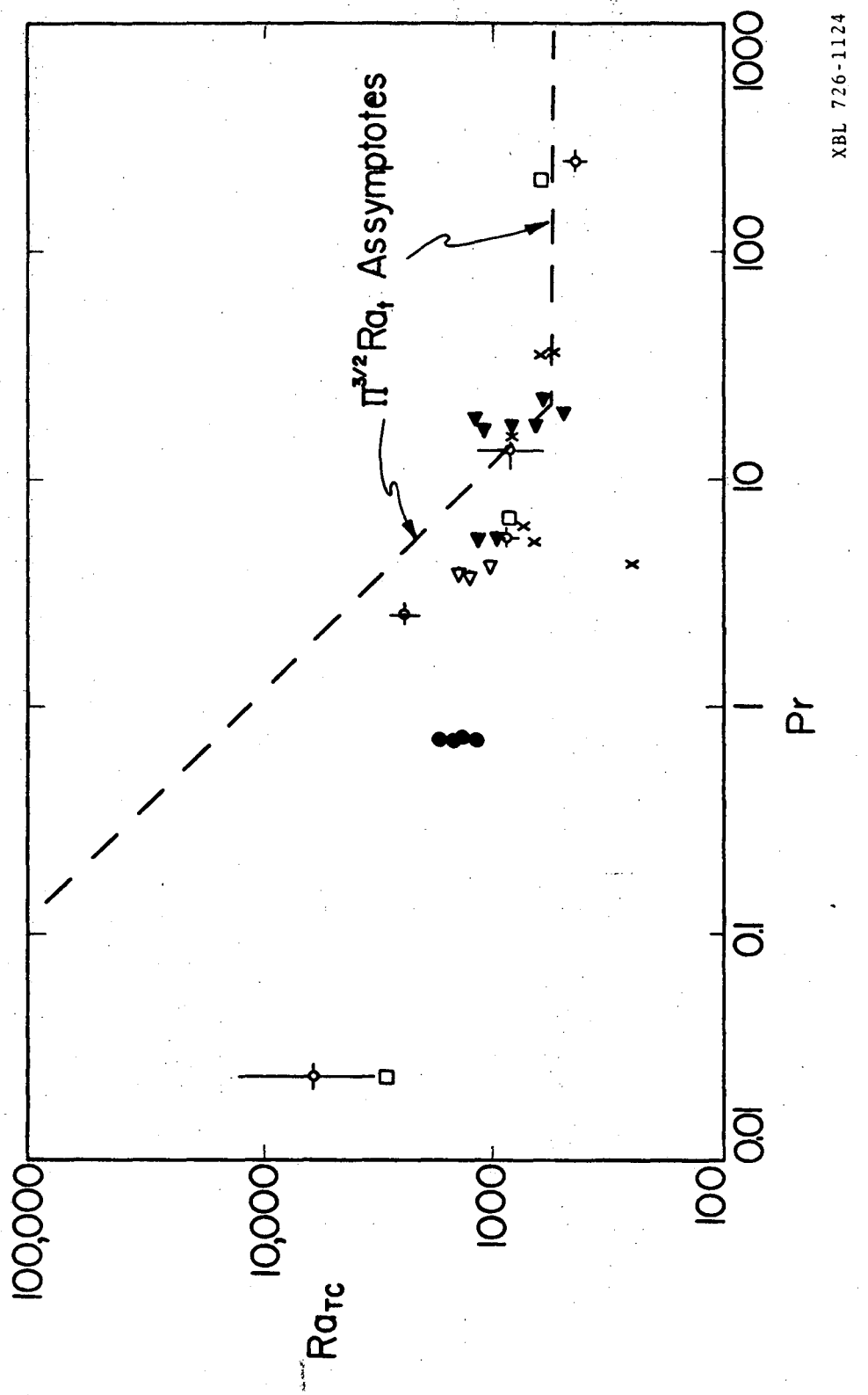

Fig. VIII-1. Comparison of Experimental Steady State Natural Convection Heat Transfer Data, Ra_{TC}, with Convection Initiation Data, $\pi^{3/2} Ra_t$. ● Mull and Reinhner (1930), Δ Malkus (1954), ✣ Globe and Dropkin (1958), X Silveston (1958), □ Rossby (1966), ▲ Somerscales and Gazda (1969).

The result $Ra_{TC} = Ra_t$ (approximately) holds reasonably well for Pr greater than 2, even though there is a large amount of scatter. At low values of Pr the experimental data fall below the above relation, which indicates that, as Pr decreases, the ratio of conduction to convection influence in the initiation mechanism changes with respect to that in the steady-state mechanism.

(2) Effect of Surface Rigidity. Results of Chapter VII, Sec. 1.6. show that Ra_t was independent of the rigidity of the surface. However, it can be anticipated that the ability of a surface to deform and the possibility of surface tension effects at a gas-liquid surface will produce different values of the transfer coefficient at a gas-liquid surface and at a solid-liquid surface. There are no transfer data available to use for evaluation of this effect.

(3) Effect of Fluid Vibration and Bulk Fluid Motion. Since the initiation in the initial onset of convection is probably on a different scale than the initial motion of a thermal in steady state convection, it can be anticipated that bulk fluid effects will have different effects on Ra_t and Ra_{TC}. There are no data available to evaluate the significance of this effect.

(4) Fluid-Depth Dependence. The results of Chapter V, Sec. 2. showed that the initiation phenomenon was independent of the depth of the fluid for fluid depths greater than about twice the penetration depth. However, in the production of thermals, the depth of the bulk fluid associated with the production and dissipation of the thermals is much greater than the penetration depth. This can be seen from the photos

of Sparrow, et al. (1970) of established thermals. The fluid depth necessary for fluid-depth independence in the thermal action has not been evaluated. Depth appears to be significant for Ra_H as high as 10^8, as shown by the heat transfer coefficients being correlated by an exponent less than 0.33 on Ra_H (Somerscales and Gazda, 1969).

4. Models Using Ra_t to Predict Steady-State Transfer Coefficients

(1) Foster (1970) used a theoretical analysis to study pseudo two-dimensional, finite-amplitude thermal convection in a fluid with an infinite Prandtl number. The results showed a building up and destruction of the density boundary layer in accordance with Howard's model. The form of the disturbance was assumed to be similar to that used in Amplification Theory for onset of convection, which incorrectly predicted that Ra_t was dependent on the surface rigidity. The onset of instability had to be arbitrarily pre-defined, but with these limitations and those associated with linear theory the study showed that Howard's model could be mathematically simulated.

(2) Burger (1970) measured the onset conditions and transfer coefficients in the absorption of sulfur dioxide into water for periods up to 20 times the onset time. The onset conditions were correlated with $Ra_t = 320$. Sc was 600, and the pressure driving force was a step function followed by a slow decay as gas was dissolved.

A model based on Howard's theory (1966) was compared with the experimental transfer coefficients. The theoretical coefficient was in the form of Eq. (VIII-6), and the period was assumed equal to the onset

time. The experimental values were about 20% lower than those predicted from the model, so that $Ra_{TC} = 1.73\ Ra_t$, which is different from the fixed surface results discussed in Sec. 2. where $Ra_{TC} = Ra_t$ for large values of Pr or Sc.

In light of the results of Chapter VI, Sec. 1.2., where the effect of surface waves on gas-liquid convection initiation was observed, it would be expected that Ra_{TC} at a gas-liquid surface would be lower than that at a solid-liquid surface because of surface deformation and surface-tension effects. These effects are probably more pronounced in the presence of thermal action than for the initiation mechanism. The difference between Burger's results and previous experimental results for fixed surfaces is not readily explicable.

5. Evaluation of Using Ra_t to Predict Ra_{TC}

The approach of determining Ra_{TC} from Ra_t appears limited. However, the initiation mechanism and steady-state mechanism have some similarities (i.e., production of convection from a conduction boundary layer) which should indicate important directions for further work in expanding information on transient and steady-state transfer coefficients, which are important in equipment design and general predictions.

IX. CONCLUSIONS AND FUTURE WORK

1. Conclusions

(1) The Rayleigh number in the form Ra_ℓ has been found to describe the onset of convection in a transient, low-vibration, one-dimensional system over a wide range of fluid depths and shapes of density profiles.

(2) Convection onset has been found experimentally to be independent of the rigidity of the surface, provided the surface is planar.

(3) Convection onset has been found experimentally to be only slightly affected by vibration, not including the effect of surface waves which might be produced by vibration at a free surface.

(4) Ra_ℓ at high values of Pr has been experimentally observed to be essentially constant in deep and shallow pools. The deep-pool value is slightly less than the shallow-pool value because of the difference in rigidity at the fluid-side edge of the density boundary layer in each case.

(5) Ra_ℓ is dependent on Pr for deep-pool cases. For low Pr, the onset conditions are well represented by $Ra_\ell \cdot Pr = 24{,}500$, while for high Pr, the relation $Ra_\ell = 1200$ applies.

(6) Ra_ℓ is independent of Pr in shallow-pool cases.

(7) Ra_ℓ is independent of the density-profile shape for high Pr fluids. The relationship for low Pr fluids has still to be verified.

(8) The Q.S.A. theoretical approach is inadequate for predicting Ra_ℓ in deep pools because it erroneously considers the bulk fluid beyond the density layer to be a destabilizing influence.

(9) The Amplification Theory appears inadequate to describe experimental observations. It develops relative terms, i.e. amplification

factor, which are not constant as experimental conditions change, i.e., variation in Pr.

(10) The experimental results show that Ra_ℓ can be calculated for the deep pool case and high Pr using the marginal stability assumption, and a density boundary layer gradient approximation. Presently, there is no model which adequately predicts the low-Pr, deep-pool values of $Ra_\ell \cdot Pr$.

(11) Surface-tension effects upon the onset of convection are absent in a truly one-dimensional transient system down to much smaller depths and much higher Marangoni numbers than has been concluded from previous experiments.

(12) Surface-tension-driven motion appears to be stimulated by surface deformation (i.e., surface waves), meniscuses, and surface tension gradients along the surface.

(13) Density convection initiators present in the fluid prior to the establishment of the adverse density field appear to fall into two categories: Primary, i.e. possibly bulk fluid motion; and Secondary, i.e., possible density variations in the fluid and surface waves.

(14) There is experimental evidence to suggest that the density boundary layer in steady-state, deep pool convection at solid-liquid surface is not destroyed during the production of the thermal, in contrast to Howard's (1966) model. This follows from a close examination of experimental data and comparing it with the deep pool, steady-state convection model of Howard (1966).

2. Recommended Future Work

Density-Driven Convection: Initiation

(1) Visual observation of first motion in the initiation phenomenon to identify the primary and secondary sources stimulating instability.

(2) Development of the low-Pr model for convection initiation in deep pools. The high-Pr model appears adequately defined by the model outlined in Conclusion 10, using a time-independent wave form to describe the first form of motion.

(3) Determining the effect of bulk motion on Ra_ℓ

(4) Examining whether Ra_ℓ is independent of density-profile shape at low Pr.

(5) Extending shallow-pool, free-surface data to high values of $\frac{\alpha t}{H^2}$ to determine when the surface rigidity and surface-tension-driven motion effects become significant.

Density-Driven Convection: Steady State

(6) Deep-pool data for a wide range of Pr in a sufficiently deep container in which the walls do not interfere with the thermal action, including period, density profile, and transfer coefficient.

(7) Visual observation of the thermal-production cycle to understand better the basic mechanism.

Surface-Tension-Driven Convection: Initiation

(8) Theoretical and experimental development of the relationship between the effects of surface waves and/or bulk fluid motion on the surface-tension-driven convection initiation phenomena.

Surface-Tension-Driven Coupled with Density-Driven Convection

(9) Influence of surface disturbances on the density-driven convection initiation at gas-liquid surfaces (either surface waves or bulk fluid motion).

(10) Extension of gas-liquid experimental results to liquid-liquid systems.

(11) Measurement of relative contribution of surface tension and density forces in the steady state for convection at a gas-liquid interface.

ACKNOWLEDGMENTS

I would like to express my sincere gratitude to Prof. C. Judson King for his insight, support, and enthusiasm to explore many areas associated with this work.

Many others to whom I am indebted include Prof. G. Pimental for the use of his laboratory in the early stages of this work, Miss G. Steel of the Lawrence Berkeley Laboratory for making available the vibrationless table, and to Prof. R. A. Seban and Prof. R. L. Pigford for their part in the preparation of this thesis.

Above all I am thankful for the encouragement and support from my wife, Dianne.

Work was performed under the auspices of the U. S. Atomic Energy Commission.

APPENDIX A. CALCULATIONS FOR INTERPRETATION OF LITERATURE RESULTS

The calculations included in this appendix are not included in the original papers. The work has been gathered together here to substantiate conclusions made in this report. First-named authors are in alphabetical order.

Definitions: The definitions of the Rayleigh number and the Marangoni number, used in the literature, vary with the length scale used in these dimensionless groups. In this report, the length scale for the transient problem is $\sqrt{\alpha t}$. The relevant groups are listed in Chapter I, Table 1, and the Nomenclature.

Blair and Quinn (1969)

Data were presented to distinguish between surface-tension-driven convection and density-driven convection in the system ethyl ether desorbing from a monochlorobenzene-10% ethyl ether solution. An estimation of the Marangoni number is made below. The Rayleigh number for the contrasting density-driven experiment was measured at 300 (approximately).

$$\frac{Ra_t}{M_t} = \frac{g \frac{\partial \rho}{\partial \psi} \mathscr{D}}{\frac{\partial \sigma}{\partial \psi}} \left(\frac{t_R^3}{t_M} \right)^{1/2}$$

Liquid properties at 20° C (International Critical Tables, 1928)

	Viscosity (c.p.)	Mol. Wt.	Density (gm/cc)	Mol. Vol. (cc/mole)	Surface Tension (dyne/cm)
Chlorobenzene (1)	0.80	110	1.1066	100	33.56
Ether (2)	0.233	74	0.714	103	17.01

Assuming a linear variation of viscosity with mole fraction,

$\mu_L = 0.743$ c.p.

Calculating diffusivities from the Wilke-Chang correlation

$$\mathscr{D}_{12} = 5 \times 10^{-5} \text{ cm}^2/\text{sec}$$

$$\mathscr{D}_{21} = 1.78 \times 10^{-5} \text{ cm}^2/\text{sec}$$

$$\mathscr{D}_L = \frac{\mathscr{D}_{12}\,\mu_2 + (\mathscr{D}_{21}\,\mu_1 - \mathscr{D}_{12}\,\mu_2)\psi_L}{\mu_L}$$

$$= 1.9 \times 10^{-5} \text{ cm}^2/\text{sec}$$

Assume no change of volume on mixing at this dilution

$$\frac{\partial \rho}{\partial \psi} = \frac{\partial \rho}{\partial \eta}\frac{\partial \eta}{\partial \psi} \qquad \begin{pmatrix} \eta = \text{mass fraction} \\ \psi = \text{mole fraction} \end{pmatrix}$$

$$= 0.392 \times 0.625$$

$$\frac{\partial \rho}{\partial \psi} = 0.245 \text{ gm/cc mole fraction}$$

Assume linear variation of surface tension with mole fraction

$$\frac{\partial \sigma}{\partial \psi} = \gamma_1 - \gamma_2 = 16.55 \text{ dynes/cm mole fraction}$$

From the experimental data at a driving force of 0.085 atm, the critical time for surface-tension-driven convection was 2 seconds; for the density-driven convection the critical time was 62 seconds.

The estimated value of the mass-transfer-driven Marangoni number is 3100 at an estimated Sc of 390. The estimated value of the mass-transfer-driven Rayleigh number for the free surface experiments was in the range $1.7 < Ra_t < 12.5$.

Clark and King (1970); Brown and King (1969)

A rectangular channel device was used by Clark and King (1970) to evaporate four solutes--carbon disulphide, n-pentane, cyclopentane, and ethyl ether from n-tridecane solvent into a flowing nitrogen stream. The authors found that the onset of convection could be described by a unique value of the Marangoni number (= 4500) for all the systems studied.

Estimations of the Rayleigh numbers and the thermal-driven Marangoni number are made below.

The composition-driven Rayleigh number was found from Table 1, and liquid properties listed in Clark's thesis (Clark, 1967). The results are as follows:

Solute	Ra_t(composition-driven)
n-Pentane	2.32
Ethyl ether	1.08
Cyclopentane	0.73

The thermal-driven Rayleigh number was reported for the n-pentane/tridecane system only; Ra = 28 at $(\psi_S - \psi_B) = 0.05$. The heat transfer and low flux mass transfer relations for dilute solutions were simplified to

$$(T_S - T_B) = \sqrt{\frac{\Theta}{\pi}} \frac{1}{K} (\psi_S - \psi_B) \Delta H_{vap} \quad .$$

For this experimental system

$$Ra_t = \left[\frac{g \frac{\partial \rho}{\partial T} \alpha^{1/2}}{\mu}\right] \left[T_S - T_b\right] t_c^{3/2} \quad .$$

The first bracket is almost constant in dilute solutions, the contact time (t) is identical for each run, and $(T_c - T_B)$ is almost proportional to $(\psi_S - \psi_B)\ \Delta H_{vap}$. It follows that

$$Ra_t \propto (T_S - T_b) \propto (\psi_S - \psi_B)\ \Delta H_{vap} \quad .$$

Thus the thermal-driven Rayleigh and Marangoni numbers at cellular onset can be estimated by $Ra_t/(\psi_S - \psi_B)\ \Delta H_{vap}$ = constant, $M_t/(\psi_S - \psi_B)\ \Delta H_{vap}$ = constant, where the constants are found from the n-pentane/tridecane system at $(\psi_S - \psi_B) = 0.05$.

Solute	Ra(thermal)	M(thermal)	Sc
n-pentane	16	30	1780
ethyl ether	2.3	4.3	1690
Cyclopentane	42	80	1800

For the Carbon Disulphide-Tridecane system, the thermal-driven Rayleigh number for the onset of convection was reported as $Ra_t = 285$. The corresponding composition-driven Rayleigh number was found from Table 1, Eq. (7) to be Ra = -40, the negative sign indicating a stabilizing composition gradient.

As in the density-driven system, the surface tension considerations indicate both a stabilizing and a destabilizing effect. From Table 1, Eq. (5), the composition-driven Marangoni number is M = 3150 at Sc = 2000, and from Table 1, Eq. (8), the thermal-driven Marangoni number was estimated at M = -1700 at Pr = 20.

The ratio of gas phase resistance to liquid phase resistance at convection initiation in the CS_2-tridecane system was approximately unity. This corresponded to a shape factor of about 0.62 (refer to Appendix G, Fig. G-3).

Brown and King (1969) varied the liquid flow rate in the apparatus used by Clark and King (1970). The results were as follows:

Re(approximately)	900	360	150
Mt	850	1690	4500
	Turbulent		Laminar

$$Re = \frac{(\text{hydraulic radius}) \cdot (\text{flow rate})}{(\text{viscosity})}$$

Currie (1967)

The approach used was to find the most unstable mode using the Q.S.A. segment approximation (refer Chapter II) and the marginal stability assumption. The published results were in the form Ra_H versus ε, where $\varepsilon = \ell/H$ (defined in Chapter II, Fig. II-2). The parameter ε was dependent upon the thermal conditions of the two fixed boundaries enclosing the liquid. For a linear decay in surface temperature at the heating surface and a constant temperature at the other surface (refer to Appendix H)

$$\frac{\ell}{H} = 1 - \frac{8}{\tau} \sum_{o}^{\infty} \frac{1}{(2n+1)^4 \pi^4} (1 - \exp - (2n+1)^2 \pi^2 \tau)$$

where

$$\tau = \frac{\alpha t}{H^2} \quad .$$

In order to arrange the data in the form Ra_ℓ vs τ for comparison with the present experimental data, ℓ/H vs τ was plotted in Appendix H, Fig. H-3 and then cross-plotted with Ra_H vs ℓ/H from Currie's (1967) paper to give Ra_ℓ vs τ. The results have been plotted in Chapter VII, Fig. VII-2 in the form of Ra_ℓ vs τ.

T. D. Foster (1965)

The author evaporated water from a quiescent pool and recorded the surface temperature as a function of time. From this measurement and from Schlieren techniques, he recorded convection initiation at the following conditions.

Run	Liquid Ht. (cm)	$(\frac{\partial T_s}{\partial t})_{av}$ (10^{-3} °C/sec)	t_c (sec)	$(\frac{\partial T_s}{\partial t})_{av} t_c^{5/2}$ (°C(sec)$^{3/2}$)	$\frac{\alpha t}{H^2}$ (10^{-3})
1	6.9	2.9	84	190	2.56
2	4.8	5.2	65	178	4.1
3	2.4	17.0	45	233	11.3
4	4.8	8.9	53	185	3.35
5	7.3	7.4	63	233	1.72
6	4.8	4.6	69	183	4.35
7*	10.0	5.1	70	211	1.0

The bulk temperature was kept at 28°C, and the physical properties for water at that temperature are listed in Appendix D. From the above results, the average Rayleigh number Ra_t was calculated as 256. The Marangoni number was calculated to be in the range 890 to 1670.

Foster reports that his surface temperature profiles were linear, but evaporation normally has a constant heat flux at its surface, which produces a parabolic temperature ($T_s \alpha t^{1/2}$) rather than a linear decay. In the evaporation case,

$$\frac{\text{area under parabola}}{\text{area if surface temperature were a step change}} = \frac{\int_T dt}{Tt} = \frac{\int_t^{3/2} dt}{t^{3/2}} = \frac{2}{3}$$

*Result taken from Spangenberg and Rowland (1961).

Foster (1969)

Estimation of Ra_t for Shallow Pool results:

Water was heated from below with liquid depths varying from 0.5 cm to 30 cm. At depths greater than 5 cm, the critical conditions were independent of depth. However, under identical heating conditions, the time for convection initiation increased from 70 seconds at greater than 5 cm to 300 seconds at 0.5 cm. The Rayleigh number could not be evaluated because the temperature difference across the liquid layer was not reported. However, it can be estimated from the heat conduction solution with the temperature at the lower boundary increasing linearly with time, and the upper surface insulated (air-liquid interface). This solution was taken from Carslaw and Jaeger (1962), p. 104, and was simplified using the parameters of Foster's experiment ($\frac{\alpha t}{H^2} = 1.8$):

$$(\Delta T)_{t=300} = 0.5\ \beta H^2/\alpha \quad \text{where} \quad \beta = \frac{\partial T_s}{\partial t}$$

The increase in Ra_t at the shallow depth can be found from

$$Ra_t \propto \Delta T\ t_c^{3/2}$$

$$\frac{(Ra_t)_{t=300}}{(Ra_t)_{t=70}} = \frac{(\Delta T)_{t=300}}{(\Delta T)_{t=70}} \times \left(\frac{300}{70}\right)^{3/2} = 10.7$$

From the results published by Foster (1969) the deep-pool Rayleigh number (Ra_t) was in the range 1000 - 1200; thus, the shallow pool Rayleigh number (Ra_t) would be in the range 10,700 - 12,800.

Mayr, Brian, and Vivian (1971); Mayr (1970)

Desorption was carried out in a short, vertical, wetted-wall column with solutes, acetone, ethyl ether and tri-ethyl-amine desorbing from aqueous solutions into a nitrogen stream. In a vertical liquid flow, the surface tension forces are acting in both the horizontal direction of gravity. Mayr et al., assumed that the gradients in the vertical direction were insignificant to the gradients in the horizontal direction (penetration direction). Thus only penetration results were reported.

Solute	M_t	Biot No.	$\pi^{1/2} M_t$ (Mayr, 1970 p. 168)
Acetone	115	0.055	274
Ether	3700	1.73	6500
T.E.A.	5700	0.296	10,000

Rippling was observed in the acetone desorption experiments, but was not observed for the other solutes. Such a rippling effect could decrease the stability of the system, invalidate the basis for comparison of the acetone with the other solutes, and weaken the experimental argument that the Biot number influences the Marangoni number. A possible cause of the rippling, advanced by the authors, and Ludvikson and Lightfoot (1971) is surface tension gradients along the liquid surface. It is not clearly understood why the acetone showed this effect preferentially, but the acetone was much less soluble in water than the other solutes and consequently the magnitude of the surface tension gradients along the interface was less.

The composition-driven Rayleigh number was found from Table 1, Eq. (5), and using liquid properties listed in Mayr's (1970) thesis and Perry's Chemical Engineers Handbook 4th ed. (1963).

Solute	Ra_t
Acetone	10^{-3}(approx)
Ether	10^{-4}(approx)

The maximum value of the thermal-driven Marangoni number was estimated at 28 with Pr = 7. The thermal-driven Rayleigh number was estimated at 0.02 from Table 1, Eq. (6).

Soberman (1959)

Soberman studied convection initiation by heating a silicone oil enclosed between two fixed surfaces, the lower surface being heated with a constant heat flux and the upper surface having an adiabatic character. The results were published with the incipient Rayleigh number, based on the total fluid depth, plotted against the product Ra · Nu, where Nu was the Nusselt number. The coordinate Ra · Nu was used to describe the nonlinearity of the density profile, but a more descriptive coordinate is $\frac{\alpha t}{H^2}$, which was used to correlate shallow pool density convection in Chapters V and VI. The reasons for this preference are:

(1) A clearer identification of the physical process as it passes from a mechanism based on the fluid depth to a mechanism based on the penetration depth.

(2) A uniformity in reporting results for different lower surface temperature profiles. The coordinate $\frac{\alpha t}{H^2}$ is the simplest available to describe shallow pool convection.

Soberman's data were replotted with $\frac{\alpha t}{H^2}$ as the descriptive coordinate. The data were replotted with Ra as a function of Nu. The Nusselt number was then found as a function of $\frac{\alpha t}{H^2}$ from

$$(Nu) = 1 + \frac{8}{\pi^2} \sum_{n_{odd}} \frac{\exp(-\pi^2 n^2 \frac{\alpha t}{H^2})}{n^2} .$$

This is the solution reported by Carslaw and Jaeger (p. 63) for a constant flux at one boundary and zero flux at the other boundary. From these two plots Ra was found as a function of $\frac{\alpha t}{H^2}$. The results are tabulated on the following page:

$\alpha t/H^2$	Ra_H
0.5	2500
0.3	2500
0.23	2600
0.17	2800
0.073	3500
0.029	5700
0.013	7800
0.006	10,500
0.0024	14,000

Somerscales and Gazda (1969)

Experimental temperature profiles for deep pool steady state convection were published by these authors. Their data was used to evaluate Ra_δ for use in Chapter VIII, Sec. 2. The data is from the original paper. The data were fitted well by Howard's (1966) approximation given by Eq. (VIII-8) in Chapter VIII. The value of Ra_δ is found as follows,

$$\xi = \frac{z}{\delta}\sqrt{4/\pi} = \frac{1}{1.89}\frac{z}{z_\alpha}$$

Thus

$$\delta = 2.13\, z_\alpha$$

(note: The original paper erroneously lists 1.89 in the numerator rather than in the denominator. The mistake is obvious when comparing Elder's (1965) data in Somerscales and Gazda (1969) and Howard (1966).)

$$Ra_\delta/Ra_H = \frac{1}{2}\left(\frac{\delta}{L}\right)^3 = \frac{1}{2}\left(\frac{z_\alpha}{L}\right)^3\left(\frac{\delta}{z_\alpha}\right)^3 = 4.82\left(\frac{z_\alpha}{L}\right)^3$$

the coefficient $\frac{1}{2}$ arises from the temperature ratios in Ra_H and Ra_δ.

Experimental results

Ra_H	$\frac{z_\alpha}{L}$	Ra_δ
1.47×10^7	0.026	1250
3.21×10^8	0.01	1550

APPENDIX B. IDENTIFICATION AND ELIMINATION OF TWO-DIMENSION EFFECTS IN A TEMPERATURE PROFILE AT A GAS-LIQUID INTERFACE

One of the major objectives of this study has been the isolation of a vertical one-dimensional temperature field in a liquid. This has been for two reasons. First, theoretical predictions are for vertical one-dimensional temperature fields. Very little has been published on the horizontal or two-dimensional fields which would enable one to correct for any two-dimensional character in an experiment. The second reason is connected with uncontrollable surface-tension-driven flow in free surface experiments. The conditions under which this effect is produced and its results are discussed below.

From the onset of this project, the objective was to identify surface convection motion, especially with gas-liquid interfaces. The literature survey had shown that previous work in this field had involved mass transfer and heat transfer experiments. The latter were attractive (ref. Chapter IV) and had utilized evaporation as the means of producing a temperature gradient at the surface. For this reason, our earliest work was with evaporation of pure organic liquids.

Previous published work had been limited by the range of evaporation which was used in the experiments. In the present work, the evaporation rate, and hence the surface cooling rate, was varied over a wide range by sucking a controlled air draught over the liquid surface. The apparatus is described in Fig. B-1. Air at room conditions is sucked over the liquid surface and under the lip of the funnel. Some runs were taken with the thermocouple at different radial positions, and a radial temperature profile was found. As mentioned above, a two-dimensional temperature profile

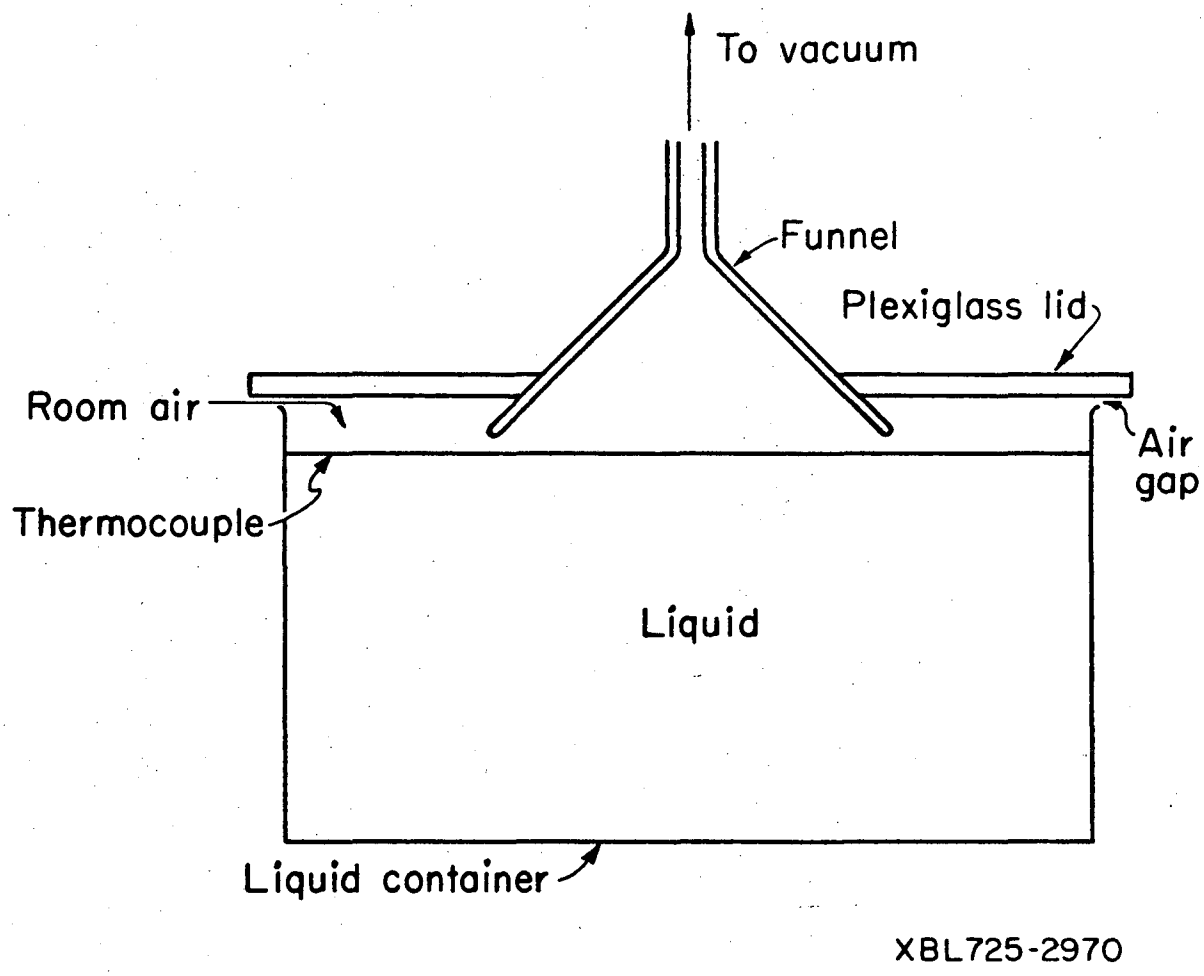

Fig. B-1. Apparatus using Forced Draught to Produce Evaporation During the Free Surface Preliminary Experiments.

presented a difficulty for correlation, scale-up and reproducibility. The results of these experiments and the experience of the published evaporative work indicated that cooling by evaporation with a constant liquid bulk temperature was limited in its use of verifying existing theory and providing data for correlations. This led to cooling by suspending a cold body above the liquid surface, as an alternative to evaporative cooling.

The simplest design tried first for conductive heat transfer experiments (Fig. B-2) used a liquid in a thermos flask with an epoxy collar supporting a flat-bottomed metal can. Cold solvent (e.g., methanol) with temperatures varying from 15°C to -60°C was poured into the metal can to produce the cooling effect. The liquid surface temperature response was almost linear and often showed a smooth minimum followed by periodic maxima and minima. However, the usual response was very jagged and only a semblance of a minimum could be seen. To improve the quality of the response, the jagged character had to be removed from the temperature response.

One of the first undesirable effects to be noted was for non-viscous liquids, which generally have a higher vapor pressure than viscous liquids. The evaporative liquid would condense on the base of the cold metal surface, causing liquid droplets to form and run down the sides of the collar, making liquid contact between cold metal surface and liquid meniscus. As the work of Ludvikson and Lightfoot (1971) has shown, this led to surface-tension-driven motion along the surface of the liquid, thus destroying heat transfer by simple conduction. This type of interference with one-dimensional heat transfer by conduction was repeated in different forms until eventually the preferred

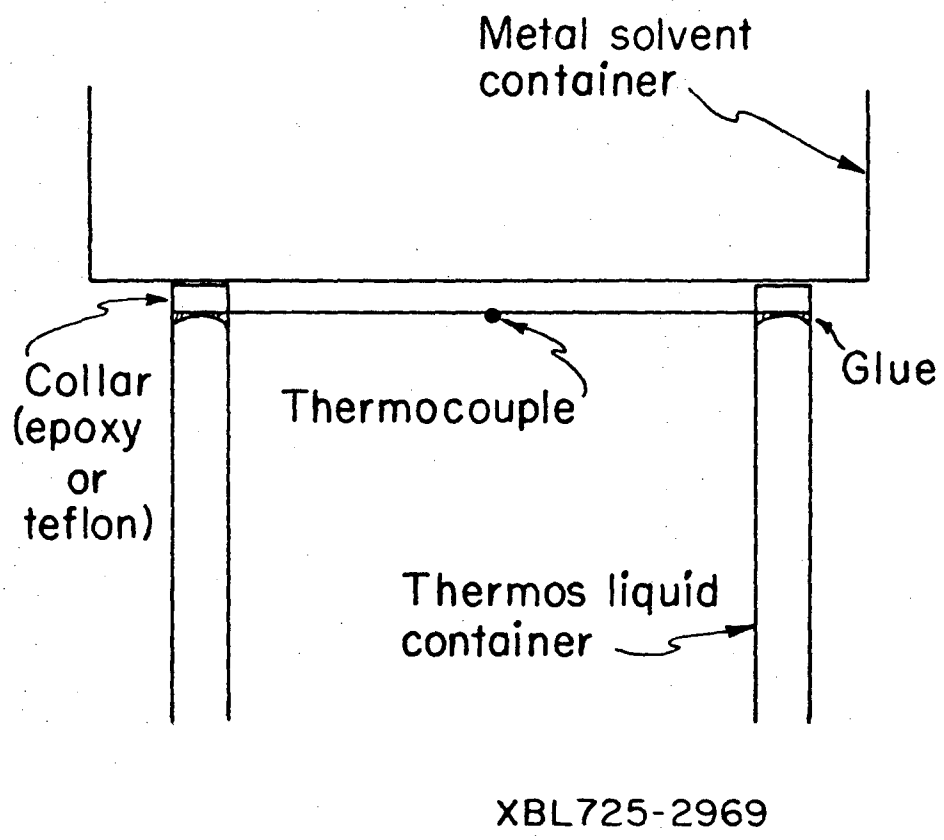

Fig. B-2. Apparatus using cold solvent and a Thermos with a meniscus on the liquid surface During the Free Surface Preliminary Experiments.

type of heat transfer was isolated. The driving force for surface-tension-generated motion lies in a gradient in the surface tension along the liquid surface. Since surface tension increases with decreasing temperature for most organic liquids, a thermal gradient along the liquid surface will produce motion.

Non-evaporating liquids were used, but the liquid surface temperatures during a run became more jagged the longer the liquid remained in the vessel. The collar, made of epoxy, was observed to become wetter (i.e., the epoxy was slightly porous) the longer it stayed in contact with the liquid, and this allowed the meniscus to creep further up the sides of the container. The liquid at the top of the meniscus was closer to the cold plate than the bulk of the liquid and thus could cool faster than the bulk liquid. This resulted in a temperature gradient along the liquid surface, but because the liquid was not in contact with the metal plate, the surface tension gradient could not sustain itself, and, after a brief burst of motion in which the temperature gradient along the surface was reduced, the liquid surface began to cool again under conduction conditions. These brief bursts of surface tension motion apparently led to the erratic character of the temperature profile, and their inconsistent timing and effect on the liquid surface temperature was the apparent reason for the nonreproducibility of the larger convective effect. In an attempt to decrease the meniscus and collar wetting effects, the epoxy collar was replaced by a Teflon collar. The results became more reproducible within a certain range of experimental conditions. Outside this range the temperature minimum was a different shape and did not follow the correlation of the other experimental range.

The source of the irregular motion was suspected as a surface tension gradient along the liquid surface. Since the surface was flat, and the temperature gradient along the liquid surface had to be a result of differences in heat transfer resistance between the cold plate and radial position on the liquid surface, the site for these differences could occur at the wall-air-liquid junction. Here there was a difference in heat transfer resistance through the air and through the solid. Because of the differences in thermal properties of the solid and the air, the liquid below the air would initially cool much faster than the liquid surface next to the solid wall.

Thermocouples were placed on the liquid surface in the center of the liquid and at the liquid-air-wall junction, and the responses were recorded during a run in which the liquid was heated rather than cooled. Heating produced a density-stable situation in the liquid, but did not change the heat flow paths and hence the expected source of surface tension motion. A thermocouple was also placed in the air space above the thermocouple on the liquid surface and halfway between hot plate and liquid surface.

The results (see Fig. B-3) show the temperature at the wall lower than the liquid temperature initially, but after a short period the wall temperature was warmest. The air temperature rapidly reached a pseudo-steady state, indicating that the temperature gradient in the air space was almost linear. After a certain time, the responses of all thermocouples changed rapidly and simultaneously. After this event the liquid temperature decreased and then increased so as to maintain a constant temperature difference with the wall temperature. The most dramatic

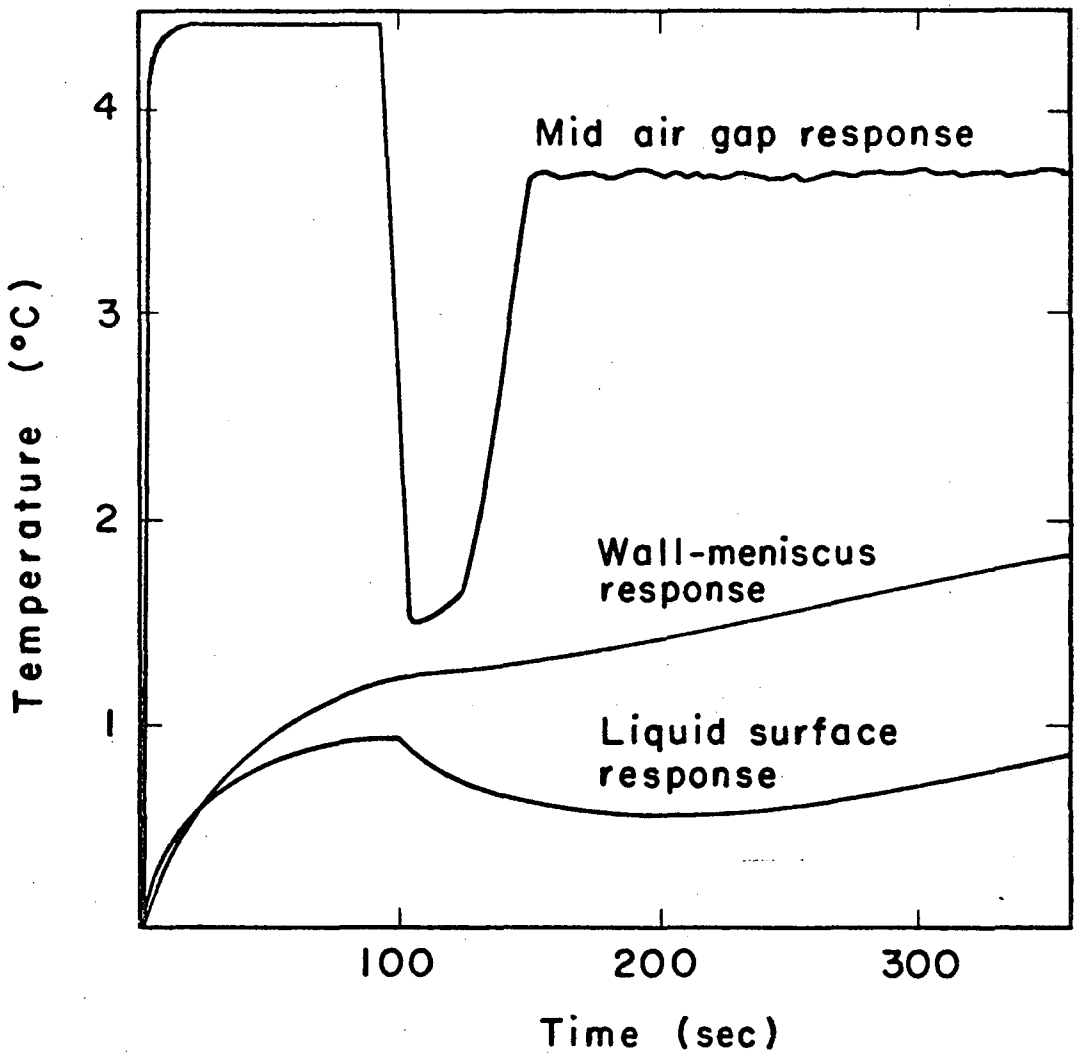

Fig. B-3. Temperature Responses in the Apparatus described in Fig. B-2 showing the effect of surface tension motion.

change was in the air temperature, which showed a sudden decrease from its pseudo-steady state value to a third of that value, and then maintained that temperature level until it increased to about 80% of the original pseudo-steady state temperature. The air temperature curve could be explained by rotation in the air space which transported heat much faster than the conduction process, especially in decreasing the half-gap temperature to a third of its conduction value. The speed of the air temperature decrease indicated that the surface tension-driven motion must have been rapid enough to generate the speed of the air gap convection. The greatest intensity on the surface-tension-driven motion must have lasted only for a short period before moving into a quieter phase of motion, as indicated by the intensity of the convection required to maintain the air gap temperature at its various levels.

Similar runs were repeated and it was found that $\Delta T\ t_c^{1/2}$ was approximately constant, where ΔT was the difference between the wall and the bulk-liquid surface temperature and t_c was the time taken for motion to begin. The air temperature was a good indicator of the presence and intensity of motion. However, rather than exploring this phenomenon at this time, since there appeared to be no theory available as a guide, the design was modified by using a foam for the collar which had similar thermal properties as air. Thus the cooler support was no longer a preferred path for heat transfer and the temperature in the liquid was one-dimensional.

With these modifications, the liquid surface temperature responses were smooth (i.e., no erratic characteristic) and reproducible. The onset, the transient, and steady state convection were clearly observed.

APPENDIX C. PHYSICAL PROPERTIES OF FLUIDS AND PLASTICS AT 25°C

The physical property data were found from the literature and presented in the following tables with these dimensions; density (ρ) gm/cc, viscosity (μ) c.p., heat capacity (c) cal/gm °C, heat conductivity (k) cal/gm sec °C, thermal diffusivity (α) cm^2/sec, coefficient of thermal expansion (β) $°C^{-1}$, surface tension (σ) dynes/cm. The thermal diffusivity and Prandtl numbers were calculated from the values of the other physical properties.

The key to the reference literature from which the data were obtained is given in the bracket following the value of the datum. The list of references is at the end of the appendix.

Table C-1. Thermal Properties of Plastics

	$K \times 10^4$	$\alpha \times 10^{+3}$
MMA Styrene Copolymer	3.0 - 4.0 (8)	0.82 to 1.11 (8)
Phenolic Cast Resin	3.5 (8)	0.68 to 0.9 (8)
Polystyrene	2.4 - 3.2 (8)	0.71 - 0.97 (8)
Plexiglass	4.0 - 6.0 (8)	0.95 - 1.4 (8)

Table C-2. Thermal Properties of Foam and Air

	$K \times 10^{+5}$	$\rho \times 10^2$	C	α
Polystyrene Foam	7.8 (8)	3.8 (8)	-	
Air	6.6 (9)	0.14 (9)	0.25 (9)	0.18

Table C-3. Surface Tension Data

Surface Tension (dynes/cm)

	15°C	20°C	25°C	30°C
n-Butanol (5)	25.00	24.57	24.2	23.7
n-Octanol (3,5)	26.50	26.00	--	25.21

Table C-4. Typical Physical Properties of Fluids at 25°C

Fluid	ρ	μ	C	$K \times 10^4$	$\alpha \times 10^3$	$\beta \times 10^3$	Pr
Methanol	0.79 (1)	0.55 (1)	0.68(1)	5.05(1)	1.05	1.2 (1)	7.4
Water	0.99 (1)	0.836(1)	1.0 (1)	14.5 (1)	1.45	0.285(1)	5.8
n-Decane	0.727(2)	0.87 (2,3)	0.52(2)	3.40(5)	0.90	1.03 (2)	13.7
n-Undecane	0.737(2)	1.10 (2,3)	0.52(2)	3.40(5)	0.865	0.983(2)	16.9
n-Butanol	0.808(3)	2.78 (3,1,4)	0.57(3)	3.67(4)	0.80	0.95 (3)	43
n-Hexanol	0.816(2)	4.64 (2,3)	0.56(2)	3.75(5)	0.82	0.85 (2)	69
n-Octanol	0.827(1,2)	7.9 (1,2,3)	0.53(5)	3.85(4,1)	0.88	0.82 (2,5)	108
Silicone Oil 50 cs	0.96 (6)	48.0 (6)	0.35(6)	3.6 (6)	1.03	1.04 (6)	465
Silicone Oil 100 cs	0.97 (6)	97.0 (6)	0.34(6)	3.7 (6)	1.10	0.98 (6)	890
Silicone Oil 1000 cs	0.97 (6)	971.0 (6)	0.33(6)	3.8 (6)	1.14	0.96 (6)	8500

References

(1) "Handbook of Physics and Chemistry" 40th ed. (1928).

(2) J. Timmermans, "Physico-Chemical Constants of Pure Organic Compounds", (1950).

(3) International Critical Tables (1928).

(4) R. C. Reid and T. K. Sherwood, "Properties of Gases and Liquids", (1966).

(5) J. H. Cline and D. H. Andrews, J. Am. Chem. Soc. 53, 3669 (1931).

(6) Bulletin #05-061, Dow Corning Chemical Products Division, (1963).

(7) B. C. Sakiadis and J. Coates, A.I.Ch.E.J. 1, 275 (1955).

(8) Modern Plastics Encyclopedia (1970).

(9) R. H. Perry, "Chemical Engineers Handbook", 4th ed. (1963).

APPENDIX D. FIXED SURFACE RESULTS

Table D-1. Deep Pool Runs (No Dependence on Depth, Wall Effects)

Methanol Pr = 7.4

Run	Ht(cm)	ΔT(°C)	t_c(sec)	Ra_t	$\frac{\alpha t}{H^2} \times 10^3$	Dia(cm)	Ra_ℓ
1	3.65	0.226	96	1150	6.8	3.65	3900
2	"	0.328	74	1150	5.3	"	3900
3	"	0.121	144	1150	10.3	"	3900

n-Decane Pr = 13.7

Run	Ht(cm)	t_c(sec)	ΔT(°C)	Ra_t	$\frac{\alpha t}{D^2} \times 10^{+3}$	Dia(cm)
1	2.8	84	0.45	875	2.16	5.9
2	"	82	0.385	720	2.10	"
3	"	110	0.235	685	2.83	"
4	"	118	0.240	775	3.03	"
5	"	100	0.331	835	2.57	"
6	4.0	44	1.16	855	0.50	8.9
7	"	29	2.26	890	0.33	"
8	"	26	2.45	820	0.30	"
9	"	29	2.28	900	0.33	"
10	"	26	2.65	890	0.30	"
11	"	42	1.27	875	0.48	"
12	"	38	1.54	910	0.435	"
13	"	64	0.69	890	0.73	"
14	"	50	0.94	840	0.57	"

(continued)

Table D-1. (continued)

n-Butanol Pr = 43

Run	Ht(cm)	t(sec)	ΔT(°C)	Ra_t	$\frac{\alpha t}{H^2} \times 10^3$	Dia(cm)	Ra_ℓ
1	5.6	64	1.80	700	1.5	8.9	2370
2	"	34	5.4	820	0.85	"	2770
3	"	40	3.17	615	1.0	"	2080
4	"	47	2.57	640	1.2	"	2170
5	"	48	2.76	700	1.2	"	2370
6	"	37	3.75	640	0.92	"	2170
7	3.65	92	1.04	700	5.6	3.65	2370
8	2.9	95	0.93	660	5.5	6.9	2230
9	"	112	0.75	680	6.7	"	2300
10	"	140	0.55	700	8.3	"	2370
11	"	175	0.38	675	10.5	"	2280

n-Octanol Pr = 108

Run	Ht(cm)	t(sec)	ΔT(°C)	Ra_t	Dia(cm)	$\frac{\alpha t}{D^2} \times 10^4$
1	5.65	109	1.66	475	8.9	11.9
2	"	124	1.37	475	"	13.5
3	"	204	0.77	560	"	22.2
4	"	152	1.06	500	"	16.5
5	"	50	5.8	510	"	5.5
6	"	63	4.2	525	"	6.8
7	"	57	4.7	505	"	6.2

(continued)

Table D-1. (continued)

n-Octanol Pr = 108

Run	Ht(cm)	t(sec)	ΔT(°C)	Ra_t	Dia(cm)	$\frac{\alpha t}{D^2} \times 10^4$
8	5.65	76	3.1	515	8.9	8.3
9	"	51	5.7	520	"	5.5
10	"	143	1.03	440	"	15.6
11	"	84	2.58	495	"	9.1

50 cs Dow Corning Silicone Oil Pr = 465

Run	Ht(cm)	t(sec)	ΔT(°C)	Ra_t	$\frac{\alpha t}{H^2} \times 10^3$	Dia(cm)	Ra_ℓ
1	5.65	163	2.37	330	5.5	8.9	1120
2	"	230	1.48	350	7.8	"	1190
3	"	133	3.32	350	4.5	"	1190
4	"	84	9.1	475	2.9	"	1610
5	"	73	11.6	490	2.5	"	1660
6	"	96	8.2	520	3.3	"	1770
7	"	106	7.4	540	3.6	"	1830
8	"	108	7.4	540	3.7	"	1830
9	"	100	6.6	450	3.4	"	1530
10	"	120	4.3	385	4.1	"	1310
11	"	200	2.25	430	6.8	"	1460
12	"	194	2.25	415	6.6	"	1410
13	"	244	1.45	375	8.3	"	1270
14	"	254	1.50	415	8.8	"	1410
15	"	140	3.45	390	4.8	"	1330

(continued)

Table D-1. (continued)

100 cs Dow Corning Silicone Oil, Pr = 890

Run	Ht(cm)	Dia(cm)	t(sec)	ΔT(°C)	Ra_t
1	5.65	8.9	380	1.25	310
2	"	"	182	3.9	320
3	"	"	275	2.17	330
4	"	"	129	5.8	285
5	"	"	120	7.7	340
6	"	"	200	3.55	340
7	"	"	211	2.8	290
8	"	"	95	10.7	335

1000 cs Dow Corning Silicone Oil, Pr = 8500

Run	Ht(cm)	Dia(cm)	t(sec)	ΔT(°C)	Ra_t	$\frac{\alpha t}{H^2} \times 10^3$	Ra_ℓ
1	5.65	8.9	435	14.7	435	16.2	1470
2	"	"	358	19.3	425	13.3	1440
3	"	"	276	23.5	355	10.3	1200
4	"	"	617	6.9	350	22.8	1190
5	"	"	530	7.3	325	19.7	1100
6	"	"	470	9.6	325	17.5	1100
7	"	"	345	17.0	355	12.8	1200
8	"	"	416	14.3	400	15.5	1350
9	"	"	372	17.0	355	13.8	1200

Table D-2. Deep Pool Runs (Variation of Fluid Width)

n-Decane Pr = 13.7

Run	Ht(cm)	Dia(cm)	t(sec)	ΔT(°C)	Ra_t	$\frac{\alpha t}{D^2}$
1	2.5	0.57	88	0.55	1150	0.24
2	"	"	90	0.56	1200	0.25
3	"	"	106	0.64	1760	0.29
4	"	"	58	0.81	900	0.155
5	"	"	32	1.56	670	0.087
6	"	"	48	0.90	760	0.130
7	"	"	62	0.62	760	0.170

n-Octanol Pr = 108

Run	Ht(cm)	Dia(cm)	T(sec)	ΔT(°C)	Ra_t	$\frac{\alpha t}{D^2}$
1	2.5	0.87	46	5.3	415	0.053
2	"	"	55	4.15	425	0.064
3	"	"	110	1.80	520	0.128
4	"	"	86	2.80	510	0.088
5	"	0.57	112	4.55	1350	0.30
6	"	"	39	8.8	550	0.105
7	"	"	35	9.5	510	0.095
8	"	"	83	6.2	1170	0.225
9	"	"	60	4.8	560	0.160
10	"	"	166	3.13	1680	0.45
11	"	"	90	3.9	830	0.24
12	"	"	116	3.75	1180	0.31

Table D-3. Shallow Pool Runs

Methanol Pr = 7.4

Run	Ht(mm)	t(sec)	ΔT(°C)	Ra_ℓ	Ra_t	Ra_H	$\frac{\alpha t}{H^2}$	Dia(mm)
1	11.9	124	0.187	4700	1410	-	9.2×10^{-2}	36.5
2	"	136	0.169	4820	1460	-	10.2×10^{-2}	"
3	"	74	0.346	4050	1190	-	5.5×10^{-2}	"
4	6.2	213	0.124	2910	2060	4760	5.85×10^{-1}	"
5	"	128	0.205	3550	1600	7810	3.5×10^{-1}	"
6	"	86	0.385	4520	1670	14,700	2.36×10^{-1}	"
7	3.48	140	0.50	2620	4450	3340	1.21	"
8	"	64	0.57	2350	1570	3820	0.55	"
9	"	74	0.515	2300	1770	3460	0.64	"
10	"	161	0.38	2160	4240	2560	1.38	"
11	"	111	0.46	2420	2910	3110	0.96	"

(continued)

Table D-3. (continued)

n-Butanol Pr = 43

Run	Ht(mm)	t(sec)	ΔT(°C)	Ra_ℓ	Ra_t	Ra_H	$\frac{\alpha t}{H^2}$	Dia(mm)
1	11.9	102	0.68	1700	500	39,000	5.76×10^{-2}	36.5
2	"	96	0.69	1700	500	39,500	5.4×10^{-2}	"
3	"	95	0.96	2310	680	55,000	5.4×10^{-2}	"
4	"	102	0.70	1870	550	40,000	5.8×10^{-2}	"
5	"	150	0.35	1650	485	19,500	8.5×10^{-2}	"
6	6.2	148	0.95	3050	1320	7700	0.322	"
7	"	102	1.01	2230	795	8150	0.213	"
8	"	92	1.13	2230	760	9150	0.192	"
9	"	42	2.27	1650	480	18,300	8.7×10^{-2}	"
10	"	63	2.06	2500	782	16,700	0.131	"
11	"	61	2.06	2400	750	16,700	0.13	"
12	"	39	3.32	2130	625	27,000	0.08	"
13	"	108	1.03	2440	890	8350	0.225	"
14	"	80	1.45	2400	790	11,750	0.167	"
15	3.48	164	2.05	2300	3290	2900	1.08	"

(continued)

Table D-3. (continued)

n-Butanol Pr = 43

Run	Ht(mm)	t(sec)	ΔT(°C)	Ra_ℓ	Ra_t	Ra_H	$\frac{\alpha t}{H^2}$	Dia(mm)
16	3.48	260	2.30	2780	7350	3260	1.72	36.5
17	"	346	1.67	2450	10,000	2800	2.38	"
18	"	376	1.97	2280	9310	2370	2.40	"
19	"	96	2.36	2200	1690	3360	0.63	"
20	"	36	6.0	2720	1010	8550	0.24	"
21	"	54	3.7	2530	1150	5280	0.36	"
22	"	82	2.9	2530	1630	4120	0.54	"
23	2.06	332	5.0	1490	23,100	1490	6.3	"
24	"	202	6.1	2370	13,500	1830	3.7	"
25	"	240	5.7	1610	16,100	1690	4.55	"
26	"	448	4.85	1440	35,400	1440	8.5	"
27	"	127	6.25	1650	6850	1870	2.4	"
28	"	66	7.9	1900	3240	2340	1.25	"
29	"	66	7.9	1870	3230	2340	1.25	"
30	"	52	9.3	2150	2690	2780	0.98	"

(continued)

Table D-3. (continued)

n-Butanol Pr = 43

Run	Ht(mm)	t(sec)	ΔT(°C)	Ra_ℓ	Ra_t	Ra_H	$\frac{\alpha t}{H^2}$	Dia(mm)
31	2.06	117	6.35	1660	6150	1890	2.2	36.5
32	"	95	6.9	1890	4900	2050	1.80	"

50 cs Dow Corning Silicone Fluid Pr = 465

Run	Ht(mm)	t(sec)	ΔT(°C)	Ra_ℓ	Ra_t	Ra_H	$\frac{\alpha t}{H^2}$	Dia(mm)
1	11.9	377	1.87	2320	945	5950	0.29	36.5
2	"	164	4.20	1950	600	13,400	0.126	"
3	"	230	3.7	2620	875	11,700	0.177	"
4	"	685	1.1	2170	1350	3500	0.53	"
5	"	292	2.72	2390	920	8650	0.255	69 mm
6	"	142	5.85	2210	670	18,700	0.109	"
7	"	192	3.97	2270	710	12,600	0.142	"
8	6.2	480	5.2	1960	3700	2300	1.36	36.5
9	"	288	6.85	2270	2270	3050	0.82	"

(continued)

Table D-3. (continued)

50 cs Dow Corning Silicone Fluid Pr = 450

Run	Ht(mm)	t(sec)	ΔT(°C)	Ra_ℓ	Ra_t	Ra_H	$\frac{\alpha t}{H^2}$	Dia(mm)
10	6.2	433	5.2	1900	3170	2300	1.23	36.5
11	19.6	270	2.08	2030	600	--	0.078	"

APPENDIX E. FREE SURFACE RESULTS

Table E-1. Deep Pool Results (Thermoelectric Cooler)

n-Decane Pr = 13.7

Run	t(sec)	ΔT(°C)	Ra_t
1	28	1.54	575
2	38	1.48	875
3	40	1.55	990
4	56	0.61	650
5	47	1.0	810
6	38	1.50	885
7	60	0.64	750
8	24	1.83	540
9	110	0.193	560
10	83	0.32	610

n-Butanol Pr = 43

Run	t(sec)	ΔT(°C)	Ra_t	M_t	$\frac{\alpha t}{H^2} \times 10^{+3}$
1	38	2.26	405	1520	2.3
2	140	0.405	515	525	8.4
3	120	0.87	870	1040	7.2
4	170	0.48	820	670	10.2
5	48	1.75	446	1320	2.9
6	106	0.81	680	910	6.4
7	112	0.485	440	560	6.7
8	31	2.7	360	1640	1.9

(continued)

Table E-1. (continued)

n-Butanol Pr = 43

Run	t(sec)	ΔT(°C)	Ra_t	M_t	$\frac{\alpha t}{H^2} \times 10^{+3}$
9	60	1.45	520	1225	3.6
10	84	0.91	540	910	5.0
11	200	0.39	850	600	12.0
12	72	1.16	540	1070	4.3
13	62	1.28	620	1100	3.7

n-Octanol Pr = 108

Run	t(sec)	ΔT(°C)	Ra_t	Ma_t
1	166	1.0	535	477
2	100	2.29	570	850
3	62	4.08	500	1190
4	73	3.12	485	990
5	128	1.26	455	530
6	282	0.515	610	310
7	190	0.60	395	310
8	97	1.70	410	620
9	88	2.33	480	810
10	174	0.85	490	415

(continued)

Table E-1. (continued)

100 cs Silicone Oil Pr = 890			
Run	t(sec)	ΔT(°C)	Ra_t
1	90	7.5	215
2	150	4.22	260
3	210	2.35	240
4	108	5.4	205
5	118	6.45	275
6	155	3.0	195
7	78	7.1	165
8	190	2.25	200
9	255	1.55	210
10	95	6.0	185
11	135	4.1	215

Table E-2. Deep Pool Results (Spray Cooler)

n-Decane Pr = 13.7

Run	Ra_t	S
1	275	0.694
2	262	0.630
3	305	0.611
4	400	0.50
5	118	0.843
6	165	0.786
7	111	0.816
8	161	0.810
9	355	0.505
10	206	0.761
11	206	0.625
12	121	0.938
13	160	0.727
14	121	0.777

n-Undecane Pr = 16.9

Run	Ra_t	S
1	179	0.757
2	157	0.791
3	157	0.851
4	405	0.623
5	296	0.547

(continued)

Table E-2. (continued)

n-Undecane Pr = 16.9

Run	Ra_t	S
6	151	0.897
7	145	0.782
8	181	0.767
9	221	0.704
10	179	0.825
11	380	0.53
12	165	0.779
13	140	0.769
14	123	0.883
15	193	0.813
16	109	0.873
17	145	0.735
18	460	0.52
19	280	0.608
20	307	0.559
22	390	0.621
23	385	0.533

n-Butanol Pr = 43

Run	Ra_t	S
1	421	0.522
2	123	0.791

(continued)

Table E-2. (continued)

n-Butanol Pr = 43

Run	Ra_t	S
3	325	0.558
4	118	0.860
5	124	0.861
6	135	0.750
7	129	0.876
8	101	0.861
9	118	0.718
10	109	0.861
11	138	0.843
12	146	0.802
13	166	0.714
14	130	0.672
15	208	0.628

n-Hexanol Pr = 69

Run	Ra_t	S
1	135	0.860
2	270	0.824
3	166	0.843
4	142	0.866
5	148	0.830
6	230	0.679

(continued)

Table E-2. (continued)

n-Hexanol Pr = 69

Run	Ra_t	S
7	155	0.877
8	235	0.740
9	285	0.535
10	162	0.737
11	434	0.630
12	254	0.748
13	495	0.522
14	440	0.500
15	225	0.755
16	358	0.649
17	531	0.520

(n-Octanol = Pr 108)

Run	Ra_t	S
1	162	0.877
2	215	0.865
3	450	0.550
4	335	0.668
5	235	0.803
6	262	0.784
7	200	0.754
8	405	0.543

(continued)

Table E-2. (continued)

(n-Octanol = Pr 108)

Run	Ra_t	S
9	190	0.794
10	212	0.752
11	390	0.581
12	200	0.764
13	405	0.530

Table E-3. Shallow Pool (Thermo Electric Cooler)

n-Butanol Pr = 43

Run	Ht(mm)	t(sec)	ΔT(°C)	Ra_t	Ra_H	Ma_t	$\frac{\alpha t}{H^2}$
1	5.0	98	1.56	1150	6650	1690	0.31
2	"	120	1.35	1370	5700	1610	0.385
3	"	42	2.6	540	11,100	1830	0.135
4	"	185	1.20	2300	5100	1790	0.59
5	"	82	1.30	740	5550	1290	0.26
6	"	75	1.42	700	6050	1340	0.24
7	"	50	2.02	550	8600	1560	0.16
8	"	210	1.03	2400	4470	1630	0.67
9	"	90	1.20	790	5100	1240	0.29
10	"	41	3.27	660	14,000	2280	0.13
11	"						
12	3.3	47	4.08	1010	5000	2930	0.34
13	"	64	4.12	1630	5050	3600	0.47
14	"	50	3.94	1060	4850	3040	0.315
15	"	60	3.28	1170	4050	2770	0.44

(continued)

Table E-3. (continued)

n-Butanol Pr = 43

Run	Ht(mm)	t(sec)	ΔT(°C)	Ra_t	Ra_H	Ma_t	$\frac{\alpha t}{H^2}$
16	3.3	92	3.12	2120	3850	3270	0.67
17	"	180	2.33	4320	2900	3410	1.32
18	"	109	2.32	2020	2860	2640	0.80
19	"	158	2.57	4020	3140	3520	1.15
20	"	240	1.89	5370	2330	3200	1.75
21	"	255	2.15	6730	2660	3740	1.85
22	2.16	274	5.8	20,200	1980	10,500	4.65
23	"	256	6.15	19,200	2080	10,750	4.3
24	"	220	6.15	15,400	2080	9950	3.75
25	"	136	6.05	7350	2050	7700	2.3
26	"	112	6.25	5650	2130	7200	1.91
27	"	113	5.75	5300	1960	6650	1.92
28	"	88	5.95	3700	2020	6100	1.5
29	"	116	4.80	4600	1640	5650	2.0
30	"	116	5.28	5050	1800	6200	2.0

(continued)

Table E-3. (continued)

n-Butanol Pr = 43

Run	Ht(mm)	t(sec)	$\Delta T(^{\circ}C)$	Ra_t	Ra_H	Ma_t	$\frac{\alpha t}{H^2}$
31	2.16	145	4.8	6410	1640	6300	2.5
32	"	162	5.0	7900	1770	6950	2.8

Table E-4. Shallow Pool Results (Spray Cooler)

n-Butanol Pr = 43

Run	Ht(mm)	t(sec)	ΔT(°C)	Ra_t	$Ra_H \times 10^3$	M_t	$\frac{\alpha t}{H^2}$	S
1	5.0	69	1.45	635	6.2	1310	0.220	0.617
2	"	42	1.81	375	7.7	1280	0.135	0.758
3	"	87	1.39	890	5.9	1415	0.278	0.500
4	"	23	2.04	173	8.8	1070	0.0735	0.843
5	"	54	1.39	420	5.9	1115	0.173	0.650
6	"	33	1.45	420	6.2	910	0.105	0.743
7	"	80	1.01	560	4.3	985	0.256	0.500
8	"	29	1.73	212	7.4	1020	0.093	0.772
9	"	107	1.45	1230	6.2	1635	0.340	0.557
10	"	55	1.47	452	6.25	1180	0.175	0.674
11	"	41	1.60	321	6.8	1120	0.131	0.731
12	"	24	1.47	133	6.25	790	0.077	0.777
13	"	75	1.29	645	5.5	1220	0.240	0.500
14	"	53	1.35	400	5.75	1070	0.169	0.606
15	"	41	1.29	260	5.5	900	0.131	0.701

(continued)

Table E-4. (continued)

n-Butanol Pr = 43

Run	Ht(mm)	t(sec)	ΔT(°C)	Ra_t	$Ra_H \times 10^3$	M_t	$\frac{\alpha t}{H^2}$	S
16	5.0	38	1.76	318	7.5	1180	0.121	0.724
17	"	24	2.04	178	8.8	1070	0.075	0.817
18	"	74	1.28	625	5.45	1200	0.237	0.543
19	"	60	1.29	460	5.5	1090	0.192	0.575
20	3.3	82	3.15	1750	3.55	3100	0.595	0.741
21	"	35	2.22	356	2.48	1440	0.255	0.787
23	"	107	3.00	2530	3.37	3390	0.73	0.741
24	"	50	2.81	760	3.15	2170	0.365	0.749
25	"	62	2.95	1110	3.30	2540	0.455	0.760
26	"	141	2.79	3560	3.12	3610	1.03	0.647
27	"	167	3.66	6020	4.10	5150	1.22	0.685
28	"	150	2.89	4050	3.24	3850	1.09	0.672
29	"	102	2.45	1970	2.74	2700	0.75	0.712
30	"	84	2.60	1530	2.91	2600	0.61	0.750
31	"	91	3.13	2080	3.51	3260	0.66	0.751

(continued)

Table E-4. (continued)

n-Butanol Pr = 43

Run	Ht(mm)	t(sec)	ΔT(°C)	Ra_t	$Ra_H \times 10^3$	M_t	$\frac{\alpha t}{H^2}$	S
32	3.3	152	2.31	3320	2.58	3100	1.11	0.651
33	"	287	2.57	9650	2.87	4750	2.10	0.650
34	"	87	2.58	1600	2.88	2620	0.635	0.81
35	"	78	2.89	1520	3.24	2780	0.57	0.76
36	"	231	3.27	8800	3.65	4960	1.69	0.77

n-Octanol Pr = 108

Run	Ht(mm)	t(sec)	ΔT(°C)	Ra_t	Ra_H	M_t	$\frac{\alpha t}{H^2}$	S
1	5.0	91	2.89	625	3460	1020	0.32	0.70
2	"	90	3.47	735	4150	1210	0.315	0.72
3	"	139	2.62	1070	3150	1150	0.486	0.62
4	"	55	3.3	337	3960	910	0.193	0.77
5	"	53	3.05	375	3650	820	0.184	0.77
6	"	66	3.42	462	4100	1030	0.380	0.77
7	"	200	2.75	1970	3300	1430	0.702	0.50

APPENDIX F. CONVECTION ONSET IN AIR

The heating apparatus used for detecting Ra_t in organic liquids at fixed surfaces (Chapter III, Sec. 2.2.1.) was modified to measure onset conditions in air. This change was necessary because the surface temperature did not change significantly after convection. This was due to the dominance of the metal heater in determining the solid-air surface temperature. The onset conditions were detected by placing a thermocouple approximately 2 mm above the heated surface (Fig. F-1) so that it was in the thermal layer. The responses for this thermocouple and the surface temperature are shown in Fig. F-2.

The critical conditions were read off the surface temperature curve at the point corresponding to the first deviation from the conduction profile of the response in the thermal layer. These critical conditions, along with the physical properties of air obtained from the Physics and Chemistry Handbook (41^{st} ed.) are listed below.

Physical Properties of Air at 20°C.

$$\frac{\mu}{\rho} = 0.151 \text{ cm}^2/\text{sec}$$

$$\alpha = 0.220 \text{ cm}^2/\text{sec}$$

$$\beta = \frac{1}{\rho}\frac{d\rho}{dT} = \frac{1}{T}$$

$$Ra_t = 10.44\ \Delta T t_c^{3/2}$$

Run	ΔT_c (°C)	t_c (sec)	Ra_t
1	4.8	37	11,300
2	4.8	41	11,300
3	7.0	32	13,100
4	5.75	33.5	11,700
5	5.85	33	11,500
6	5.65	34	11,700
7	6.4	33	12,650
8	5.1	36.5	11,700
		Avg.	11,850

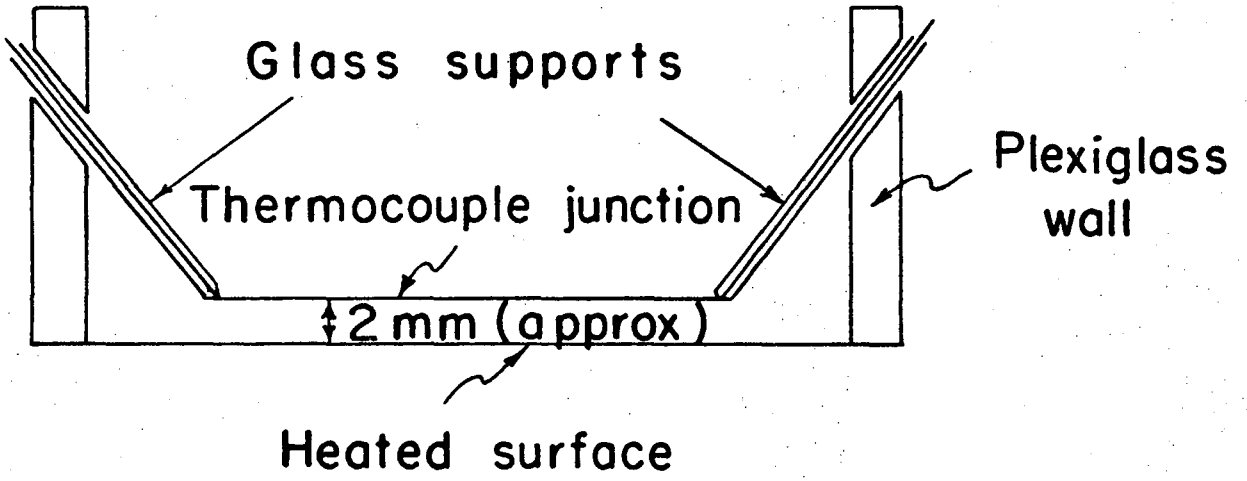

Fig. F-1. Position of Thermocouple Used to Measure the Onset of Convection in Air in the Deep Pool Apparatus Described in Fig. III-2.

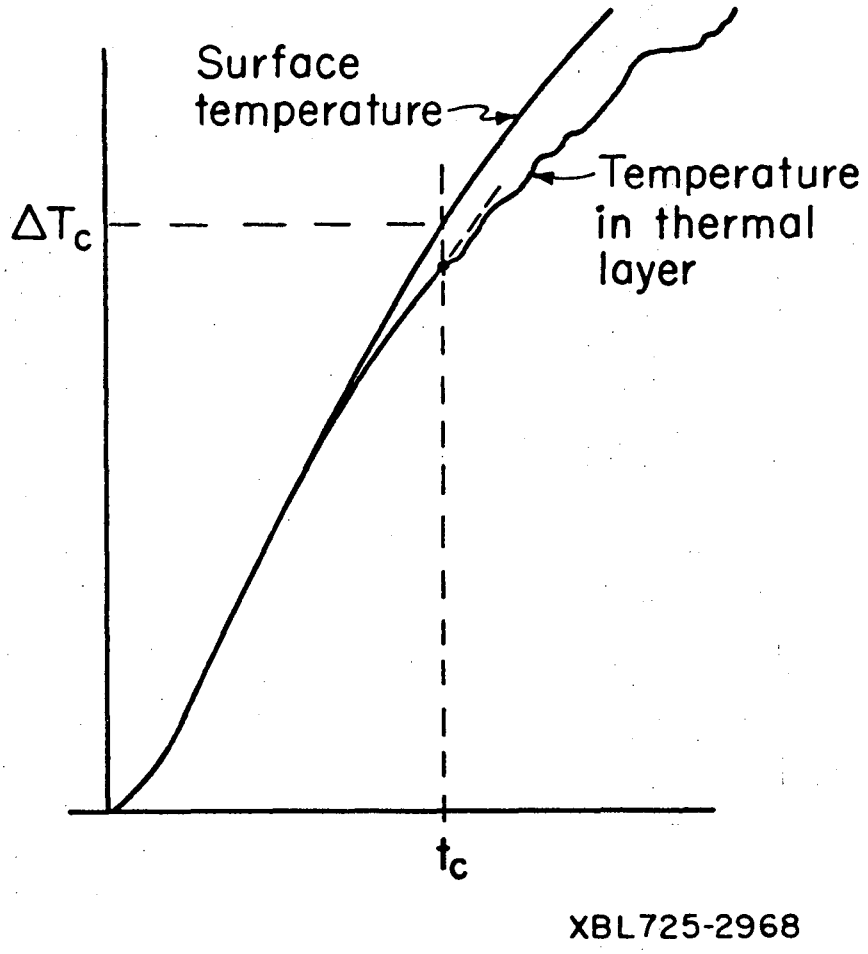

Fig. F-2. Temperature Response of the Thermocouple described in Fig. F-1 and on the Air-Metal Surface.

APPENDIX G. ALTERNATE DESCRIPTIONS OF THE SURFACE-TEMPERATURE-TIME CURVES

A simple scheme to describe the shape of the time dependent surface temperature curve was outlined in Chapter V. This method was based on normalization of the area enclosed within the surface-temperature curve and the time axis.

An alternate method of curve description used by many authors is to assume gas phase and liquid transport resistances and then describe the shape of the curve in terms of the ratio of the two resistances. The mathematical model is shown in Fig. G-1.

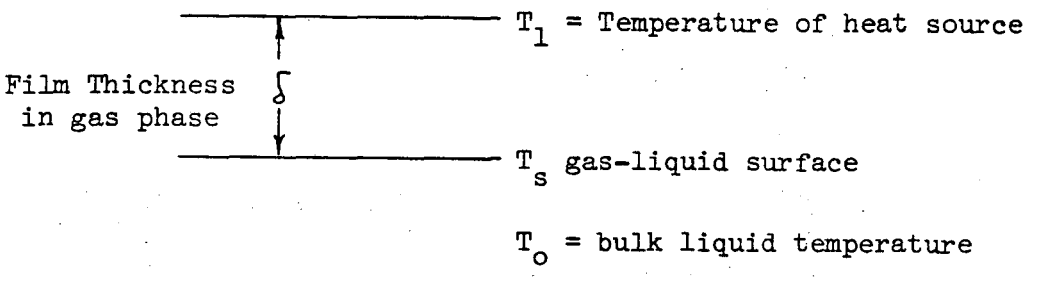

Fig. G-1

When the hot medium is exposed to the liquid, the air film thickness is assumed to be established rapidly while the temperature of the hot side of the film is constant. In the limit, this will represent a step change in the temperature T_1 at a finite distance from the gas-liquid surface. If the temperature profile in the air phase can be assumed to be almost linear immediately after exposure, which is true for an air film thickness of 3 mm after 0.1 seconds at room conditions,

then the heat conduction solution can be found from Carslaw and Jeager (1962), p. 300;

$$\frac{T_s - T_o}{T_l - T_o} = 1 - \exp R \operatorname{erfc} R \qquad \text{(G-1)}$$

where T_s, T_o, T_l, are described above in Fig. G-1.

$$R = \frac{k_{air}\sqrt{\alpha t}}{\delta\, k_{liq}} = \text{ratio of gas phase to liquid phase resistance}$$

α = diffusivity

t = time of exposure

The shape of the curve is nearly a step function at high values of R, whereas it is nearly linear for small values of R (refer to Fig. G-2).

The relationship between R and the shape factor S, described in Chapter V, can be found by normalizing the area enclosed between the surface temperature curve and the time axis. Thus

$$S = \frac{\int_o^t (T_s - T_o)dt}{(T_s - T_o)\big|_t\, t}$$

$$= \frac{\int_1^R (1 - \exp \psi \operatorname{erfc} \psi)d\psi}{(1 - \exp R \operatorname{erfc} R) \cdot R} \qquad \text{(G-2)}$$

This relationship has been plotted on Fig. G-3.

Another method of describing the shape of the surface curve, used in linear analysis, is derived from a heat balance at the heat transfer surface.

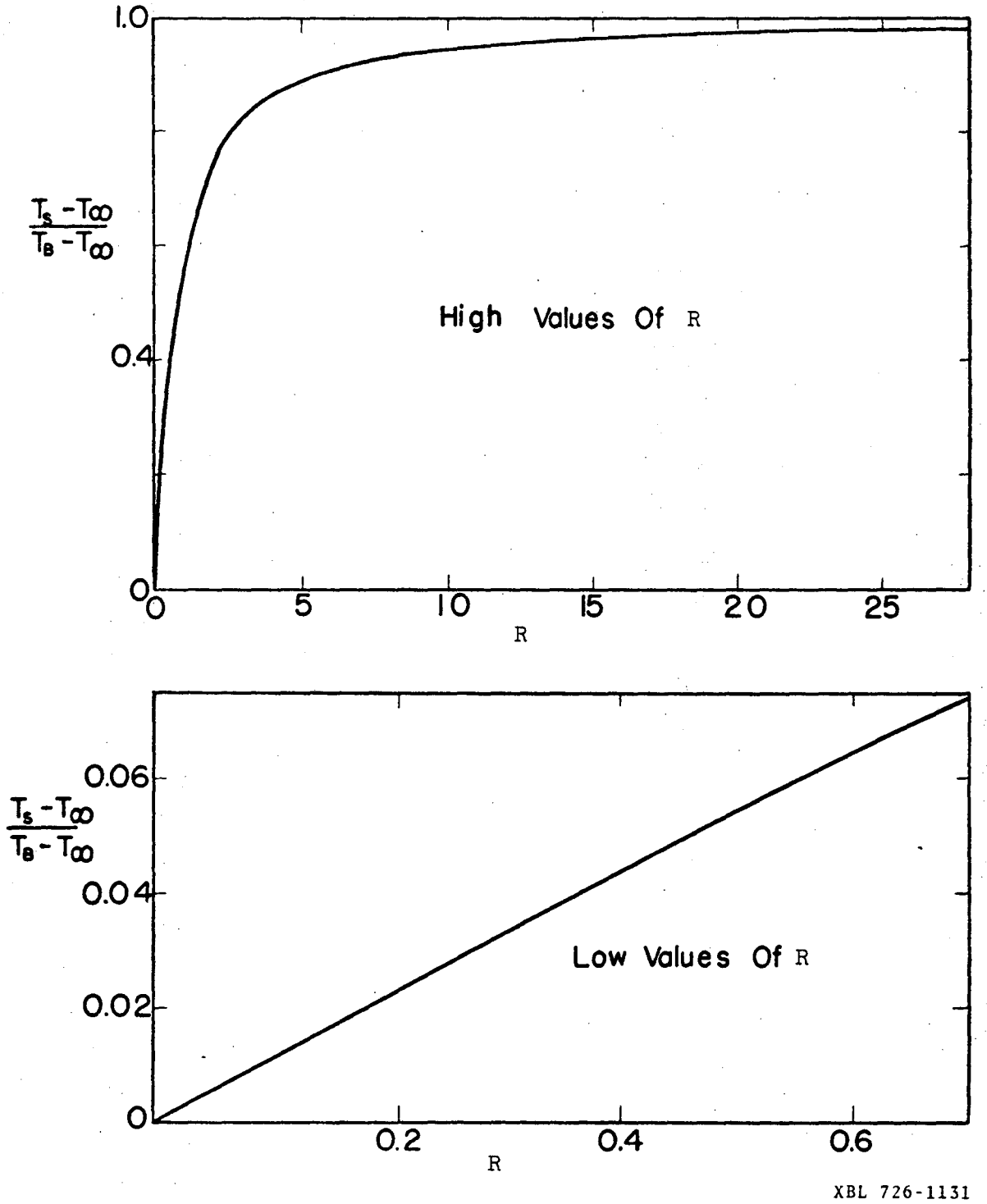

Fig. G-2. Shapes of Curves Described by Eq. G-1, for high and low values of R.

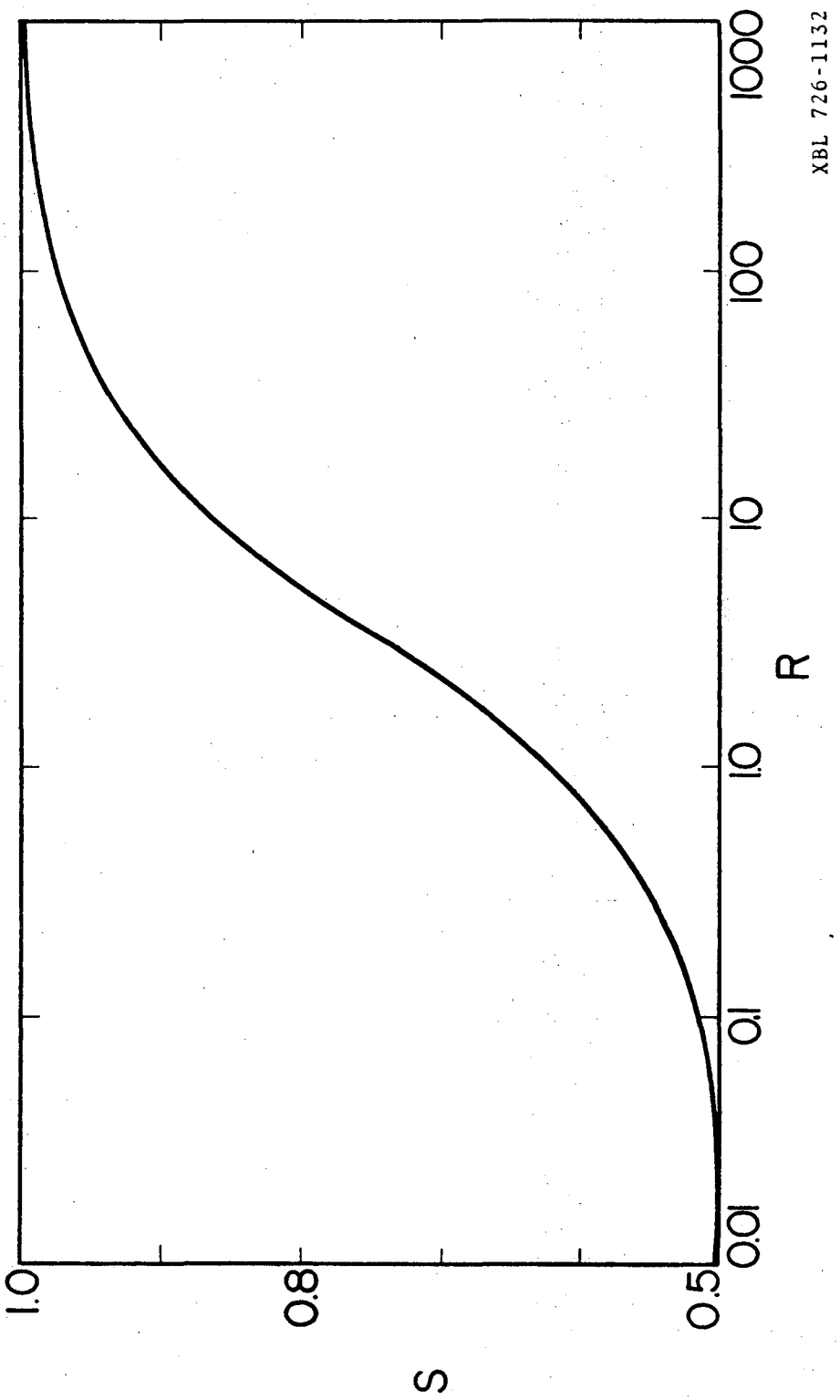

Fig. G-3. Relationship Between the Shape Factor, S, and the Biot number, R given by Eq. G-2.

$$k_{liq} \frac{\partial T_s}{\partial \psi} = k_{air} \frac{(T_s - T_l)}{\delta} \qquad (G\text{-}3)$$

When made dimensionless and linearized around the steady state linear profile in the liquid, the above form becomes

$$\nabla T_s = N_\ell T_s \qquad (G\text{-}4)$$

where N_ℓ = Evaporation number = ratio of gas phase resistance to liquid phase resistance.

The advantages of using the normalized area over the ratio R (or N_ℓ) are as follows:

(1) The set of curves described by the model from which R is derived represents a section of the possible curve shapes. If the convection is sensitive to curve shape, R would be a better parameter than S for the particular series of curves described by (R = constant). This is true because S would be too general. However, the results of Chapter VI indicate that for density-driven convection S is adequate. This may not be true for surface-tension-driven convection.

(2) If there is chemical reaction of any other complicating factor in the production of the surface temperature or composition curve, it would be easier to plot the curve and find a value of S rather than fit the curve with a relevant value of R.

APPENDIX H. TRANSFORMATION OF Ra_t INTO Ra_ℓ

By definition

$$Ra_\ell = Ra_t \left(\frac{\ell A}{\sqrt{\alpha t}}\right)^3 \tag{H-1}$$

where

$$\ell . A_\circ = \sqrt{\alpha t}$$

A is the proportionality constant (H-2)

1) Variation of "A" with Surface Temperature-Versus-Time Curve (Shape Factor S)

The solution for conduction into a semi-infinite medium with $T_s = k\, t^{n/2}$ is given by Carslaw and Jaeger (1962), p. 63, as:

$$T(z,t) = k\, \Gamma(n+1)\, (4t)^{n/2}\, i^n \operatorname{erfc} \frac{2}{\sqrt{4\alpha t}} \tag{H-3}$$

Substitution of (H-3) into

$$\frac{1}{2} T_s \ell = \int_0^\infty T(z,t)\, dz \tag{H-4}$$

yields

$$A = \frac{\ell}{\sqrt{\alpha t}}\ \Gamma\left(\frac{n}{2}+1\right)\, 2^{n+2}\, i^{n+1} \operatorname{erfc} 0 \tag{H-5}$$

n	0	1	2	3	4	5
$\Gamma(\frac{n}{2}+1)$	1	$\frac{1}{2}\sqrt{\pi}$	1	$\frac{3}{4}\sqrt{\pi}$	2	$\frac{15}{8}\sqrt{\pi}$
2^{n+2}	4	8	16	32	64	128
$i^{n+1}\operatorname{erfc} 0$	0.5642	0.250	0.09403	0.03125	0.00940	0.002608
A	2.2568	1.772	1.504	1.3293	1.2032	1.109557

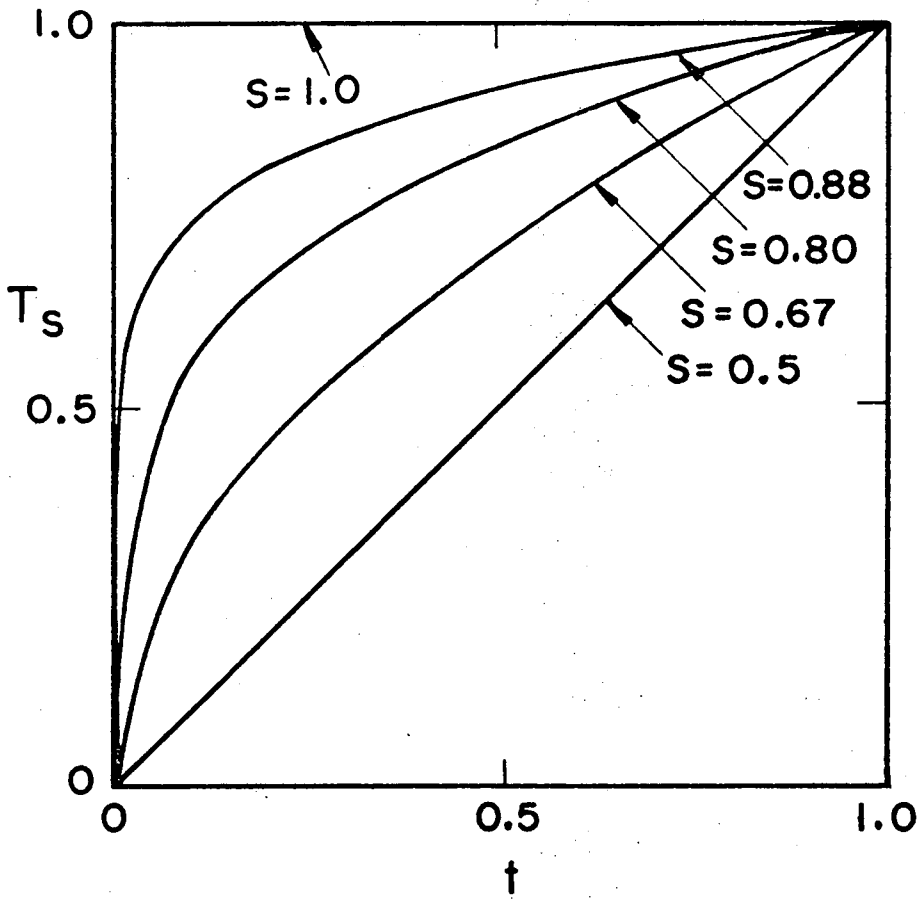

Fig. H-1. Family of Surface Temperature vs. time curves for the relation $T_S = kt^{n/2}$. The variable parameter is the Shape Factor, S.

By definition

$$S = \frac{\int_0^t T_s(\tau)d\tau}{T_s(t) \cdot t} \qquad (H\text{-}6)$$

$$= \frac{2}{n + 2}$$

n =	0	1	2	3	4	5
S =	1.0	0.67	0.5	0.4	0.33	0.285

The relationship between A vs. n and S vs. n were cross-plotted to determine A vs. S. Values of A for S between 1.0 and 0.5 were interpolated from the curve of A vs. S and presented on Fig. H-2.

2) Variation of A with Height Factor $\frac{\alpha t}{H^2}$ for a Step Function and a Linear Change of T_s

The solution for conduction into a fluid with depth H, one surface at a constant temperature, and the other surface showing a linear change of temperature with time is given by Carslaw and Jaeger (1962), p. 104, as:

$$T = (z - 1)\,\tau + \frac{2}{\pi^2} \sum_1^\infty \frac{\sin n\pi z}{n^3} (1 - e^{-n^2\pi^2\tau}) \qquad (H\text{-}7)$$

From the definition of ℓ, Eq. (H-4), and Eq. (H-7)

$$\frac{\ell}{\sqrt{\alpha t}} = A_L = \frac{1}{\sqrt{\tau}} \left[1 - \frac{8}{\pi^4\tau} \sum_0^\infty \frac{1}{(2n + 1)^4} \left[1 - e^{-(2n + 1)^2\pi^2\tau}\right]\right] \qquad (H\text{-}8)$$

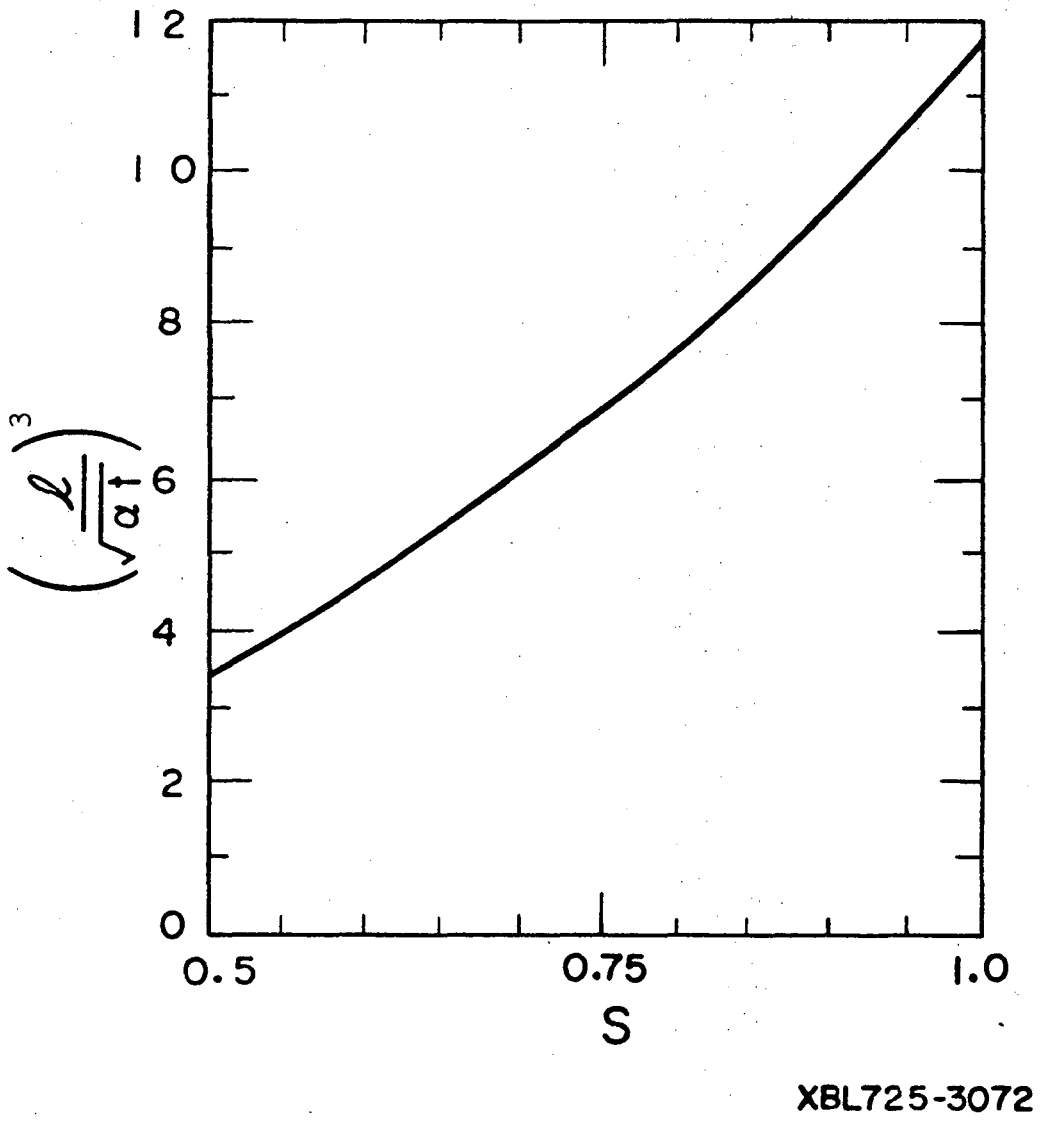

Fig. H-2. Ratio of cube of Effective density layer depth $(\ell)^3$ to the cube of the Thermal Diffusion Scale Length $(\alpha t)^{3/2}$ as a Function of Shape Factor (S) for the Family of Curves $T_s = kt^{n/2}$.

A similar analysis for a step change in surface temperature was performed using the solution given by Carslaw and Jaeger (1962), p. 104, for this case:

$$T = (z - 1) + \frac{2}{\pi} \sum_{1}^{\infty} \frac{\sin n\pi z}{n} e^{-n^2\pi^2\tau}$$

and

$$\frac{\ell}{\sqrt{\alpha t}} = A_s = \frac{1}{\sqrt{\tau}} \left[1 - \frac{8}{\pi^2} \sum_{0}^{\infty} \frac{1}{(2n + 1)^2} e^{-(2n + 1)^2\pi^2\tau}\right]$$

The relationships between (A_s, A_L) and τ ($= \frac{\alpha t}{H^2}$) have been plotted on Fig. H-3. The limiting solutions for very small τ are equivalent to the semi-infinite medium solutions discussed in Sec. 1 of this appendix.

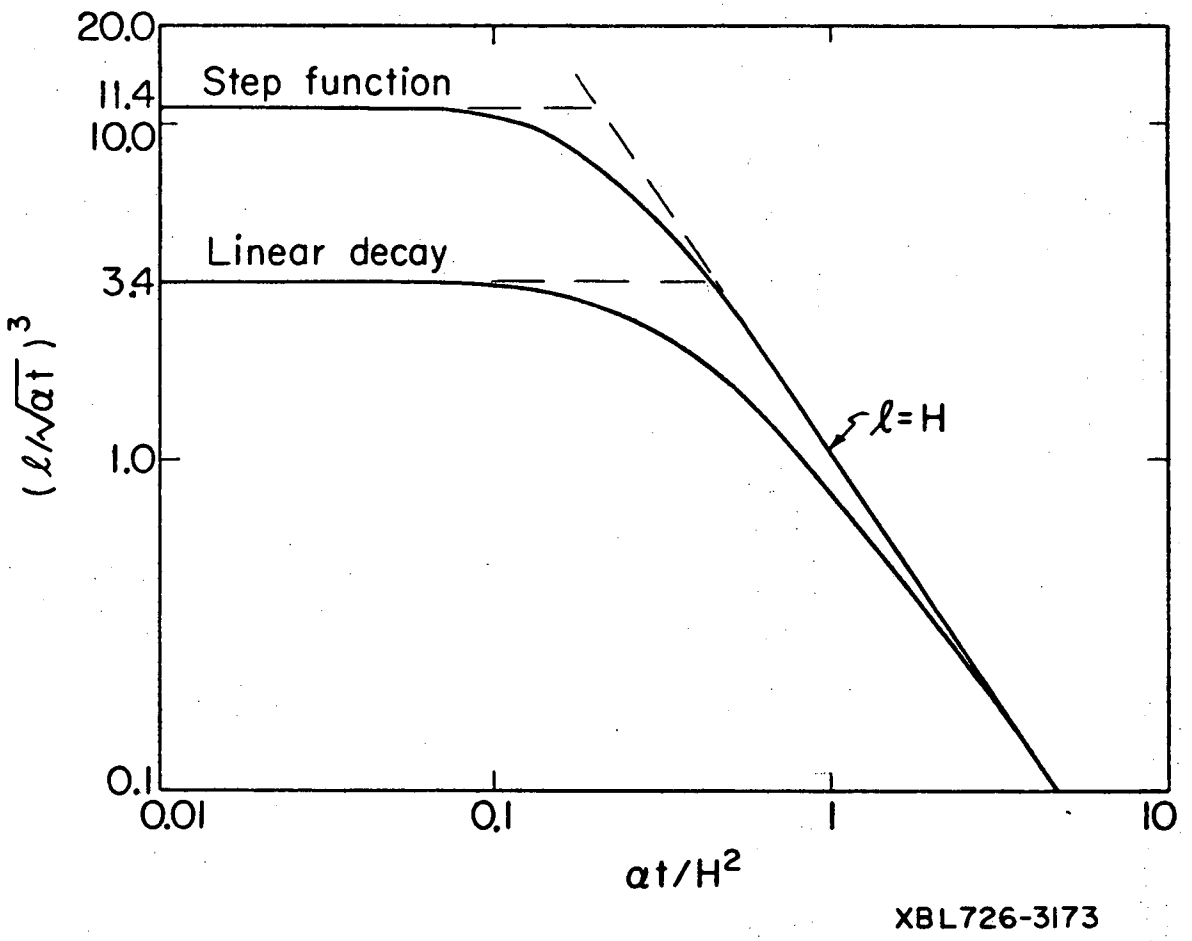

Fig. H-3. Ratio of the cube of the Effective Density layer depth, ℓ^3, to the cube of the thermal diffusion scale length $(\alpha t)^{3/2}$ as a Function of Depth Factor $(\alpha t/H^2)$ for a Step Change and Linear Time Decay of Surface Temperature.

τ	$A_L \tau^{1/2}$	$A_s \tau^{1/2}$
10.0	0.9917	1.0
5.0	0.9833	1.0
2.5	0.9667	1.0
1.25	0.9334	1.0
0.625	0.8669	0.9983
0.312	0.7454	0.9629
0.156	0.5791	0.8266
0.0781	0.4196	0.6250
0.0391	0.2974	0.4459
0.0195	0.2103	0.3154
0.00977	0.1487	0.2230
0.00408	0.1052	0.1577

$$\lim_{\tau \to \infty} (A_L \tau^{1/2}, A_s \tau^{1/2}) = 1$$

$$\lim_{\tau \to 0} (A_L, A_s) = (1.504, 2.2568)$$

APPENDIX I. SHAPE FACTOR(S) DATA FOR CONVECTION INITIATION AT A FIXED SURFACE

Preliminary experimentation showed that variation of the shape of the surface temperature vs. time curve could be best obtained using the spray cooler to cool a gas-liquid surface. However, some spray-cooler results showed the influence of surface waves which were produced from the spray action (Chapter VI, Sec. 1.2.). Comparison of thermo-electric and spray-cooler results for linear changes (S = 0.5) of surface temperature with time (Chapter VI, Fig. VI-11) showed that surface-wave influence was negligible for n-octanol. However, it was not certain that the results of surface temperature-vs-time curves with other values of S were free of surface-wave influence since the severity of the spray action was increased to produce curves with higher values of S.

This problem was answered by producing surface temperature-vs-time curves with a wide range of S at a fixed interface. The development of this experiment came after the spray cooler results. The principle of the apparatus was to use the thermo-electric heat pump to produce a heated surface, and control the temperature of the heated surface by controling the current to the heat pump. The design was based on principles discussed in Chapter III, Sec. 2.2. and is shown in Fig. I-1. The isothermal heating surface was designed according to Chapter IV, Sec. 3.4. The metal cylinder acted as the heat sink for the thermo-electric heat pump.

The number of experiments was limited to verifying the spray-cooler results for n-octanol. The results are listed below and plotted in Chapter VII, Fig. VII-1. They show that surface-wave influence in the

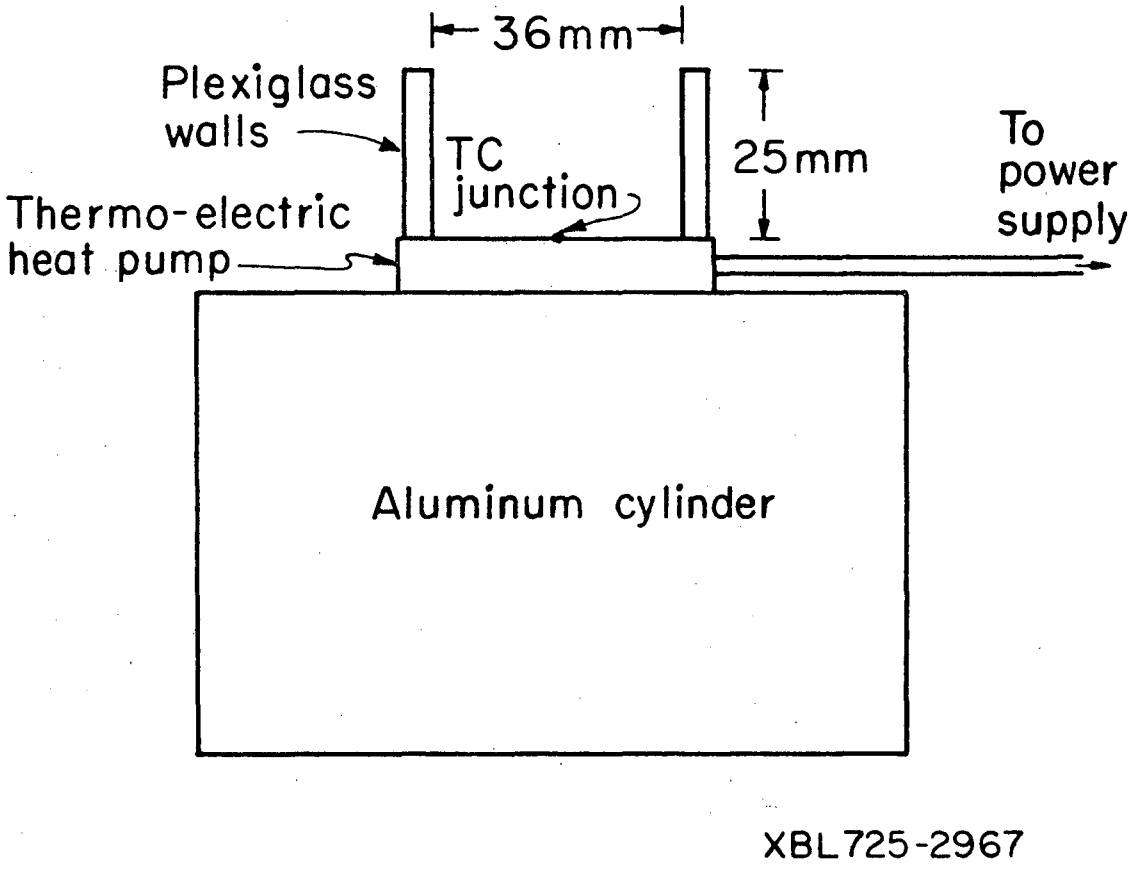

Fig. I-1. Fixed Surface, Deep Pool Apparatus used to Determine the Shape Factor Data.

spray-cooler results for n-octanol was negligible for the range of S investigated in the spray-cooler experiments.

Results for n-octanol

	$\Delta T(^{\circ}C)$	t_c(sec)	Ra_t	Ra_ℓ	S
1	0.98	74	156	420	0.87
2	1.55	82	280	475	0.67
3	1.17	64	150	420	0.89
4	4.25	57	460	485	0.515
5	1.63	90	348	500	0.615
6	2.50	50	246	445	0.75
7	1.11	68	156	400	0.86

APPENDIX J. INFLUENCE OF TEMPERATURE GRADIENTS ALONG A GAS-LIQUID SURFACE

Mitchell and Quinn (1968) observed oscillations in surface temperature accompanied by surface movement when a thin film of liquid was heated from below by a point source. This phenomenon was explained in terms of surface-tension forces which arose from the temperature gradients along the liquid surface. A mechanistic description of this type of surface-tension-driven motion has been developed by Biddulph and Ellis (1966) in explaining a similar situation, the interaction between surface waves and surface-tension gradients. The phenomenon appears to be driven by point-source variations in surface tension along the surface. An obvious case to study is one where a strictly increasing surface tension gradient exists along the gas-liquid surface with no point sources or surface deformation. The results of a study of this case for a thin film or liquid are reported in the following:

The uniform surface-tension gradient along the gas-liquid surface was investigated in a shallow pool apparatus shown in Fig. J-1. The liquid container was made from polycarbonate (0.75 mm thick) with the dimensions shown. The thermoelectric heat pumps were positioned at each end of the liquid container and provided a uniform temperature across the liquid, perpendicular to the direction of heat transfer between the pumps. These heat pumps could produce either a cooling or a heating effect by choosing the direction of the current in them. A copper plate was placed above the liquid, leaving an air gap of approximately 2 mm. This was done to produce a linear temperature profile in the air gap.

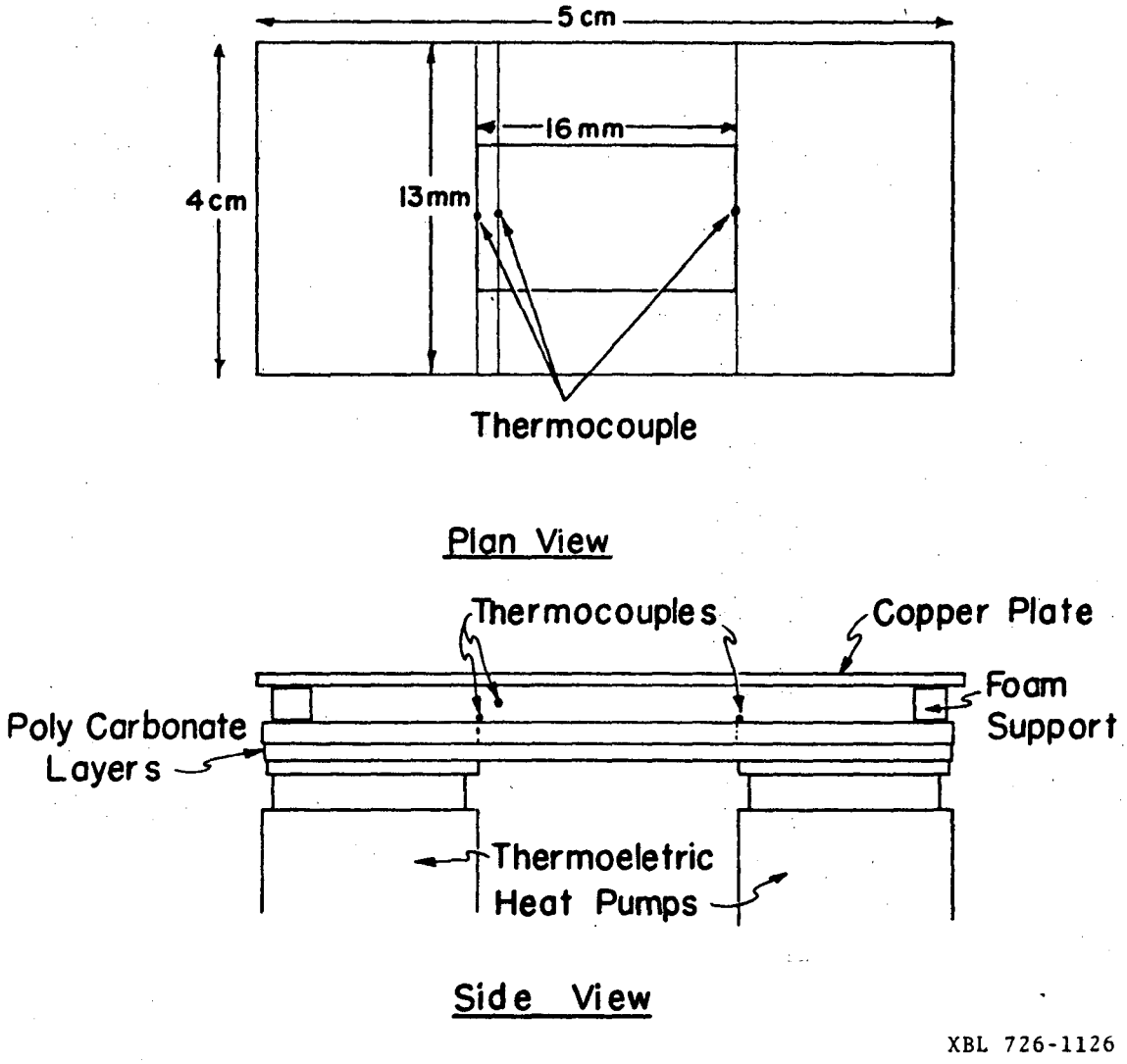

Fig. J-1. Apparatus used for the investigation of the effect of a uniformly increasing or decreasing Surface Temperature Gradient along a Thin Liquid Layer.

The temperatures at both ends of the liquid layer were monitored, as was the temperature of the air near one end of the liquid and approximately 1 mm above the liquid surface. From the discussion of surface convection in Appendix B, it was expected that a sudden change in surface liquid or air temperature would indicate the onset of surface convection.

Several liquids were tested, with the top level being such that there was no meniscus. The heat pump close to the end where the air temperature was being measured was switched on to heat the liquid. The results showed no oscillations, nor deviations from a smoothly increasing liquid and air temperature response. The most severe conditions were for decane (viscosity of 0.87 cp.) where the temperature gradient was 3° C/cm, established in 180 seconds. However, when the liquid was allowed to run over the edges of the container so that there was fluid on the top surface of the container, strong convection effects were observed. In this case the liquid had a bump in surface, which led to two-dimensional gradients and geometry.

The results of Quinn and Mitchell were verified by using the gas-liquid cooling equipment described in Chapter V, with a thermoelectric heat pump. A thin copper wire was attached to the base of the cooler. The tip of the wire was positioned close to the thermocouple junction, but did not enter the fluid. The resulting temperature profile produced when the gas-liquid surface was heated (to inhibit density-driven flow) showed oscillations as Quinn and Mitchell observed. When the thin rod touched the liquid and the experiment repeated, the bottom of the cooler was covered with liquid. Obviously, the liquid ascended the rod under surface tension action, which agrees with the observation of Ludvikson and Lightfoot (1971).

The conclusion from these studies is that a lateral surface tension gradient on a gas-liquid planar surface does not show instability, even though cases with point source variations and surface deformations do. This suggests that the following conditions are required, but not necessarily sufficient, for surface tension motion

(1) a surface tension gradient along the surface

and (2) a meniscus, surface wave or point source

APPENDIX K. VALUES OF EXPERIMENTAL Ra_{TC} and Ra_t

1. Deep-Pool Heat Transfer Coefficients from the Literature

The following data was taken from the literature in the form of Nu vs. Ra_H for deep pools ($Ra_H > 10^5$) so as to calculate Ra_{TC} and its dependence on Pr. The results have been plotted as Ra_{TC} vs. Pr on Fig. VIII-1.

Somerscales and Gazda (1969)

Ra_H	Nu	$\frac{Ra_H}{2Nu^3} = Ra_{TC}$	Pr
7.34×10^5	9.02	500	20.2
1.76×10^6	11.1	645	16.8
6.4×10^6	17.4	605	19.7
1.47×10^7	20.4	850	17.6
5.97×10^7	29.3	1200	18.5
1.30×10^8	38.5	1150	17.1
3.72×10^7	26.9	970	5.64
3.21×10^8	50.8	1200	5.56

Silveston (1958)

Ra_H	Nu	Ra_{TC}	Pr
2.47×10^5	5.5	750	6.07
3.8×10^5	6.59	670	5.43
1.25×10^5	6.26	260	4.23
1.86×10^5	5.30	620	35.0
0.93×10^5	4.39	555	35.2

Globe and Dropkin (1958) (estimated from plot of results)

$Nu/Ra^{1/3}$	Ra_{TC}	Pr
(appears in error compared with Rossby (1966)		8700
0.105	425	250 - 400
0.074 - 0.095	1200 - 570	10 - 20
0.80	900	5.5
0.057	2450	2.5
0.057 - 0.035	3400 - 13,000	0.02

Malkus (1954)

Ra_H	Nu	Ra_{TC}	Pr
1.7×10^5	4.4	1000	4.0 (estimate)
4.25×10^5	5.5	1300	4.0
8.6×10^5	6.7	1400	4.0

Mull and Reihner (1930) - (Air, Pr = 0.7)

Log Nu	Log Ra_H/Pr	Ra_{TC}
0.55 - 0.6	5.2	1150
0.76	5.88	1500
0.84	6.2	1750
1.05	6.58	1250
1.17	6.92	1250

Rossby (1966)

Ra_H	Nu	Ra_{TC}	Pr
4×10^5	4.1	2900	0.023
10^6	8.4	850	6.8
10^6	9.2	650	200

2. Value of $\pi^{3/2} Ra_{t/STEP}$ to Compare with Ra_{TC}

Values of $\pi^{3/2} Ra_t$ for a step change can be found from values of Ra_t for a linear decay and multiplying by the appropriate length scale factor discussed in Appendix H.

From Fig. H-3,

$$Ra_{t/STEP} = \frac{3.4}{11.4} Ra_{t/LINEAR}$$

$$= 1/3.35 \; Ra_{t/LINEAR}$$

Large Pr Asymptote:

From Fig. VII-3,

$$Ra_{t/LINEAR} = 350$$

$$\pi^{3/2} Ra_{t/STEP} = 350 \times (1/3.35) \times 5.57$$

$$= 570$$

Small Pr Asymptote

From Fig. VII-3,

$$Pr \; Ra_{t/LINEAR} = 7200$$

$$\pi^{3/2} Ra_{t Pr/STEP} = 7200 \times (1/3.35) \times 5.57$$

$$= 12{,}000$$

APPENDIX L. NOMENCLATURE

a = wave number of initial vibration

C_p = heat capacity at constant pressure (cal/gm°C)

$\mathscr{D}$ = mass diffusivity (cm^2/sec)

D = fluid width (cm)

g = gravity constant (cm/sec^2)

h = heat transfer coefficient for a single thermal layer

H_o = overall heat transfer coefficient

H = fluid depth (cm)

ΔH_{vap^n} = heat of vaporization (cal/gm-mole)

k = thermal conductivity (cal/cm sec °C)

ℓ = effective density layer thickness

M_H = Marangoni number based on fluid depth = $\frac{\Delta\sigma\ H}{\mu\alpha}$

M_t = Marangoni number-time dependent = $\frac{\Delta\sigma\ t^{1/2}}{\mu\alpha^{1/2}}$

M_{Ho} = Marangoni number calculated without considering density effects

ΔP = Mass transfer driving force in pressure units

R = Biot number = ratio of heating phase transfer resistance to heated phase transfer resistance

Ra_H = Rayleigh number based on fluid depth H = $\frac{\rho g\beta\ \Delta T\ H^3}{\mu\alpha}$

Ra_t = Rayleigh number-time dependent = $\frac{\rho g\beta\ \Delta T\ \alpha^{1/2}t3/}{\mu}$

Ra_δ = Rayleigh number derived from steady state convection temperature profile

Ra_{TC} = Rayleigh number derived from steady-state natural convection heat transfer data

Ra_P = Rayleigh number based on period of motion

Ra_{Ho} = Rayleigh number calculated without considering surface tension effects

Sc = Schmidt number

t = time (sec)

t^*, tp = length of period (sec)

T = temperature (°C)

v = velocity perturbation term

w = amplification factor

z = vertical coordinate

$\frac{\alpha t}{H^2}$ = fluid depth factor

$\frac{\alpha t}{D^2}$ = fluid width factor

Variable Subscripts

1 = air

2 = liquid

S = interface

b,∞ = bulk conditions

c = conditions at onset of convection

w = wall

Greek Letters

α = thermal diffusivity (cm^2/sec)

β = volumetric coefficient of thermal expansion $(°C)^{-1}$

λ = wavelength of initial vibration (cm)

μ = viscosity tension (centipoise)

σ = surface tension (dynes/cm)

$\Delta\sigma$ = difference in surface tension between surface liquid and bulk liquid (dynes/cm)

ρ = density (gm/cc)

ξ = perturbation expansion term

θ = temperature perturbation

η = mass fraction

ψ = mole fraction

π_n = dimensionless groups

δ = penetration depth

Mathematical Operators

∇ = differential operator = $\frac{\partial}{\partial\psi} + \frac{\partial}{\partial y} + \frac{\partial}{\partial z}$

∇_2 = differential operator = $\frac{\partial}{\partial\psi} + \frac{\partial}{\partial y}$

REFERENCES

Bakker, C. A. P., van Buytenen, P. M., and Beek, W. J., Chem. Eng. Sci. 21, 1039 (1966)

Ball, J. G. and Himmelblau, D. M., Advances in Chemical Physics 13, 267 (1968)

Bénard, H., Revue Generale des Sci. pure et appl. 11, 1261, 1309 (1900)

Berg, J. C., Ph.D. Dissertation, University of California, Berkeley (1964)

Berg, J. C. and Acrivos, A., Chem. Eng. Sci. 20, 737 (1965)

Berg, J. C., Acrivos, A., and Boudart, M., J. Fluid Mech. 24, 721 (1966)

Berg, J. C., Boudart, M., and Acrivos, A., "Advances in Chem. Eng.", 6, Academic Press (1966)

Berg, J. C. and Morig, C. R., Chem. Eng. Sci. 24, 937 (1969)

Berg, J. C. and Palmer, H. J., J. Fluid Mech. 47, 779 (1971)

Blair, L. M. and Quinn J. A., J. Fluid Mech. 36, 385 (1969)

Brian, P. L. T., A.I.Ch.E.J. 17, 765 (1971)

Brown, W. H. and King, C. J., Lawrence Berkeley Laboratory Report No. UCRL-18974 (1969)

Burger, E. D., Ph.D. Dissertation, University of Illinois, Urbana-Champaign (1971)

Bulletin #05-061, Dow Corning Chemical Products Division (1963)

Busse, F. H., J. Math. Phys. 46, 140 (1967)

Busse, F. H. and Whitehead, J. A., J. Fluid Mech. 47, 305 (1971)

Carslaw, H. S. and Jaeger, J. C., "Conduction of Heat in Solids", Oxford University Press, 2nd ed., New York (1959)

Chandrasekhar, S., "Hydrodynamic and Hydromagnetic Stability", The Clarendon Press, Oxford (1961)

Chen, M. M. and Whitehead, J. A., J. Fluid Mech. 31, 1 (1968)

Clark, M. W., Ph.D. Dissertation, University of California, Berkeley (1967)

Clark, M. W. and King, C. J., A.I.Ch.E.J. 16, 69 (1970)

Cline, J. K. and Andrews, D. H., J. Am. Chem. Soc. 53, 3669 (1931)

Currie, I. G., J. Fluid Mech. 29, 337 (1967)

Davenport, I. F. and King, C. J., Chem. Eng. Sci., in press (1972)

Davis, S. H., J. Fluid Mech 30, 465 (1967)

Davies-Jones, R. P., J. Fluid Mech. 44, 695 (1970)

Debler, W. R. and Wolf, L. W., J. Heat Transfer 92, 351 (1970)

Ellis, S. R. M. and Biddulph, M., Chem. Eng. Sci. 21, 1107 (1966)

Foster, T. D., Phys. Fluids 8, 1249 (1965)

Foster, T. D., Phys. Fluids 8, 1770 (1965)

Foster, T. D., Phys. Fluids 11, 1257 (1968)

Foster, T. D., Phys. Fluids 12, 2482 (1969)

Foster, T. D., Geophysical Fluid Dynamics 2, 201 (1971)

Fugii, T., Takeuchi, M. T., Fujii, M., Suzaki, K., and Vehra, H., Int. J. Heat Mass Transfer 13, 753 (1970)

Globe, S. and Dropkin, D., J. Heat Transfer 81, 24 (1959)

Gresho, P. M. and Sani, R. L., Int. J. Heat Mass Transfer 14, 207 (1971)

Heitz, W. L. and Westwater, J. W., J. Heat Transfer 93, 188 (1971)

Hodgeman, C. D., "Handbook of Physics and Chemistry", 40th ed. Chemical Rubber Pub. Co., Cleveland (1959)

Howard, L. N., Proc. Eleventh Int. Congress Appl. Mech., 1109-1115, Berlin: Springer (1966)

Ibl, N. and Mueller, R. H., J. Electrochemical Soc. 105, 346 (1958)

International Critical Tables, Vol. 1-7, 1st ed., McGraw-Hill, New York (1928)

Hrma, P., Chem. Eng. Sci. 25, 1679 (1970)

Kayser, W. V. and Berg, J. C., Ind. Eng. Chem., Fundamentals 10, 526 (1971)

Kenny, D. B. R., Appl. Mech. Rev. 21, 1101 (1968)

Koshmeider, E. L., Beitr. Phys. Atmos. 39, 1 (1966)

Koshmeider, E. L., J. Fluid Mech. 30, 9 (1967)

Krishnamurti, R., J. Fluid Mech. 33, 445, 457 (1968)

Krishnamurti, R., J. Fluid Mech. 42, 295, 309 (1970)

Levich, V. G., "Physico-Chemical Hydrodynamics", Prentice Hall, New Jersey (1962)

Ludvikson, V. and Lightfoot, E. N., A.I.Ch.E.J. 17, 1166 (1971)

Lick, W., J. Fluid Mech. 21, 565 (1965)

Mahler, E. G., Schechter, R. S., and Wissler, E. H., Phys. Fluids 11, 1901 (1968)

Mahler, E. G., Ph.D. Thesis, The University of Texas, Austin, Texas (1969)

Mahler, E. G. and Schechter, R. S., Chem. Eng. Sci. 25, 955 (1970)

Malkus, W. V. R., Proc. Roy. Soc. A225, 196 (1954)

Malkus, W. V. R. and Veronis, G., J. Fluid Mech. 4, 225 (1958)

Mayr, S. T., Sc.D. Dissertation, Massachusetts Institute of Technology (1970)

Mitchell, W. T. and Quinn, J. A., Chem. Eng. Sci. 23, 503 (1968)

Modern Plastics Encyclopedia 46, 931 (1970)

Morton, B. R., Quart. J. Mech. Appl. Math. 10, 433 (1957)

Mull, W. and Reihler, H., Beitr Z. Gesandheitstech-Ing. 1, 28 (1930)

Mueller, R. H., Ph.D. Dissertation, Erdgenossiche Technische Hochschule, Zurich (1956)

Neild, D. A., J. Fluid Mech. 19, 341 (1964)

Onat, K. and Grigull, V., Wärme and Stoffübertragung 3, 103 (1970)

Orell, A. and Westwater, J. W., A.I.Ch.E.J. 8, 350 (1962)

Palm, E., J. Fluid Mech. 8, 183 (1960)

Pearson, J. R. A., J. Fluid Mech. 4, 489 (1958)

Perry, R. H., "Chemical Engineers Handbook", 4th ed., McGraw-Hill Book Co., Inc., New York (1963)

R. E. and Quinn, J. A., A.I.Ch.E.J. 12, 894 (1966)

(Lord) Rayleigh, Phil. Mag. 32, 529 (1916)

Reid, R. C. and Sherwood, T. K., "Properties of Gases and Liquids", 2nd ed., McGraw-Hill Book Co., Inc., New York (1966)

Robinson, J. L., J. Fluid Mech. 29, 461 (1967)

Rossby, H. T., Ph.D. Thesis, Massachusetts Institute of Technology (1966)

Sakiadis, B. C. and Coates, J., A.I.Ch.E.J. 1, 275 (1955)

Schmidt, R. J. and Saunders, O. E., Proc. Roy. Soc. A165, 216 (1938)

Scriven, L. E. and Sternling, C. V., J. Fluid Mech. 19, 321 (1964)

Segal, L. A. and Stuart, J. T., J. Fluid Mech. 13, 289 (1962)

Silveston, P. L., Forsch. Ing. Wes. 24, 29, 59 (1958)

Smith, K. A., J. Fluid Mech. 24, 401 (1966)

Soberman, R. K., Phys. Fluids 2, 131 (1959)

Somerscales, E. F. C. and Dougherty, T. S., J. Fluid Mech. 42 (1970)

Somerscales, E. F. C. and Gazda, I. W., Int. J. Heat Mass Transfer 12, 1491 (1969)

Spangenberg, W. G. and Rowland, W. R., Phys. Fluids 4, 743 (1961)

Sparrow, E. M., Husar, R. B., and Goldstein, R. J., J. Fluid Mech. 41, 793 (1970)

Springer, T. G. and Pigford, R. L., Ind. Eng. Chem., Fundamentals 9, 458 (1970)

Thompson, D. W., Ind. Eng. Chem., Fundamentals 9, 243 (1970)

Timmermans, J., "Physico-Chemical Constants of Pure Organic Compounds", Elsevier Pub. Co., New York (1950)

Vidal, A., Ph.D. Dissertation, Stanford University (1967)

Vidal, A. and Acrivos, A., Ind. Eng. Chem., Fundamentals 7, 53 (1968)

Vivian, J. E., Brian, P. L. T., and Mayr, S. T., Ind. Eng. Chem., Fundamentals 10, 75 (1971)

Willis, G. E. and Deardorff, J. W., J. Fluid Mech. 23, 337 (1965)

Wilke, C. R. and Pin Chang, A.I.Ch.E.J. 1, 264 (1955)

Willis, G. E. and Deardorff, J. W., Phys. Fluids 10, 1861 (1967)

Willis, G. E. and Deardorff, J. W., J. Fluid Mech. 44, 661 (1970)

TECHNICAL INFORMATION DIVISION
LAWRENCE BERKELEY LABORATORY
UNIVERSITY OF CALIFORNIA
BERKELEY, CALIFORNIA 94720